BBSRC London Interdisciplinary Biosciences PhD Programme

Fatty acid-induced stress signalling in adipocytes

A dissertation submitted to the University of London in candidature for the degree of Doctor of Philosophy by Léa Brochard

Supervisors: Dr Lazaros Foukas, Prof Jürg Bahler

20th September 2018

STATEMENT

This thesis is an account of research conducted at the Department of Genetics, Evolution and Environment at University College London, between March 2015 and September 2018. I, Lea Brochard, confirm that the work presented in this thesis is my own. Where information has been derived from other resources, I confirm that this has been indicated in the thesis.

ABSTRACT

Insulin resistance has been shown to be caused by saturated fatty acids (SFA), especially palmitate found in abundance in the Western diet. The enzyme phosphatidylinositol 3 kinase (PI3K) has been identified as a key modulator of SFA-induced insulin resistance. To further the current understanding of the molecular mechanisms at play, we performed a transcriptome analysis comparing the gene expression profiles of 3T3-L1 adipocytes treated with palmitate, in the presence or absence of an inhibitor selective for p110α, one of the catalytic subunits of class IA PI3K. It revealed that the expression of a number of genes induced by type I interferon (IFN) is stimulated in response to palmitate, an effect abrogated by p110α inhibition. Such finding was of particular interest as IFN is known, like palmitate, to trigger insulin resistance. We studied the molecular links between IFN- and palmitate-mediated insulin resistance in both murine and human pre- and mature adipocytes. This allowed the confirmation of the positive metabolic effect of inhibiting p110α. The effect of palmitate on components of the IFN pathway was further explored and led to the establishment of a pivotal role of IFN-stimulated genes (ISGs) in the development of SFA-induced metabolic dysfunctions in adipocytes.

IMPACT STATEMENT

The material presented in this thesis constitutes primary research on the topic of insulin resistance. This metabolic dysregulation is one of the principal causes of type 2 diabetes (T2D) and is associated with obesity. With an estimated 422 million of type 2 diabetic adults in 2014 and obesity reaching a toll of 650 million adults in 2016 worldwide, tackling this pandemic is now at the forefront of the public health agenda (World Health Organisation 2016). To this end, it is critical to further investigate the molecular mechanisms at the core of insulin resistance in hope of improving the treatment and prevention of the aforementioned metabolic diseases.

Dietary saturated fatty acids (SFAs) have been implicated in the development of insulin resistance. We investigated the molecular signalling underlying the onset this state following SFA overload in mouse and human adipocytes. More specifically, we focused our attention on the cellular consequences of palmitate overload, a SFA found in abundance in the Western diet. For the first time, its effect on the phosphorylation of the downstream effectors of the IFN pathway (signal transducer and activator of transcription 3 [STAT3] and STAT1) was explored in adipocytes. We were able to demonstrate that palmitate induced the activation of STAT3 in mouse fat cells, thus establishing a role for the IFN signalling pathway amongst the molecular mediators of obesity as a sustained state of inflammation. Furthermore, our study stands as the first investigation exploring the palmitate-mediated modulation of the autophagic response of 3T3-L1 pre-adipocytes and

evidences the pro-autophagic role of SFA. In addition, we provide new insight on the role of a key IFN pathway component, namely *Isg15*, in the modulation of the metabolic effect of insulin and of autophagy in the context of SFA overload.

Collectively, these results outline a new axis of research that aims to better understand and cure metabolic disorders such as obesity and T2D exploiting components of cell signalling pathways as potential therapeutic targets. Further work will be needed to ascertain these findings and testing them into animal models and, eventually, translate them to clinical applications.

TABLE OF CONTENTS

LIST OF ABBREVIATIONS

AC	Adenylyl cyclase
AMPK	Adenosine monophosphate-activated serine/threonine protein kinase
ANOVA	Analysis of variance
ARs	Adrenergic receptors
ATG	Autophagy related gene protein
ATP	Adenosine triphosphate
AS160	Akt substrate of 160 kDa
ATGL	Adipose triglyceride lipase
BAT	Brown adipose tissue
BMI	Body mass index
BSA	Bovine serum albumin
BSA FAF	BSA fatty acid free
cAMP	Cyclic adenosine monophosphate
CBP	CREB binding protein
CCT	Chaperonin containing T-complex protein 1
CD	Cluster of differentiation
C/EBP	CCAAT-enhancer binding proteins
CERS	Ceramide synthase
CMV	Cytomegalovirus
cPPT	Central polypurine tract
CREB	Cyclic adenosine monophosphate response element-binding protein

CRTC	CREB regulated transcription coactivator
CRISPR	Clustered regularly interspaced short palindromic repeats
CST	Cell Signaling Technology
CT-1	Cardiotrophin-1
DAVID	Database for annotation, visualisation and integrated discovery
DAG	Diacylglycerol
DMEM	Dulbecco's modified eagle's medium
DMSO	Dimethyl sulfoxide
DTT	Dithiothreitol
DNA	Deoxyribonucleic acid
dsRNA	Double-stranded ribonucleic acid
EDTA	Ethylenediaminetetraacetic acid
EFP	Estrogen-responsive finger protein
EIF2	Eukaryotic translation initiation factor 2
ER	Endoplasmic reticulum
ERK	Extracellular signal-regulated kinases
FA	Fatty acid
FBS	Fetal bovine serum
FetA	Fetuin-A
FFA	Free fatty acid
FGF2	Fibroblast growth factor 2
FOXO	Forkhead box O
GAS	Gamma-activated sequences
GFP	Green fluorescent protein
GLUT	Glucose transporter type

GPCR	G protein-coupled receptors
GPD1	Glycerol-3-phosphate dehydrogenase 1
Gp130	Glycoprotein 130
GRB	Growth factor receptor-bound protein
GS	Glycogen synthase
GSK3β	GS kinase-3β
G3P	Glycerol-3-phosphate
HBS	Hepes buffered saline
HECT	Homologous to E6AP carboxyterminus
HEK	Human embryonic kidney cells
HERC	HECT and RCC1 containing protein
HFD	High-fat diet
HG	High glucose
HHARI	Human homolog of drosophila Ariadne
hMADS	Human multipotent adipose-derived stem cells
HSD	Honest significant difference
HSL	Hormone-sensitive lipase
HSP	Heat shock protein
IBMX	3-isobutyl-1-methylxanthine
IFIT	Interferon-induced protein with tetratricopeptide repeats
IFI	Interferon-induced protein
IFN	Interferon
IFNAR	Interferon-α/β receptor
IFNGR	Interferon-γ receptor
IFNLR	IFN-λ receptor

IgG	Immunoglobulin G
IIGP	Interferon-inducible GTPase
IL	Interleukin
IL6R	Interleukin 6 receptor
IP	Immunoprecipitation
IR	Insulin receptor
IRAK	Interleukin-1 receptor associated kinase
IRES	Internal ribosomal entry site
IRF	Interferon-regulatory factor
IRG	Immunity-related GTPase
IRS	Insulin receptor substrate
ISG	Interferon-stimulated genes
ISGF	Interferon-stimulated genes factor
ISRE	Interferon-stimulated responses element
JAK	Janus kinase
JNK	c-Jun N-terminal kinase
KD	Knockdown
LC3B	Microtubule-associated protein 1B-light chain 3
LDHA	Lactate dehydrogenase A
LFA-1	Leukocyte function-associated antigen-1
LG	Low glucose
LIF	Leukemia inhibitory factor
LPS	Lipopolysaccharide
LSD	Least significant difference
LTR	Long terminal repeat

MAG	Monoacylglycerol
MAPK	Mitogen-activated protein kinase
MDH1	Malate dehydrogenase 1
MDI	Methyl-isobutyl-xanthine, dexamethasone, insulin induction media
MD-2	Myeloid differentiation factor-2
MEFs	Mouse embryonic fibroblasts
MEK	MAPK/ERK kinase
MGL	Monoacylglycerol lipase
mRNA	Messenger ribonucleic acid
mTORC	Mammalian target of rapamycin complex
MyD88	Myeloid differentiation primary response 88
NADH	Nicotinamide adenine dinucleotide
NCBI	National Center for Biotechnology Information
NF-κB	Nuclear factor-κB
PACT	Protein activator of the interferon-induced protein kinase
p-Akt	Phosphorylated-Akt
PBS	Phosphate buffered saline
PDK	Phosphoinositide-dependent kinase
PE	Phosphatidylethanolamine
PI	Phosphatidylinositol
PI(3)P	Phosphatidylinositol 3-phosphate
PI(3,4)P_2	Phosphatidylinositol (3,4)-bisphosphate
PI(3,4,5)P_3	Phosphatidylinositol (3,4,5)-trisphosphate
PI3K	Phosphatidylinositol 3-kinase
PI(4)P	Phosphatidylinositol 4-phosphate

PI(4,5)P_2	Phosphatidylinositol (4,5)-bisphosphate
PKA	Protein kinase A
PKC	Protein kinase C
PKR	Protein kinase R
PLAA	Phospholipase A2
PPIA	Peptidylprolyl isomerase A
PPARγ	Peroxisome proliferator-activated receptor-γ
P/S	Penicillin/streptomycin
PSMC6	Proteasome 26S subunit protein
RCC	Regulator of chromosome condensation
RNA	Ribonucleic acid
RNAi	RNA interference
RRE	Rev response element
SFA	Saturated fatty acid
SDS-PAGE	Sodium dodecyl sulfate polyacrylamide gel electrophoresis
SF	Serum free
SGBS	Simpson-Golabi-Behmel syndrome
SH2	Src homology 2
shRNA	Short hairpin ribonucleic acid
SIK	Salt inducible kinase
SIN LTR	Self-inactivating long terminal repeat
siRNA	Short interfering ribonucleic acid
SOCS	Suppressor of cytokine signalling
SOS	Son of sevenless
SPT	Serine palmitoyl transferase

SREBP	Sterol regulatory element-binding protein
STAT	Signal transducer and activator transcription
STRING	Search tool for the retrieval of interacting genes/protein
S6K	Ribosomal protein S6 kinase
TAG	Triacylglycerol
TBS-T	Tris-buffered saline-Tween 20
TCP1	T-complex protein 1
TEMED	Tetramethylethylenediamine
TIRAP	Toll-interleukin-1 resistance domain-containing adapter protein
TLR	Toll-like receptor
TNFα	Tumour necrosis factor α
TRAM	TRIF-related adapter molecule
TRIF	TIR domain-containing adapter-inducing interferon-β
TSC	Tuberous sclerosis complex
TYK	Tyrosine kinase
TX	Triton-X
T2D	Type 2 diabetes
T3	Triiodothyronine
Ub	Ubiquitin
UBA1	Ubiquitin-like modifier activating enzyme 1
UBC	Ubiquitin C
UBCH8	Ubiquitin-conjugating enzyme H8
UBE1L	Ubiquitin-activating enzyme E1-like
UPR	Unfolded protein response
USP	Ubiquitin-specific peptidase

VPS34 Vacuolar protein-sorting defective 34

WAT White adipose tissue

WPRE Woodchuck hepatitis post-transcriptional regulatory element

WT Wild type

LIST OF TABLES AND FIGURES

CHAPTER 1. INTRODUCTION

I. 1. Insulin, a critical regulator of metabolism

I. 1. 1. The regulation of glucose homeostasis

Glucose homeostasis is essential to sustain bodily functions. Through the secretion of various hormones, the pancreas is able to maintain the extracellular concentration of this simple sugar within the narrow range of 4 to 6 mM (Roder 2016). Pancreatic endocrine cells form clusters known as islets of Langerhans, accounting for only 1 to 2% of the organ's mass. Five distinct cell types constitute these structures: α-, β-, γ-, δ- and ε-cells. As shown in *table 1*, α- and β-cells form the bulk of the islets and secrete glucagon and insulin, respectively. These two hormones work in tandem to promote opposite effects on circulating blood glucose.

Table 1. *The five endocrine cell types constituting the pancreatic islets of Langerhans.* Each hormone secreted has a specific function. For instance, while glucagon increases blood glucose levels, insulin promotes the opposite effect. Although the overall cellular composition of the islets is conserved across vertebrates, the details of their cytoarchitecture can vary considerably from species to species (Roder 2016).

Cell type	*Occurrence (%)*	*Hormone secreted*
α-cells	15-20	Glucagon
β-cells	65-80	Insulin Amylin C-peptide
δ-cells	3-10	Somatostatin
γ-cells	3-5	Pancreatic polypeptide
ε-cells	<1	Ghrelin

In a postprandial state, pancreatic β-cells are able to detect a rise in exogenous glucose levels, prompting the release of insulin into the bloodstream. This hormone down-regulates glucose concentration through three processes (Aronoff 2004): firstly, it promotes glucose uptake in its target cells such as adipocytes and muscle cells; secondly, insulin stimulates hepatic glycogenesis hence allowing for excessive glucose to be converted into glycogen (H. K. Han 2016); and lastly, this hormone stalls liver-mediated glucose production by inhibiting both glycogenolysis and gluconeogenesis (*Figure 1*). In addition to modulating blood glucose homeostasis, insulin promotes a range of anabolic reactions including lipogenesis and protein synthesis (Aronoff 2004). Conversely, as illustrated in *figure 1*, the fasting state is characterised by a combination of catabolic processes initiated by glucagon-secreting α-cells. While an overall switch from glucose to fat burning occurs, glucose-dependent tissues, such as the brain, are fuelled by endogenous glucose released via hepatic glycogenolysis and gluconeogenesis (Roder 2016).

Disturbances of the endocrine system described above are becoming increasingly prevalent, especially insulin resistance, which refers to the failure of a known quantity of insulin to stimulate glucose uptake in an individual compared to a healthy population (Lebovitz 2001). This common pathophysiological condition seeds a range of metabolic symptoms such as obesity, hyperlipidemia, hypertension and hyperglycemia, clustered under the umbrella term “Syndrome X” or “metabolic syndrome” (Moller 2005, Reaven 1988). The metabolic syndrome constitutes a key risk factor for T2D, a chronic disease affecting over 422 million adults worldwide in 2014 (World Health Organisation 2016). Such disorder is characterised by the inability of pancreatic β-cells to produce sufficient levels of insulin leading to the

release of abnormally large amounts of hepatic glucose into the bloodstream (Lebovitz 2001). The World Health Organisation defines the diagnostic criteria for T2D as a fasting plasma glucose concentration ≥ 7.0 mmol/L or a plasma glucose concentration ≥ 11.1 mmol/L two hours after the oral dose used in a glucose tolerance test (World Health Organisation 2006).

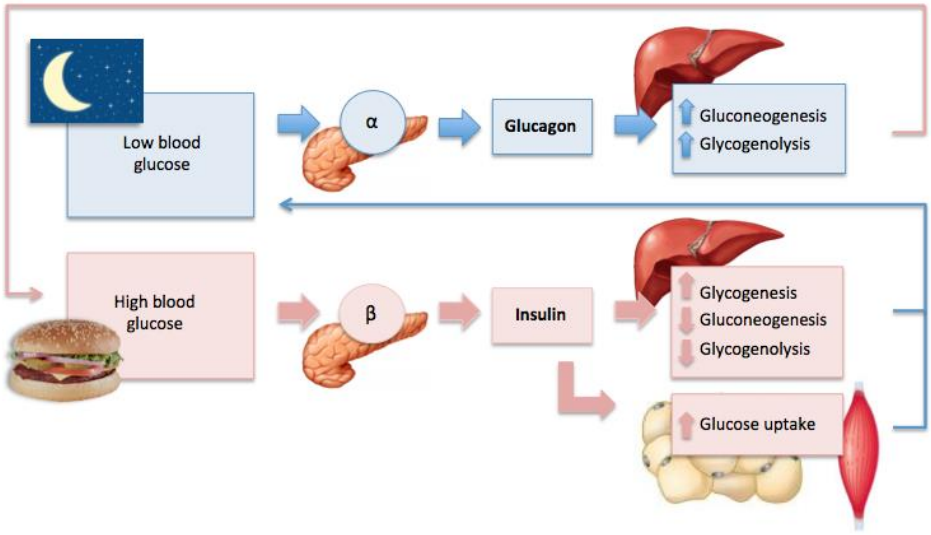

Figure 1. *The complementary role of insulin and glucagon in glucose homeostasis.* After a meal, the pancreatic β-cells secrete insulin into the bloodstream. This hormone promotes the storage of energy by stimulating glycogenesis in the liver. Meanwhile, insulin inhibits hepatic glucose production through the down-regulation of gluconeogenesis and glycogenolysis. In target tissues such as skeletal muscles and adipose tissue, glucose uptake is then enhanced. Together these reactions lower blood glucose concentration. When the latter reaches a certain threshold, the α-cells of the pancreas secrete the catabolic hormone glucagon, which induces hepatic gluconeogenesis and glycogenolysis to increase circulating glucose levels.

I. 1. 2. Overview of the insulin pathway

In order to improve the treatment and prevention of T2D, it is critical to thoroughly understand the molecular signalling mediating insulin action. *Figure 2* presents an overview of the cascades activated by this hormone. These are initiated by the binding of insulin to the extracellular α-subunit of its receptor that dimerises to form the $\alpha_2\beta_2$ complex. This event allows for the autophosphorylation of the

insulin receptor (IR) β-subunits (Guo 2014). Upon activation, the receptor recruits and phosphorylates various substrates including IR substrate-1 to 4 (IRS1-4) and the adaptor Src homology 2 (SH2) domain-containing transforming protein (SHC), which serve as docking sites for other downstream signalling proteins. In turn, these proteins promote the activation of two main branching pathways: the Ras/mitogen-activated protein kinase (MAPK) and the PI3K/Akt cascades, involved in the regulation of cell growth, metabolism and survival (Guo 2014). As shown in *figure 2*, the former is induced by the interaction of SHC with the docking protein growth factor receptor-bound protein 2 and the guanine nucleotide exchange factor son of sevenless. The resulting complex drives the activation of the downstream Ras-Raf-MAPK-extracellular signal-regulated kinase (ERK) pathway through a series of phosphorylation events (Van den Berghe 2004).

On the other hand, the PI3K cascade stems from the binding of tyrosine phosphorylated IRS to the SH2 domain of PI3K. By phosphorylating phosphatidylinositol (4,5)-bisphosphate to generate phosphatidylinositol (3,4,5)-triphosphate, this enzyme, which will be the focus of the next section, enables the activation of 3-phosphoinositide dependent protein kinases -1 and -2 (PDK1 and PDK2). Together, these kinases are responsible for the stimulation of the protein kinase Akt at residues Thr^{308} and Ser^{473}, respectively (Guo 2014). The functional role of the putative PDK2 is exerted by the mammalian target of rapamycin complex 2 (mTORC2), one of two multi-protein complexes implicated in the regulation of the mTOR pathway.

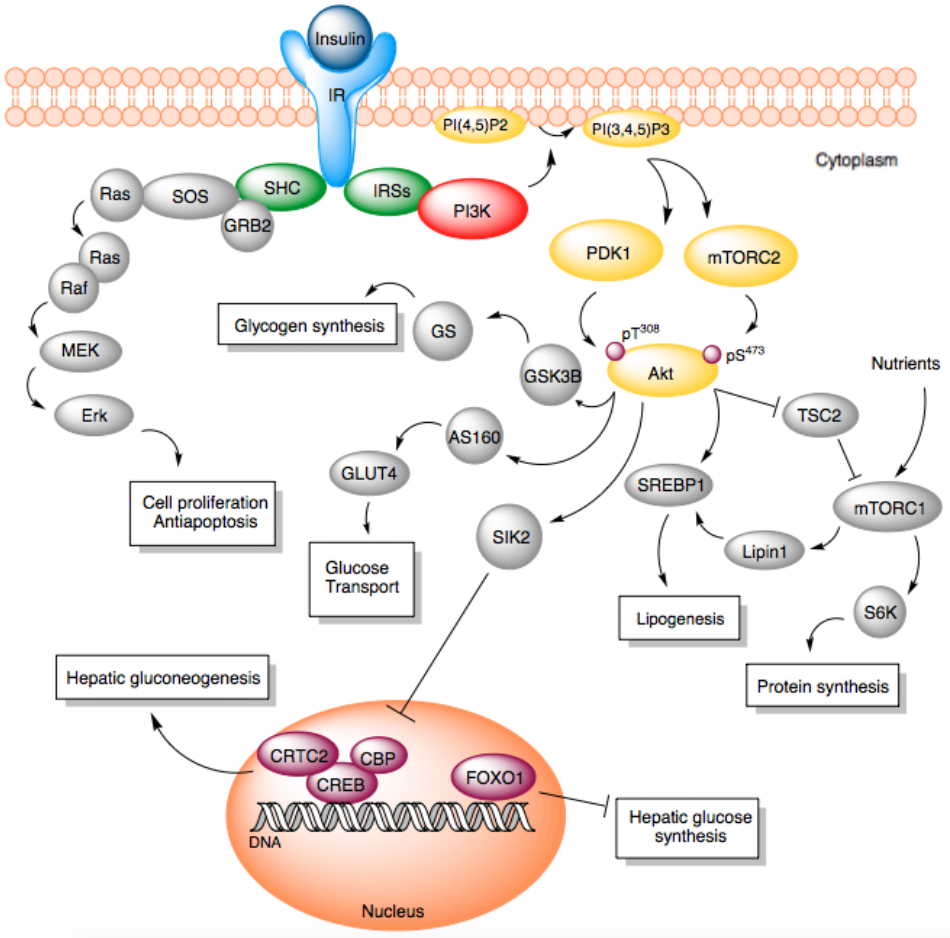

Figure 2. *Overview of the insulin signalling and its relevance to cell metabolism.* The binding of insulin to its receptor triggers an array of downstream reactions initiated by the phosphorylation of insulin receptor substrates (IRS) and the adaptor Src homology 2 (SH2) domain-containing transforming protein (SHC). Phosphatidylinositol 3-kinase (PI3K) is then stimulated inducing, in turn, the phosphorylation of Akt at Thr^{308} and Ser^{473} through the activation of protein kinase 1 (PDK1) and mammalian target of rapamycin complex 2 (mTORC2), respectively. This results in the modulation of a range of cellular functions including glucose transport, lipogenesis, protein synthesis, hepatic glucose synthesis and hepatic gluconeogenesis, as well as cell proliferation and apoptosis. *AS160*: Akt substrate of 160 kDa; *CBP*: CREB binding protein; *CREB*: cyclic adenosine monophosphate response element-binding protein; *CRTC2*: CREB regulated transcription coactivator 2; *DNA*: deoxyribonucleic acid; *ERK*: extracellular signal-regulated kinases; *FOXO1*: forkhead box O1; *GLUT4*: glucose transporter type 4; *GRB2*: growth factor receptor-bound protein 2; *GS*: glycogen synthase; *GSK3β*: glycogen synthase kinase-3β; *IR*: insulin receptor; *MEK*: mitogen-activated protein kinase (MAPK)/Erk kinase; *PI(3,4,5)P*$_3$: phosphatidylinositol (3,4,5)-triphosphate; *PI(4,5)P*$_2$: phosphatidylinositol (4,5)-bisphosphate; *SIK2*: salt inducible kinase 2; *SOS*: son of sevenless; *SREBP1*: sterol regulatory element-binding protein 1; *S6K*: ribosomal protein S6 kinase; *TSC2*: tuberous sclerosis complex 2.

As illustrated in *figure 2*, the downstream effects of Akt activation are numerous and diverse. For instance, mTORC2-mediated serine phosphorylation of Akt induces hepatic lipid and cholesterol synthesis by activating sterol regulatory

element-binding protein 1 (SREBP1). Akt stimulation also results in the inhibition of tuberous sclerosis complex 2 (TSC2), thereby up-regulating mTORC1, the other mTOR complex. The latter is implicated in an array of cellular functions including the modulation of protein synthesis (Sengupta 2010). Moreover, mTORC1 was found to induce lipogenesis through promoting the nuclear translocation of Lipin1 and, in turn, activating SREBP1. The intricacy of the signalling network presently described demonstrates the interdependence of the PI3K and the mTOR pathways (Sarbassov 2006).

In addition to TSC2 and SREBP1, Akt targets many other mediators of metabolic homeostasis. For instance, it hinders the activity of glycogen synthase kinase-3β (GSK3β), thus switching on glycogen synthesis via glycogen synthase. It also promotes glucose transport through the regulation of Akt substrate of 160 kDa, which controls the translocation of glucose transporter type 4 (GLUT4) (Guo 2014). Furthermore, Akt is responsible for mediating the expression of many genes by modulating the activity of transcription factors such as forkhead box O1 (FOXO1) and cyclic adenosine monophosphate (cAMP) response element-binding protein (CREB) (*Figure 2*) (Altarejos 2011). The molecular mechanisms regulated by the latter are explored in further detail in Chapter 4.

I. 2. The pivotal role of PI3Ks in the insulin signalling pathway

I. 2. 1. PI3K classification

Due to their critical role in the insulin signalling pathway, PI3Ks have been identified as potential therapeutic targets in the treatment of metabolic disorders

(Engelman 2006). These evolutionary conserved enzymes are divided into three classes (I-III) on the basis of sequence homology and substrate preference (*Table 2*). Various isoforms of the catalytic and regulatory subunits can exist depending on the organism considered (*Figure 3*). Members of this family of enzymes are specialised in the phosphorylation of the 3'-hydroxyl group of the inositol ring of phosphatidylinositol and phosphoinositides. This reaction is at the intersection of several intracellular signalling pathways implicated in vesicle trafficking, cell metabolism, survival and polarity (Engelman 2006).

Table 2. *Substrate preference of PI3K family members* in vitro. While, class I PI3K can phosphorylate phosphatidylinositol (PI), phosphatidylinositol 4-phosphate [PI(4)P] and PI(4,5)P_2 to generate phosphatidylinositol 3-phosphate [PI(3)P], phosphatidylinositol (3,4)-bisphosphate [PI(3,4)P_2] and PI(3,4,5)P_3, respectively, class II enzymes preferentially react with PI and PI(4)P and class III with PI (Engelman 2006).

Substrate	*Class of PI3K*	*Product*
PI	I, II and III	PI(3)P
PI(4)P	I and II	PI(3,4)P_2
PI (4,5)P_2	I	PI (3,4,5)P_3

With each class of PI3Ks involved in specific cellular functions, class I PI3Ks have been shown to mediate growth and metabolism by acting downstream of an insulin-like receptor (*Figure 2*). Such function was conserved throughout eukaryotic evolution with corresponding orthologues of class I PI3K pathway components found in *Caenorhabditis elegans*, in *Drosophila melanogaster* and in mammals (LoPiccolo 2008, Vanhaesebroeck 2010, Engelman 2006). As detailed in the previous section, class I PI3Ks permits the phosphorylation of Akt through activating PDK1 and mTORC2. It also ensures the phosphorylation of other kinases, such as protein kinase C (PKC), key in modulating cell growth and metabolism in

response to multiple cues including nutrients, energy status and growth factors (Sarbassov 2006).

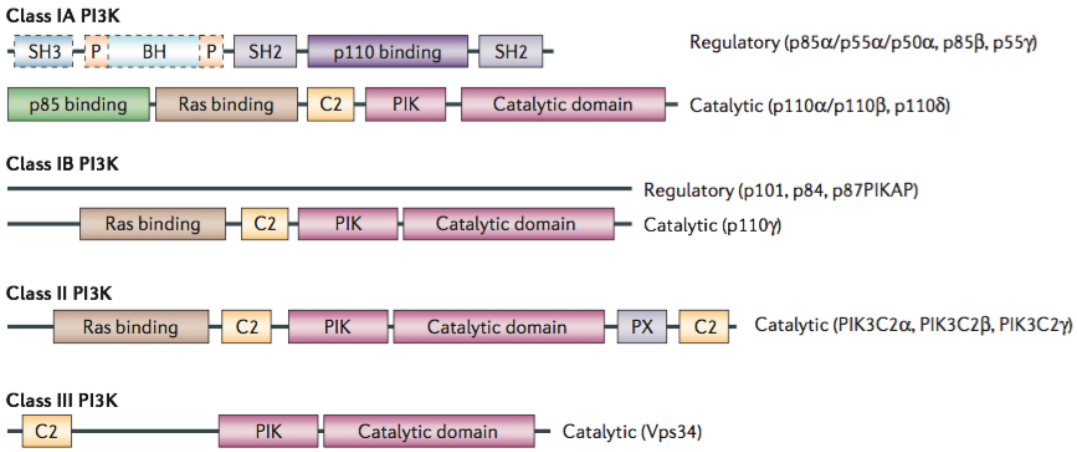

Figure 3. *Domain structures of PI3K family members*. Class I PI3Ks are composed of a regulatory and a catalytic subunit. Class IA consists of a p85 regulatory subunit counting three isoforms (p85α, p85β and p55γ) and a p110 catalytic subunit also comprising three isoforms (p110α, p110β and p110δ). Class IB is formed of a regulatory subunit (p101, p84 and p87PIKAP) and a single isoform of the p110 catalytic subunit, p110γ. Class II, on the other hand, counts only a single p110-like subunit existing as three isoforms (PIK3C2α, PIK3C2β and PIK3C2γ). Lastly, Class III is represented by a single member, vacuolar protein-sorting defective 34 (VPS34) (Engelman 2006). Permission to reproduce this figure has been granted by Springer Nature.

I. 2. 2. The consequences of blunted PI3K signalling

A large body of studies has investigated the metabolic consequences of blunted PI3K signalling and established a direct link of causality with the development of insulin resistance (Guo 2014). The down-regulation of PI3K activity can be attributed to the over-consumption of SFAs and in particular palmitate (Hla 2014). Found in abundance in Western diets, this SFA serves as primary substrate for synthesis of ceramides, lipid molecules composed of a sphingosine base linked to a fatty acid (FA) (Hla 2014). Although alternative theories exist to explain palmitate-induced insulin resistance, recent studies propose that the deleterious effect associated with this SFA results from its promoting the synthesis of a specific

species of ceramide ($C_{16:0}$) found to be involved in the attenuation of PI3K signalling (Hla 2014).

Indeed, Turpin and colleagues report an elevation of $C_{16:0}$-ceramide levels in mice fed a high-fat diet (HFD), along with an increased expression of ceramide synthase 6 (CERS6), the enzyme involved in $C_{16:0}$-ceramide production (Turpin 2014). Deleting this enzyme, not only reduced $C_{16:0}$-ceramide levels, but also protected the mice from diet-induced obesity and glucose intolerance. In line with these findings, the insulin-stimulated phosphorylation of downstream effectors of PI3K, Akt and GSK3β, were reportedly enhanced in the liver of knockout *CerS6* mice compared to wild type (WT) (Turpin 2014). In addition, evidence indicates that $C_{16:0}$-ceramide antagonises mitochondrial electron transport inducing the suppression of β-oxidation and obesogenic symptoms such as hindered FAs disposal (*Figure 4*) (Turpin 2014). This is consistent with the findings of Hommelberg and colleagues showing that palmitate induces the accumulation of diacylglcerol (DAG) in insulin-resistant skeletal muscle cells (Hommelberg 2011). This lipid metabolite plays a critical role in insulin signalling as the increase in its intracellular concentration drives the activation of PKC in both hepatocytes and skeletal muscle cells. PKC then hinders IRS1 and IRS2 tyrosine phosphorylation required for PI3K induction thereby promoting insulin resistance (Erion 2010).

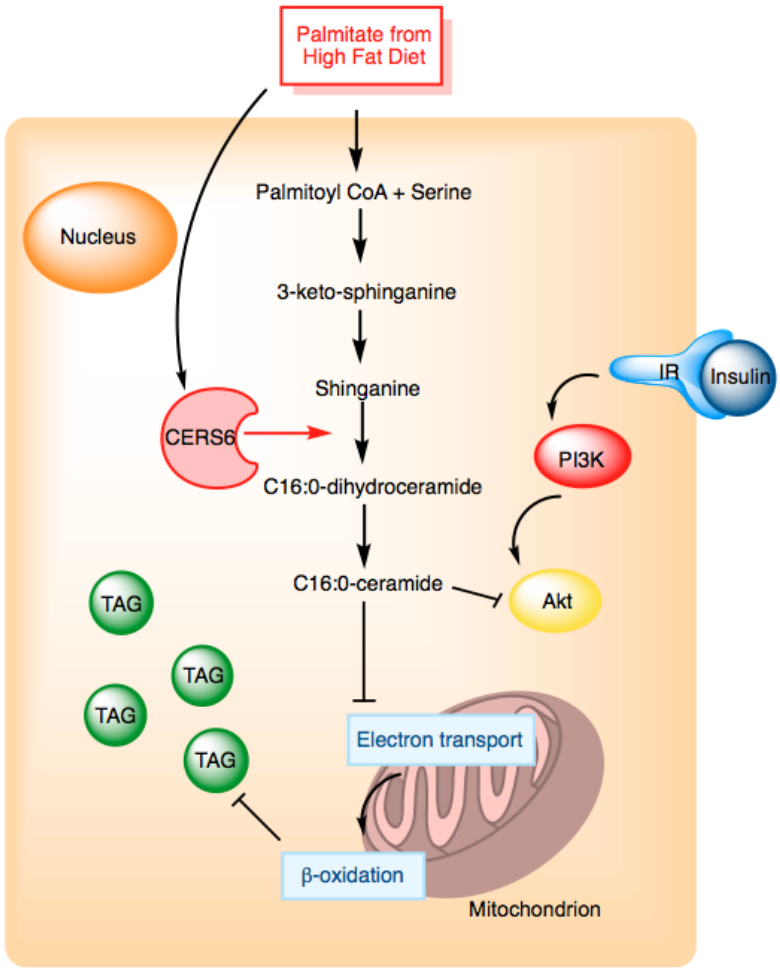

Figure 4. *The stimulation of $C_{16:0}$-ceramide synthesis induced by a high-fat diet (HFD) in the context of insulin resistance.* Palmitate from HFD promotes the synthesis of $C_{16:0}$-ceramide in two ways: firstly, it serves as primary substrate in the pathway and secondly, it directly stimulates the activity of ceramide synthase 6 (CERS6), which catalyses the conversion of sphinganine to $C_{16:0}$ dihydroceramide. The production of $C_{16:0}$-ceramide inhibits Akt as well as the electron transport chain in the mitochondria, driving a rise in the accumulation of triacylglycerols (TAGs) in the cell.

Investigating the consequences of blunted PI3K signalling, the work of Foukas and colleagues has highlighted the pivotal role of p110α – one of three isoforms of the catalytic subunit of class IA PI3K (p110) (L. C. Foukas 2006). Having generated a strain of mice carrying a loss-of-function mutation of p110α (D933A), they observed that while homozygosity caused embryonic lethality, the heterozygous genotype was associated with a substantial attenuation of the signalling mediated by insulin-receptor substrate proteins (L. C. Foukas 2006). As expected,

this translated phenotypically by pre-diabetic symptoms such as hyperinsulinemia, glucose intolerance, hyperphagia and increased adiposity in young mice. Unexpectedly, their results focusing on the long-term effects of reduced p110α signalling revealed an age-dependent beneficial impact on metabolism overriding the negative short-term effects in early life (L. B. Foukas 2013). Consistent with this, a recent study demonstrated that treatment of obese mice and rhesus monkeys with pharmacological inhibitors of PI3K resulted in a considerable reduction of adiposity and liver steatosis (Ortega-Molina 2015). The positive effect of long- term p110α inhibition points to potential isoform specific interventions in T2D treatments.

I. 3. The importance of adipose tissue in insulin resistance

I. 3. 1. Adipose tissue, an endocrine organ involved in the regulation of energy homeostasis

Across eukaryotes, lipid droplets can be found as a form of energy storage. Vertebrates, however, are the only subgroup having evolved specialised lipid storing cells named adipocytes (Rosen 2014). These cells are found in abundance in adipose tissue, which is also composed of additional cell types described as the stromal vascular fraction, including stem cells, pre-adipocytes, endothelial cells and immune cells such as neutrophils and macrophages (Rafols 2014). Pre-adipocytes In mammals, two distinct types of adipose tissues exist: brown adipose tissue (BAT) and white adipose tissue (WAT). Adipocytes observed in the latter are characterised by a unique large lipid droplet accounting for over 95% of the cellular mass and significantly fewer mitochondria compared to BAT. Therefore, it was traditionally understood that while BAT was mainly involved in thermogenesis, WAT was an

inert organ specialised in fat storage. However, evidence is accumulating in favour of a more complex role of WAT (Coelho 2013). Indeed, as reviewed by Zwick *et al*., WAT exerts a range of organ- and tissue-specific functions. For instance, it buffers mechanical shock when adjacent to a skeletal structure. WAT depots at the surface of the skin and intestine also appear to be a critical player in systemic immune response by sensing and responding to bacterial infection (Zwick 2018).

Aside from these organ-specific functions, WAT has surfaced as a metabolically dynamic organ, pivotal in glucose and lipid metabolism (Rosen 2014). It is in fact the largest endocrine tissue in the human body with cells able to secrete various hormones, growth factors, enzymes and cytokines, known as adipokines (Coelho 2013). Discovered in 1994, leptin - encoded by the notorious *ob* gene - was the first adipocyte-derived factor identified (Y. P. Zhang 1994). This anorexigenic adipokine is sensed by the central nervous system, as well as some peripheral tissues where it promotes energy expenditure. Regulation of leptin secretion is mediated by a mosaic of factors, some stimulating it, such as glucose, amino acids, insulin and overfeeding; others inhibiting it, for instance, free fatty acids (FFA), thyroid hormones and fasting (Moon 2013). Interestingly, intrinsic differences in leptin expression levels exist between adipose tissue depots. For example, the adipokine is synthesised in larger quantities in subcutaneous compared to visceral fat (Coelho 2013).

Since the discovery of leptin, a large number of additional adipocyte-secreted factors have been identified, such as adiponectin. Evidence support that this 30 kDa peptide exists as three individual complexes: a high-molecular weight complex, a

low-molecular weight complex and a trimeric one. Schraw and colleagues demonstrated plasma concentration of the former to be inversely correlated with fat mass in human subjects (Schraw 2008). In the liver, adiponectin promotes insulin sensitivity as well as FA oxidation, while hindering hepatic glucose production along with the influx of FFA. Meanwhile, in skeletal muscles, the adipokine induces glucose uptake and FA oxidation. Similarly to leptin, the effect of adiponectin is also mediated through the hypothalamus, which enables it to stimulate appetite and down-regulate energy expenditure (Coelho 2013).

More recently discovered is resistin, a short peptide of 108 amino acids (Steppan 2001). As with leptin, the expression of this adipokine is depot-specific. However, in the case of resistin, expression levels are significantly greater in visceral compared to subcutaneous adipose tissue (Kershaw. E. and Flier 2004). *In vivo* experiments indicate that resistin impairs glucose tolerance, a metabolic effect thought to reflect the ability of the peptide to antagonise insulin action and hinder its downstream signalling (Steppan 2001).

Aside from adipokines, adipose tissue also secretes various pro-inflammatory cytokines such as tumour necrosis factor α (TNFα) (Kershaw. E. and Flier 2004). In its circulating form, TNFα is a 17 kDa peptide produced by adipocytes as well as macrophages present in the stromal vascular fraction. As evidenced by Ruan and colleagues, this cytokine is able to modulate gene expression in various target tissues, including adipose tissue and the liver (H. M. Ruan 2002). Indeed, having infused rats with TNFα, they recorded significant alterations in adipocyte gene expression profile, promoting FFA, glucose and cytokine release (e.g. adiponectin

and interleukin-6 [IL-6], another pro-inflammatory cytokine secreted by adipose tissue), while also suppressing transcription factors implicated in adipogenesis and lipolysis. In addition, such intervention stimulated FFA and cholesterol synthesis through changes in liver gene expression (H. M. Ruan 2002). Furthermore, TNFα has been demonstrated to directly interfere with insulin signalling through the indirect inhibition of IRS1 and IRS2. This effect was found strengthened by TNFα-mediated increase in FFA serum concentration, which, as discussed in the previous section, also impairs insulin signalling (Kershaw. E. and Flier 2004).

The ability of adipose tissue to secrete factors such as leptin, adiponectin, resistin, TNFα and IL-6 positions this organ as a key modulator of energy homeostasis and metabolism. Importantly, this organ not only secretes a biochemical message but is also able to sense and integrate those emitted by other endocrine organs. This crosstalk is mediated through the variety of receptors expressed in the adipose tissue, which also enables responses to external cues. Such receptors are specific for endocrine hormones such as insulin, glucagon and growth hormone, but also bind some of the aforementioned cytokines, including leptin, IL-6 and TNFα (Kershaw. E. and Flier 2004). In addition, adipocytes were found to express β- and α-adrenergic receptors (β-ARs and α-AR), thus permitting catecholamine-induced lipolysis to occur within their lipid droplet. This three-step metabolic process, which ensures the breakdown of triacylglycerol (TAG) into glycerol and FA, will be the further explored in Chapter 4. Thus the capacity of adipose tissue to integrate and respond accordingly to the metabolic status of the whole body makes it a critical player in the pathogenesis of T2D and insulin resistance.

I. 3. 2. Adipose tissue in obesity

An outstanding characteristic of adipose tissue is its ability to expand unlike any other non-neoplastic tissues. This can occur through two distinct processes: hypertrophy, by which individual cells becomes larger, or hyperplasia, which describes the recruitment of new adipocytes (Rosen 2014). In humans, over-nutrition induces hypertrophy up to the critical threshold of 0.7-0.8 µg per cell across depots. Past this weight, Krotkiewski and colleagues were able to establish that the number of fat cells rapidly rises, marking the onset of hyperplasia (Krotkiewski 1983). Location of fat depots may also influence the type of process at play, with evidence indicating hypertrophy to be involved in the expansion of upper body subcutaneous fat, while hyperplasia appears to mediate the plasticity of depots found in the lower body (Tchoukalova 2010).

Obesity is a direct consequence of overfeeding and is defined by the World Health Organisation as an "abnormal and excessive fat accumulation that may impair health" (World Health Organisation n.d.). Body mass index (BMI), which integrates measures of an individual's weight and height, is the most commonly used tool to diagnose obesity. Such index is associated with mortality following a U-shaped distribution. The minimal mortality corresponds to the healthy BMI range of 18.5 to 25 kg/m^3. Values below the lower end of this interval are defined as underweight, while those beyond the top end are classified as overweight. Above a BMI of 30 kg/m^3, an individual is recognised as obese (M. a. Muller 2017). It is important to note the limitation of this index in the diagnosis of obesity as it fails to provide insight on fat mass and distribution and poorly predicts the health of the patient.

At the cellular level, the expansion of adipose tissue in the context of obesity has a considerable impact on the endocrine function of the organ and is associated with the onset of insulin resistance. This is clearly illustrated by the metabolic effects of genetic leptin deficiency: the *ob*/*ob* mouse, unable to successfully synthesise leptin, develops early-onset obesity, while also exhibiting hyperphagia, insulin resistance and diabetes (Moon 2013). After two weeks of daily intraperitoneal injections of recombinant leptin, Halaas *et al*. recorded a 30% reduction in the body weight of the mutant mice while the WT strain was not affected by the intervention (Halaas 1995). In contrast, diet-induced obesity is characterised by increased circulating leptin levels, which are found to diminish with caloric restriction and weight loss (Kershaw. E. and Flier 2004).

Aside from leptin, the secretion of many additional adipokines is affected by obesity. Adiponectin plasma concentration, for instance, decreases in obesity and is restored after weight loss. An inverse correlation also exists between the total concentration of this adipokine and both circulating glucose and TAG levels, insulin resistance as well as visceral fat accumulation (Nigro 2014). Administration of recombinant adiponectin was reported to rescue these phenotypes (Kershaw. E. and Flier 2004). Further validating the importance of adiponectin in the modulation of insulin signalling, Combs *et al.* reported that a transgenic over-expression of the peptide in rodents resulted in enhanced insulin sensitivity and glucose tolerance (Combs 2004). Similarly, circulating resistin levels were found elevated in murine models of diet-induced obesity as well as in genetic models of the condition (Steppan 2001). After treatment with recombinant resistin, WT mice exhibited both impaired glucose tolerance and insulin resistance. Also vouching for the critical role

of adipose tissue in the modulation of systemic insulin sensitivity and energy expenditure, a study by Blüher and colleagues reveals that the adipose tissue-specific deletion of the IR gene in mice induces the development of obesity and its related metabolic dysregulation (Bluher 2002).

Excessive adiposity also alters the secretion of the cytokines previously mentioned, TNFα and IL-6. Indeed, plasma concentration of both peptides is increased in obesity (Coelho 2013). In the case of TNFα, this up-regulation not only impairs insulin sensitivity of local adipocytes but also dampens hepatic and muscle insulin sensitivity (Hotamisligil 1993). Corroborating such findings, genetic knockout of TNFα or its receptor ameliorates insulin resistance in murine models of obesity (H. a. Ruan 2003). IL-6, on the other hand, was shown to hinder insulin signalling by down-regulating the expression of elements of its molecular cascade, while simultaneously stimulating the expression of suppressor of cytokine signalling 3 (SOCS3), an inhibitor of IR and IRS1 tyrosine phosphorylation (J. K. Senn 2003).

This obesity-associated rise in pro-inflammatory cytokines is thought to be the result of the larger population of M1 macrophages. Unlike the M2 macrophages implicated in tissue healing and remodelling, M1 macrophages promote inflammation through the secretion of pro-inflammatory cytokines including TNFα and IL-6. While M2 macrophages are predominant in lean mice, with obesity the M1/M2 ratio shifts in favour of a larger M1 population (Rosen 2014). Histological evidence in both obese mice and humans revealed that these cells infiltrated adipose tissue to create “crown-like structures” around adipocytes. As macrophage infiltration was found particularly pronounced in visceral depots compared to

subcutaneous depots, the location of WAT depots is determinant in the profile of adipokines produced. This seeds the notion that visceral adiposity may be more metabolically detrimental than subcutaneous adiposity (Cinti 2005). In addition to macrophages, a mosaic of immune cells was also found to be more abundant in obese adipose tissue, including neutrophils, B and T lymphocytes, and each cell type was involved in the promotion of insulin resistance (Rosen 2014). Together, these findings support obesity as a state of low-grade inflammation.

I. 4. Lipid metabolism in adipocytes

I. 4. 1. The role of lipolysis in lipid mobilisation

Obesity not only impacts the hormonal and cytokine profiles of adipose tissue, it also alters the metabolism of lipid molecules within adipocytes through the promotion of low-grade systemic inflammation. More specifically two processes are affected, namely lipolysis and autophagy. The former describes the process by which TAG stores are hydrolysed to release FAs and glycerol into the circulation for endogenous use, thus allowing cells to cope with starvation. This process takes place in all tissues and cells containing lipid droplets in which TAGs accumulate. Vertebrates have developed tissues specialised in the deposition and mobilisation of TAGs, known as WAT (M. E. Schweiger 2014). By regulating the rates of lipolysis and lipogenesis (metabolic formation of fat), WAT maintains a tight control over energy homeostasis. The lipolytic process can be broken down into three coordinated steps catalysed by individual lipases: adipose triglyceride lipase (ATGL), which converts TAG to DAG, hormone-sensitive lipase (HSL), which guaranties the hydrolysis of DAG to monoacylglycerol (MAG), and lastly monoglyceride lipase,

which generates glycerol from MAG (*Figure 5*) (J. a. Jocken 2008). Each step of this chain reaction releases FAs, which can either enter the bloodstream or migrate to the mitochondria to undergo β-oxidation. Alternatively, FAs can be re-esterified to TAG using glucose imported in the adipocyte via GLUTs (Altarejos 2011).

Because lipolysis is as critical determinant of cellular energy levels, a range of factors is implicated in its regulation. As illustrated by *figure 5*, WAT lipolysis is principally mediated through the release of insulin and catecholamines (neurotransmitters including dopamine, epinephrine and norepinephrine) (Kobayashi 2001). These bind to β-ARs, which induce adenylyl cyclase (AC) activity (Altarejos 2011). Once activated, the latter catalyses synthesis of cAMP. Increased cellular concentration of this secondary messenger allows it to bind to the regulatory subunits of protein kinase A (PKA), resulting in the dissociation of the catalytic subunits of the kinase. The activated catalytic subunit of PKA then phosphorylates HSL at Ser^{659} and Ser^{660}, permitting its translocation to the lipid droplet where it catalyses the second step of lipolysis. In parallel to activating HSL, PKA also stimulates lipolytic rates through the phosphorylation of ATGL and perilipin, a protein found at the surface of the lipid droplet. This reaction induces a conformational change of the protein, which exposes the core of the droplet to p-HSL hence promoting lipolysis (J. a. Jocken 2008).

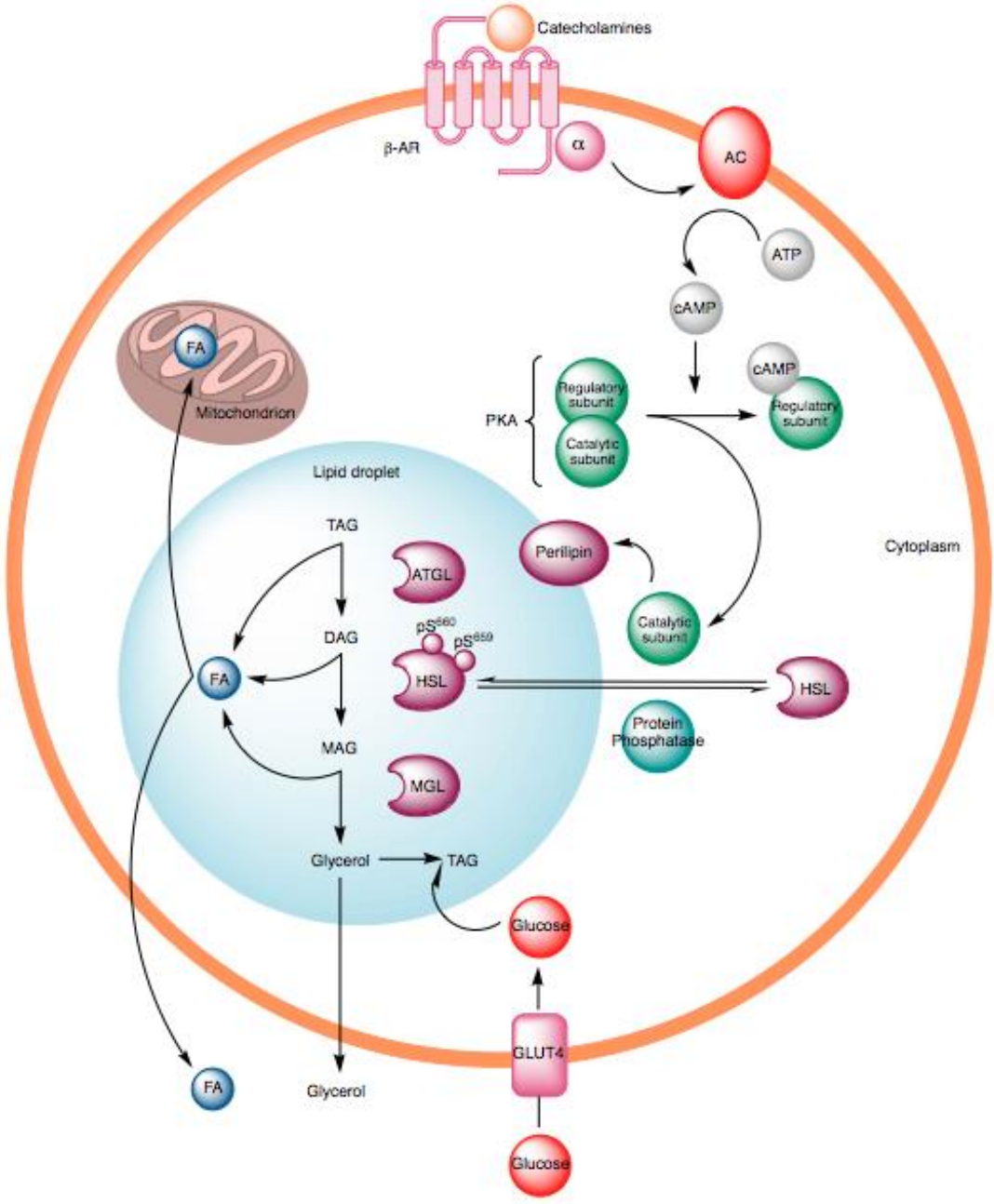

Figure 5. *Catecholamine-mediated activation of lipolysis.* Upon binding of the neurotransmitter to its receptors, β-adrenergic receptors (β-ARs), adenylyl cyclase (AC) is stimulated allowing for the cellular concentration of cyclic adenosine monophosphate (cAMP) to rise, hence the up-regulation of protein kinase A (PKA) activity. The kinase phosphorylates both hormone-sensitive lipase (HSL) and perilipin, two enzymes promoting lipolysis. This three-step metabolic process occurring in the lipid droplet converts TAG into glycerol and fatty acids (FA) to provide energy to the cell. *ATGL*: adipose triglyceride lipase; *DAG*: diacylglycerol; *MAG*: monoacylglycerol; *MGL*: monoacylglycerol lipase.

I. 4. 2. Autophagy, a process regulated by nutrient concentration and energy homeostasis

The second key metabolic even disrupted by obesity in adipocytes is autophagy. It is defined as the catabolic process by which the cell degrades, through lysosomal activity, defective or threatening constituents including damaged organelles, intracellular pathogens and unfolded proteins (Cahova 2015). Three different types of autophagy have so far been characterised namely macro-, micro- and chaperone-mediated autophagy. While in macro-autophagy cytosolic components are engulfed by the lysosome through the intermediate of a so-called autophagosome (a double membrane-bound vesicle), in micro-autophagy, the targets are directly absorbed by the lysosome. Both mechanisms are able to cope with large cytosolic cargo and can be either selective or non-selective. Chaperone-mediated autophagy, on the other hand, has the particularity of relying on the formation of protein complex between the target and chaperone proteins recognised by the lysosomal membrane receptor lysosomal-associated membrane protein 2A (Glick 2010). The following section is centred on macro-autophagy later simply referred to as autophagy.

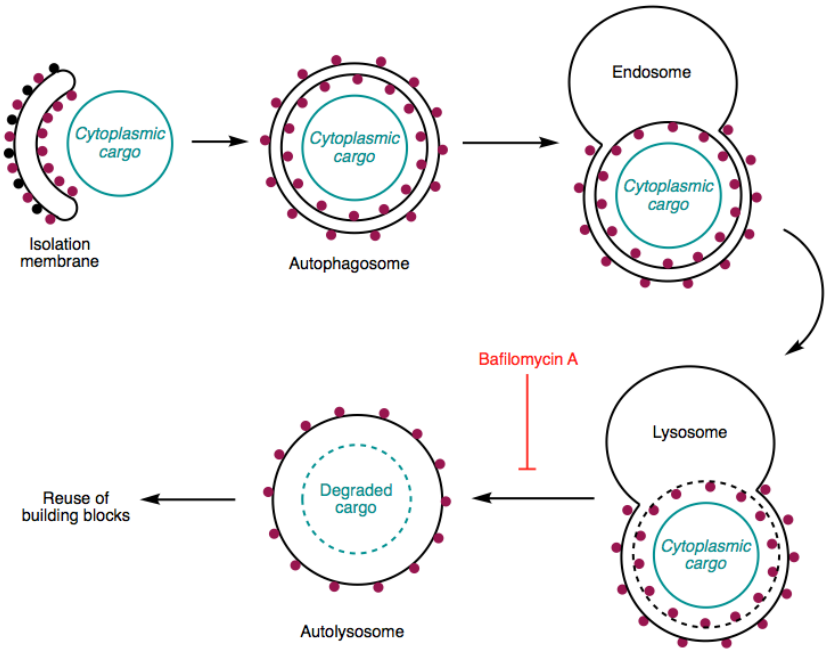

Figure 6. *A step-by-step overview of autophagy.* The self-degradative process of autophagy is initiated by the formation of the isolation membrane, which eventually engulfes the targeted cytosolic cargo. At this point, the phagophore interacts with elements of two ubiquitin-like systems: on the one hand, autophagy related protein (ATG) 5-ATG12 conjugated complexes (illustrated by black dots), and on the other hand microtubule-associated protein 1B-light chain 3 (LC3B-II) (represented by red dots). The former is involved in the assymetric recruitment of the later to the membrane, thus inducing the curvature around the cargo and the formation of the autophagosome. The outer membrane of this organelle fuses with the endosome and in turn the lysosome. The resulting autolysosome ensures the degradation of the cargo through the activity of lysosomal hydrolases. It is this step of the process that can be inhibited by bafilomycin A1. The building blocks of the digested cargo can then be exported to the cytosol for reuse.

Figure 6 provides an overview of the molecular mechanisms at play during autophagy. The process is initiated with the *de novo* formation of an isolation membrane, known as phagophore, mostly originated from the endoplasmic reticulum (ER) (Biazik 2015). The phagophore extends around the cytosolic cargo, thus producing an autophagosome. This double-membrane vesicule is able to fuse with the lysosome, unloading its content, which can then be degraded by the lysosomal proteases. By-products of autophagy are exported back to the cytoplasm where they can be recycled for protein synthesis and used as substrate for adenosine triphosphate (ATP) production (Glick 2010).

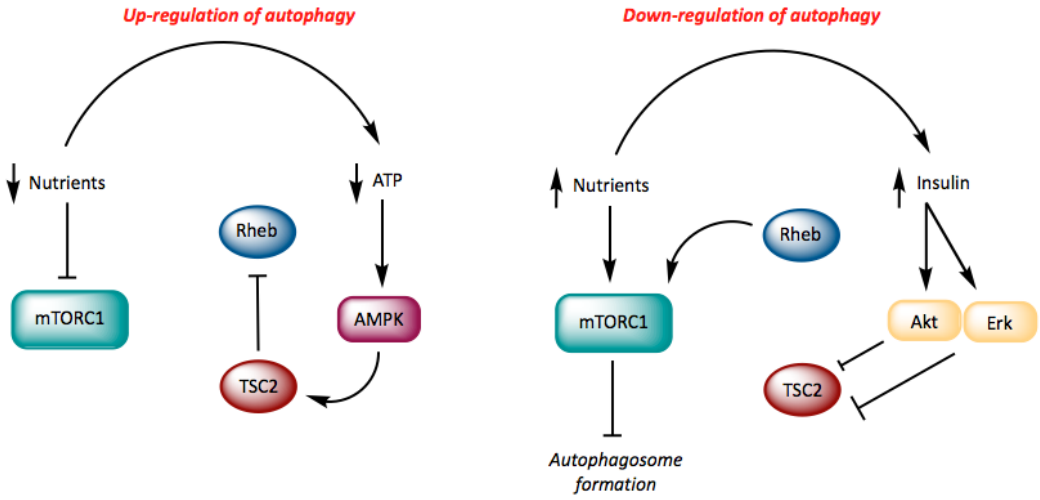

Figure 7. *Autophagy is regulated by the nutrient-sensing complex mTORC1.* If nutrients are scarce, mTORC1 is inhibited and no longer hinders autophagosome formation. Autophagy is therefore up-regulated. mTORC1 activity is also blocked through the stimulation of adenosine monophosphate-activated serine/threonine protein kinase (AMPK), resulting from the decrease in intracellular adenosine triphosphate (ATP) concentration. This kinase promotes TSC2-mediated inhibition of Rheb, which would otherwise induce mTORC1. Alternatively, if nutrients are readily available, mTORC1 hampers autophagosome formation and down-regulates autophagy. The inhibitory effect of TSC2 on Rheb is prevented through the activity of Akt and Erk, which both block TSC2 activity. These kinases are stimulated by the rise in insulin levels prompted by the increase in nutrients.

Although basal rates of autophagy are maintained in most cell types to guaranty the integrity of their organelles and proteins, the homeostatic process can be stimulated by variations in nutrients concentration (Glick 2010). Indeed, while nutrients are readily available, growth-promoting mTORC1 inhibits autophagosome formation. Inversely, amino acid deprivation and hypoxia repress the activity of this protein multicomplex, thus prompting a rise in autophagy levels (Cahova 2015). In addition, a dip in intracellular ATP ensuing from nutrients depletion stimulates adenosine monophosphate-activated serine/threonine protein kinase (AMPK). The kinase phosphorylates and activates TSC2, thus further down-regulating mTORC1. Indeed, as shown in *figure 7*, activated TSC2 promotes the inhibition of Rheb, a

small Ras-like GTPase found to directly induce mTOR kinase, the core component of mTORC1 (Shaw 2009).

Lastly, fluctuations in the activity of downstream effectors of the insulin pathway also influence mTORC1 and in turn autophagic rates. For instance, both Erk and Akt are able to stimulate mTORC1 by blocking TSC2 activity. Furthermore, Akt inhibits the activity of an mTORC1 inhibitor, the proline-rich Akt substrate of 40 kDa (Shaw 2009). Aside from stimulating mTORC1, Akt also regulates autophagy through FOXO1, as this transcription factor was found to mediate the transcription of four key pro-autophagic genes: *Vps34*, *Atg12*, *Atg14* and *Gabarpl1* (H. H. Liu 2009). Overall, inhibition of mTORC1 paired with the dephosphorylation of FOXO1 boost autophagic turnover thereby guarantying the availability of amino acids necessary for protein synthesis and substrate for metabolism.

I. 5. Transcriptome analysis investigating the impact of p110α inhibition on FA-induced insulin resistance

I. 5. 1. The findings of the transcriptome analysis

With the advent of bioinformatics, it is now possible to perform high-throughput transcriptome analyses to identify novel effectors in signalling pathways. The present work originates from such an analysis carried out in the Foukas lab using ribonucleic acid (RNA) extracted from mouse 3T3-L1 adipocytes. The study compared the transcriptome of samples treated with palmitate in the presence or absence of a p110α-selective inhibitor (A66) (S. F. Jamieson 2011). Sequencing analysis allowed the identification of an array of genes of which expression was

altered in response to the treatments. Notably, the expression of a number of genes known to be induced by IFN was up-regulated in response to palmitate. This effect was abrogated by adding A66 to the SFA treatment (*Table 3, the gene list can be found in its entirety in table 14*). IFNs are cytokines produced by cells in response to parasites, viruses, bacteria and tumour cells (S. S.-K. Kaur 2008). Their classification relies on the type of receptors mediating their signal: while type I IFNs (IFN-α, -β, -ο, -ε, -κ, -τ and -δ) interact with the IFN-α/β receptor (IFNAR), type II IFN (IFN-γ) requires IFN-γ receptor (IFNGR) and type III IFNs (IFN-λ1, IFN-λ2, IFN-λ3 and IFN-λ4) are specific to IFN-λ receptor complex, formed of the specific IFN-λ receptor chain 1 and the shared IL-10 receptor chain 2 (De Weerd 2007, Vilcek 2003, Wack 2015). Of the genes presented in *table 3*, all but *Iigp1*, induced by IFN-γ, are stimulated by type I IFN (Uthaiah 2003).

The downstream signalling of each type of IFN has been studied extensively since the early 1990s (L. Platanias 2005). Hundreds of genes mediating a range of biological responses were found induced by these cytokines, with some genes regulated by more than one type of IFNs and others modulated by a specific type of IFN. Of the many IFN-dependent pathways, the Janus kinase (JAK) -STAT cascade has been the most extensively studied. Evidence supports its involvement in various biological processes, such as immune responses, cellular differentiation and the regulation of energy homeostasis (Richard 2014). As illustrated by *figure 8*, type I IFN receptor IFNAR was found to engage the JAK1 and tyrosine kinase 2 (TYK2), while evidence supports that IFNGR associates with JAK1 and 2. These tyrosine kinases are responsible for the phosphorylation of the cytoplasmic STAT transcription factors, more particularly, STAT1, STAT2, and STAT3 in most cell

types and STAT4, STAT5A, STAT5B and STAT6 in certain types. Once activated, the STAT proteins dimerise and translocate to the nucleus to initiate transcription by interacting with the promoter regions of ISGs (Ivashki 2014).

Table 3. *List of genes modulated by IFN identified by the transcriptome analysis*. The name of the genes is followed by their symbol, their National Center for Biotechnology Information (NCBI) ID and their Ensembl ID in brackets. *Ifit*: interferon-induced protein with tetratricopeptide repeats; *Irf*: IFN-regulatory factor; *Ifi*: IFN-induced protein; *Iigp*: IFN-inducible GTPase.

	Down-regulated by palmitate	***Up-regulated by palmitate***	***Down-regulated by A66***	***Up-regulated by A66***
Effect abrogated by A66	-	Interferon-induced protein with tetratricopeptide repeats 1, *Ifit1* (15957) [ENSMUSG00000034459] Interferon-induced protein with tetratricopeptide repeats 3, *Ifit3* (15959) [ENSMUSG00000074896]	-	-
Effect abrogated by palmitate	-	-	Interferon regulatory factor 9, *Irf9* (16391) [ENSMUSG00000002325] Interferon regulatory factor 7, *Irf7* (54123) [ENSMUSG00000025498] Interferon-induced protein 44, *Ifi44* (99899) [ENSMUSG00000028037] Interferon-induced protein with tetratricopeptide repeats 1, *Ifit1* (15957) [ENSMUSG00000034459] Interferon stimulated gene 15, *Isg15* (100038882) [ENSMUSG00000035692] Interferon activated gene 203, *Ifi203* (15950) [ENSMUSG00000039997] Interferon inducible GTPase 1, *Iigp1* (60440) [ENSMUSG00000054072] Interferon induced protein with tetratricopeptide repeats 1B like 2, *Ifit1bl2* (112419) [ENSMUSG00000067297]	-

For instance, type I IFN induces the formation of STAT1/STAT2 heterodimers, which can then form a tri-molecular complex with IRF9, known as ISG factor 3 (ISGF3). By interacting with a unique consensus sequence, IFN-stimulated responses element (ISRE), ISGF3 regulates the transcription of a subset of ISGs involved in the cell's antimicrobial response (Schoggins 2011). Alternatively, both type I and II IFN can induce the formation of other STATs dimers, such as STAT1 or STAT3 homodimers. These bind gamma-activated sequences (GAS) present in the promoter of certain ISGs, thereby initiating the transcription of these pro-inflammatory genes (L. Platanias 2005). As reviewed by Ivashki and Donlin, the pleiotropic nature of type I and type II IFN-mediated signalling is likely to reflect the wide range of STATs activation patterns triggered by the interaction of IFN receptors with the STAT family members (Ivashki 2014).

The set of genes regulated by type III IFNs and type I IFNs overlap and promote a strong antiviral state in cells. However, while most nucleated cells respond to type I IFNs, only cells found in tissues with a high risk of viral exposure and infection - such as the cells of mucosal epithelial tissues - respond to type III IFNs (Wack 2015). This permits the host to limit inflammatory cost to only certain tissues. Upon ligand binding, the IFN-λ receptor complex activates JAK1 and TYK2, similarly to IFNAR. This allows the recruitment and phosphorylation of STAT1 and STAT2, which interact with IRF9 to form the tri-molecular complex ISGF3 also induced by type I IFN (Zhou 2007). Thus, despite being mediated via different receptors, similar transcriptional responses are promoted by type I and type III IFN. Nevertheless, the dynamism of the gene expression differs between the two types of cytokines. Indeed, as revealed by Bolen *et al.*, the induction driven by IFN-β

and IFN-λ is significantly longer lasting than that mediated by IFN-α (Bolen 2014). This difference is thought to reflect the inhibitory activity of ubiquitin-specific protease 18 (USP18) on the latter but not the former two IFNs (Wack 2015).

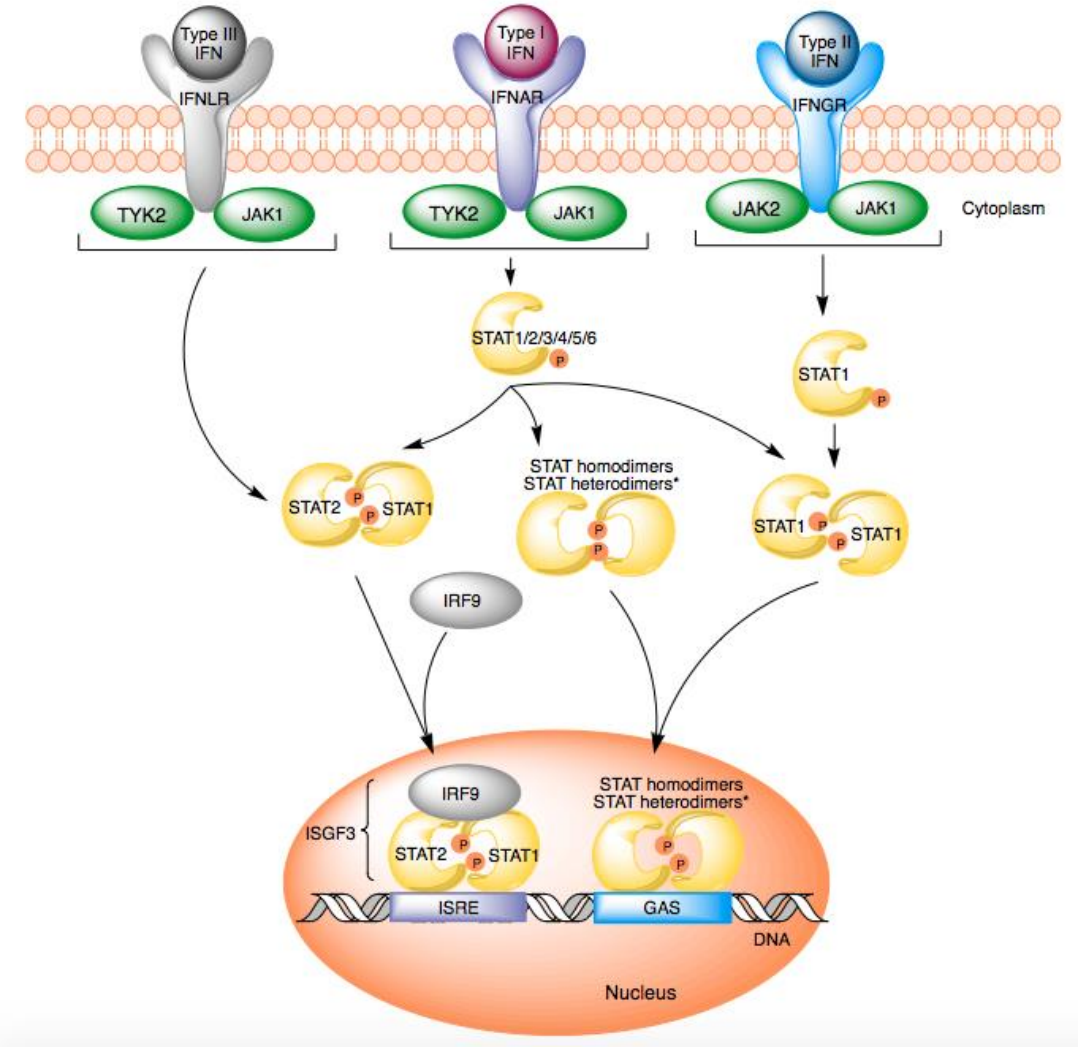

Figure 8. *The downstream signalling of type I, II and III interferons (IFN).* Type I IFN interacts with IFN-α/β receptor (IFNAR) extracellularly to activate tyrosine kinase 2 (TYK2) and Janus kinase 1 (JAK1) at the intracellular level. This results in the phosphorylation of signal transducer and activator transcription 1, 2, 3, 4, 5 and 6 (STAT1 to STAT6), which then form homo- and heterodimers. The STAT1-STAT2 heterodimer binds IRF9 to constitute the IFN-stimulated gene (ISG) factor 3 (ISGF3) complex that modulates the transcription of a subset of ISGs by interacting with IFN-stimulated response element (ISRE). The other STAT dimers bind gamma-activated sequences (GAS), thereby regulating another subset of ISGs. On the other hand, type II IFN docks onto its receptor, IFN-γ receptor (IFNGR), inducing the activation of JAK1 and JAK2. In turn, STAT1 is stimulated and homodimerises in order to translocate to the nucleus where it can bind GAS. Type III IFNs specifically induce the dimerisation of STAT1 and STAT2 through the IFN-λ receptor (IFNLR)-mediated activation of TYK2 and JAK1. This drives the formation of ISGF3 and in turn the transcription of a subset of ISGs also induced by type I IFNs. * Possible STAT homodimers: STAT1, STAT3, STAT4, STAT5 and STAT6; possible STAT heterodimers: STAT1/STAT2, STAT3, STAT4 or STAT5; STAT2/STAT3 and STAT5/STAT6 (Hervas-Stubbs 2011).

I. 5. 2. IFNs as key players in insulin resistance

Interestingly, PI3K was reported to play a key role in IFN-mediated signalling. As early as 1995, Uddin and colleagues established the ability of IFN-α to stimulate the tyrosine phosphorylation of IRS1 and promote the association of PI3K with the latter (S. Y. Uddin 1995). The following year, this group reported similar effects of IFN-α and -β on IRS2, while type II IFN was found to activate PI3K signalling in an IRS-independent manner (L. U. Platanias 1996). Interestingly, type I IFN-mediated activation of PI3K was reported to be STAT-independent, hence suggesting an absence of interplay between the PI3K and STAT pathways in IFN signalling (S. M. Uddin 2000). However, Nguyen and colleagues established that phosphorylation of STAT1 Ser^{727} by IFN-γ requires PI3K and Akt activity (Nguyen 2001). Consistently, subsequent studies found that PKC-δ, one of fifteen isoforms of PKC known to be activated by PI3K, was stimulated following both type I and II IFN treatments and formed a complex with STAT1 (Deb 2003, S. S. Uddin 2002). In addition, both pharmacological and genetic inhibition of PKC-δ blocked STAT1-mediated gene transcription through GAS or ISREs.

This link with PI3K resonates with the body of work advocating IFNs as key players in the development of insulin resistance. Veikko and colleagues provided an initial line of evidence supporting this theory with their insulin-clamp studies establishing that IFN treatment induce impaired glucose tolerance and insulin sensitivity in the context of viral infections (Koivisto 1989). More recent publications shed light on the molecular mechanisms at play by establishing that type II IFN treatment impairs insulin signalling through the down-regulation of IR, IRS1 and GLUT4 and the reduction of phosphorylation levels of Akt (p-Akt) in

human and mouse adipocytes (McGillicuddy 2009). This seemingly contradicts the early study of Platanias and colleagues, which supported an IRS-independent activation of PI3K by IFN-γ (L. U. Platanias 1996). The insulin resistance triggered by IFN-γ treatment is likely to reflect a sustained activation of STAT1 and SOCS1 and to a lesser extent of STAT3 and SOCS3 (McGillicuddy 2009). SOCS proteins are known to be involved in a negative feedback loop which minimises the amplitude of type I IFN responses and thereby avoiding potential toxicity for the host cell. They are indeed able to compete with STATs for binding of IFNAR and suppress JAK activity (Ivashki 2014).

I. 5. 3. ISGylation, an event analogous to ubiquitination

Isg15 became of particular interest in the present investigation because the aforementioned transcriptome analysis evidenced that its expression was affected by the A66 treatment in mouse adipocytes. Furthermore, the nature of the peptide encoded by this gene, discussed in this section, led ISG15 to be identified as a potential modulator of the pathways regulating adipocyte metabolism discussed so far. *Isg15* is one of the most strongly induced ISGs by IFN-α and –β, pathogen infections and lipopolysaccharide (LPS) (Pohl 2012). Studying human corneal cells, Taylor and colleagues also identified IFN-γ as a stimulus for ISG15 production. However, the response to type II IFN was delayed and less intense compared to that elicited by type I IFN with ISG15 production peaking 24 h later in response to IFN-γ treatment (Taylor 1996).

As illustrated by *figure 9*, the 17 kDa peptide encoded by this gene is

characterised by two ubiquitin-like domains prompting a comparison to di-ubiquitin (Sadler 2008). In a sequence of biological events analogous to ubiquitination, ISG15 has the specificity of being able to conjugate to over 200 cellular proteins (Dai 2011). Indeed, ISG15 has the ability to conjugate to a large number of proteins via a reaction similar to ubiquitination, know as ISGylation (Zhang 2011). Thus, ISG15 is likely to affect the activity of various cellular processes including those mediated by palmitate. In addition, a cytokine role has emerged for unconjugated ISG15, which could be another way by which this peptide could alter SFA-dependent cellular processes. This topic will be discussed in depth in Chapter 5.

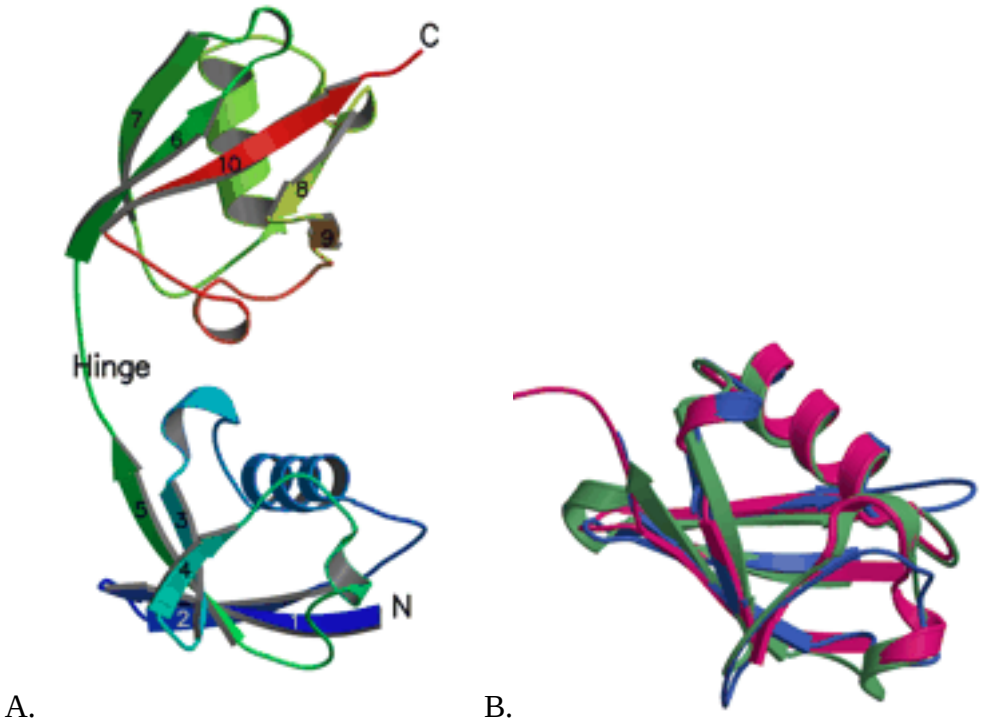

Figure 9. A. *The tertiary structure of murine ISG15.* The ribbon diagram of Narasimhan *et al*. shows the two ubiquitin-like domains of ISG15 characterised by a so-called β-grasp fold. The N-terminus (in blue) is connected to the carboxyterminus (in red) by a hinge (in green). The last four residues of the C-terminal are disordered and unresolved, suggesting a highly flexible region. **B.** *Overlay of the structures of the N-terminus (in blue), the carboxyteminus (in green) and the ubiquitin structure (in pink) revealing the similarity of the three folds.* Each includes a five-strand mixed β-sheet within which is found a three-turn α-helix, along with two 3_{10} helices (Narasimhan 2005). Permission to reproduce this figure has been granted by the American Society for Biochemistry and Molecular Biology.

I. 6. Hypothesis and aims of the investigation

The experiments presented herein were formulated to test the hypothesis that palmitate-induced insulin resistance is mediated through effectors of the IFN pathway, such as ISG15. To validate this hypothesis, the present work aimed at identifying the mechanism underlying development of insulin resistance by dietary FA and the impact of insulin pathway activity on this process. The study used two cell-based models: the extensively used murine 3T3-L1 adipocyte model and primary human multipotent adipose-derived stem (hMADS) as a human model to further ascertain the therapeutic potential of the findings. Experiments were performed in both pre-adipocytes and differentiated cells as both cell types are present in adipose tissue. The goals of the investigation can be summarised as follows:

1) Characterise the signalling pathways shown by transcriptome analysis to be affected by FA in a PI3K dependent manner.
2) Test the effect of inhibition of specific PI3K isoforms on SFA-induced insulin resistance.
3) Delineate the downstream pathways in order to identify novel ‘druggable’ targets.

CHAPTER 2. MATERIAL AND METHODS

II. 1. Procedures in mammalian cell culture

II. 1. 1. Cell lines and culture media

Two cell lines were used: 3T3-L1 derived from mouse and hMADS. While the former were kept in 10% calf serum/Dulbecco's modified eagle's medium (DMEM) supplemented with penicilin/streptomycin (P/S) (both from *Life Technologies, Gibco*), the latter were grown in complete media (*Lonza*) (*see appendix VII. 1 for media preparation*). Cells were cultured in sterile cell culture filter cap T75 flasks (*Greiner Bio-One, Cellstar*) and kept at 37ºC in a Binder C 150 incubator with 5% CO_2. At approximately 80% confluency, the cells were sub-cultured following the protocol below.

<u>*Sub-culturing 3T3-L1 cells:*</u>

The following manipulations were performed using aseptic techniques. Fresh medium was pre-heated for 30 min in a 37ºC water bath:

1. When the desired confluency was reached, the media was discarded and replaced by 10 mL of sterile phosphate buffered saline (PBS) (*Life Technologies, Gibco*). After gently tipping the flask a few times, the PBS was discarded.
2. 2 mL of trypsin-ethylenediaminetetraacetic acid (EDTA) (*Sigma-Aldrich*) were added to the culture, rolling the flask to ensure contact with all cells. The flask was incubated at 37ºC until full cell detachment was achieved.

3. As soon as the cells detached, 8 mL of culture media was added for a total volume of 10 mL. The suspension was pipetted up and down to ensure homogeneity.
4. The volume of suspension necessary to achieve the desired split ratio was discarded and fresh medium was added for a total volume of 15 mL. Homogeneity was maintained by pipetting up and down.
5. The cells were returned to the incubator.

Sub-culturing hMADS:

These cells were sub-cultured according to the protocol of Rodriguez and colleagues and Zaragosi and colleagues (Zaragosi 2006, Rodriguez 2005). Human fibroblast growth factor 2 (FGF2) (*PeproTech*) was added to the cell medium irrespectively of passage stage.

II. 1. 2. Adipocyte differentiation

See *appendix VII. 2* for preparation of reagents and differentiation media. Cells were plated in 6-well Nunc™ Cell-Culture Treated 6 dishes (*Thermo Fisher Scientific*), in Nunclon™ Delta cell culture dishes (10 cm in diameter, a.k.a 10 cm Ø) (*Thermo Fisher Scientific*) or in Cellstar cell culture dishes (6 cm Ø) (*Greiner Bio-One, Cellstar®*).

3T3-L1 adipocytes differentiation:

1. Cells were plated in 10% fetal bovine serum (FBS)/DMEM high glucose (HG) supplemented with P/S (*Life Technologies, Gibco*) and incubated at

37°C in a Binder C 150 CO_2 incubator.

2. After two days post confluency, the cells were stimulated with methyl-isobutyl-xanthine, dexamethasone, insulin (MDI) induction media (day 0), resulting in a distinct change in the morphology of the cells in the next two days.
3. Two days after the addition of the MDI induction media was replaced with insulin media.
4. Two days later the media was changed to 10% FBS/DMEM (HG) supplemented with P/S. Media was then replaced every two days until full differentiation was achieved by day 8.

hMADS adipocytes differentiation:

1. Cells were plated in hMADS complete media supplemented with human FGF2 and incubated at 37°C in a Binder C 150 CO_2 incubator.
2. After two days post confluency, the media was replaced to hMADS complete media without FGF2.
3. The following day, the cells were stimulated with hMADS differentiation media.
4. Three days later, the media was switched to hMADS differentiation media without 3-isobutyl-1-methylxanthine (IBMX) or dexamethasone, which was replaced every three days with fresh media until treatment.

II. 1. 3. Cell treatments

Both mature and pre-adipocytes were washed with PBS before treatments. The latter were treated once 80% confluency was reached. PBS was then aspirated and replaced with pre-warmed medium. The chosen treatment was then carried out. Suppliers and protocols for stock solutions of palmitate, IFN, LPS, inhibitors, insulin and isoproterenol are summarised in *table 4*. Following treatment, the cells were placed on ice and washed with ice cold PBS. 1% Triton X (TX)-100 lysis buffer was then added to the monolayer (*see appendix VII. 4 for 1% TX-100 lysis buffer preparation*).

Table 4. *The reagents used for cell treatments, the company they were purchased from, the solvent used to dilute them and the concentrations of stock and working dilutions.* * Note two successive working dilutions were made to carry out the isoproterenol treatment.

	Purchased from	*Solvent*	*Stock concentration*	*Working dilution*
Recombinant IFN-α murine	BioLegend	MilliQ water	100 ng/µL ($2 - 10 \times 10^7$ U/mg)	5 ng/µL
Recombinant IFN-α 2A human	PeproTech	MilliQ water	100 ng/µL ($\geq 5 \times 10^6$ U/mg)	5 ng/µL
Recombinant IFN-γ murine	PeproTech	MilliQ water	100 ng/µL ($\geq 5 \times 10^6$ U/mg)	5 ng/µL
Recombinant IFN-γ human	PeproTech	MilliQ water	100 ng/µL ($\geq 2 \times 10^7$ U/mg)	5 ng/µL
Recombinant IFN-λ 2 murine	PeproTech	MilliQ water	100 ng/µL	5 ng/µL
Recombinant ISG15 human	Sino Biological	MilliQ water	100 µg/µL	50 µg/µL
LPS	Sigma-Aldrich	PBS	1 mg/mL	10 ng/µL
A66	Tocris Bioscience	DMSO	10 mM	1 mM
D030 (IC87114)	Symansis	DMSO	10 mM	1 mM
TAK 242	Cayman Chemical	DMSO	10 mM	1 mM
Myriocin	Cayman Chemical	DMSO	10 mM	1 mM
Bafilomycin A1	Cayman Chemical	DMSO	1 mM	5 µM
C16	Cayman Chemical	DMSO	10 mM	1 mM
Bovine insulin	Sigma-Aldrich	MilliQ water	1 mM	10 µM
Human insulin	Sigma-Aldrich	MilliQ water	1 mM	10 µM
Isoproterenol	Sigma-Aldrich	MilliQ water	10 mM	1. 100 µM; 2. 10 µM*

II. 1. 4. Quantitative immunoblot analysis

Cell lysis and protein content quantification:

1. The cells were scraped off the dish in lysis buffer and transferred into pre-cooled eppendorf tubes.
2. The suspension was centrifuged at 13,300 g at 4ºC in an AccuSpin Micro 17R centrifuge (*Fisher Scientific*) for 5 min.
3. The concentration of protein in the supernatant was determined using either the Quick Start Bradford or the Pierce bicinchoninic acid protein assay kits (*Bio-Rad*). The absorbance of the samples was measured using an Infinite M200 multimode reader (*Tecan*) coupled with Magellan 6 software for data analysis.
4. Sample protein concentrations were standardised using 1% TX-100 buffer and a solution of electrophoresis sample buffer containing dithiothreitol (DTT) (*AGTC Bioproducts*) was added at a 1:5 ratio (*see appendix VII. 5 for electrophoresis sample buffer preparation*).
5. The lysates were then heated at 100ºC for 5 min and stored at -20ºC.

Protein separation by sodium dodecyl sulfate polyacrylamide gel electrophoresis (SDS-PAGE):

See *appendix VII. 6* and *appendix VII. 7* for gel preparation 10%, 15% SDS acrylamide gels and 12% Tris-tricine gels, respectively. Equal amount of lysate protein was loaded per lane and 5 μL of Precision Plus Protein All Blue standards (*Bio Rad*). 10% SDS acrylamide gels were run for 2 h at 110 V. To improve the resolution of Tris-tricine gels, a lower voltage (60 V) was applied while samples were migrating though the stacking to the separating gel. The voltage was then

increased to 110 V.

Western blot:

After discarding the stacking gel, the separating gel was added to the transfer stack. The polyvinylidene fluoride membrane used (pore size: 0.45 μm) (*Immobilon®, Merck Millipore*) was activated with methanol (*VWR International*) then rinsed in deionised water and transfer buffer. The transfer was run for 1 h 30 min at 0.45 A (*see appendix VII. 6. D for transfer buffer composition*).

Antibody probing and immune-complex detection:

All subsequent washes and incubations were performed on a see-saw rocker SSL4 (*Stuart*):

1. The membrane was blocked with milk (5% fat-free milk powder diluted in Tris-buffered saline – Tween 20 [TBS-T] (*Acros Organics*)) for 1 h at room temperature.
2. The membrane was then washed in TBS-T three times for 5 min at room temperature.
3. The membrane was incubated overnight with the primary antibody at 4ºC (*see table 5 for the various primary antibodies used*). The protocol for preparing the primary antibody solution can be found in *appendix VII. 8.*
4. The washes (step 2) were repeated.
5. The membrane was incubated for 1 h at room temperature with a fluorescent secondary antibody diluted in 5% milk (1:5,000). Dylight™ 800 Conjugated anti-mouse immunoglobulin G (IgG) (H+L) (goat) (*Rockland*) and Alexa Fluor 680 goat anti-rabbit IgG (H+L) (*Invitrogen*) were used after incubation

with a mouse and a rabbit primary antibody, respectively.

6. The membrane was washed (step 2) and the signal was measured using the Odyssey CLx Imager (*Li-Cor*) coupled to the software Image Studio Version 5.

Table 5. *Primary antibodies used for immunoblot analysis. CST*: Cell Signaling Technology.

	Purchased from	*Catalogue number*	*Type*	*Dilution*	*Molecular weight of target (kDa)*
β-actin	Sigma-Aldrich	A2228	Mouse IgG2a	1:5,000	42
Akt (Pan) (40D4)	CST	2920	Mouse IgG1	1:1,000	60
ISG15	CST	2743	Rabbit antibody	1:1,000	15
LC3B	CST	2775	Rabbit antibody	1:1,000	14, 16
Perilipin (D1D8)	CST	9349	Rabbit IgG	1:1,000	62
Phospho-Akt (T308) (C31E5E)	CST	2965	Rabbit IgG	1:1,000	60
Phospho-HSL (S660)	CST	4126	Rabbit antibody	1:1,000	81, 83
Phospho-PKA substrate (RRXS*/T*) (100G7E)	CST	9624	Rabbit IgG	1:1,000	-
Phospho-STAT1 (S727) (D3B7)	CST	8826	Rabbit IgG	1:1,000	91
Phospho-STAT1 (Y701) (58D6)	CST	9167	Rabbit IgG	1:1,000	84, 91
Phospho-STAT3 (S727)	CST	9134	Rabbit antibody	1:1,000	86
Phospho-STAT3 (Y705) (D3A7)	CST	9145	Rabbit IgG	1:1,000	79, 86
PKR (B-10)	Santa Cruz	6282	Mouse IgG2a	1:200	68
p62/SQSTM1 (2C11)	Novus Biologicals	M01	Mouse IgG2a	1:1,000	75
STAT3 (124H6)	CST	9139	Mouse IgG2a	1:1,000	79, 86
Vinculin	Sigma-Aldrich	V9131	Mouse IgG1	1:5,000	124
Total HSL	CST	4107	Rabbit antibody	1:1,000	81, 83

II. 2. RNA interference (RNAi) experiments

This section presents the RNAi technique used to silence the target gene *Isg15*. It relies on the delivery of a short hairpin RNA (shRNA) into the cells through viral infection. This approach has the benefit of producing long-term silencing of the gene and thus allows for experiments to be performed in both pre- and mature-adipocytes. *Figure 10* details the process of producing the two stable cell lines: one transduced with the pGIPZ vector carrying the *Isg15*-targeting shRNA construct and the other transduced with the empty pGIPZ vector, used as control. shRNA are integrated within the host genome following a reverse transcription step, allowing for long-term knockdown of the target gene. Once transcribed, the shRNA translocates to the cytosol where it is processed into short interfering RNA (siRNA) duplexes by the Dicer enzyme. The oligonucleotides are thus able to associate with the target messenger RNA (mRNA), which is then degraded endogenously by the RNA-induced silencing complex (Moore 2010).

More specifically, the technique employed to deliver the shRNA within the cell is refered to as the calcium phosphate co-precipitation developed in 1973 by Graham and van der Eb (Graham 1973). It involves on the formation of a calcium-phosphate-deoxyribonucleic acid (DNA) co-precipitate from mixing calcium chloride in a buffered saline/phosphate solution. The co-precipitate is then dispersed onto target cells which engulf the DNA through endocytocis. Calcium phosphate stimulates this process by promoting the binding of the DNA to the cell surface.

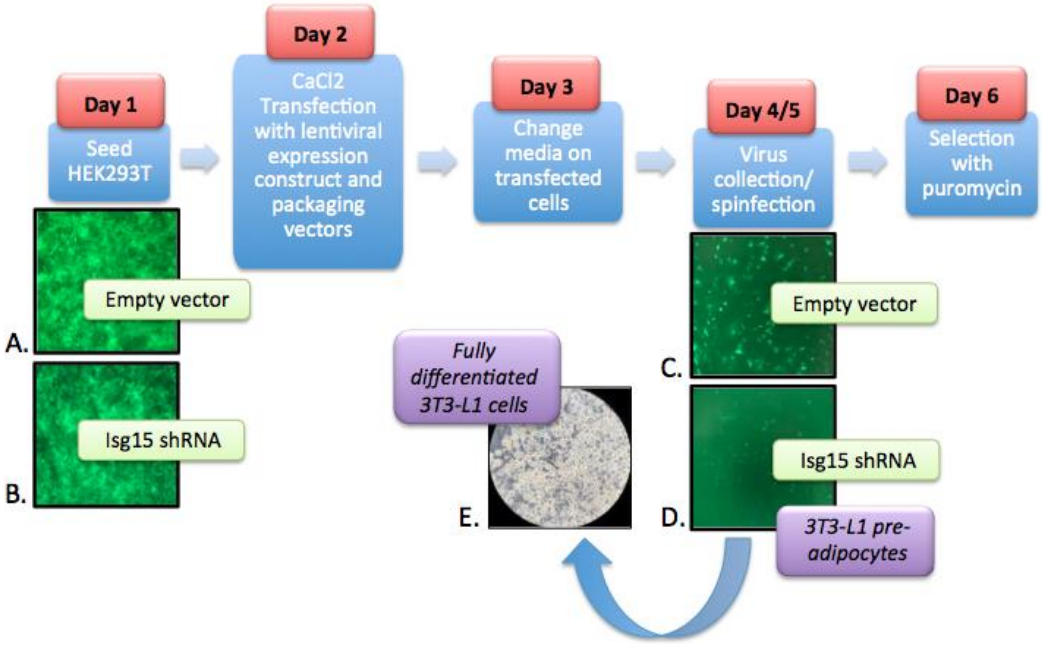

Figure 10. *Flow chart detailing the process used to produce a stable 3T3-L1* Isg15-*knockdown (KD) cell line.* The first day, human embryonic kidney (HEK) 293T cells were seeded in two 10 cm dishes. The following day, the 3T3-L1 target cells were plated and the HEK 293T cells were transduced with the plasmids (including the two packaging plasmids and the pGIPZ-*Isg15* shRNA construct or the pGIPZ empty vector) using the calcium phosphate co-precipitation method. 24 h post-transduction, the media of the HEK 293T cells was changed. On days 4 and 5, the lentivirus-containing supernatant of the HEK 293T cells was collected and used to replace the media of the target 3T3-L1 cells. The infection of the murine cells included a centrifugation step, thus the name "spinfection". Because the pGIPZ vector includes a turbo green fluorescent protein (*turboGFP*) reporter, it is possible to monitor transduction efficiency (as shown on pictures A, B, C and D included in the figure). Moreover, the plasmid counts a puromycin-resistance gene to allow for selection of successfully transduced cells. As demonstrated on picture E, the stable cell line produced could be fully differentiated.

Day 1: human embryonic kidney (HEK) 293T cells were seeded into two 10 cm dishes with 10 mL of 10% FBS/DMEM (HG) supplemented with P/S (*Life Technologies, Gibco*) and incubated at 37ºC (1.5 million cells per dish);

Day 2: 3T3-L1 target cells were plated in following the protocol below:

1. When the stock flask of 3T3-L1 reach confluency, wash with 10 mL of PBS and add 2 mL of trypsin EDTA.

2. Stop the trypsinisation process by adding 8 mL of antibiotics-free 10% FBS/DMEM (HG).
3. Leave 2 mL of the suspension in the stock flask and add 13 mL of 10% calf/ DMEM (HG) supplemented with P/S.
4. Transfer the remaining 8 mL of suspension to a 15 mL falcon tube and centrifuge at 1,000 rpm for 5 min using a Multifuge x3R Heraeus (*Thermo Scientific*).
5. The supernatant was discarded and the cells were resuspended in 5 mL of antibiotics-free 10% FBS/DMEM (HG).
6. The cells were then plated in a 6-well dish at a density of 20×10^3 cells per well.

24 h following seeding, the HEK 293T cells were transduced:

- In a 1.5 mL eppendorf, 61 µL $CaCl_2$ (*Sigma-Aldrich*) (2 M), 1 µg p8.91 (*Addgene*), 1 µg pMDG (*Addgene*) and either 1.5 µg pGIPZ lentivirus expression construct (*Dharmacon, see table 6 for details*) or 1.5 µg of pGIPZ empty vector were diluted to a total volume of 500 µL with MilliQ water (*see figure 11 for pGIPZ vector elements*).
- This solution was added dropwised to a second eppendrof containing 500 µL 2X hepes buffered saline (HBS) buffer while forcing air bubles into the mix (*see appendix VII. 9 for HBS buffer preparation*).
- Following a 20 min incubation at room temperature, the DNA-$CaCl_2$-HBS buffer mix was added dropwise to the cells.

Day 3: 24 h after the transduction, the cells were washed with pre-warmed PBS and the medium was replaced to 10 mL of antibiotics-free 10% FBS/DMEM supplemented with 1% bovine serum albumine (BSA).

Day 4 and 5: The lentivirus-containing supernatant was harvested 24 and 48 h after media change and was used to replace the media of target cells. The media was sterile filtered (0.45 μm Minisart filter, *Sartorius*) and supplemented with Polybrene (*Sigma-Aldrich*) (1:1,000). Target cells are rinced with pre-warmed PBS before adding 2 mL of media containing the virus. After changing the media the cells were "spinfected" - 45 min at 800 g at 37°C and returned to the incubator.

Day 6: Target cells were returned to 10% FBS/DMEM supplemented with P/S (2 mL/well) and puromycin (*Clontech Laboratories, Inc.*) was added to the media (4 μg/mL).

Table 6. *Information on the GIPZ mouse* Isg15 *shRNA.*

Clone ID	V2LMM_25376
Sequence of mature antisense	TAAGCGTGTCTACAGTCTG
Accessions	NM_015783
Vector map	pGIPZ

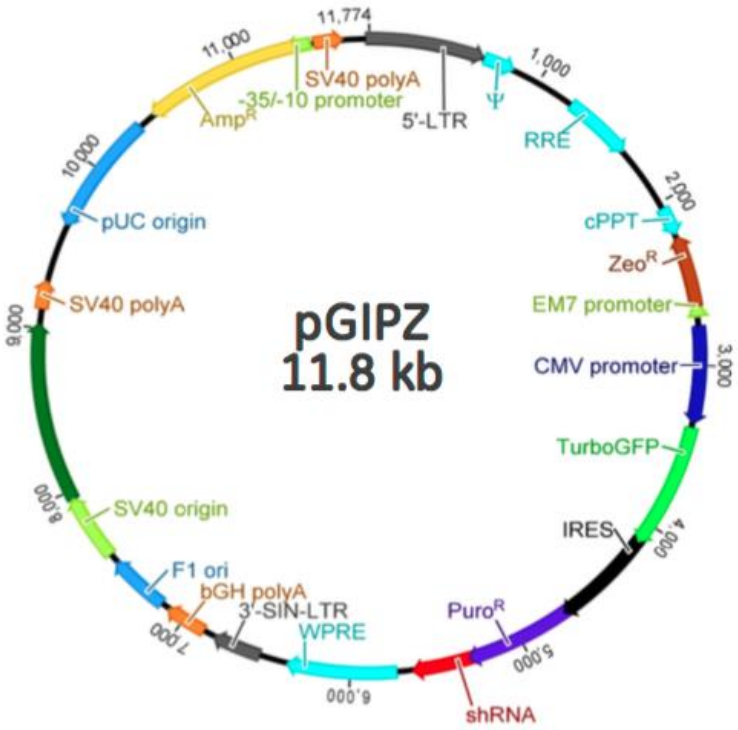

Figure 11. *pGIPZ vector elements (*Dharmacon*).* Short hairpin RNA (shRNA) targeting the gene of interest; woodchuck hepatitis post-transcriptional regulatory (WPRE) element to enhance transgene expression in the target cells; 3' self-inactivated long terminal repeat (3' SIN LTR) for enhanced safety when working when lentivirus; SV40 and bGH polyA: mammalian terminator of transcription; F1 ori: origin of bacteriophage replication; pUC ori which marks the origin of replication in *Escherichia coli* and SV40 ori allowing this in mammalian cells expressing the SV40 large T-antigen; *Amp*^{R}, *Zeo*^{R} and *Puro*^{R}: ampicillin, Zeocin and pruomycin resistance genes allowing for antibiotic-mediated selection of transduced cells; 5' long terminal repeat (5' LTR); Psi (Ψ) packing sequence, which permits viral genome packing through lentiviral packaging systems; Rev response element (RRE) promoting packaging efficiency of full-length viral genomes thus increasing titre; central polypurine tract (cPPT) promotes the translocation of viral vector into the nucleus of non-dividing cells; EM7: prokaryotic promoter that allows expression of antibiotic genes; cytomegalovirus (CMV) promoter ensuring strong transgene expression; *turboGFP* reporter, which permits to monitor transduction efficiency; internal ribosomal entry site (IRES) which enables the expression of *turboGFP* and *Puro*^{R} in a single transcript (GIPZ Lentiviral shRNA n.d.).

II. 3. Mass spectrometric analysis of protein ISGylation

II. 3. 1. Treatments and cell lysis

3T3-L1 cells were differentiated in Nunclon^{TM} Delta cell culture dishes (10 cm Ø) according to the protocol detailed in section II. 1. 2 of the present chapter. *Table 7* details the treatments performed on the differentiated cells before processing them. The differentiated cells were rinced with PBS and the media was replaced before treating them.

Table 7. *Treatments carried out in 3T3-L1 mature adipocytes before processing them for the mass spectrometry experiment.*

Dish number	*Treatment (concentration)*	*Duration (in h)*	*Type of media*
Dish 1	Untreated	12	10% FBS/DMEM
Dish 2	IFN-α (20 ng/mL)	12	10% FBS/DMEM
Dish 3	IFN-α (20 ng/mL)	12	10% FBS/DMEM
Dish 4	Palmitate 3:1 BSA (500 µM)	12	10% FBS/DMEM

Cell lysis and protein content quantification:

1. Once the treatments completed, the dishes were placed on ice and the media was aspirated. Cells were rinsed with ice-cold PBS before lysing in 100 µL of buffer (10 mM Tris-HCl, pH 8, 150 mM sodium chloride, 2% SDS, plus protease inhibitors used in 1% TX-100 lysis buffer recipe detailed in *appendix VII. 4*).
2. Cells were scraped off the dishes and transferred into pre-chilled eppendorf tubes on ice.
3. Lysates were passed through a 23 gauge needle to shear the DNA and incubated at 100ºC for 5 min.
4. Lysates were diluted with 900 µL 1% TX-100 lysis buffer.
5. Suspensions were centrifuged at 13,300 g at 4ºC in an AccuSpin Micro 17R centrifuge for 5 min.
6. The concentration of protein in the supernatant was determined using the Pierce bicinchoninic acid protein assay kit. The absorbance of the samples was measured using an Infinite M200 multimode reader coupled with Magellan 6 software for data analysis.

7. Sample concentrations were standardised using 1% TX-100 buffer. For the first and second experiments a concentration of 1.4 mg/mL was used and for the third experiment a concentration of 0.7 mg/mL was used. The total volume was 1 mL for all samples.

II. 3. 2. Immunoprecipitation (IP)

1. The antibodies were added to the samples according to *table 8* and the samples were incubated for 2 h on a rotator SB3 (*Stuart*) at 20 rpm at 4ºC.
2. 15 µL protein-G Sepharose beads (*GE Healthcare*) were added to each sample followed by a second 2 h-long incubation on the rotating wheel at 20 rpm at 4ºC.
3. The beeds were washed three times with 0.5 mL lysis buffer, followed by three washes with 0.5 mL ammonium bicarbonate (25 mM).
4. Pellets were stored at -80ºC until transported on dry ice to the mass spectrometry laboratory.

Table 8. *Summary of the antibodies added to the various samples during the immunoprecipitation (IP) experiment.* The b3-AR antibody was used as negative control to account for background detection.

Treatment (concentration)	*Antibodies*
Untreated	*2 µg ISG15 antibody*
IFN-α (20 ng/mL)	*2 µg β3-AR antibody*
IFN-α (20 ng/mL)	*2 µg ISG15 antibody*
Palmitate 3:1 BSA (500 µM)	*2 µg ISG15 antibody*

Table 9. *Antibodies used for IPs.*

	Purchased from	*Catalogue number*	*Type*	*Molecular weight of target (kDa)*
ISG15(F-9)	Santa Cruz	166755	Mouse IgG1	15
β3-AR (C-5)	Santa Cruz	515763	Mouse IgG2a	68

II. 3. 3. Mass spectrometry and data analysis

The mass spectrometry data was generated by the mass spectrometry lab (Barts Cancer Institute, Queen Mary University of London) in collaboration with Dr Pedro Cutillas and Dr Vinothini Rajeeve. The data analysis on the protein hits was performed using Excel. The signal intensities obtained for a sample incubated with an antibody specific for β3-AR (antibody specific to an unrelated target) were subtracted to the values obtained for the samples incubated with the ISG15-specific antibody as a control for unspecific binding. The database for annotation, visualisation and integrated discovery (DAVID) (version 6.8) was employed for gene functional classification (Dennis 2003). The search tool for the retrieval of interacting genes/protein (STRING) software was used to unravel interactions and visualise networks of gene clusters (Szklarczyk 2015).

II. 4. Statistical analysis

Experimental results were reported as averages ± SEM. Differences were analysed using one-way and two-way analyses of variance (ANOVA) from IBM

SPSS2.2 software package. For the former, Tukey honest significant difference (HSD) test was performed as a *post hoc* test. A p-value < 0.05 was deemed significant. For additional insight when the p-value was close to 0.05, a two-tailed paired student t-test was used to compare effects of treatments within the same cell line or an unpaired t-test when comparing two cell lines.

CHAPTER 3. THE EFFECT OF PALMITATE ON INSULIN AND IFN SIGNALLING PATHWAYS

III. 1. Overview of Chapter 3

As discussed in the introduction, the present work stems from a transcriptome analysis, which compared the gene expression profile of 3T3-L1 adipocytes treated with the SFA palmitate in the presence or absence of a pharmacological inhibitor (A66) targeting p110α, one of the catalytic subunits of class IA PI3K. The data analysis revealed that the expression of a number of genes induced by IFN was stimulated by palmitate and such effect was negated by the addition of A66. This chapter presents the preliminary steps towards validating the findings of the transcriptome profiling experiment. The groundwork involved establishing models of palmitate- and IFN-mediated insulin resistance in both murine and human adipocytes. The consequence of p110α inhibition in such models was then explored to gain further insight on the findings of Foukas *et al.* regarding the beneficial phenotypic effect of such inhibition in the $p110\alpha^{D933A/WT}$ mice (L. C. Foukas 2006). To confirm the interaction between palmitate and the IFN pathway, a series of experiments was performed investigating the effect of the SFA on the phosphorylation of two downstream effectors of IFN, STAT1 and STAT3. These transcription factors were of particular interest as McGillicuddy and colleagues demonstrated that IFN-induced insulin resistance is dependent on their sustained activation (McGillicuddy 2009). Having demonstrated the palmitate-induced

activation of STAT3, further experiments were carried out to probe the molecular pathways involved in this crosstalk.

III. 1. 1. Aim of Chapter 3

The aim of the present chapter was to develop a model of both palmitate- and IFN-induced insulin resistance. To this end the phosphorylation of a pivotal effector of the insulin signalling pathway (Akt) was assessed following treatments with either SFA or IFN. In addition, we wanted to verify a potential interaction between the palmitate and the IFN pathways. As mentioned previously, this was done through monitoring the activation of STAT1 and STAT3 in response to palmitate. A range of pharmacological inhibitors was used to shed light on the interaction unveiled between palmitate and STAT3. Experiments were performed in both pre- and mature 3T3-L1 adipocytes and these were mirrored in hMADS adipocytes to further ascertain the therapeutic relevance of potential findings. As mentioned in Chapter 1, both pre- and mature adipocytes are present in adipose tissue and ensure the metabolic function of the organ. Pre-adipocytes have the ability to proliferate and differentiate into mature adipocytes. Studying the response of each cell type individually provides therefore valuable insight on the molecular mechanism underlying the onset of insulin resistance in adipose tissue.

III. 2. Introduction of Chapter 3

III. 2. 1. The crosstalk between STAT3 and modulators of obesity

In Chapter 1, the mechanisms of palmitate- and IFN-induced insulin resistance were discussed. In light of the findings of the transcriptome analysis indicating the existence of a crosstalk between the two pathways, we hypothesised that palmitate-induced insulin resistance was modulated by elements of the IFN cascade. As evidenced by McGillicuddy and colleagues, IFN-γ-mediated insulin resistance is driven by the sustained activation of STAT1 and to a lesser extent STAT3 (McGillicuddy 2009). Therefore, assessing the effect of palmitate on the activation of these transcription factors constituted a valid approach to probe a potential interaction between SFAs and the interferon signalling.

A body of studies implicates these two transcription factors in the pathogenesis of obesity. In the present section, the specific role of STAT3 will be explored, focusing initially on the link between STAT3 and adipokines/cytokines involved in modulating the development of obesity. For instance, IL-6, which rates of secretion are up-regulated in obese individuals, induces the phosphorylation of STAT3 in a JAK-dependent manner (Vogt 2011). Furthermore, Jiang and colleagues revealed that STAT3 modulated adiponectin expression in cultured 3T3-L1 adipocytes (C. K. Jiang 2013). Using both chromatin IP and luciferase assays, the authors were able to confirm the existence of a functional STAT3-binding site within the adiponectin promoter.

In HEK 293T, leptin exposure was found to induce the phosphorylation of STAT3 in a biphasic manner including an initial acute phase 15 min following leptin

stimulation and a second chronic phase of lesser intensity starting 1 h 35 post-induction (C. W. Han 2016). The authors were also able to confirm the ability of TNFα, another key adipokine implicated in the biochemistry of obesity, to stimulate STAT3 phosphorylation. (C. W. Han 2016). The link between leptin and STAT3 had been evidenced as early as 1996, when Vaisse and colleagues discovered that the adipokine promoted STAT3 activation in the hypothalamus of WT and *ob*/*ob* mice (Vaisse 1996). Seven years later, Bates *et al*. confirmed the importance of STAT3 signalling in leptin-mediated regulation of energy expenditure (Bates 2003). Indeed, they observed the onset of obesity and hyperphagia in mice bearing a genetic mutation of the leptin receptor long form (Y1138S), a residue known to specifically mediate the activation of STAT3.

In addition to adipokines, the activation of STAT3 was found modulated by insulin resistance-inducing nutrients in a variety of metabolic tissues. Indeed, a study performed by Kim and colleagues in HepG2 cells demonstrated that silencing *stat3* ameliorated amino acid-mediated suppression of insulin signalling. Furthermore, amino acids were found to induce the phosphorylation of STAT3 (J. Y. Kim 2009). In WAT and liver, insulin-resistance inducing arginine chronic treatment stimulated STAT3 tyrosine phosphorylation in rats (de Castro Barbosa 2009). Relevantly to the present work, Oberbach and colleagues evidenced palmitate treatment to enhance STAT3 activation in human bladder smooth muscle cells (Oberbach 2010). More specifically, the SFA stimulated p-STAT3 Tyr^{705} levels following an 8 h palmitate treatment. However, beyond this time point the SFA had an inhibitory effect on both *stat3* mRNA and p-STAT3 Tyr^{705} levels with a maximal down-regulation at 48 h of treatment. Inversely, immunofluorescence analysis in cells treated for 48 h with

palmitate revealed that both *socs3* mRNA and SOCS3 protein expression was enhanced in presence of the SFA (Oberbach 2010). The authors postulate that these observations manifest the existence of a negative feedback loop mediated by SOCS3 targeting IL-6 signalling, which concentration they found significantly increased following palmitate stimulation at all time points tested.

The effect of palmitate on STAT3 activation was also investigated by Mashili and colleagues (Mashili 2013). Having exposed L6 cultured myotubes (derived from rat skeletal muscles) to palmitate for 24 h, they noted a significant increase in the phosphorylation of STAT3 Tyr^{705}. This was coincident with a stimulation of SOCS3 expression and a reduction in p-Akt Ser^{473} levels following insulin stimulation compared to untreated control (signifying development of insulin resistance). Palmitate-induced activation of STAT3 was sustained after 36 h of treatment. Together these results suggest that, at least in skeletal muscle, palmitate-mediated insulin resistance is likely to involve a STAT3-dependent mechanism (Mashili 2013). Aligning with the findings of Mashili and colleagues, Weigert *et al*. demonstrated that a 20 h-long palmitate treatment stimulated both IL-6 protein and mRNA expression in a nuclear factor-κB (NF-κB)-dependent manner in human myotubes (Weigert 2004). In turn, IL-6 was evidenced to induce STAT3 tyrosine phosphorylation.

The study Mashili and colleagues also demonstrates that the sustained phosphorylation of STAT3 is determinant in the onset of skeletal muscle insulin resistance in T2D (Mashili 2013). Comparing biopsies from overweight, glucose tolerant individuals with T2D patients matched for age and BMI, the investigation

reveals a 2-fold increase in p-STAT3 Tyr^{705} in the latter group. Furthermore, a positive correlation was observed between plasma FFA levels and skeletal muscle p-STAT3 concentration, which was negatively correlated with insulin sensitivity in the control group (Mashili 2013).

To gain further insight into the metabolic role of STAT3, researchers have attempted to knockout *stat3* in mice, however no conclusions could be drawn as this manipulation induces early embryonic lethality (K. N. Takeda 1997). Instead, tissue-specific disruptions were performed using the Cre-*loxP* technique to silence the gene during later life. Using this system, Cernkovich and colleagues proceeded to create mice bearing an adipocyte-specific disruption of *stat3*. They reported that the transgenic mouse shows increased weight and adiposity linked to adipocyte hypertrophy although it does not exhibit hyperphagia or reduced energy expenditure. The authors explained these phenotypes through the observed dysregulation of leptin-induced lipolysis (Cernkovich 2008).

III. 2. 2. The crosstalk between STAT1 and modulators of obesity

The role of STAT1 in the context of obesity is mainly understood through its interaction with IFN-γ. This cytokine, whose expression is up-regulated in obesity, was shown to activate STAT1 (McGillicuddy 2009, Balhoff 1998). IFN-γ-induced STAT1 was evidenced to bind the murine promoter of lipoprotein lipase *in vitro* (Hogan 2003). This enzyme is specialised in the hydrolysis of serum TAGs into FFAs then stored in fat depots. Both muscle- and liver-specific overexpression of lipoprotein lipase in transgenic mice was reported to cause insulin resistance in the

corresponding tissues (J. F.-C. Kim 2001). In accordance with these findings, Delezie *et al.* demonstrated that the overexpression of this lipase in muscle and adipose tissue promoted obesogenic phenotypes in mice (Delezie 2012).

In addition to IFN-γ, oncostatin-M was shown to promote the tyrosine phosphorylation of STAT1 in 3T3-L1 adipocytes (J. L. Stephens 1998). This cytokine, also reported to induce STAT3, belongs to the gp130 family, which includes leukemia inhibitory factor (LIF), IL-6, IL-11, IL-27, cardiotrophin-1 (CT-1), neuropoietin, CT-1-like cytokine and ciliary neurotrophic factor (U. a. White 2011). Although not secreted by adipocytes, oncostatin-M is produced by the cells of the stromal vascular fraction in human adipose tissue, as well as by murine macrophages (Sanchez-Infantes 2014). Its release may also be induced by exposing neutrophils and dendritic cells to LPS or granulocyte/macrophage-colony stimulating factor (Hergovits 2017). Throughout the literature, this cytokine has been associated with metabolic dysregulation.

Indeed, it was reported to hinder adipogenesis through the down-regulation of peroxisome proliferator-activated receptor-γ (PPARγ) and adiponectin, while also promoting insulin resistance in 3T3-L1 adipocytes (U. S. White 2008). Furthermore, oncostatin-M was found to stimulate plasminogen activator inhibitor-1 and IL-6 in this cell type. The former, expressed by adipose tissue, is associated with the onset of T2D as well as being critical in the pathogenesis of obesity (Sanchez-Infantes 2014). Sanchez-Infantes *et al.* established the existence of a positive correlation between expression levels of oncostatin-M in human adipose tissue and body weight. Inversely, they reported a negative correlation between oncostatin-M and insulin

levels. Expression levels of the cytokine were also found increased in epididymal fat of *ob*/*ob* and HFD-fed mice (Sanchez-Infantes 2014).

Evidence also supports aforementioned LIF to induce STAT1, along with STAT3, in 3T3-L1 adipocytes (J. L. Stephens 1998). This gp130 class cytokine is synthesised by pre-adipocytes and promotes differentiation through stimulation of adipogenic transcription factors PPARγ and CCAAT-enhancer binding proteins (C/EBPs) (Aubert 1999). The process of adipogenesis and the role of these transcription factors will be further discussed in the following section. LIF was also reported to down-regulate the activity of lipoprotein lipase through transcriptional regulation in adipocytes (Marshall 1994). In the context of obesity, inhibition of this cytokine in mice was associated with the development of glucose intolerance, insulin resistance and increased adiposity along with hyperphagia and increased expression of pro-inflammatory cytokines including TNFα and IL-6. Collectively, these observations support a protective role for LIF in the onset of obesity (Fioravante 2017).

CT-1, another member of the gp130 family, was also found to activate STAT1 and STAT3 in 3T3-L1 adipocytes. Like LIF, CT-1 is anti-inflammatory and has been reported to signal through the LIF receptor, resulting in the induction of the JAK/STAT cascade (Zvonic 2004). Using a gene targeted *ct-1*$^{-/-}$ mouse model, Moreno-Aliaga revealed that CT-1 is pivotal in the modulation of energy homeostasis and metabolism. Indeed, deleting the gene inhibited energy expenditure in mice, which also exhibited obesogenic phenotype, T2D and hypercholesterolemia. Exposure of *ob*/*ob* mice and HFD-fed mice to recombinant CT-1 alleviated

symptoms of both obesity and T2D (Moreno-Aliaga 2012). Interestingly, CT-1 serum concentration was reported to be elevated in obesity potentially in an effort to counteract associated metabolic dysfunctions.

In light of these findings, the observations of Zvonic and colleagues seem rather unexpected: their study reveals that chronic treatment of 3T3-L1 adipocytes with CT-1 hinders the expression of FA synthase and IRS1, while triggering the onset of insulin resistance (Zvonic 2004). Moreno-Aliaga *et al.* address this discrepancy focusing on the crosstalk between CT-1 and the STATs cascade known to down-regulate insulin signalling: they emphasise that because SOCS3 is overexpressed in WAT of murine obese models, the detrimental metabolic effect of CT-1 reported by Zvonic *et al*. is likely to be tissue specific rather than systemic (Moreno-Aliaga 2012). In addition, the authors note CT-1 expression is relatively low in WAT *versus* other metabolic tissues such as skeletal muscles.

Although *stat3* deletion causes lethality in mice, *stat1* deletion is viable and its pathophysiology has been extensively studied in the context of immunity. It is only recently that Sisler and colleagues examined the metabolic consequences of *stat1* deficiency (Sisler 2015). Although no change in body weight was measured between the $stat1^{-/-}$ mice and the $stat1^{+/+}$ control, the former exhibited increased adiposity paired with reduced lean mass. During fasting, the authors reported a down-regulation of adrenergic-stimulated lipolysis manifested by an impaired lipid and glycerol release in the WAT of $stat1^{-/-}$ mice. Paradoxically, these traits coincided with enhanced energy expenditure in the knockout model. To explain their observations, Sisler *et al.* propose that FFAs are re-esterified to TAG in the WAT of

stat1$^{-/-}$ mice. Furthermore, mitochondrial functions were hindered by the loss of *stat1*. Together, this data suggest a critical role for STAT1 in energy homeostasis, TAG turnover and mitochondria biogenesis (Sisler 2015).

III. 2. 3. The role of STATs in adipogenesis

Collectively, the aforementioned studies demonstrate STATs to be key players in the onset of obesity through their role in the regulation of systemic insulin sensitivity and inflammation. This role is reinforced by the involvement of these transcription factors in adipogenesis, a cellular process describing the differentiation of pre-adipocytes into mature adipocytes. Adipocyte development is regulated by a number of transcription factors including PPARγ and C/EBPs (K. G. Zhang 2011). These transcriptional effectors of adipogenesis modulate different stages of the differentiation process: C/EBPβ and C/EBPδ promote the initial mitotic clonal expansion phase, while C/EBPα and PPARγ stimulate the terminal differentiation phase, characterised by a rise in lipid accumulation and insulin sensitivity (Sarjeant 2012).

In 1996, Stephens *et al*. reported a substantial induction of STATs 1, 3 and 5 during the differentiation of 3T3-L1 adipocytes. The expression of STAT6, however, was unchanged. Following TNFα exposure, which stalled the process of differentiation, the expression of STATs 1 and 5 was hindered, but that of STAT3 was unaffected. They concluded that because of the tight correlation of STATs 1 and 5 to the adipocyte phenotype, these transcription factors were involved in adipogenesis (J. M. Stephens 1996). Interestingly, upon differentiation of human

subcutaneous pre-adipocytes, Harp and colleagues recorded a decrease in STAT1 expression, coinciding with an increase in STATs 3 and 5 expression. In line with the observations of Stephens *et al*., they reported STAT6 to be unaffected (Harp 2001).

The specific role of STAT3 in adipogenesis was further investigated by Deng *et al*. who demonstrated that STAT3 was activated during the proliferative phase and that protein inhibitor of activated STAT3 down-regulated adipogenic gene expression in 3T3-L1 cells (Deng 2006). Having also established the inhibitory effect of suppressing STAT3 on adipogenesis through the use of pharmacological inhibitor and siRNA targeting of *stat3,* Wang and colleagues differentiated 3T3-L1 pre-adipocytes in the presence or absence of PPARγ agonist troglitazone. The study unveiled that troglitazone-induced activation of PPARγ rescued the suppression of adipogenesis mediated by STAT3 inhibition (Wang 2009). C/EBPβ was also implicated in the modulation of adipocyte differentiation by STAT3. Indeed, luciferase reporter assay experiments performed by Zhang *et al*. identified a direct binding of STAT3 to C/EBPβ during the early stages of the adipogenic process (K. G. Zhang 2011).

As discussed in Chapter 1, the study of McGillicuddy and colleagues evidenced the ability of IFN-γ to provoke insulin resistance in human adipocytes (McGillicuddy 2009). They also reported that the cytokine inhibits adipogenesis and lipid storage through down-regulating the expression of PPARγ, FA synthase, perilipin and adiponectin. The anti-adipogenic effect of IFN-γ had been reported nearly twenty years prior by Grégoire *et al*. in rodent pre-adipocytes (Gregoire

1992). Inhibiting in turn JAK1 and the JAK2 through pharmacological inhibitors allowed McGillicuddy and colleagues to conclude that JAK1-STAT1 activation – but not JAK2-STAT3 - is critical in the modulation of the anti-adipogenic action of IFN-γ. Indeed, blocking JAK1 signalling rescued the effect of the cytokine on adipocyte functions, while targeting JAK2 had no effect (McGillicuddy 2009).

III. 2. 4. Toll-like receptor 4 (TLR4), a point of overlap in palmitate- and IFN-induced pathways

In addition to investigating the effect of palmitate on the phosphorylation of STATs 1 and 3, the present chapter will also focus on a point of overlap between palmitate and IFN-γ signaling: TLR4. This 839 amino acids-long peptide is one of ten human and twelve murine homologs of type I transmembrane proteins characterised by a cytoplasmic domain containing a conserved region (the Toll/IL-1 receptor domain) and an extracellular domain featuring leucine-rich repeats. While most TLRs (including TLR4 and 2) are located on the cell surface, some are found on the surface of endosomal/lysosomal compartments (O'Neill 2013).

This class of proteins is principally involved in the induction of inflammatory cytokines as part of the immune system in response to various cues. TLR4 has been established as the primary receptor for the gram-negative bacterial outer membrane LPS (Faure 2001). The binding of LPS requires the association of TLR4 with myeloid differentiation factor-2 (MD-2), made distinctive by a β-cup fold, ideal for interacting with flat hydrophobic ligands such as LPS. Another modulator of TLR4 signalling is cluster of differentiation 14 (CD14). This leucine-rich repeat family

member recruits LPS to the TLR4-MD-2 complex thus triggering the downstream cascade illustrated in *figure 12* (B. a. Park 2013).

Upon ligand engagement, TLR4 interacts with its two pairs of adaptor proteins: myeloid differentiation primary response 88 (MyD88) and Toll-IL-1 resistance domain-containing adapter protein (TIRAP), and TIR domain-containing adapter-inducing IFN-β (TRIF) and a TRIF-related adapter molecule (TRAM) (Laird 2009). The recruitment of TIRAP to the membrane requires binding to $PI(4,5)P_2$ and allows cytosolic MyD88 to interact with TLR4. Once MyD88 is associated with TLR4, IL-1 receptor associated kinase 1 (IRAK1) and IRAK4 are recruited to the signalling complex (Laird 2009). While both pairs of adaptors mediate the activation of the MAPK and NF-κB cascades, TRIF/TRAM exclusively induces IRF3 activation and IFN-β production (Schilling 2013). Relevantly to the present work, many studies have reported that members of the TLR family are able to stimulate class IA PI3K. For instance, Ojaniemi and colleagues provide evidence that TLR4 promotes the formation of a PI3K-MyD88 complex, which in turn stimulates TLR4 downstream signalling (Ojaniemi 2003).

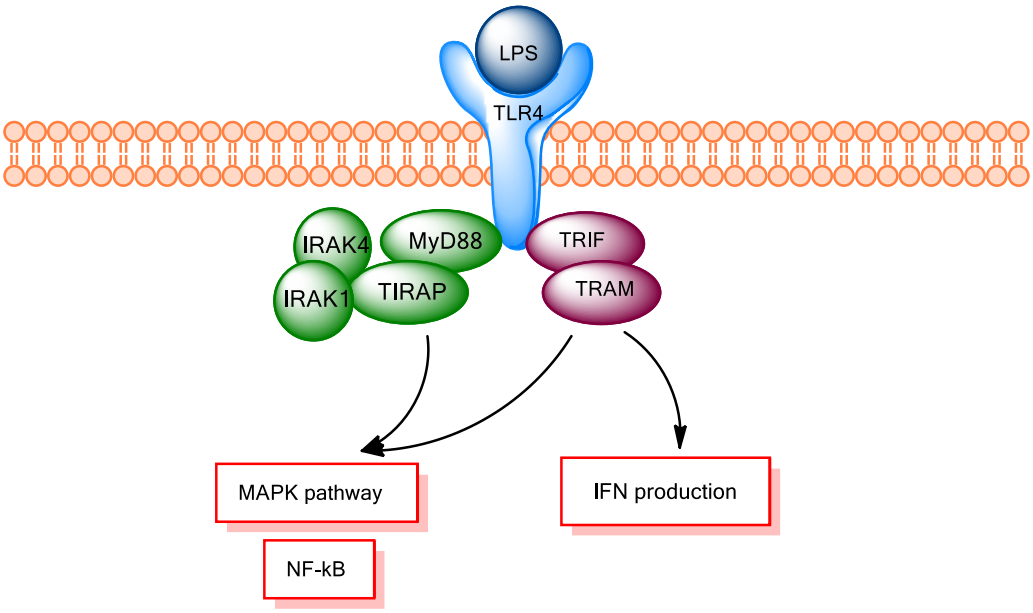

Figure 12. *Overview of the Toll-like receptor 4 (TLR4) signalling pathway.* Upon binding of LPS, TLR4 activates a pair of adaptor proteins: myeloid differentiation primary response 88 (MyD88) and Toll-interleukin-1 resistance domain-containing adapter protein (TIRAP), and TIR domain-containing adapter-inducing IFN-β (TRIF) and TRIF-related adapter molecule (TRAM). The former then recruits interleukin-1 receptor associated kinase 1 (IRAK1) and IRAK4 to the complex. Both pairs of adaptors allow the stimulation of the MAPK pathway and nuclear factor-κB (NF-κB), but only TRIF/TRAM induces IFN production.

A large body of evidence indicates a critical role for TLR4 in metabolic homeostasis through mediation of FFA signalling. Indeed, Shi and colleagues demonstrated that mice lacking TLR4 were protected from the deleterious effects of systemic lipid infusion on insulin signalling and glucose metabolism (Shi 2006). In addition, SFAs were also reported to activate the TLR4 cascade, thereby stimulating the rates of *de novo* ceramide synthesis in skeletal muscle cells (Holland 2011). Further emphasising the importance of TLR4 in palmitate-mediated ceramide synthesis, Schilling and colleagues reported a synergistic increase in *de novo* $C_{16:0}$-ceramide production in macrophages treated with a combination of palmitate and LPS (Schilling 2013). In addition, they demonstrated that FFA-induced

inflammatory response was reduced in the absence of the receptor in both adipocytes and macrophages (Shi 2006).

The same year, Song and colleagues established that *Tlr4* mRNA expression was enhanced during 3T3-L1 adipogenesis as well as in adipose tissue of obese *db/db* mice (M. K. Song 2006). LPS- or FFA-mediated stimulation of TLR4 was reported to stimulate NF-κB cascade along with the expression of pro-inflammatory cytokines (TNFα and IL-6) in the differentiated fat cells, which had become insulin resistant (M. K. Song 2006). More recently Kim and colleagues compared the impact of diet- and genetically-induced obesity in the activation of TLRs cascades (S. C. Kim 2012). Interestingly, it appears that although both types of obesity elicit the up-regulation of the TLR1, TLR4, TLR5, TLR8, TLR9 and TLR12 genes as well as their downstream targets in murine visceral adipose tissue, the magnitude of the effect is larger in diet-induced obesity.

Despite the many studies linking TLR4 to FFA-induced metabolic dysregulation, the molecular mechanisms involved remained unclear until 2012. That year Pal *et al.* provided strong evidence that TLR4 interacts with SFA through a liver secretory glycoprotein known as fetuin-A (FetA) thereby modulating SFA-induced insulin resistance (Pal 2012). Indeed, silencing *fetA* protected mice from the onset of HFD-induced insulin resistance. Furthermore, targeted mutation experiments revealed the ability of FetA to directly bind TLR4 through its galactoside terminal. Cleaving this terminal prevented the onset of FFA-induced insulin resistance. More recently, a direct interaction between palmitate and the

hydrophobic binding pocket of TLR4 adaptor protein MD-2 was evidenced by Nicholas *et al*. in human monocyte derived dentritic cells (Nicholas 2017).

Having highlighted the pivotal role of TLR4 in palmitate-induced insulin resistance, it is interesting to focus on the evidence supporting the TLR4 as an inducer of the IFN pathway. This topic has been extensively studied over the past decade. So far five of the ten human TLRs (TLR3, 4, 7, 8 and 9) have been implicated in the induction of type I IFNs (Noppert 2007). Despite some differences in downstream effectors, all TLRs were reported to activate the TANK binding kinase or the inhibitor of κB kinase ε. This permits the phosphorylation of IRFs, in turn leading to the stimulation of IFN genes. LPS, a TLR4 ligand was also found to activate a range of type II IFN response genes, including IFN-γ-inducible protein 10, as well as type I IFN induced gene such as *Isg15* (T. T. Kawai 2001). Likewise, IFN-γ was reported to induce TLR2 and TLR4 expression in human endothelial cells. Interestingly, IFN-γ and LPS were found to act synergistically: while both molecules induced TLR2 expression, their effect was enhanced when the cells were treated with IFN-γ and LPS simultaneously (Faure 2001).

In the same cell type, LPS-mediated activation of TLR4 was found to drive the phosphorylation of STAT3 (Ying 2013). In addition, TLR4 was shown to stimulate STAT1 in a PKCδ-dependent manner in macrophages (Rhee 2003). Such findings are in line with the study of Dasu and colleagues, showing that TLR4 expression was reduced upon inhibition of PKC-δ in human monocytes under diabetic conditions (Dasu 2008). Although most studies were carried out in macrophages, monocytes and dendritic cells, these results point at TLR4 as a key

element linking IFN- and palmitate-induced insulin resistance in adipocytes. The crosstalk between STATs and the NF-κB/pro-inflammatory cytokines signalling explored in this introduction suggests that these two models of insulin resistance are likely to integrate both TLR4 and STATs as cornerstones.

III. 3. Results of Chapter 3

III. 3. 1. Establishing cell models of FA- and IFN-γ-induced insulin resistance

III. 3. 1. 1. Using 3T3-L1 cell line

We first intended to reproduce the established model of palmitate- and IFN-γ-induced insulin resistance using 3T3-L1 pre-adipocytes, a prerequisite for further investigations. We assessed insulin sensitivity at the signalling level using Akt phosphorylation as a convenient read-out. As mentioned in the introduction, PDK1 mediates in the phosphorylation of Thr^{308}, while mTORC2 promotes the phosphorylation of Akt at Ser^{473} (Guo 2014). The phosphorylation of residues is necessary for maximal activation of Akt, thus both residues can be probed to assess insulin sensitivity. Because Foukas *et al.* had previously demonstrated the importance of p110α in the insulin signalling pathway of 3T3-L1 cells by investigating the phosphorylation of pAkt Thr^{308}, this residue was selected as read-out in the experiments presented in the present work (L. B. Foukas 2013).

Cells were treated with palmitate (500 μM) or IFN-γ (50 ng/mL) for 24 h and lysed following acute insulin stimulation (10 nM for 5 min). This preliminary experiment was performed in presence or absence of serum. As expected, p-Akt drastically increased in response to insulin, indicating enhanced PI3K activity *(Figures 13A* and *B*). However, contrary to the accepted molecular model, palmitate treatment drove a further Akt activation in insulin-stimulated cells. The magnitude of the increase was lesser in serum-deprived cells (< 10%) than in those treated in the presence of serum (30%). The effect of IFN-γ treatment on insulin-stimulated p-Akt levels also appeared to be impacted by serum deprivation: while cells treated in

serum containing medium showed a 27% increase in p-Akt signal compared to insulin control (*Figure 13A*), p-Akt levels in cells treated in serum free (SF) medium was decreased by 10% compared to insulin-treated control (*Figure 13B*).

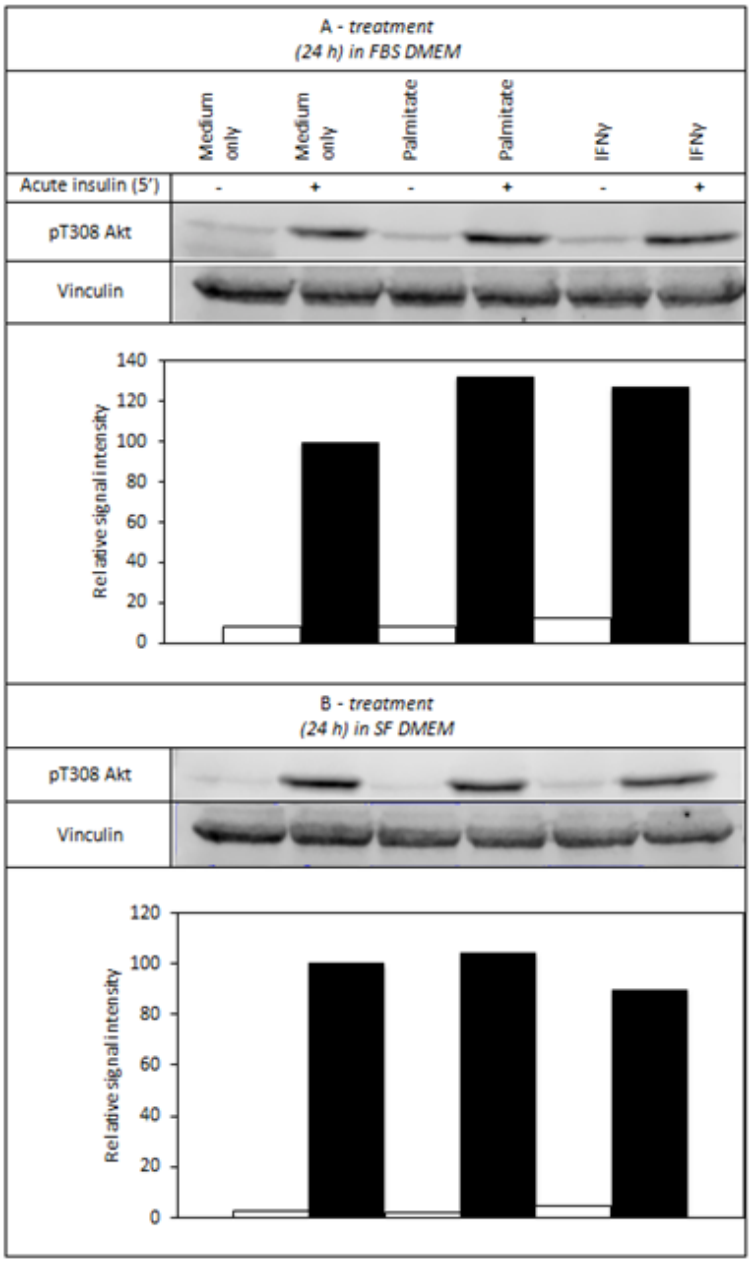

Figure 13. *Effect of palmitate and IFN-γ treatment on insulin sensitivity in **3T3-L1 pre-adipocytes**.* 3T3-L1 pre-adipocytes were treated for 24 h in 10% FBS/Dulbecco's modified eagle's medium (DMEM) (HG) (**A**) or SF DMEM (HG, 0.2% BSA) (**B**). Palmitate 500 µM was added to the medium (24 h treatment) (lanes 3 and 4) or IFN-γ 50 ng/mL (24 h treatment) (lanes 5 and 6). Insulin stimulation was with 10 nM for 5 min. In the presence of serum both treatments induced a slight increase in p-Akt levels. In the absence of serum palmitate treated cells showed a subtle increase in p-Akt compared to the untreated control, while there was a 10% decrease in p-Akt level in IFN-γ treated cells. Cells were lysed with 150 µL 1% triton X (TX)-100 lysis buffer. 110 µg of protein were loaded

per lane (10% sodium dodecyl sulfate [SDS]-acrylamide gel). Data shown are from a single experiment.

In order to magnify the effect of palmitate treatment while maintaining physiological significance, cells were treated in serum containing medium for 24 h followed by a 3 h-long serum starvation. The pre-adipocytes were then stimulated for 15 min with 100 nM insulin (*Figure 14A*). Under such conditions, the SFA induced a 50% decrease in p-Akt signal compared to insulin-stimulated control in line with the current paradigm. This effect fell short of reaching statistical significance using the one-way ANOVA ($F(4,14) = 45.65$, p-value = 0; Tukey HSD *post hoc* test between "insulin-stimulated control" and "insulin-stimulated, palmitate treatment": p-value = 0.11), however a paired student t-test produced a p-value of 0.04. Adding the p110α-selective inhibitor, A66, during treatment abrogated the palmitate-mediated inhibition, thus restoring Akt phosphorylation to insulin-stimulated control levels. When treated with A66 alone, the phosphorylation levels following insulin stimulation were more than doubled compared to the insulin-stimulated control. In light of the previous results (*Figure 13*), the IFN-γ treatment was carried out in SF media. The modest inhibition of insulin-stimulated Akt activity caused by the cytokine depicted in *figure 13B* could not be reproduced (*Figure 14B*). Nevertheless, when combined with A66, IFN-γ treatment promotes a two-fold increase of p-Akt levels following insulin stimulation compared to insulin control. Such activation of Akt appears to surpass that mediated by the inhibitor alone plus insulin.

The experiments presented above were repeated in mature 3T3-L1 adipocytes. We were able to show a statistically significant 40% decrease of insulin-stimulated p-Akt levels in response to palmitate treatment compared to insulin-stimulated control. Such effect was rescued by inhibiting p110α (*Figure 15A*). Having lowered the concentration of IFN-γ ten-fold to reproduce the conditions used by McGillicuddy and colleagues we recorded a statistically significant 25% reduction in insulin-stimulated p-Akt levels following IFN-γ treatment (*Figure 15B*) (McGillicuddy 2009). The trend suggests that A66 rescues the effect of the cytokine treatment although the difference between the insulin-stimulated p-Akt signal recorded following IFN-γ treatment alone and combined with A66 is not statistically significant (one-way ANOVA $F(4,18) = 40.64$, p-value = 0.00; Tukey HSD *post hoc* test between "insulin-stimulated, IFN-γ treatment" and "insulin-stimulated, IFN-γ + A66 treatment": p-value = 0.38). The impact of the cytokine treatment on the phosphorylation of Akt Ser^{473} was also examined and produced an inhibition of similar amplitude compared to the insulin-stimulated p-Akt levels (*data not shown*).

Although only one of the ten IFN-stimulated genes identified by the transcriptome analysis is induced by IFN-γ, the work presented in this thesis has extensively explored the downstream effect of IFN-γ. The reason for this was that treatment of 3T3-L1 adipocytes with IFN-α followed by acute insulin stimulation had no effect on the phosphorylation levels of Akt (*data not shown)*. Although, in our hands, IFN-γ had a minor impact on insulin stimulated Akt phosphorylation, IFN-γ-induced insulin resistance in both human and murine adipocytes had been demonstrated in the literature (McGillicuddy 2009). Moreover, IFN-γ can be produced by leukocytes infiltrating the adipose tissue, whereas a source of type I

IFNs in the adipose tissue has not been reported. Thus, because the aim of our study was to explore the overlaps between two pathways involved in the onset of insulin resistance, we opted for using IFN-γ in subsequent experiments.

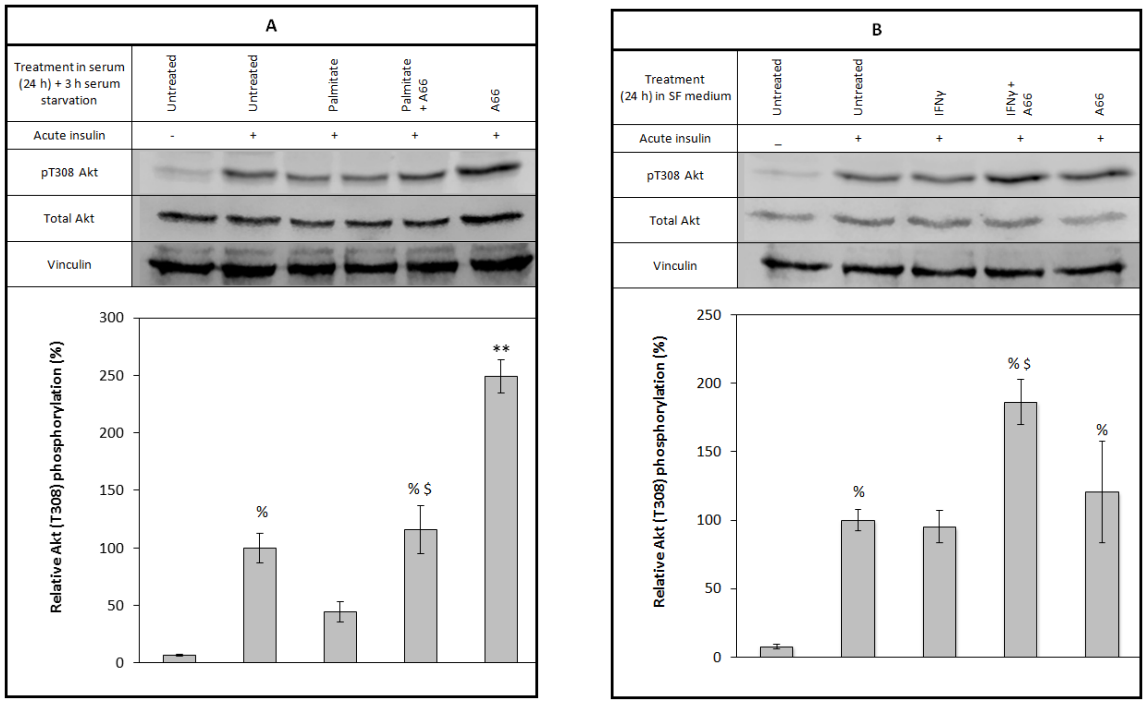

Figure 14. A. *p110α inhibition prevents palmitate-induced insulin resistance in **3T3-L1 pre-adipocytes***. The 50% decrease in p-Akt observed in palmitate treated cells (the difference between the insulin-stimulated control and the palmitate-treated cells was not statistically significant using the one-way analysis of variance [ANOVA] but the p-value was 0.04 when using a paired student t-test) is rescued by A66. 3T3-L1 pre-adipocytes were treated with palmitate (500 μM) (lanes 3 and 4) and A66 (0.5 μM) (lanes 4 and 5) in 10% FBS/DMEM (HG) for 24 h. Following a 3 h serum deprivation (SF DMEM, HG, 0.2% BSA), cells were stimulated with insulin (100 nM for 15 min). 50 μg of protein were loaded per lane (10% SDS-acrylamide gel). Data from four independent experiments. **B.** *IFN-γ treatment does not affect the phosphorylation of Akt Thr^{308} in **3T3-L1 pre-adipocytes***. Unlike palmitate, IFN-γ does not inhibit the phosphorylation of Akt. However, the cytokine considerably stimulates p-Akt in the presence of A66. 3T3-L1 pre-adipocytes were treated for 24 h in SF DMEM (HG, 0.2% BSA) with IFN-γ (200 ng/mL) (lanes 3 and 4) and A66 (1 μM) (lanes 4 and 5). Media were replaced with fresh serum-free media without any additives other than 0.2% BSA and cells were then acutely stimulated with insulin (100 nM for 15 min). 40 μg of protein were loaded per lane (10% SDS-acrylamide gel). Data from three independent experiments. For both *figures A* and *B*, cells were lysed with 75 μL 1% TX-100 lysis buffer per well and two 6-well plates were pooled together. Statistical difference between the untreated control and other treatments is indicated with %; statistical difference between the palmitate treatment and other treatments is indicated with $; ** denotes a treatment statistically different from all other treatments (p-value < 0.05). **Note:** previous work in our lab has shown that A66 alone does not cause a substantial increase in p-Akt Thr^{308} therefore this control was not included in the figure (L. B. Foukas 2013).

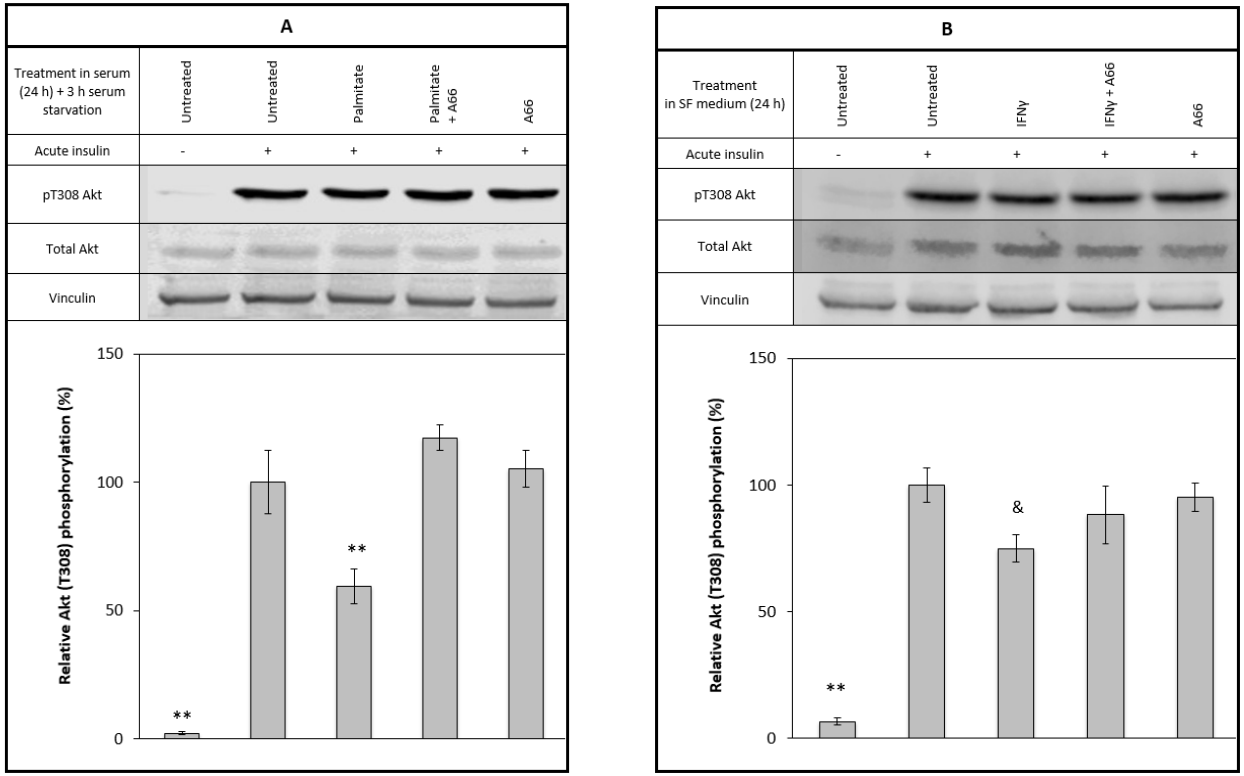

Figure 15. A. *Inhibition of PI3K p110α blocks palmitate-induced insulin resistance in **3T3-L1 mature adipocytes***. The decrease in p-Akt level observed when cells were treated with palmitate is rescued by A66. 3T3-L1 mature adipocytes were treated with palmitate (500 μM) (lanes 3 and 4) and A66 (1 μM) (lanes 4 and 5) in 10% FBS/DMEM (HG) for 24 h. Following a 3 h serum deprivation (SF DMEM, HG, 0.2% BSA), cells were stimulated with insulin (100 nM for 15 min). 100 μg of protein were loaded per lane (10% SDS-acrylamide gel). Data from three independent experiments. **B.** *IFN-γ induces insulin resistance in **3T3-L1 mature adipocytes***. Despite a trend in this direction, inhibition of PI3K p110α does not rescue the effect of the cytokine to statically significant levels. 3T3-L1 mature adipocytes were treated for 24 h in SF DMEM (HG, 0.2% BSA) with IFN-γ (20 ng/mL) (lanes 3 and 4) and A66 (1 μM) (lanes 4 and 5). Media were replaced with fresh serum-free media without any additives other than 0.2% BSA and cells were then acutely stimulated with insulin (100 nM for 15 min). 70 μg of protein were loaded per lane (10% SDS-acrylamide gel). Data from six independent experiments. For both *figures A* and *B*, cells were lysed with 100 μL 1% TX-100 lysis buffer per well. Statistical difference between the insulin stimulated control and other treatments is indicated with &; ** denotes a treatment statistically different from all other treatments (p-value < 0.05).

III. 3. 1. 2. Using hMADS cell line

The results presented in this next section sought to reproduce the experiments performed in 3T3-L1 in a human cell line, hMADS adipocytes (*Figures 16A, 16B, 17A* and *17B*). As shown in *figure 16A*, palmitate treatment of insulin-stimulated pre-adipocytes failed to elicit the expected decrease in p-Akt signal. However, IFN-γ seems to have an inhibitory effect (57% decrease in insulin-stimulated p-Akt compared to insulin-stimulated control), although this effect did not reach statistical significance. These cells were much more sensitive than the murine cells to A66 as combining palmitate or IFN-γ with the inhibitor produced considerable boost in insulin-stimulated p-Akt (3-fold increase) compared to the insulin-stimulated control. A66 alone drove a 4.5 fold increase in insulin-stimulated Akt phosphorylation.

The experiments presented in *figures 17A* and *B* performed in mature hMADS mirror those carried out in mature 3T3-L1 recorded in *figures 15A* and *B.* The human cells responded to the palmitate and A66 treatments similarly to the mouse cells, with the p110α inhibitor rescuing the deleterious effect of palmitate on insulin-stimulated p-Akt levels (*Figure 17A*). Although a similar trend could be observed with IFN-γ treatment, the cytokine did not affect significantly insulin-stimulated p-Akt levels compared to the insulin-stimulated control (*Figure 17B*). This experiment was repeated lowering insulin concentration (10 nM) to the order of magnitude used by Wada and colleagues (Wada 2011). However, still no effect of IFN-γ on p-Akt was observed (*data not shown*).

Table 10 summarises the findings exposed in this section: a model of palmitate-induced insulin resistance was successfully established in both 3T3-L1 and hMADS mature adipocytes, while that of IFN-γ-mediated insulin resistance could only be established in 3T3-L1 mature adipocytes. The trend of the data suggests that IFN-γ does inhibit p-Akt signal in hMADS pre- and mature adipocytes. Palmitate, on the other hand, appears to hinder Akt activation in 3T3-L1 pre-adipocytes.

Table 10. *Summary of the cell lines for which a model of palmitate- or IFN-γ-induced insulin resistance was successfully developed using p-Akt as read-out.* *The difference between the insulin-stimulated cells and the palmitate-treated cells reaches statistical significance using a paired student t-test but not the ANOVA.

Cell line	*Palmitate-induced insulin resistance*	*IFN-γ-induced insulin resistance*
3T3-L1 pre-adipocytes	✓ Validated model*	✗
3T3-L1 mature adipocytes	✓ Validated model	✓ Validated model
hMADS pre-adipocytes	✗	✗
hMADS mature adipocytes	✓ Validated model	✗

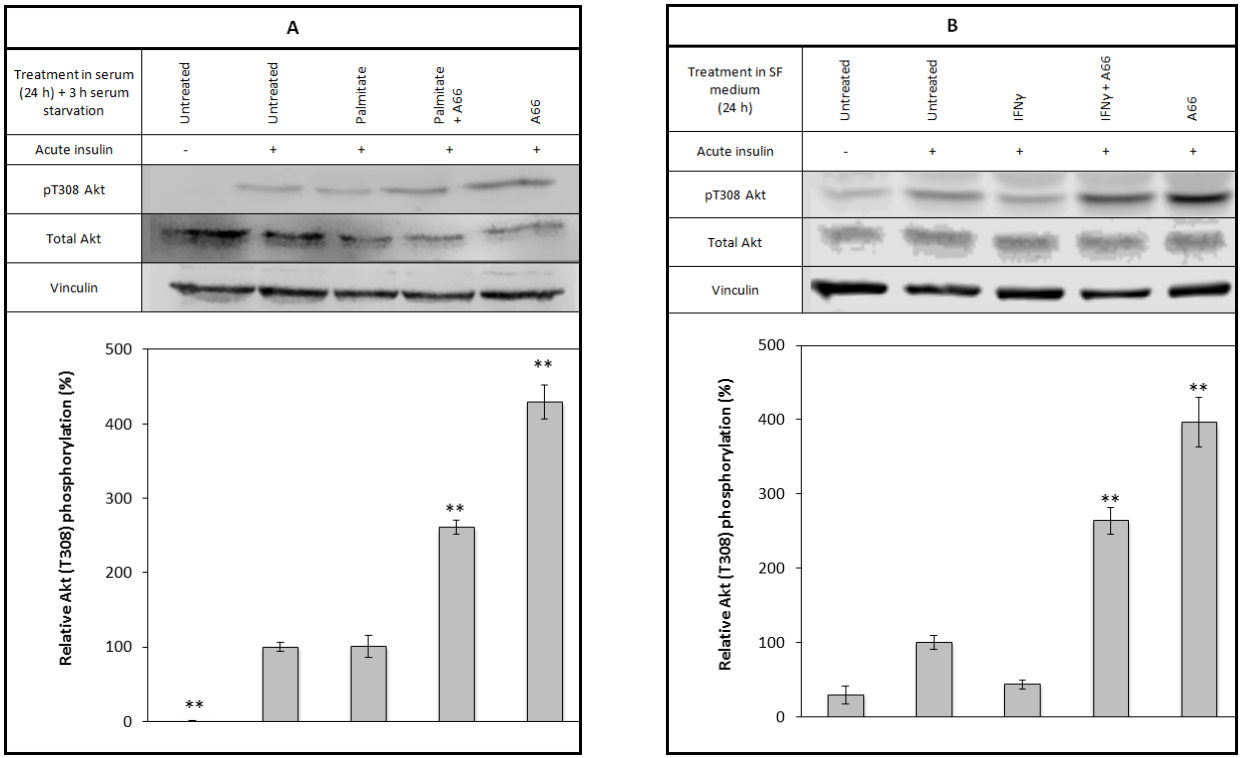

Figure 16. A. *Palmitate does not cause insulin-resistance in* ***hMADS pre-adipocytes***. p-Akt expression was unaltered after treating the cells with palmitate compared to the insulin-stimulated control. hMADS pre-adipocytes were treated with palmitate (500 µM) (lanes 3 and 4) and A66 (0.5 µM) (lanes 4 and 5) in complete DMEM (LG) for 24 h. Following a 3 h serum deprivation (SF DMEM, LG, 0.2% BSA), cells were stimulated with insulin (100 nM for 15 min). Cells were lysed with 75 µL 1% TX-100 lysis buffer per well and two 6-wells dishes plates were drawn together. 80 µg of protein were loaded per lane (10% SDS-acrylamide gel). **B.** *IFN-γ marginally inhibits the phosphorylation of Akt Thr*^{308} *in* ***hMADS pre-adipocytes****, however this effect falls short of statistical significance.* p-Akt expression was unaltered after treating the cells with palmitate compared to the insulin-stimulated control. hMADS pre-adipocytes were treated for 24 h in SF DMEM (LG, 0.2% BSA) with IFN-γ (20 ng/mL) (lanes 3 and 4) and A66 (1 µM) (lanes 4 and 5). Cells were then acutely stimulated with insulin (100 nM for 15 min) and lysed with 100 µL 1% TX-100 lysis buffer per 10 cm Ø dish. 34 µg of protein were loaded per lane (10% SDS-acrylamide gel). For both *figures A* and *B*, ** denotes a treatment statistically different from all other treatments. Data from three independent experiments.

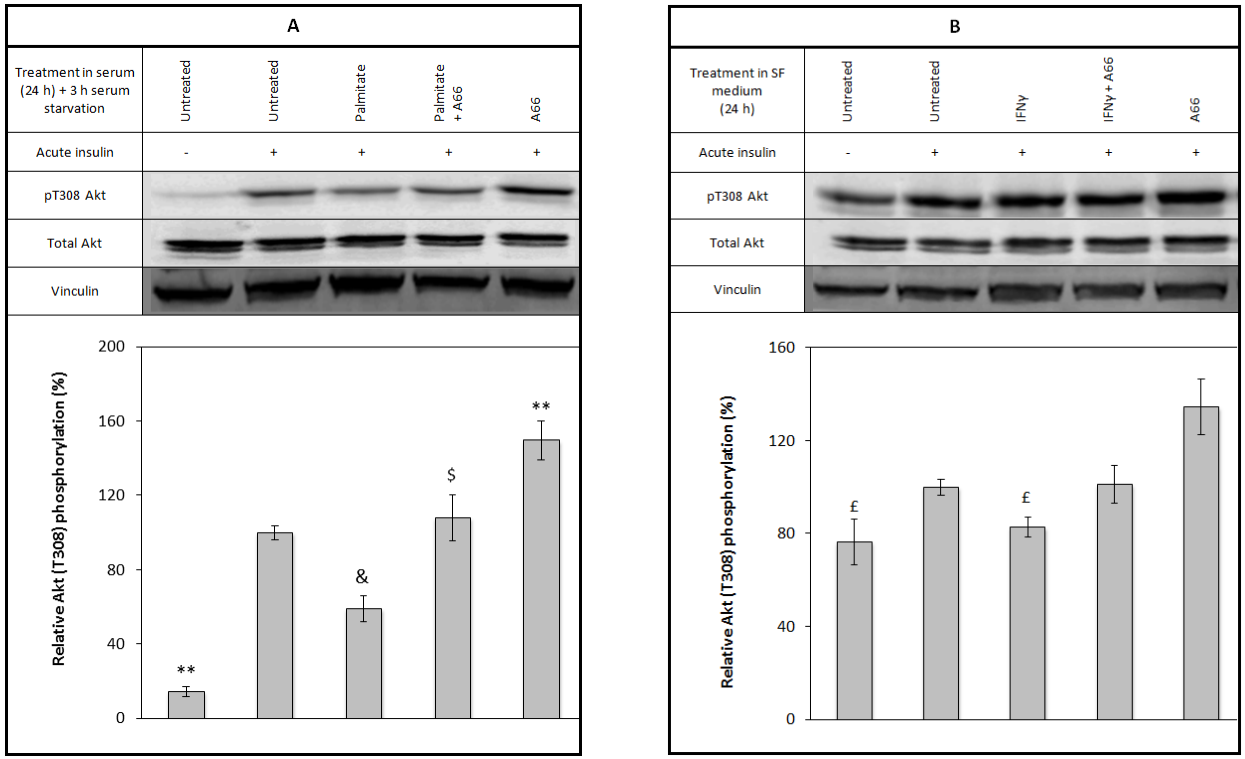

Figure 17. A. *Palmitate causes insulin resistance in* ***hMADS mature adipocytes****, rescued by inhibiting PI3K.* The decrease in p-Akt expression induced by palmitate is rescued by A66. hMADS mature adipocytes were treated with palmitate (500 µM) (lanes 3 and 4) and A66 (1 µM) (lanes 4 and 5) in complete DMEM (LG) for 24 h. Following a 3 h serum deprivation (SF DMEM, LG, 0.2% BSA), cells were stimulated with insulin (100 nM for 15 min). 100 µg of protein were loaded per lane (10% SDS-acrylamide gel). **B.** *IFN-γ does not cause insulin resistance in* ***hMADS mature adipocytes****.* p-Akt expression was unaltered by IFN-γ compared to the insulin-stimulated control. hMADS mature adipocytes were treated for 24 h in SF DMEM (LG, 0.2% BSA) with IFN-γ (20 ng/mL) (lanes 3 and 4) and A66 (1 µM) (lanes 4 and 5). Media were replaced with fresh serum-free media without any additives other than 0.2% BSA and cells were then acutely stimulated with insulin (100 nM for 15 min). 110 µg of protein were loaded per lane (10% SDS-acrylamide gel). For both *figures A* and *B*, cells were lysed with 75 µL 1% TX-100 lysis buffer per well. Statistical difference between the insulin stimulated control and other treatments is indicated with &; statistical difference between the palmitate treatment and other treatments is indicated with $; statistical difference between the A66 treatment and other treatments is indicated with £; ** denotes a treatment statistically different from all other treatments (p-value < 0.05). Data from four independent experiments.

III. 3. 2. The IFN signalling pathway effector STAT3, but not STAT1, is activated by palmitate treatment of adipocytes

Having investigated the stimulation of PI3K by palmitate and IFN-γ in the previous section, the following experiments focused on testing whether the SFA promotes activation of STAT1/3, found downstream of the IFN pathway. It has been shown that insulin resistance induced by IFN-γ treatment is mediated by the sustained activation of STAT1 and to a lesser extent STAT3, in both mouse 3T3-L1 and human Simpson-Golabi-Behmel syndrome (SGBS) adipocytes (Wada 2011, McGillicuddy 2009). Here, we sought to reproduce these findings and compare the effect of IFN-γ on STAT1/3 phosphorylation to that of palmitate. To this end, a time course experiment was performed in either serum-free or serum containing media, treating the cells for 24, 8, 4, 2 and 1 h with either palmitate (500 μM) or IFN-γ (20 ng/mL).

Four individual western blots were then run to study the phosphorylation patterns of STAT1 Tyr^{701}, STAT1 Ser^{727}, STAT3 Tyr^{705} and STAT3 Ser^{727}. As the presence of serum did not affect the response of the cells to treatment, we will present the results of the experiments performed in serum containing media for added physiological significance. However, unlike serum, the presence of BSA – used as a carrier for palmitate – did interfere with the phosphorylation of STATs. Indeed, both palmitate and the BSA control stimulated STAT3 to levels recorded in IFN-γ-treated cells (*data not shown*). Therefore the initial time course experiments were repeated using unconjugated palmitate instead of BSA-conjugated palmitate. A reason for this apparent BSA-mediated stimulation of STATs is likely due to LPS contamination of the BSA preparation, which as mentioned in the introduction of the

present chapter, is a well-established TLR4 ligand that can induce the phosphorylation of STAT1 and STAT3 (Rhee 2003, Ying 2013). Indeed, in 2009, Erridge and Samani were able to evidence that, in both macrophages and HEK 293T cells, the effect of SFA on TLR2/4 activation reflected LPS and other lipopeptide contamination found in the BSA employed in their experimental design (Erridge 2009). Such finding seeded a debate over the true role of SFAs in TLR signalling.

III. 3. 2. 1. Using 3T3-L1 cell line

Figures 18 and *19* present the time course experiment performed in 3T3-L1 pre-adipocytes, investigating STAT3 and STAT1 activation, respectively. In line with published data, we observed an increase in phosphorylation for both STAT proteins induced by IFN-γ. Consistent with the findings of McGillicuddy and colleagues, STAT3 stimulation was more modest than that of STAT1 (McGillicuddy 2009). Peak levels of tyrosine phosphorylation were recorded for both STAT1 and STAT3 at the 1 h time point with a 2,500 fold and a 2.5 fold increase, respectively, compared with the untreated control. On the other hand, serine phosphorylation peaked at the 24 h time point: p-STAT1 Ser^{727} and p-STAT3 Ser^{727} levels were multiplied by 5 and 2.5 compared with the untreated control, respectively. As shown from lanes 9 to 13, palmitate treatment failed to enhance STAT1/3 activity.

The same experimental protocol was also applied to 3T3-L1 differentiated adipocytes (*Figures 20* and 2*1*). Comparably to the trend noted in pre-adipocytes, IFN-γ triggers the activation of STAT1 and to a lesser extent STAT3. However, maximal phosphorylation levels are reached at different time points for the two cell

types. Indeed, in 3T3-L1 mature adipocytes the phosphorylation of STAT3 at Tyr^{705} and Ser^{727} residues culminates after 1 h of the cytokine treatment, while that of STAT1 at Tyr^{701} and Ser^{727} peaks at the 2 h time point. Now focusing on the effect of palmitate, it appears that the SFA fails to stimulate p-STAT3 Ser^{727}, p-STAT1 Tyr^{701} and p-STAT1 Ser^{727} levels over the time period investigated. Nevertheless, when considering the phosphorylation of STAT3 Tyr^{705}, it seems to induce a 3-fold increase at the 8 h time point compared to the untreated control.

Although this effect was not statistically significant when analysing the data using the Tukey HSD *post hoc* test (one-way ANOVA $F(12,50) = 5.81$, p-value = 0.00; Tukey HSD *post hoc* test between "untreated" and "8 h palmitate treatment": p-value = 0.27), the p-value obtained from the least significant difference (LSD) test did reach the significance threshold (LSD *post hoc* test between "untreated" and "8 h palmitate treatment": p-value = 0.00). This suggests that the change in phosphorylation observed, although modest, might be real. It would therefore be interesting to further investigate the molecular mechanisms underlying the palmitate-mediated modulation of p-STAT3 Tyr^{705} levels following an 8 h treatment.

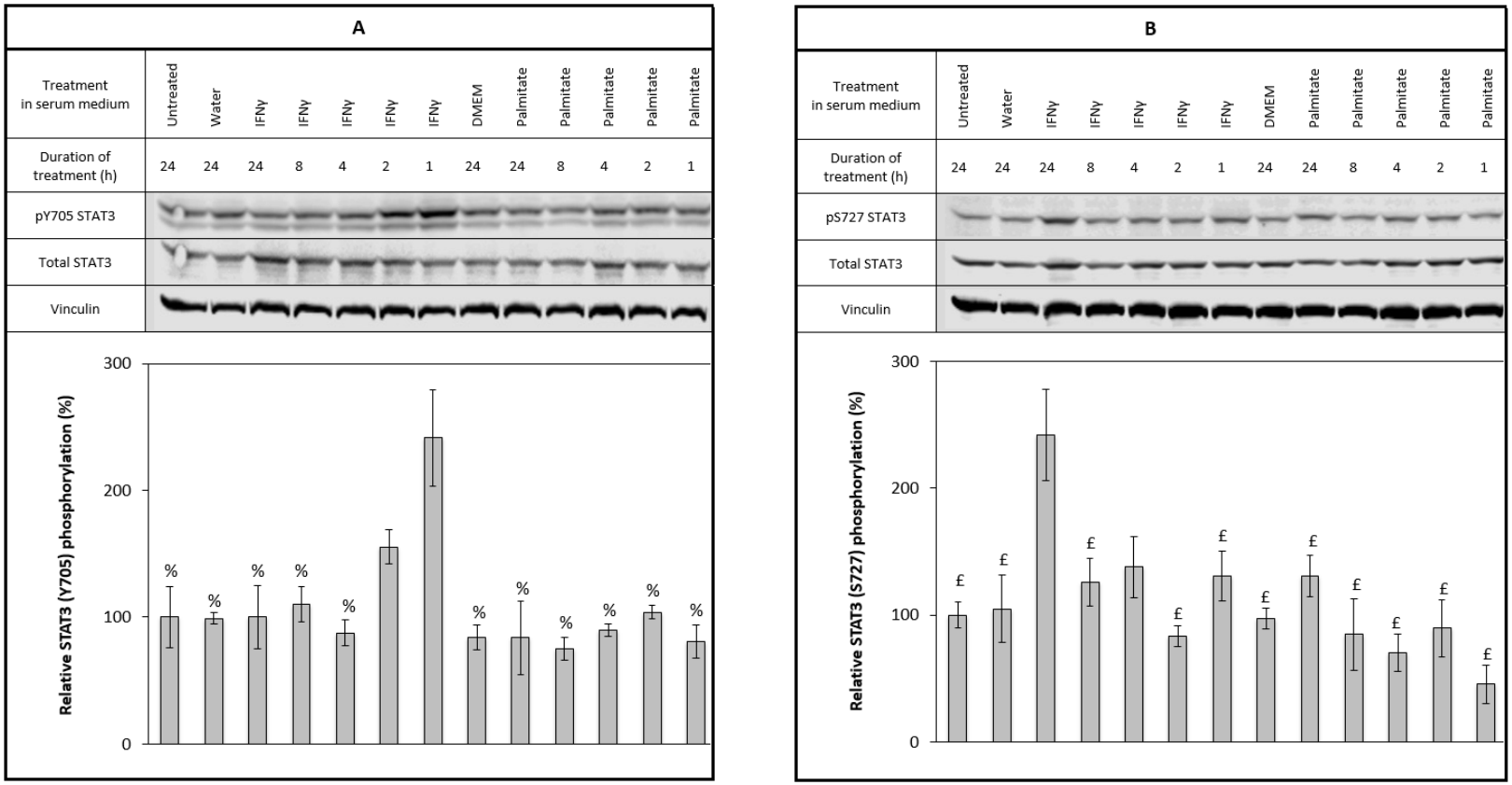

Figure 18. A. *IFN-γ but not palmitate induces the phosphorylation of STAT3 Tyr^{705} in **3T3-L1 pre-adipocytes**, however this effect falls short of statistical significance*. **B.** *IFN-γ but not palmitate induces the phosphorylation of STAT3 Ser^{727} in 3T3-L1 pre-adipocytes.* For both *figure A* and *B*, 3T3-L1 pre-adipocytes were treated with IFN-γ (20 ng/mL) (lanes 3 to 7), unconjugated palmitate (500 µM) (lanes 9 to 13) in 10% FBS/DMEM (HG). Equivalent volumes of MilliQ water (40 µL) (lane 2) and DMEM (LG) (1 mL) (lane 8) were used as control for IFN and palmitate treatments, respectively. Cells were lysed with 150 µL 1% TX-100 lysis buffer per 10 cm Ø dish. 79 µg and 66 µg of protein were loaded per lane in *figures A* and *B*, respectively (10% SDS-acrylamide gel). Statistical difference between the 24 h IFN-γ treatment and other treatments is indicated with £; statistical difference between the 1 h IFN-γ treatment and other treatments is indicated with % (p-value < 0.05). Data from three independent experiments.

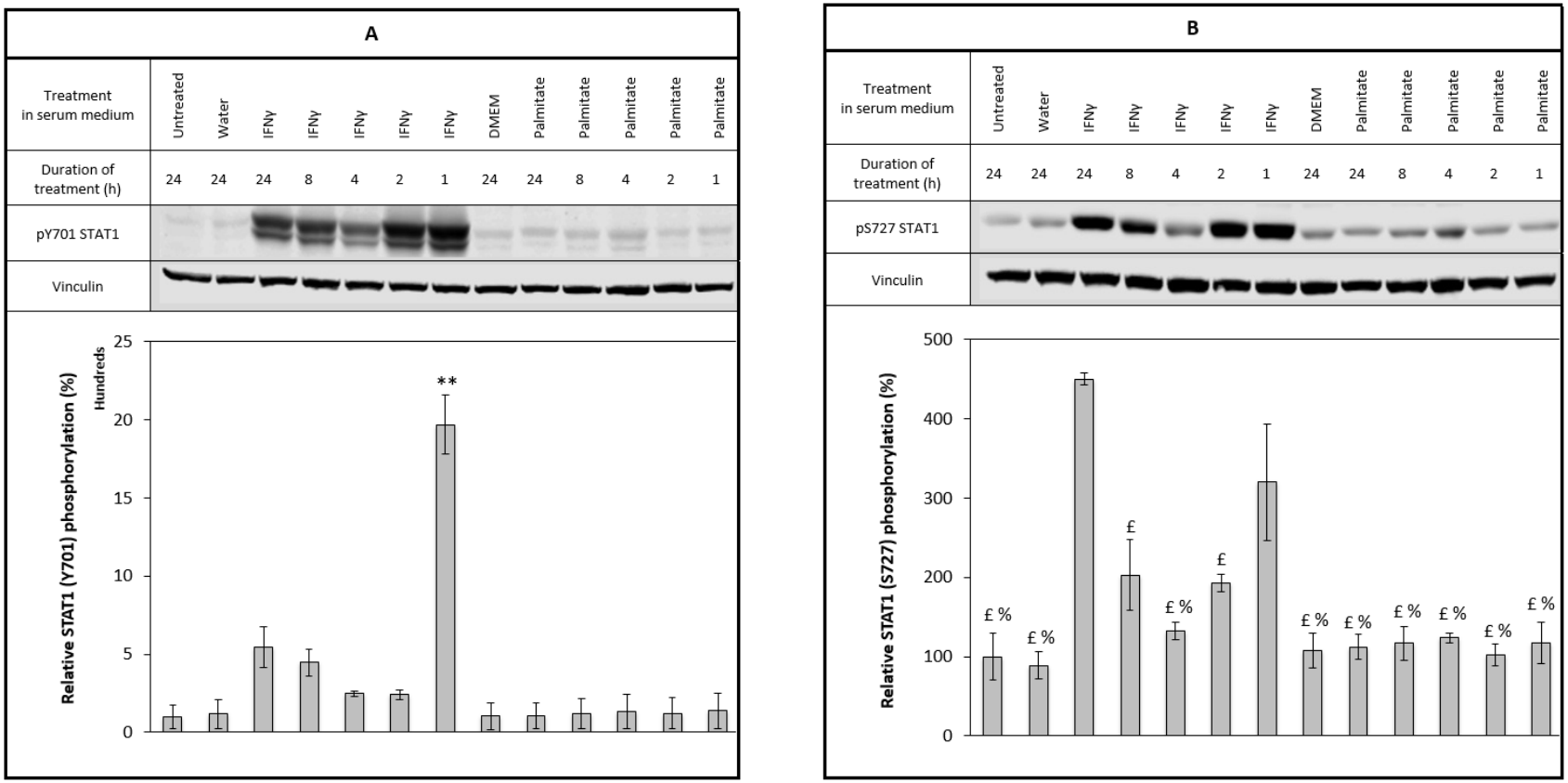

Figure 19. *IFN-γ but not palmitate induces the phosphorylation of both STAT1 Tyr[701] (A) and STAT1 Ser[727] (B) in* ***3T3-L1 pre-adipocytes***. For both *figures A* and *B*, 3T3-L1 pre-adipocytes were treated with IFN-γ (20 ng/mL) (lanes 3 to 7), unconjugated palmitate (500 µM) (lanes 9 to 13) in 10% FBS/DMEM (HG). Equivalent volumes of MilliQ water (40 µL) (lane 2) and DMEM (LG) (1 mL) (lane 8) were used as control for IFN and palmitate treatments, respectively. Cells were lysed with 100 µL 1% TX-100 lysis buffer per 10 cm Ø dish. 50 µg of protein were loaded per lane (10% SDS-acrylamide gel). Statistical difference between the 24 h IFN-γ treatment and other treatments is indicated with £; statistical difference between the 1 h IFN-γ treatment and other treatments is indicated with %; ** denotes a treatment statistically different from all other treatments (p-value < 0.05). Data from three independent experiments.

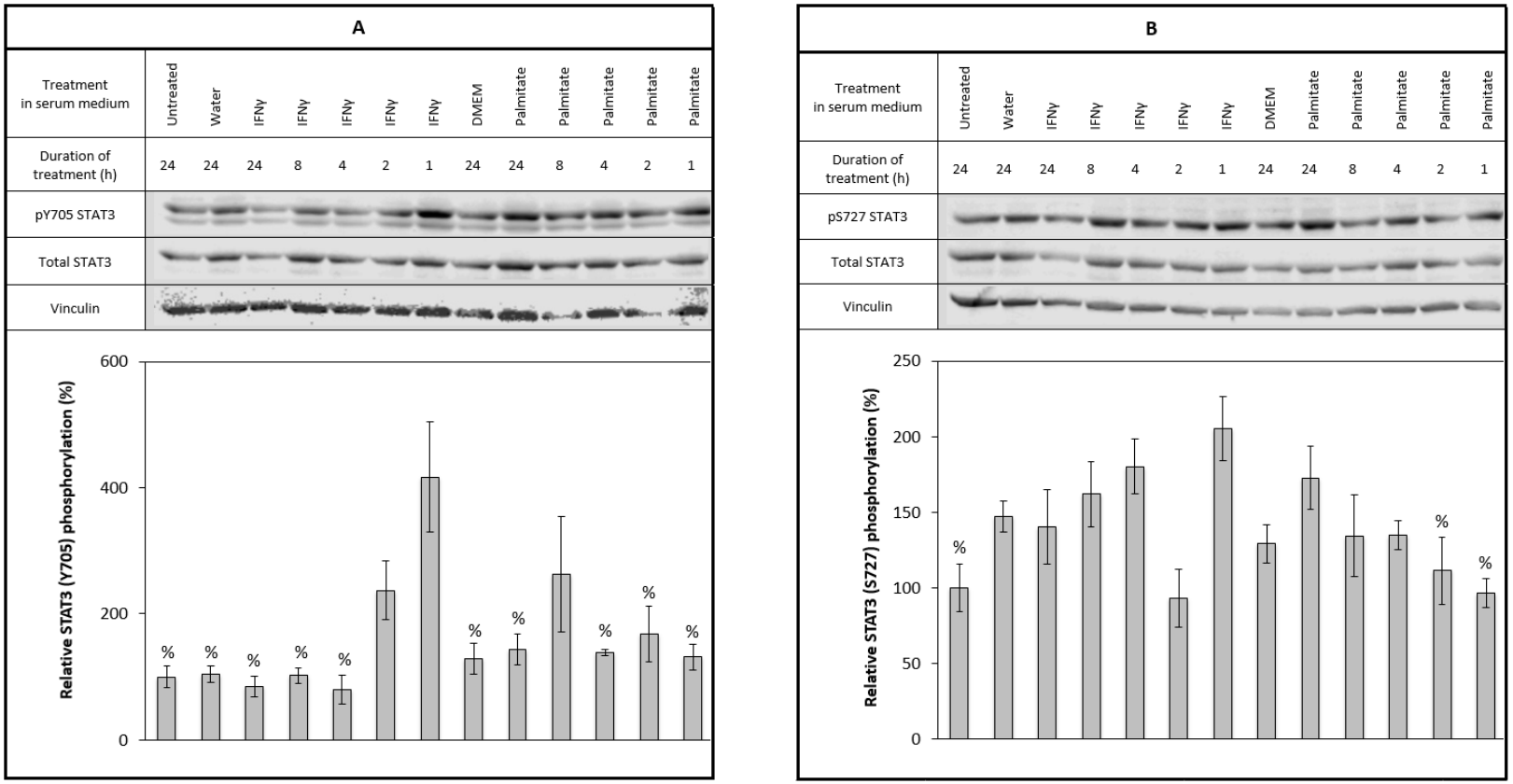

Figure 20. A. *Both IFN-γ and palmitate induce the phosphorylation of STAT3 Tyr[705] in* ***3T3-L1 mature adipocytes***. **B.** *IFN-γ but not palmitate induces the phosphorylation of STAT3 Ser[727] in 3T3-L1 mature adipocytes.* For both *figures A* and *B*, 3T3-L1 mature adipocytes were treated (HG) with IFN-γ (20 ng/mL) (lanes 3 to 7), unconjugated palmitate (500 µM) (lanes 9 to 13) in 10% FBS/DMEM. Equivalent volumes of MilliQ water (8 µL) (lane 2) and DMEM (LG) (200 µL) (lane 8) were used as control for IFN and palmitate treatments, respectively. Cells were lysed with 80 µL 1% TX-100 lysis buffer per well. 93 µg of protein were loaded per lane (10% SDS-acrylamide gel). Statistical difference between the 1 h IFN-γ treatment and other treatments is indicated with % (p-value < 0.05). Data from four independent experiments.

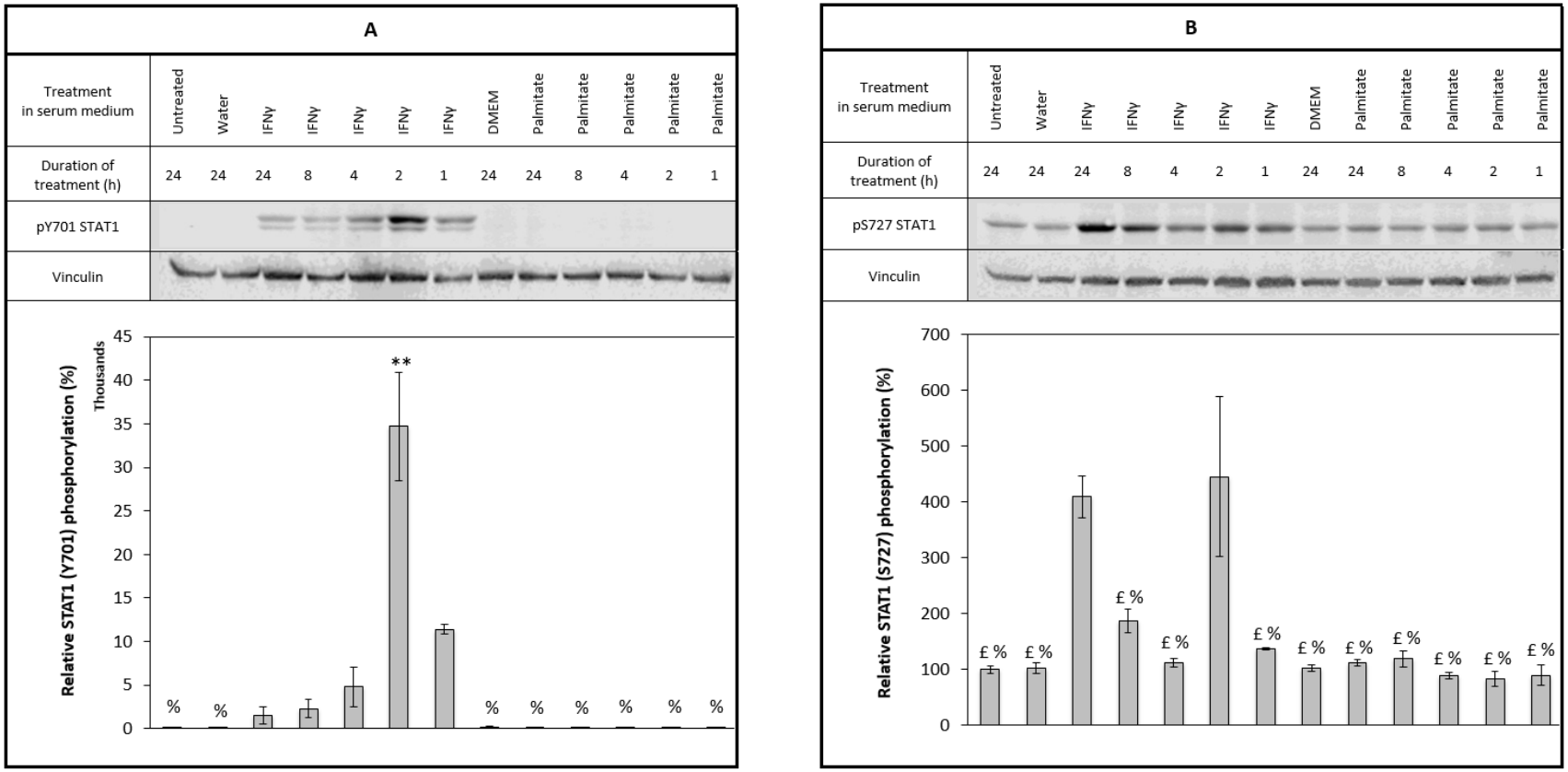

Figure 21. *IFN-γ but not palmitate induces the phosphorylation of both STAT1 Tyr[701] (A) and STAT1 Ser[727] (B) in* ***3T3-L1 mature adipocytes***. For both *figures A* and *B*, 3T3-L1 mature adipocytes were treated with IFN-γ (20 ng/mL) (lanes 3 to 7), unconjugated palmitate (500 µM) (lanes 9 to 13) in 10% FBS/DMEM (HG). Equivalent volumes of MilliQ water (8 µL) (lane 2) and DMEM (LG) (200 µL) (lane 8) were used as control for IFN and palmitate treatments, respectively. Cells were lysed with 80 µL 1% TX-100 lysis buffer per well. 82 µg of protein were loaded per lane (10% SDS-acrylamide gel). Statistical difference between the 24 h IFN-γ treatment and other treatments is indicated with £; statistical difference between the 1 h IFN-γ treatment and other treatments is indicated with %; ** denotes a treatment statistically different from all other treatments (p-value < 0.05). Data from three independent experiments.

III. 3. 2. 2. Using hMADS cell line

The experiments discussed in the previous section were reproduced in the hMADS cell line using both pre- and mature adipocytes. As shown in *figures 22* and *23*, similar trends can be noticed in human and mouse undifferentiated cells. IFN-γ yielded a much stronger stimulation of STAT1 compared to STAT3, plummeting after 1 h of treatment for all residues. While, phosphorylation levels at STAT3 Tyr^{705} are multiplied 5-fold in the presence of IFN-γ, those at STAT1 Tyr^{701} increased by over 1500%. As for the serine residues, p-STAT3 Ser^{727} levels doubled after treatment for 1 h with the cytokine - although this effect did not reach statistical significant – and p-STAT1 Ser^{727} levels were multiplied by a factor of 5. Neither STAT1 nor STAT3 was activated by the SFA.

Figures 24 and *25* present the response to IFN-γ and palmitate treatments of differentiated hMADS cells. As expected, IFN promoted the phosphorylation of STAT1 Tyr^{701} (13-fold increase at 1 h) and to a lesser degree STAT3 Tyr^{705} (2-fold increase at 1 h). Yet, although the cytokine did stimulate p-STAT1 Ser^{727} 7-fold after 2 h of treatment, its effect on p-STAT3 Ser^{727} seemed to be inhibitory with a 40% decrease compared to untreated control at the same time point (note that this difference was not statistically significant). Palmitate also reduced the basal phosphorylation of STAT3 Ser^{727} compared to the untreated control after 4 h and 1 h of treatment. However, when compared to the 24 h DMEM treated condition, no such difference could be recorded, suggesting that this palmitate-mediated effect is unlikely to be real (*Figure 24B*).

Table 11 recapitulates our findings on palmitate-mediated activation of STAT1 and STAT3 gathered so far in both 3T3-L1 and hMADS. Overall, STAT1 activity does not appear to be induced by the SFA unlike STAT3. This could indicate that palmitate does not stimulate the STAT pathway through the up-regulation of IFN secretion as this would entail both STAT proteins being activated.

Table 11. *Summary of the effect of palmitate treatment on STAT1 and STAT3 phosphorylation in mouse and human cell lines.* *effect not statistically significant when the data was analysed with the one-way ANOVA.

Cell line	***3T3-L1 pre-adipocytes***	***3T3-L1 mature adipocytes***	***hMADS pre-adipocytes***	***hMADS mature adipocytes***
p-STAT1 Ser^{727}	✗	✗	✗	✗
p-STAT1 Tyr^{701}	✗	✗	✗	✗
p-STAT3 Ser^{727}	✗	✗	✗	✗
p-STAT3 Tyr^{705}	✗	✓ 163% increase after 8 h *versus* untreated control (*)	✗	✗

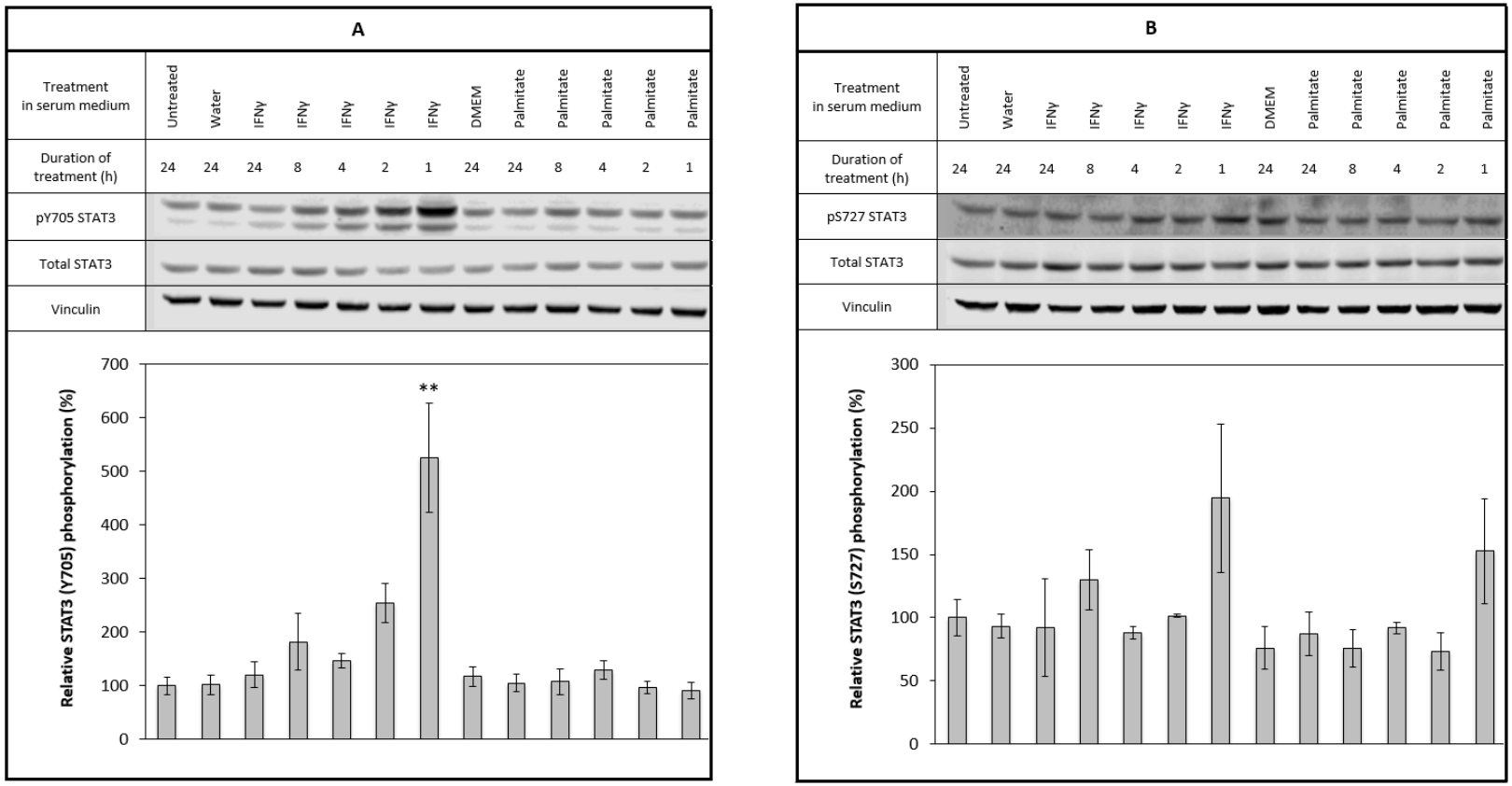

Figure 22. A. *IFN-γ but not palmitate induces the phosphorylation of STAT3 Tyr[705] in* ***hMADS pre-adipocytes****.* **B.** *Neither IFN-γ nor palmitate induces the phosphorylation of STAT3 Ser[727] in hMADS pre-adipocytes.* For both *figures A* and *B*, hMADS pre-adipocytes were treated with IFN-γ (20 ng/mL) (lanes 3 to 7), unconjugated palmitate (500 µM) (lanes 9 to 13) in complete DMEM (LG). Equivalent volumes of MilliQ water (40 µL) (lane 2) and DMEM (LG) (1 mL) (lane 8) were used as control for IFN and palmitate treatments, respectively. Cells were lysed with 100 µL 1% TX-100 lysis buffer per 10 cm Ø dish. 39 µg of protein were loaded per lane (10% SDS-acrylamide gel). ** denotes a treatment statistically different from all other treatments (p-value < 0.05). Data from three independent experiments.

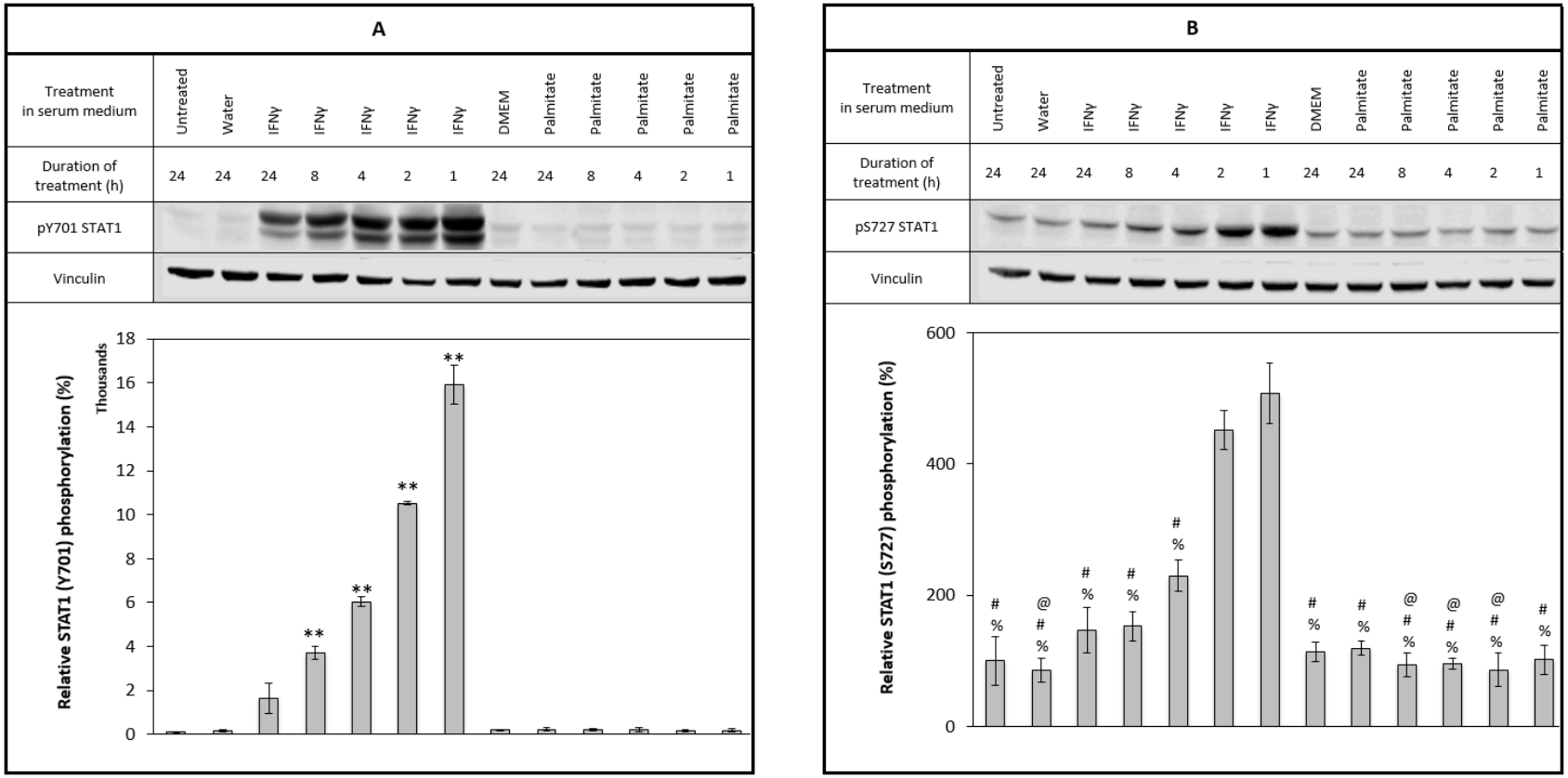

Figure 23. *IFN-γ but not palmitate induces the phosphorylation of both STAT1 Tyr^{701} (A) and STAT1 Ser^{727} (B) in* ***hMADS pre-adipocytes***. For both *figures A* and *B*, hMADS pre-adipocytes were treated with IFN-γ (20 ng/mL) (lanes 3 to 7), unconjugated palmitate (500 µM) (lanes 9 to 13) in complete DMEM (LG). An equivalent volume of MilliQ water was used as control for the IFN-γ treatments (40 µL) (lane 2) and an equivalent volume of DMEM (LG) was used as control for the palmitate treatments (1 mL) (lane 8). Cells were lysed with 100 µL 1% TX-100 lysis buffer per 10 cm Ø dish. 39 µg of protein were loaded per lane (10% SDS-acrylamide gel). Statistical difference between the 4 h IFN-γ treatment and other treatments is indicated with @; statistical difference between the 2 h IFN-γ treatment and other treatments is indicated with #; statistical difference between the 1 h IFN-γ treatment and other treatments is indicated with %; ** denotes a treatment statistically different from all other treatments (p-value < 0.05). Data from three independent experiments.

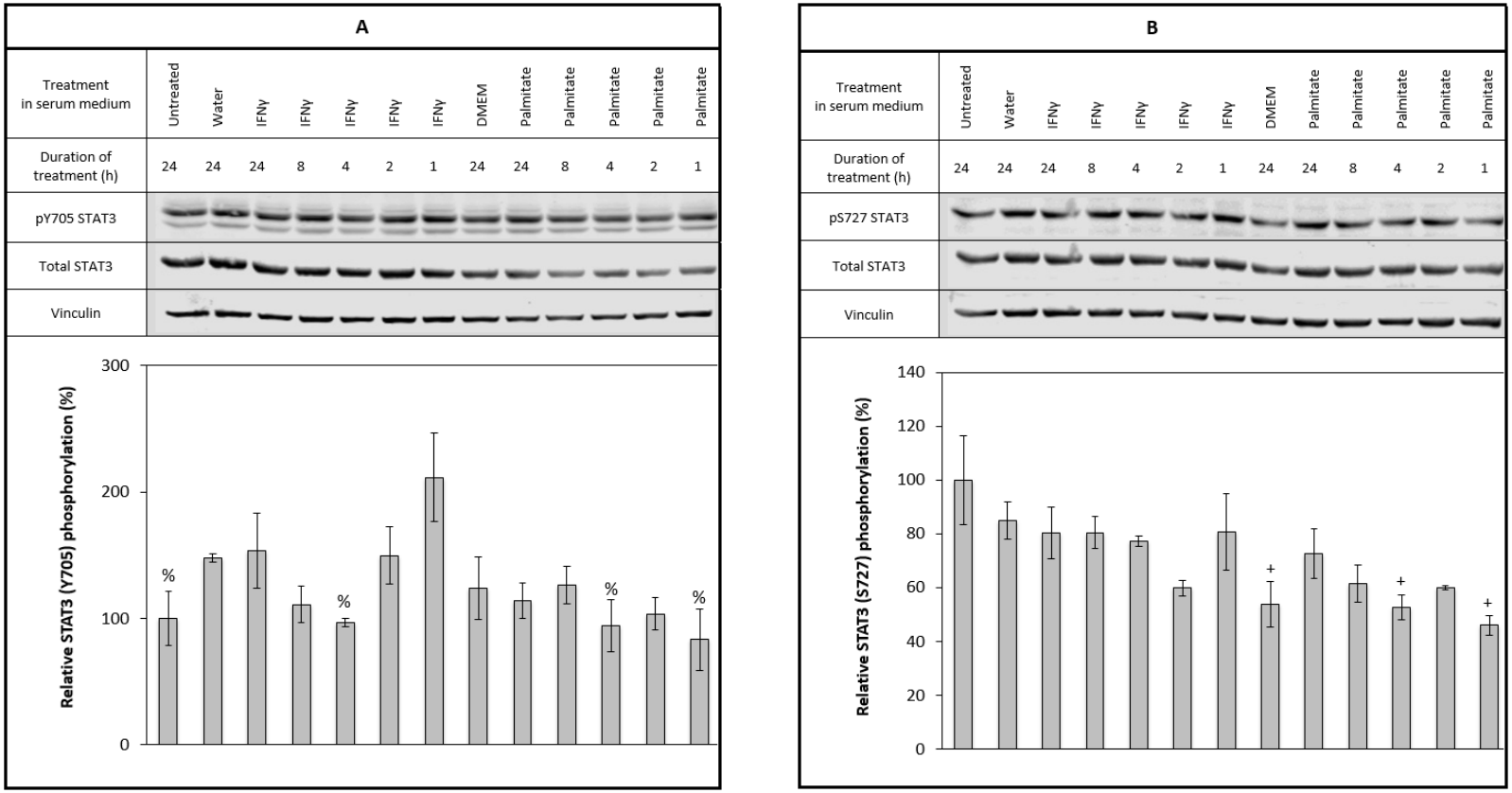

Figure 24. A. *IFN-γ but not palmitate induces the phosphorylation of STAT3 Tyr[705] in* ***hMADS mature adipocytes***. **B.** *IFN-γ and palmitate inhibit the phosphorylation of STAT3 Ser[727] in hMADS mature adipocytes.* For both *figures A* and *B*, hMADS mature adipocytes were treated with IFN-γ (20 ng/mL) (lanes 3 to 7), unconjugated palmitate (500 µM) (lanes 9 to 13) in complete DMEM (LG). Equivalent volumes of MilliQ water (8 µL) (lane 2) and DMEM (LG) (200 µL) (lane 8) were used as control for IFN and palmitate treatments, respectively. Cells were lysed with 80 µL 1% TX-100 lysis buffer per well. 46 µg of protein were loaded per lane (10% SDS-acrylamide gel). Statistical difference between the untreated control and other treatments is indicated with +; statistical difference between the 1 h IFN-γ treatment and other treatments is indicated with % (p-value < 0.05). Data from three independent experiments.

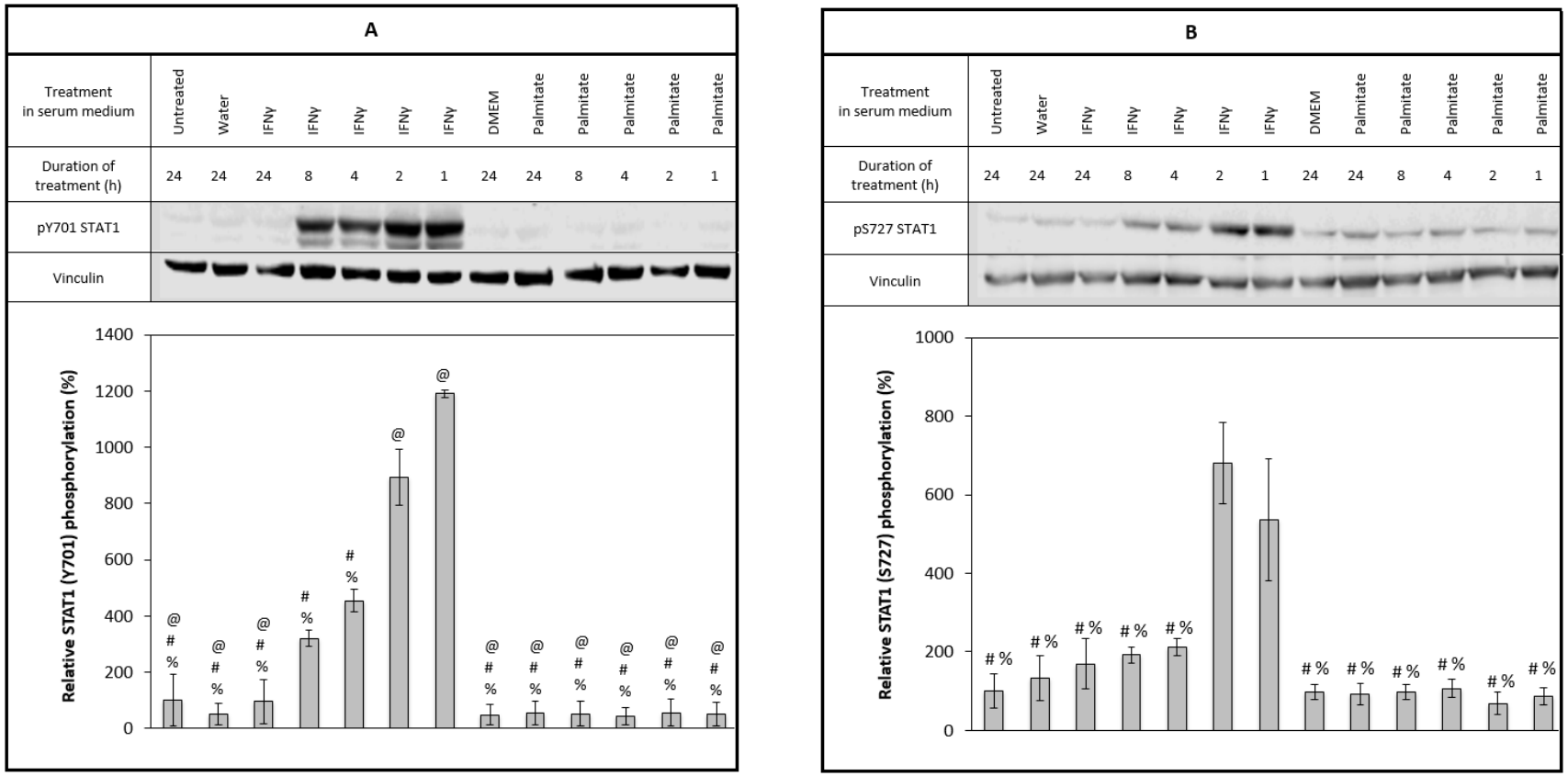

Figure 25. *IFN-γ but not palmitate induces the phosphorylation of both STAT1 Tyr[701] (A) and STAT1 Ser[727] (B) in* ***hMADS mature adipocytes***. For both *figures A* and *B*, hMADS mature adipocytes were treated with IFN-γ (20 ng/mL) (lanes 3 to 7), unconjugated palmitate (500 µM) (lanes 9 to 13) in complete DMEM (LG). Equivalent volumes of MilliQ water (8 µL) (lane 2) and DMEM (LG) (200 µL) (lane 8) were used as control for IFN and palmitate treatments, respectively. Cells were lysed with 80 µL 1% TX-100 lysis buffer per well. 24 µg of protein were loaded per lane (10% SDS-acrylamide gel). Statistical difference between the 4 h IFN-γ treatment and other treatments is indicated with @; statistical difference between the 2 h IFN-γ treatment and other treatments is indicated with #; statistical difference between the 1 h IFN-γ treatment and other treatments is indicated with % (p-value < 0.05). Data from three independent experiments.

III. 3. 3. Palmitate modulates the STAT pathway independently of IFN secretion

The results presented in the previous section suggest that palmitate has an effect on the activity of STAT3 but not STAT1 through a mechanism independent of IFN-γ secretion. To validate this hypothesis, we sought to confirm that palmitate did not trigger STAT1 phosphorylation over a shorter time course. The following section therefore compares the effect of the SFA on STAT1 (as well as STAT3) after 1 h, 30 min, 15 min and 5 min of treatment to the stimulation resulting from treating the cells for 1 h with IFN-γ. *Figures 26* to *33* clearly show that, across the cell lines tested, palmitate fails to promote the short-term activation of STAT3 and, more importantly, STAT1. This data seems to signify that the molecular mechanism by which palmitate modulates STAT3 phosphorylation occurs independently of IFN-γ secretion.

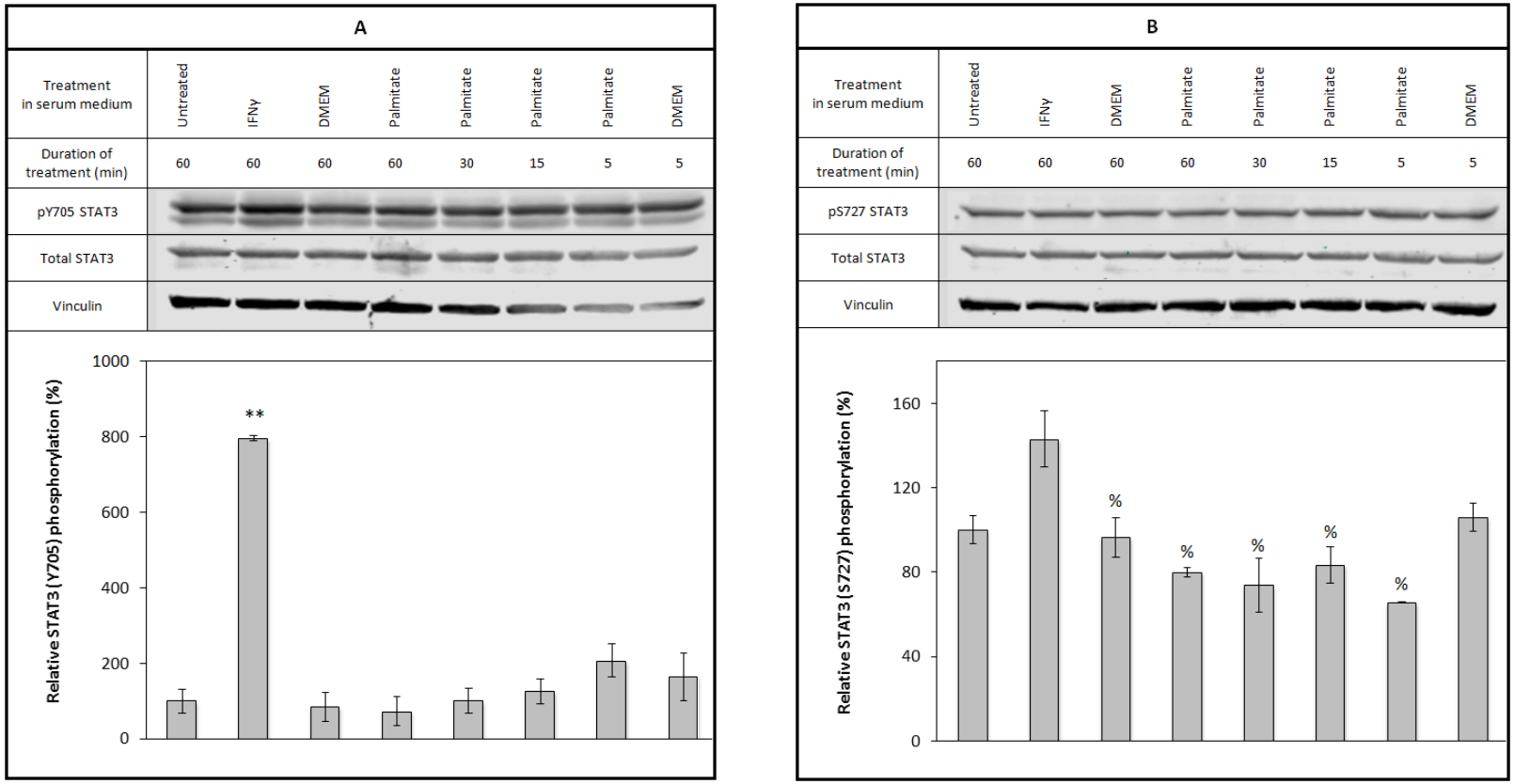

Figure 26. *Palmitate fails to induce the phosphorylation of STAT3 Tyr[705] (A) and STAT3 Ser[727] (B) in **3T3-L1 pre-adipocytes** over a short time frame.* For both *figures A* and *B*, 3T3-L1 pre-adipocytes were treated with IFN-γ (20 ng/mL) (lane 2), unconjugated palmitate (500 µM) (lanes 4 to 7) in 10% FBS/DMEM (HG). An equivalent volume of DMEM (LG) was used as control for the palmitate treatments (400 µL) (lanes 3 and 8). Cells were lysed with 100 µL 1% TX-100 lysis buffer per 6 cm Ø dish. 79 µg of protein were loaded per lane (10% SDS-acrylamide gel). Statistical difference between the 60 min IFN-γ treatment and other treatments is indicated with %; ** denotes a treatment statistically different from all other treatments (p-value < 0.05). Data from three independent experiments.

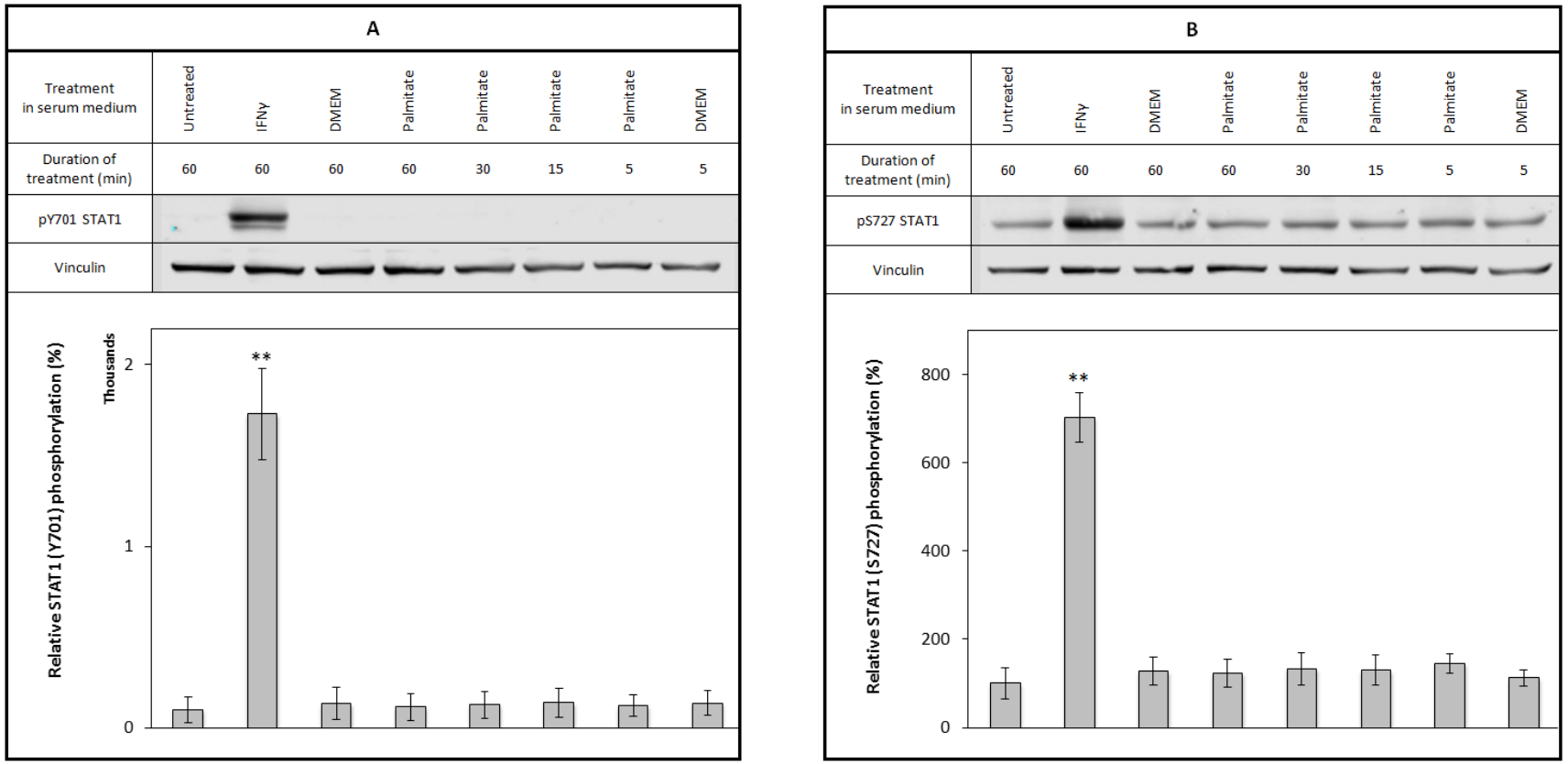

Figure 27. *Palmitate fails to induce the phosphorylation of STAT1 Tyr^{701} (A) and STAT1 Ser^{727} (B) in **3T3-L1 pre-adipocytes** over a short time frame*. For both *figures A* and *B*, 3T3-L1 pre-adipocytes were treated with IFN-γ (20 ng/mL) (lane 2), unconjugated palmitate (500 µM) (lanes 4 to 7) in 10% FBS/DMEM (HG). An equivalent volume of DMEM (LG) was used as control for the palmitate treatments (400 µL) (lanes 3 and 8). Cells were lysed with 100 µL 1% TX-100 lysis buffer per 6 cm Ø dish. 26 µg of protein were loaded per lane (10% SDS-acrylamide gel). ** denotes a treatment statistically different from all other treatments (p-value < 0.05). Data from three independent experiments.

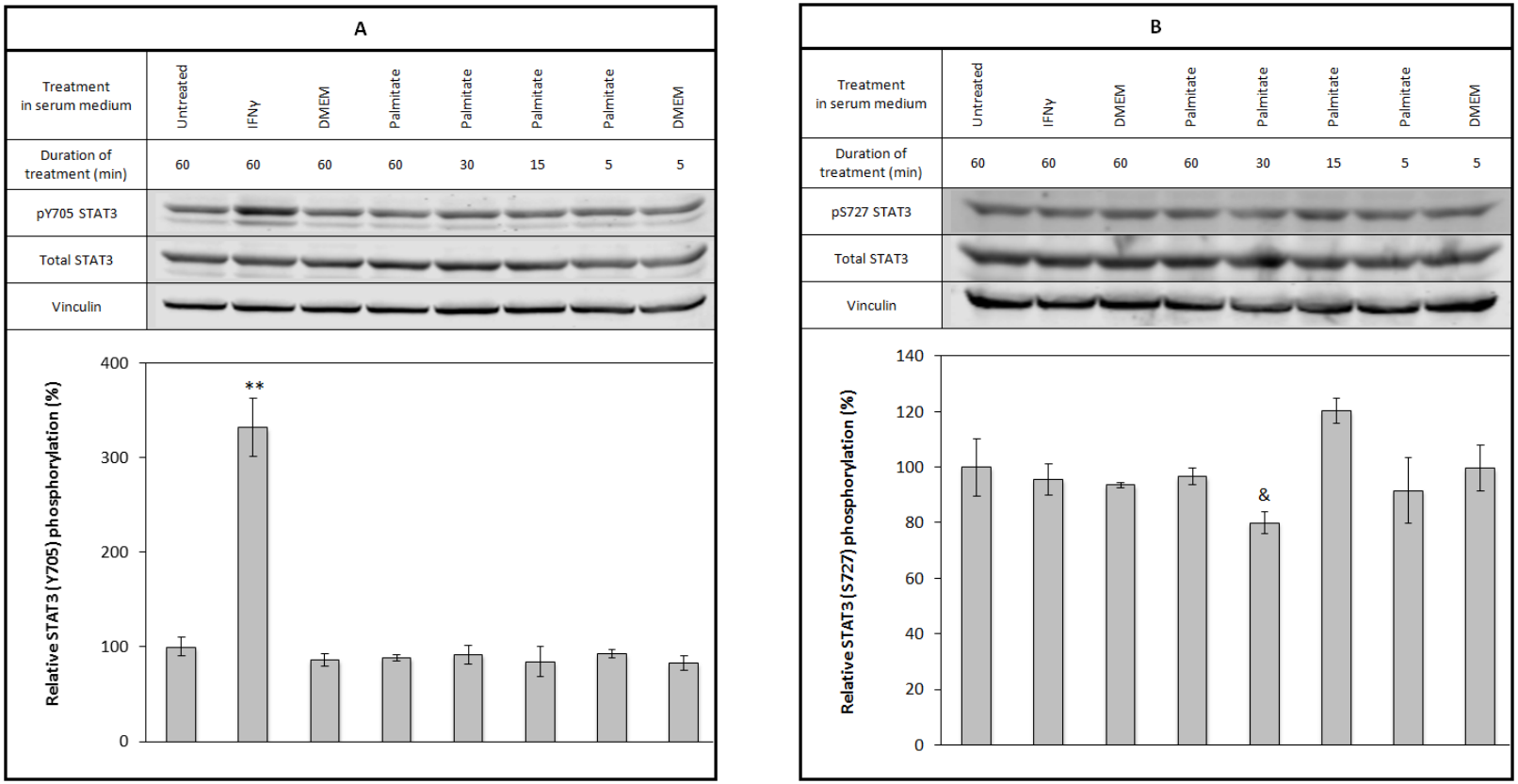

Figure 28. *Palmitate fails to induce the phosphorylation of STAT3 Tyr[705] (A) and STAT3 Ser[727] (B) in* ***3T3-L1 mature adipocytes*** *over a short time frame.* For both *figures A* and *B*, 3T3-L1 mature adipocytes were treated with IFN-γ (20 ng/mL) (lane 2), unconjugated palmitate (500 µM) (lanes 4 to 7) in 10% FBS/DMEM (HG). An equivalent volume of DMEM (LG) was used as control for the palmitate treatments (200 µL) (lanes 3 and 8). Cells were lysed with 80 µL 1% TX-100 lysis buffer per well. 70 µg of protein were loaded per lane (10% SDS-acrylamide gel). Statistical difference between the 15 min palmitate treatment and other treatments is indicated with &; ** denotes a treatment statistically different from all other treatments (p-value < 0.05). Data from three independent experiments.

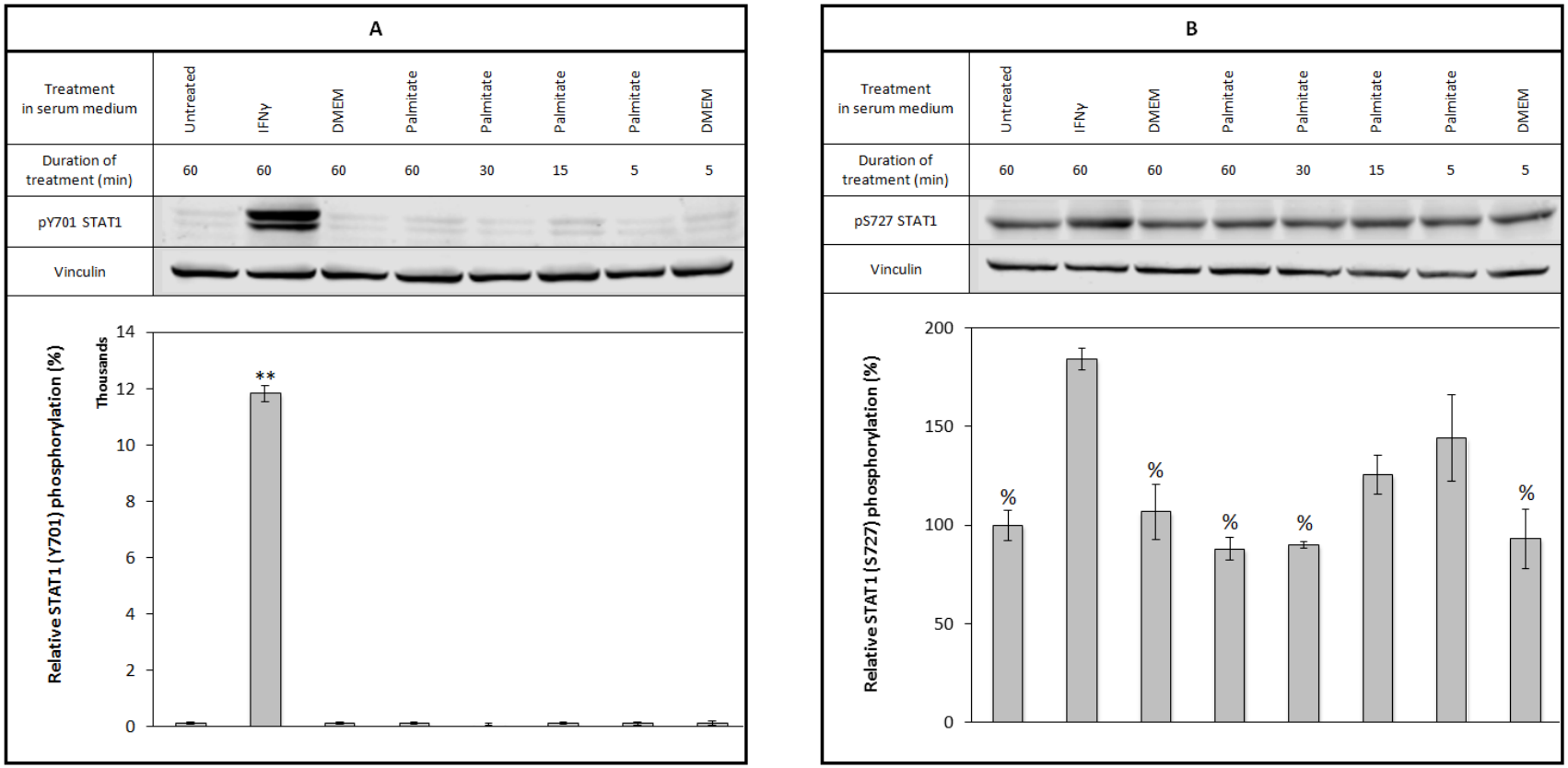

Figure 29. *Palmitate fails to induce the phosphorylation of STAT1 Tyr^{701} (A) and STAT1 Ser^{727} (B) in **3T3-L1 mature adipocytes** over a short time frame*. For both *figure A* and *B*, 3T3-L1 mature adipocytes were treated with IFN-γ (20 ng/mL) (lane 2), unconjugated palmitate (500 µM) (lanes 4 to 7) in 10% FBS/DMEM (HG). An equivalent volume of DMEM (LG) was used as control for the palmitate treatments (200 µL) (lanes 3 and 8). Cells were lysed with 80 µL 1% TX-100 lysis buffer per well. 70 µg and 78 µg of protein were loaded per lane for *figures A* and *B*, respectively (10% SDS-acrylamide gel). Statistical difference between the 60 min IFN-γ treatment and other treatments is indicated with %; ** denotes a treatment statistically different from all other treatments (p-value < 0.05). Data from three independent experiments.

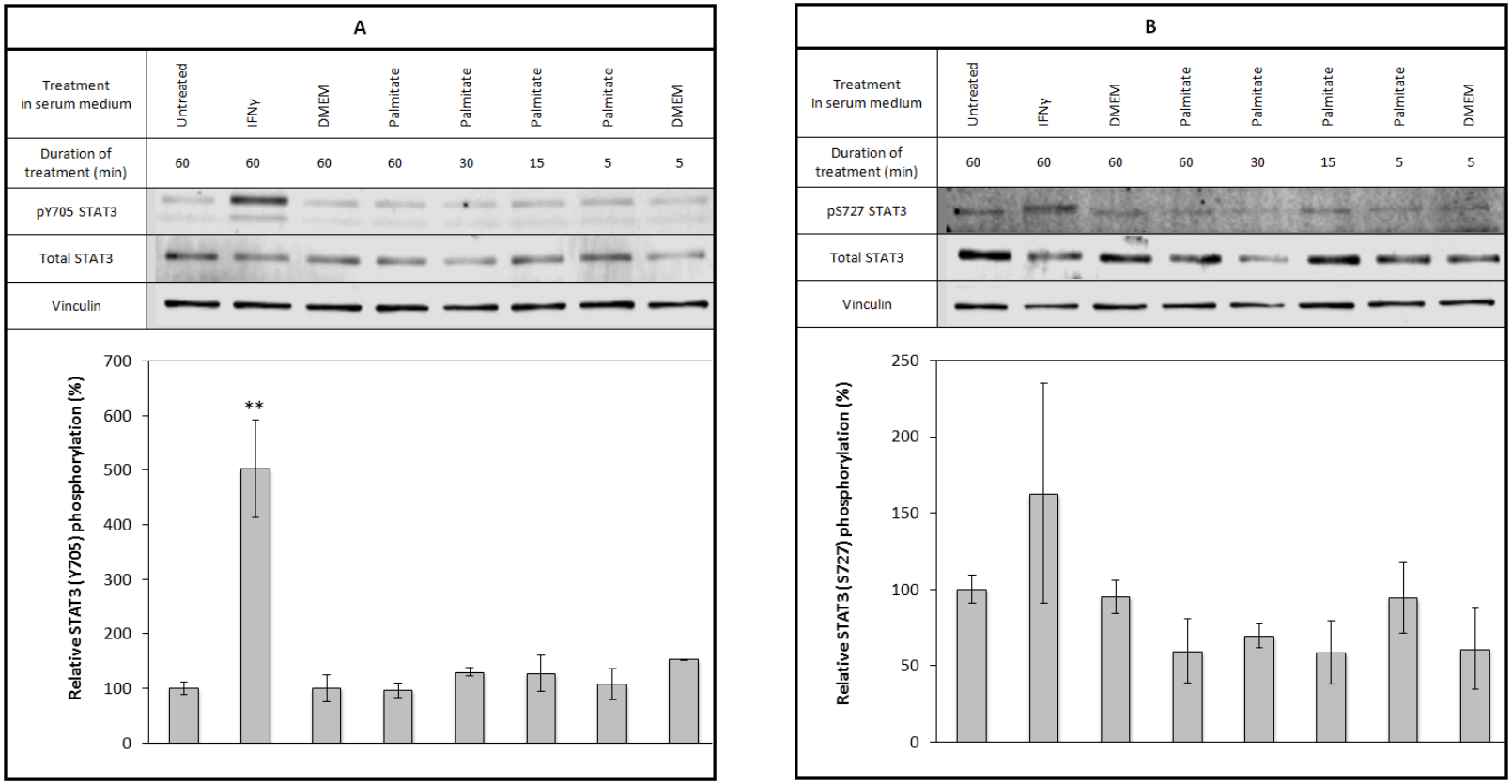

Figure 30. *Palmitate fails to induce the phosphorylation of STAT3 Tyr^{705} (A) and STAT3 Ser^{727} (B) in* ***hMADS pre-adipocytes*** *over a short time frame*. For both *figures A* and *B*, hMADS pre-adipocytes were treated with IFN-γ (20 ng/mL) (lane 2), unconjugated palmitate (500 µM) (lanes 4 to 7) in complete DMEM (LG). An equivalent volume of DMEM (LG) was used as control for the palmitate treatments (400 µL) (lanes 3 and 8). Cells were lysed with 100 µL 1% TX-100 lysis buffer per 6 cm Ø dish. 5 µg of protein were loaded per lane (10% SDS-acrylamide gel). ** denotes a treatment statistically different from all other treatments (p-value < 0.05). Data from three independent experiments.

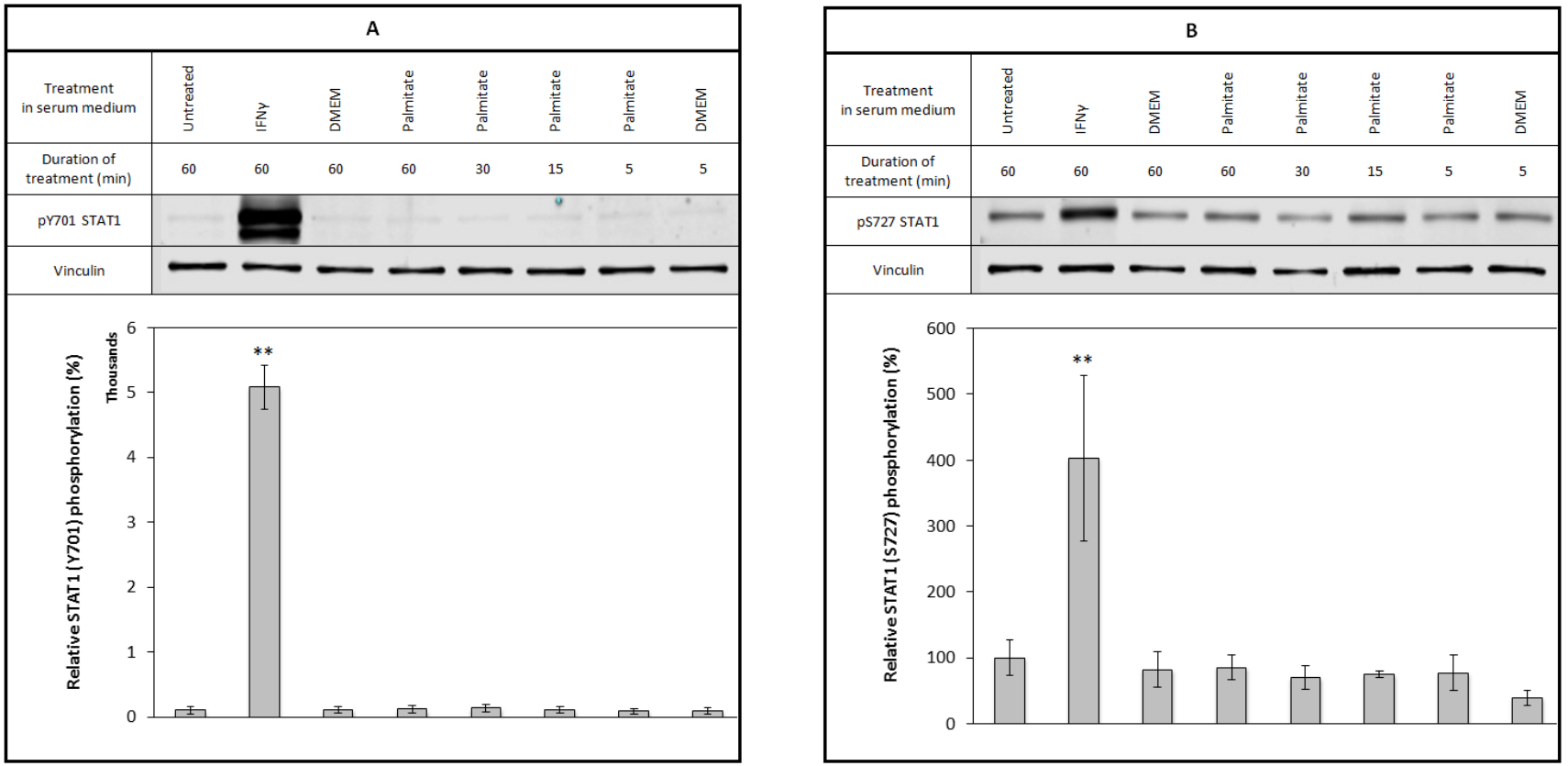

Figure 31. *Palmitate fails to induce the phosphorylation of STAT1 Tyr^{701} (A) and STAT1 Ser^{727} (B) in* ***hMADS pre-adipocytes*** *over a short time frame*. For both *figures A* and *B*, hMADS pre-adipocytes were treated with IFN-γ (20 ng/mL) (lane 2), unconjugated palmitate (500 µM) (lanes 4 to 7) in complete DMEM (LG). An equivalent volume of DMEM (LG) was used as control for the palmitate treatments (400 µL) (lane 3 and 8). Cells were lysed with 100 µL 1% TX-100 lysis buffer per 6 cm Ø dish. 4 µg of protein were loaded per lane (10% SDS-acrylamide gel). ** denotes a treatment statistically different from all other treatments (p-value < 0.05). Data from three independent experiments.

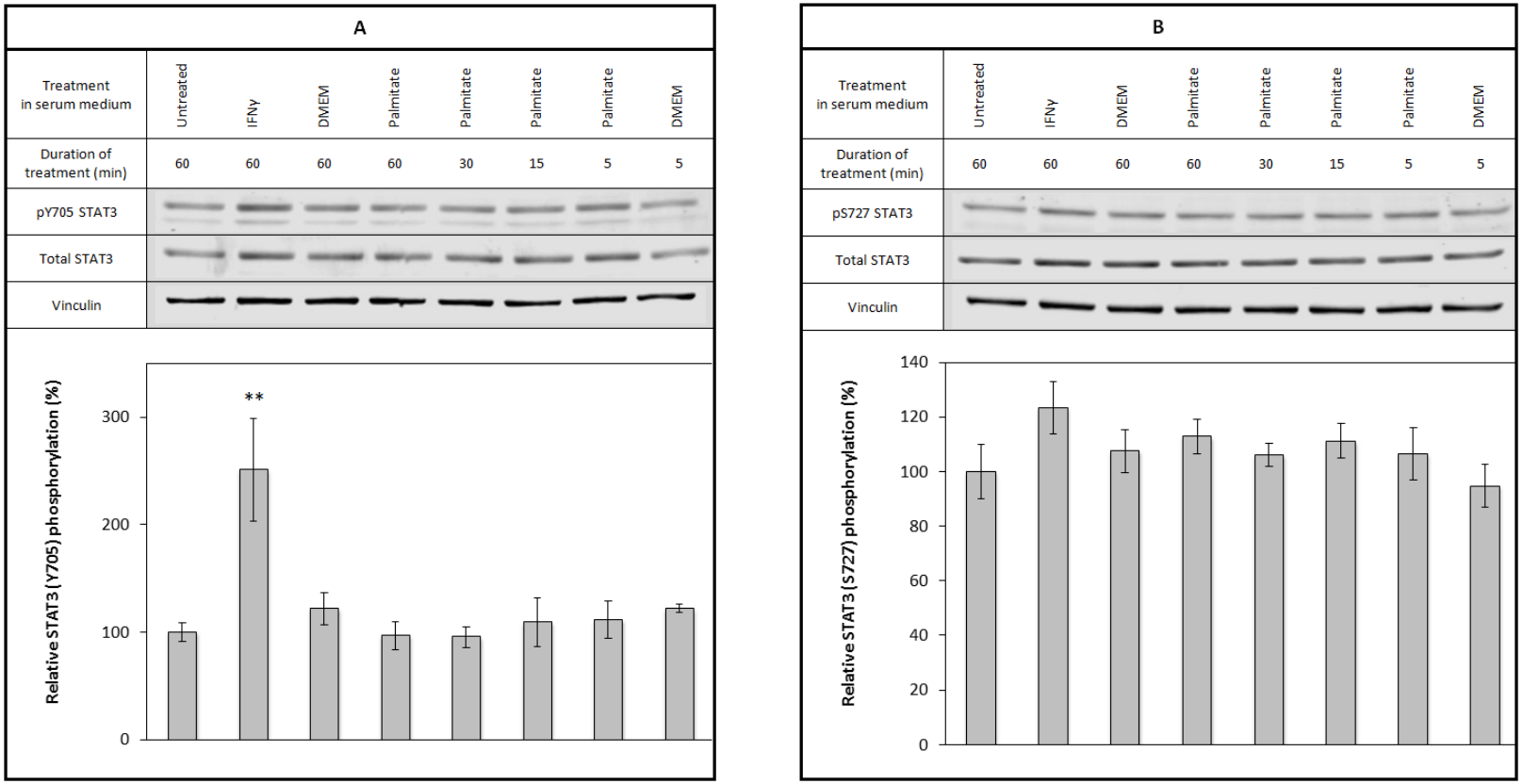

Figure 32. *Palmitate fails to induce the phosphorylation of STAT3 Tyr^{705} (A) and STAT3 Ser^{727} (B) in* ***hMADS mature adipocytes*** *over a short time frame.* For both *figures A* and *B*, hMADS mature adipocytes were treated with IFN-γ (20 ng/mL) (lane 2), unconjugated palmitate (500 µM) (lanes 4 to 7) in complete DMEM (LG). An equivalent volume of DMEM (LG) was used as control for the palmitate treatments (200 µL) (lanes 3 and 8). Cells were lysed with 80 µL 1% TX-100 lysis buffer per well. 25 µg of protein were loaded per lane (10% SDS-acrylamide gel). ** denotes a treatment statistically different from all other treatments (p-value < 0.05). Data from three independent experiments.

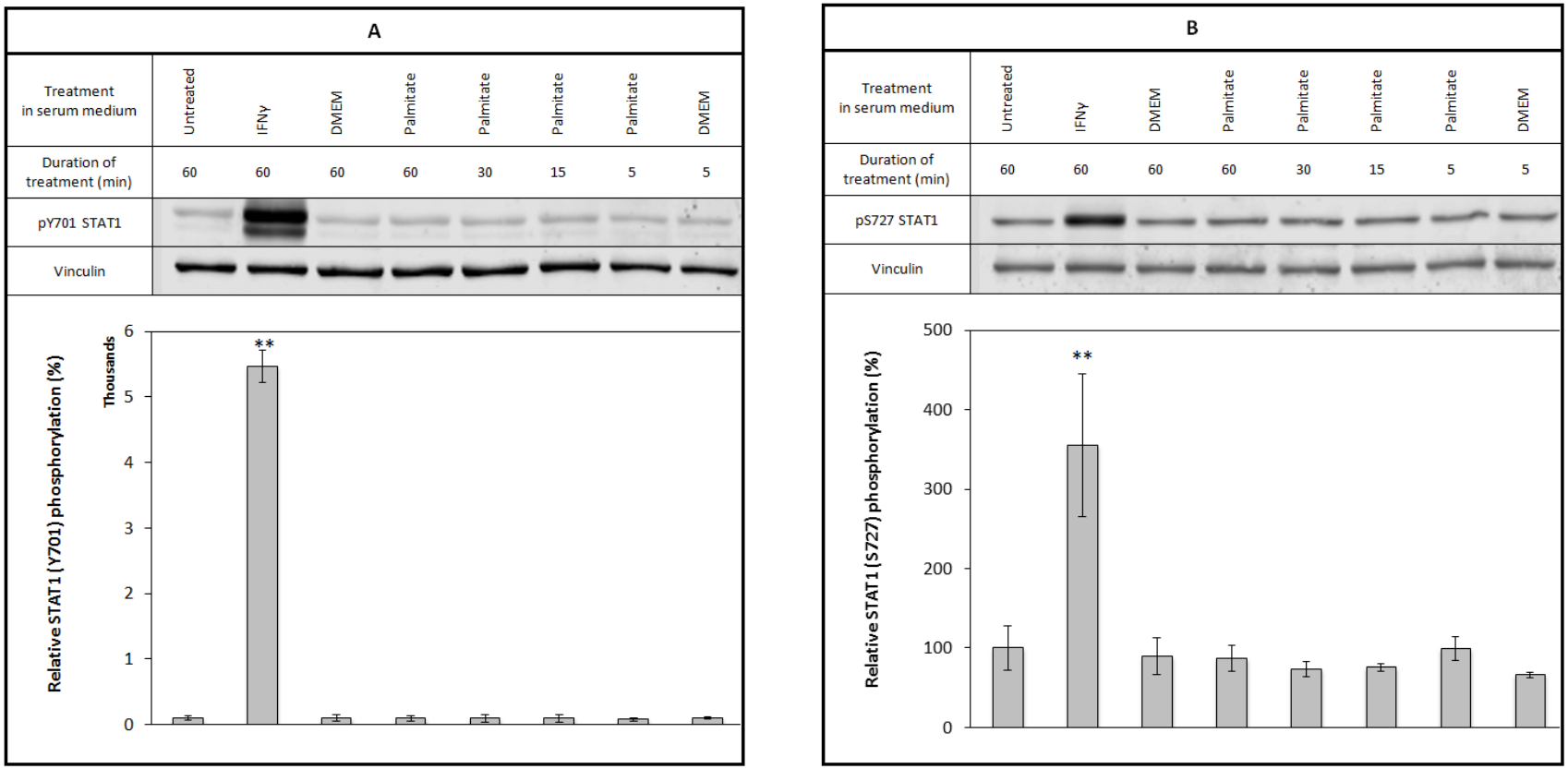

Figure 33. *Palmitate fails to induce the phosphorylation of STAT1 Tyr^{701} (A) and STAT1 Ser^{727} (B) in* ***hMADS mature adipocytes*** *over a short time frame*. For both *figures A* and *B*, hMADS mature adipocytes were treated with IFN-γ (20 ng/mL) (lane 2), unconjugated palmitate (500 µM) (lanes 4 to 7) in complete DMEM (LG). An equivalent volume of DMEM (LG) was used as control for the palmitate treatments (200 µL) (lanes 3 and 8). Cells were lysed with 80 µL 1% TX-100 lysis buffer per well. 50 µg of protein were loaded per lane (10% SDS-acrylamide gel). ** denotes a treatment statistically different from all other treatments (p-value < 0.05). Data from three independent experiments.

III. 3. 4. Palmitate-mediated STAT3 activation

We further explored the molecular mechanisms underlying palmitate-mediated modulation of STAT3 phosphorylation investigated previously. More specifically, we tested whether pharmacological inhibition of two isoforms of PI3K p110 (p110α and p110δ) or inhibition of TLR4 could protect adipocytes from the effect of the SFA. Indeed, as discussed in the introduction, the deleterious metabolic effect of palmitate was found to be mediated by PI3K (L. B. Foukas 2013, Ortega-Molina 2015). Furthermore, evidence of a crosstalk between PI3K and TLR4, the likely receptor for palmitate, was brought forward by Ojaniemi *et al*., who demonstrated that the downstream signalling of TLR4 is directly stimulated by its interaction with PI3K (Ojaniemi 2003). A66 and D030 were used to inhibit p110α and p110δ, respectively, while TAK 242 was used to block TLR4 activity. These inhibitors were tested in 3T3-L1 mature adipocytes treated for 8 h with unconjugated palmitate as palmitate was found to impact STAT3 Tyr^{705} phosphorylation under such conditions (*Figure 20A*).

As shown in *figure 34*, the palmitate-induced stimulation of pSTAT3 Tyr^{705} following 8 h of treatment recorded in *figure 20A* could successfully be reproduced. However, none of the inhibitors tested affected palmitate-induced effect on STAT Tyr^{705}. An additional experiment was carried out to further investigate the effect of TAK 242. *Figure 35* compares the tyrosine phosphorylation levels of STAT3 of mature 3T3-L1 exposed to palmitate for 8 h, in the presence or absence of TAK 242. While some cells were treated simultaneously with a combination of palmitate and TAK 242, others were pre-treated with the inhibitor for 1 h prior to adding palmitate to the media. An LPS control was included to confirm the efficiency of TLR4

inhibition. TAK 242 failed to elicit any significant effect in palmitate-stimulated cells, whether a pre-treatment was performed or not. However, in LPS-treated cells, the TLR4 inhibitor was able to rescue the endotoxin-mediated induction of p-STAT3 Tyr^{705} and pre-treatment promoted such effect.

Another inhibitor (myriocin) was tested, this time targeting serine pamitoyl transferase (SPT), the enzyme catalysing the first step of *de novo* ceramide synthesis. As discussed in Chapter 1, one of the theories explaining the negative metabolic effect of palmitate is its ability to stimulate the production of ceramide (Turpin 2014). This lipid metabolite was indeed implicated in the down-regulation of PI3K signalling thus seeding the onset of insulin resistance (Hla 2014). Moreover, it was shown to impair mitochondrial electron transport, thereby antagonising β-oxidation and FA disposal (Turpin 2014). As shown in *figure 36*, adding myriocin to the palmitate treatment had no effect on the palmitate-mediated stimulation of p-STAT3 levels.

Aside for the increase in p-STAT3 Tyr^{705} recorded in mature 3T3-L1, the other time points identified in *table 11* were investigated. However, neither the 47% nor the 54% decrease in pSTAT3 Ser^{727} compared to untreated control recorded after 4 h and 1 h of treatment, respectively, could be reproduced (*data not shown*).

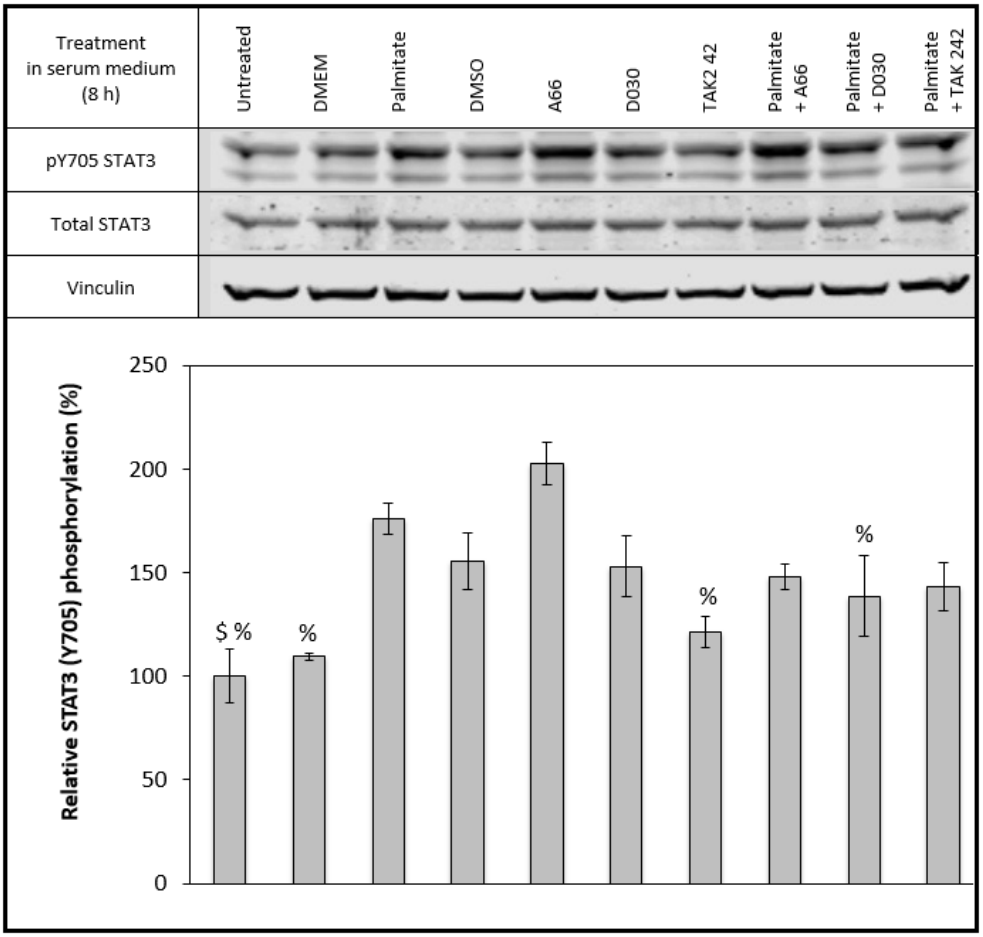

Figure 34. *Inhibition of PI3K p110α, p110δ and TLR4 do not rescue palmitate-induced phosphorylation of STAT3 Tyr[705] in* ***3T3-L1 mature adipocytes*** *after 8 h of treatment.* 3T3-L1 mature adipocytes were treated with unconjugated palmitate (500 µM) (lanes 3, 8, 9 and 10), A66 (2 µM) (lanes 5 and 8), D030 (2 µM) (lanes 6 and 9) and TAK 242 (2 µM) (lanes 7 and 10) in 10% FBS/DMEM (HG). Equivalent volumes of DMEM (LG) (200 µL) (lane 2) and DMSO (4 µL) (lane 4) were used as control for the palmitate and inhibitors treatments, respectively. Cells were lysed with 80 µL 1% TX-100 lysis buffer per well. 64 µg of protein were loaded per lane (10% SDS-acrylamide gel). Statistical difference between the palmitate treatment and other treatments is indicated with $; statistical difference between the A66 treatment and other treatments is indicated with % (p-value < 0.05). Data from three independent experiments.

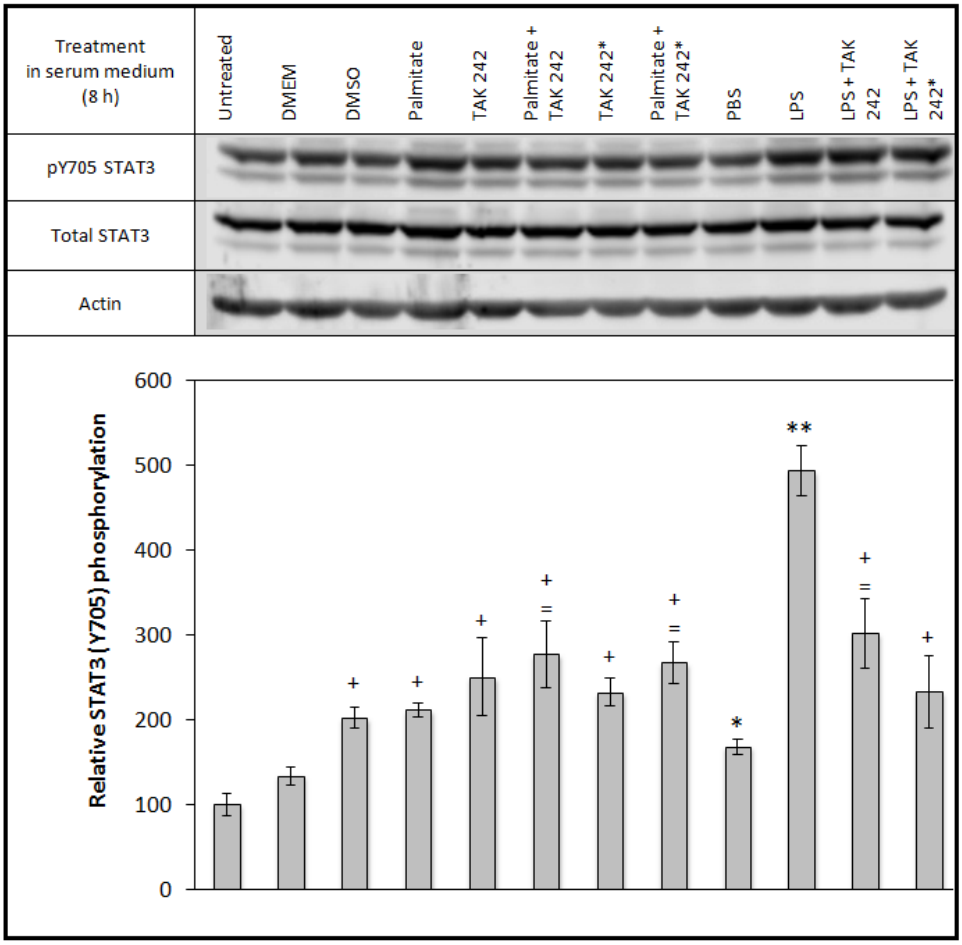

Figure 35. *Inhibiting TLR4 rescues the effect of LPS but not of palmitate on the phosphorylation of STAT3 Tyr*^{705} *in **3T3-L1 mature adipocytes** after 8 h of treatment.* 3T3-L1 mature adipocytes were treated with unconjugated palmitate (500 µM) (lanes 4, 6 and 8), LPS (100 ng/mL) (lanes 10, 11 and 12) and TAK 242 (2 µM) (lanes 5, 6, 7, 8, 11 and 12) in 10% FBS/DMEM (HG). Equivalent volumes of DMEM (LG) (200 µL) (lane 2), PBS (20 µL) (lane 9) and DMSO (4 µL) (lane 3) were used as control for the palmitate, LPS and TAK 242 treatments, respectively. For treatments marked with *, TAK 242 was added to the media 1 h prior to palmitate and LPS treatments. Cells were lysed with 80 µL 1% TX-100 lysis buffer per well. 56 µg of protein were loaded per lane (10% SDS-acrylamide gel). Statistical difference between the untreated control and other treatments is indicated with +; statistical difference between the DMEM control and other treatments is indicated with =; statistical difference between the "LPS + TAK 242" treatment and other treatments is indicated with *; ** denotes a treatment statistically different from all other treatments (p-value < 0.05). Data from three independent experiments

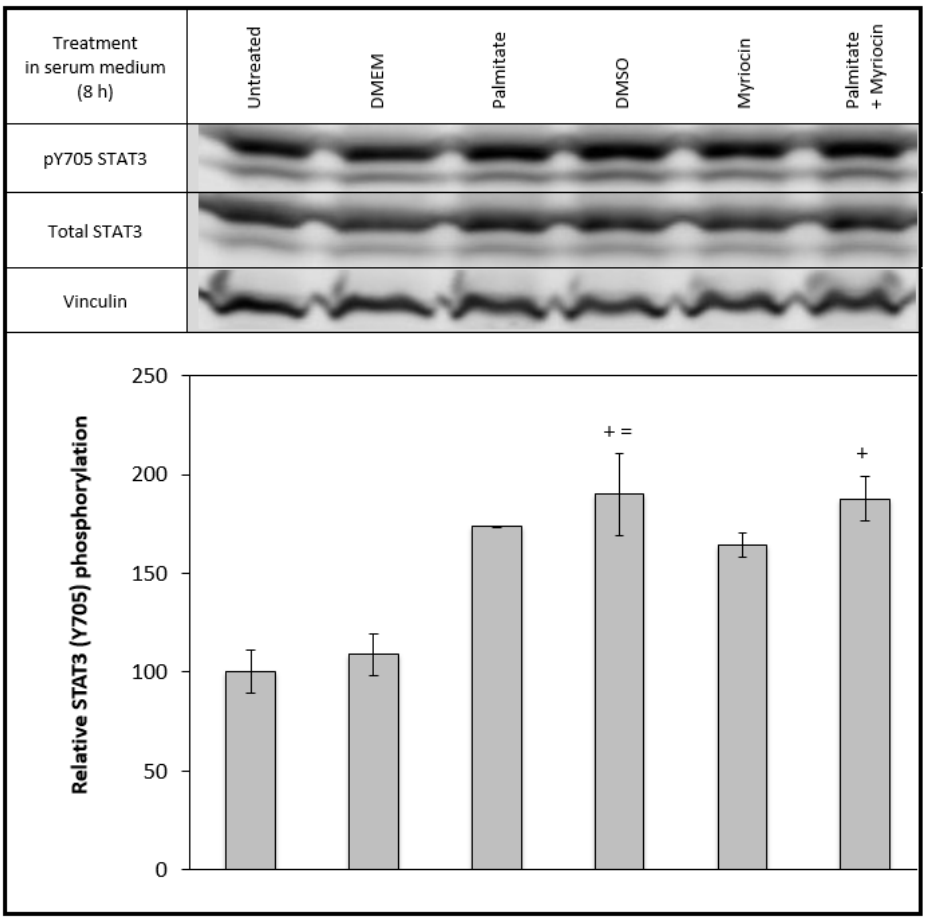

Figure 36. *Inhibiting* de novo *ceramide biosynthesis does not rescue the effect of palmitate and LPS on the phosphorylation of STAT3 Tyr[705] in* ***3T3-L1 mature adipocytes*** *after 8 h of treatment.* 3T3-L1 mature adipocytes were treated with unconjugated palmitate (500 μM) (lanes 3 and 6) and myriocin (100 nM) (lanes 5 and 6) in 10% FBS/DMEM (HG). Equivalent volumes of DMEM (LG) (200 μL) (lane 2) and DMSO (4 μL) (lane 4) were used as control for the palmitate and myriocin treatments, respectively. Myriocin and DMSO were added to the media 1 h prior to palmitate treatment. Cells were lysed with 80 μL 1% TX-100 lysis buffer per well. 156 μg of protein were loaded per lane (10% SDS-acrylamide gel). Statistical difference between the untreated control and other treatments is indicated with +; statistical difference between the DMEM control and other treatments is indicated with =; (p-value < 0.05). Data from three independent experiments.

III. 3. 5. Type I and II IFN, but not type III IFN, activate the STAT pathway

III. 3. 5. 1. Using 3T3-L1 cell line

In order to thoroughly understand the effect of the IFN family on the STAT pathway, the time course experiments investigating IFN-γ- and palmitate-mediated stimulation of STAT1 and STAT3 were repeated, this time comparing IFN-α to IFN-λ treatments. Collectively, these two sets of experiments provide a comprehensive overview of the potential role played by all three types of IFN in the activation of the two STAT proteins in adipocytes. Data from previous experiments indicates that the molecular mechanism by which palmitate modulates STAT3 phosphorylation occurs independently of IFN-γ secretion as STAT1 phosphorylation in not affected by the SFA. Testing whether type I and III IFN induce STAT1 activation would allow to extent this statement to all types of IFN. Indeed, if palmitate stimulated the production and signal through either IFN-α or IFN-λ, this would have been missed if these did not drive STAT1 phosphorylation.

Figures 37 and *38* explore the response of 3T3-L1 pre-adipocytes to these cytokines. Similarly to type II IFN, IFN-α is most potent in these cells after 1 h of treatment when considering the tyrosine residue of both STAT1 and STAT3. While the phosphorylation of the former is increased 15-fold (to levels which remain almost 5 times lower than the IFN-γ induction), that of the latter reaches 4 times basal levels (comparable to IFN-γ induction) (*Figures 37A* and *38A*). Interestingly, the phosphorylation of the serine residues was also maximal after 1 h of treatment with a 2-fold stimulation at STAT3 Ser^{727} and a 3-fold one at STAT1 Ser^{727} *versus* basal. This activation pattern differs from that of IFN-γ, which although of a similar

magnitude, peaked after 24 h of treatment (*Figures 37B* and *38B*). Strikingly, IFN-λ failed to trigger the phosphorylation of STAT across residues. As discussed in the next section, the literature on this topic seems to indicate that this type of IFN would be able to induce the phosphorylation of STAT1 (Dickensheets 2013).

Focusing on 3T3-L1 mature adipocytes, it appears that neither type I nor type III IFN are able to significantly stimulate the transcription factors (*Figures 39* and *40*). Indeed, although a subtle up-regulation can be noticed in p-STAT3 Ser^{727} after the 1 h IFN-α treatment and in p-STAT1 Tyr^{701} after 2 h of the same treatment, these were not statistically significant.

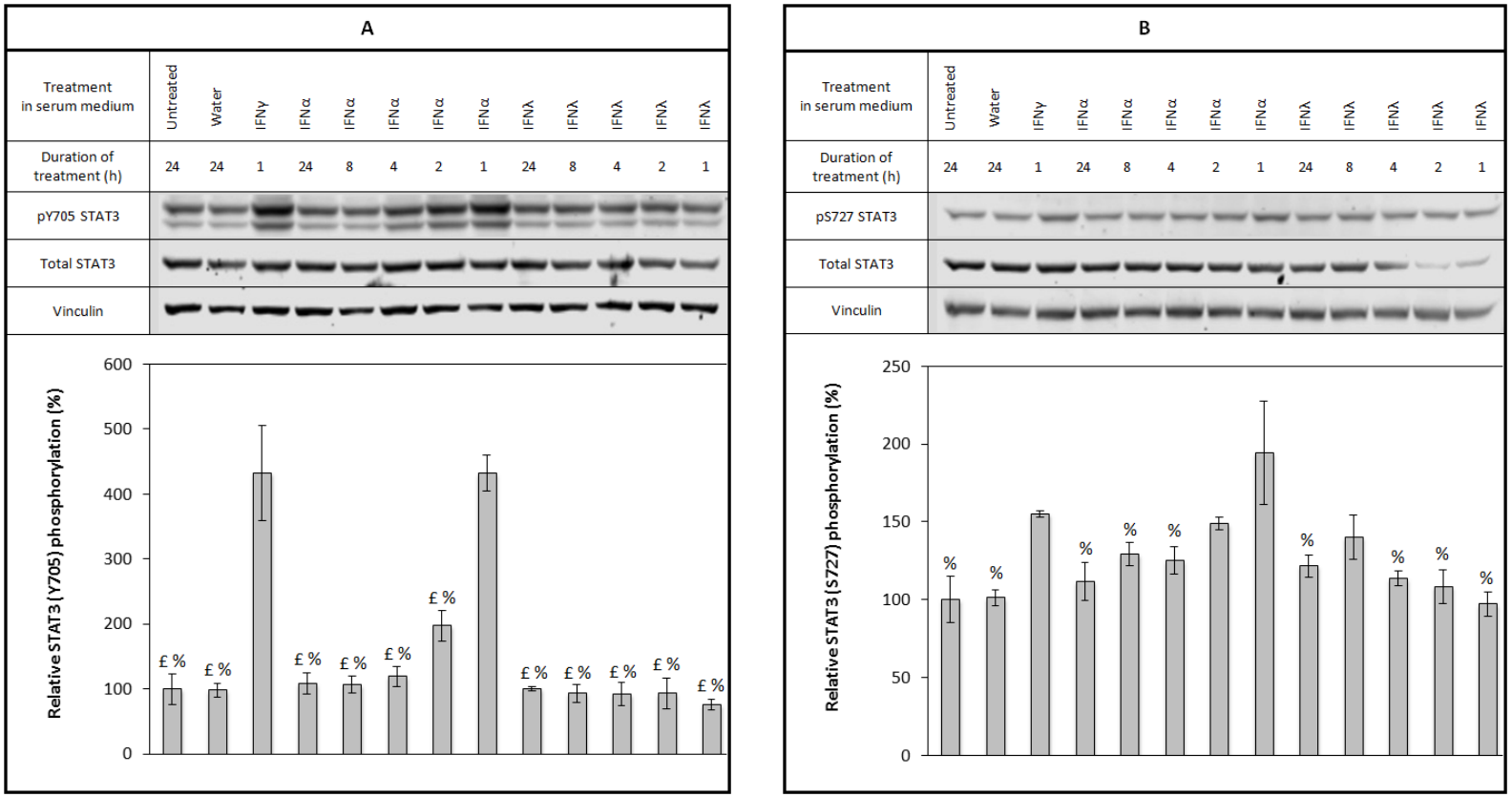

Figure 37. *Type I IFN but not type III IFN induces the phosphorylation of both STAT3 Tyr^{705} (A) and STAT3 Ser^{727} (B) in **3T3-L1 pre-adipocytes**.* For both *figures A* and *B*, 3T3-L1 pre-adipocytes were treated with IFN-γ (20 ng/mL) (lane 3), IFN-α (lanes 4 to 8) and IFN-λ (lanes 9 to 13) in 10% FBS/DMEM (HG). An equivalent volume of MilliQ water was used as control for the IFN treatments (16 µL) (lane 2). Cells were lysed with 100 µL 1% TX-100 lysis buffer per 6 cm Ø dish. 64 µg of protein were loaded per lane (10% SDS-acrylamide gel). Statistical difference between the 1 h IFN-γ treatment and other treatments is indicated with £; statistical difference between the 1 h IFN-α treatment and other treatments is indicated with % (p-value < 0.05). Data from three independent experiments.

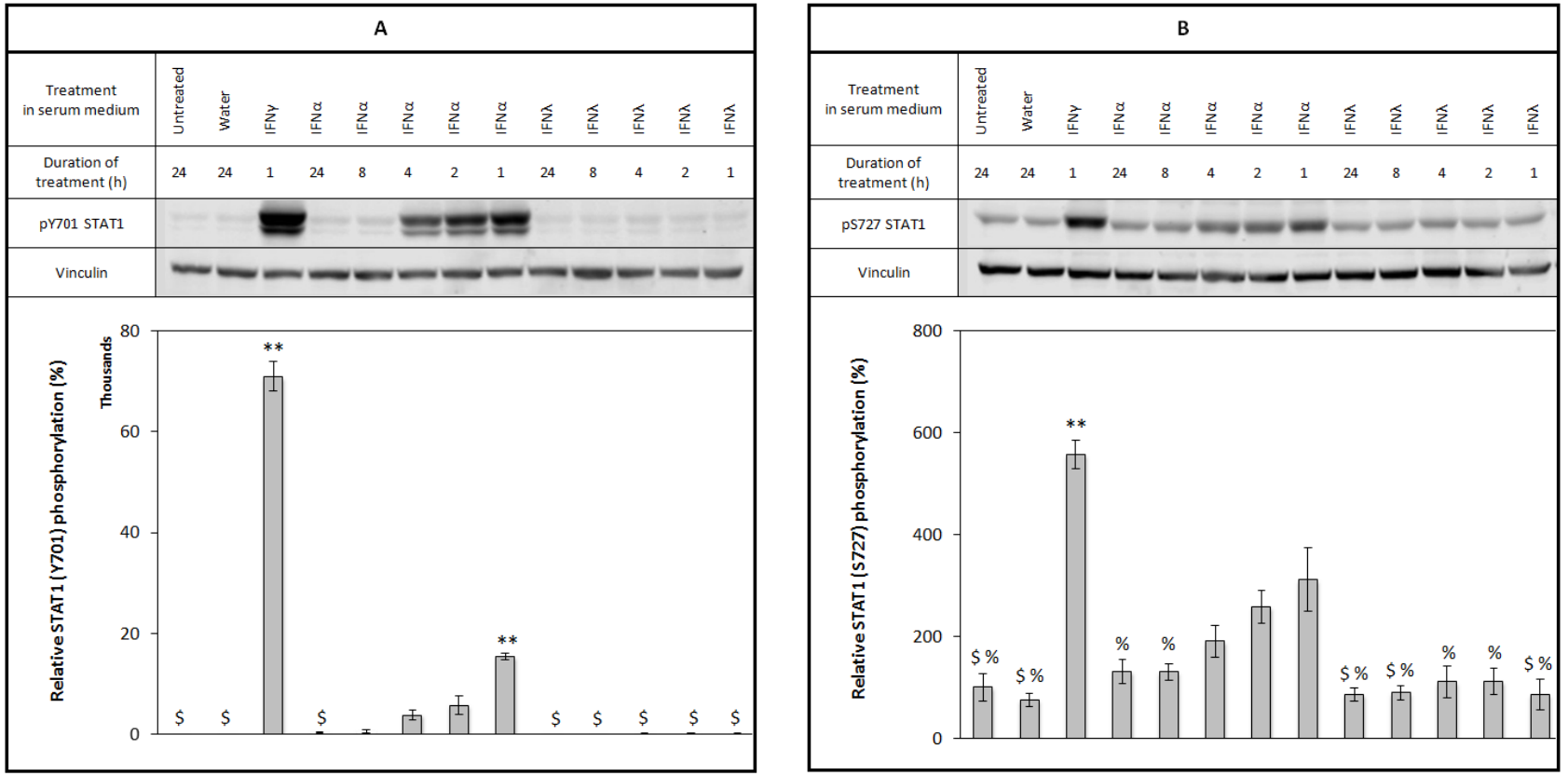

Figure 38. *Type I IFN but not type III IFN induces the phosphorylation of both STAT1 Tyr[701] (A) and STAT1 Ser[727] (B) in **3T3-L1 pre-adipocytes***. For both *figures A* and *B*, 3T3-L1 pre-adipocytes were treated with IFN-γ (20 ng/mL) (lane 3), IFN-α (lanes 4 to 8) and IFN-λ (lanes 9 to 13) in 10% FBS/DMEM (HG). An equivalent volume of MilliQ water was used as control for the IFN treatments (16 µL) (lane 2). Cells were lysed with 100 µL 1% TX-100 lysis buffer per 6 cm Ø dish. 64 µg of protein were loaded per lane (10% SDS-acrylamide gel). Statistical difference between the 2 h IFN-α treatment and other treatments is indicated with $; statistical difference between the 1 h IFN-α treatment and other treatments is indicated with %; ** denotes a treatment statistically different from all other treatments (p-value < 0.05). Data from three independent experiments.

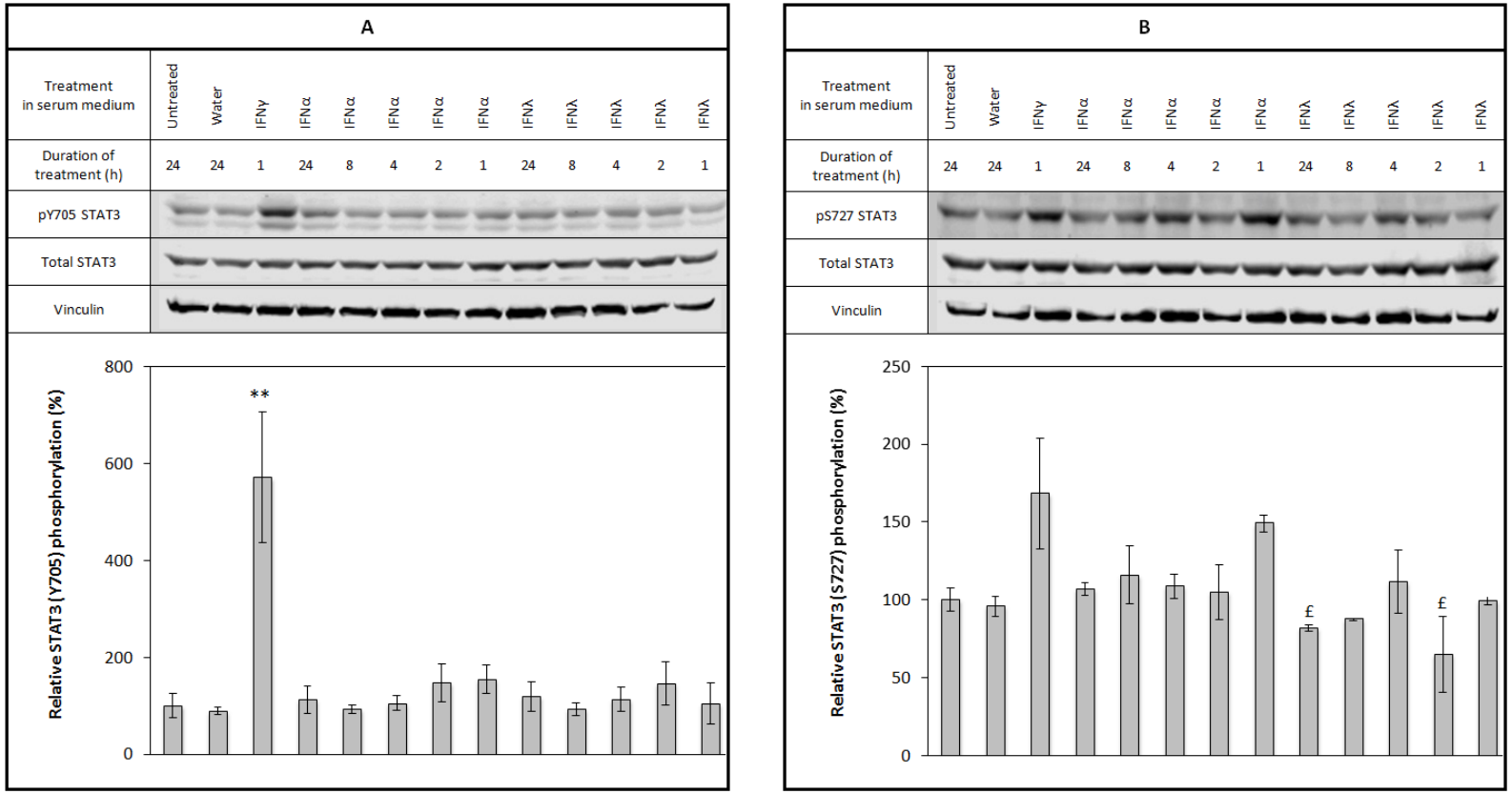

Figure 39. *Neither type I nor type III IFN induces the phosphorylation of STAT3 Tyr^{705} (A) and STAT3 Ser^{727} (B) in* ***3T3-L1 mature adipocytes***. For both *figures A* and *B*, 3T3-L1 mature adipocytes were treated with IFN-γ (20 ng/mL) (lane 3), IFN-α (lanes 4 to 8) and IFN-λ (lanes 9 to 13) in 10% FBS/DMEM (HG). An equivalent volume of MilliQ water was used as control for the IFN treatments (8 µL) (lane 2). Cells were lysed with 80 µL 1% TX-100 lysis buffer per well. 73 µg and 59 µg of protein were loaded per lane in *figures A* and *B*, respectively (10% SDS-acrylamide gel). Statistical difference between the 1 h IFN-γ treatment and other treatments is indicated with £; ** denotes a treatment statistically different from all other treatments (p-value < 0.05). Data from three independent experiments.

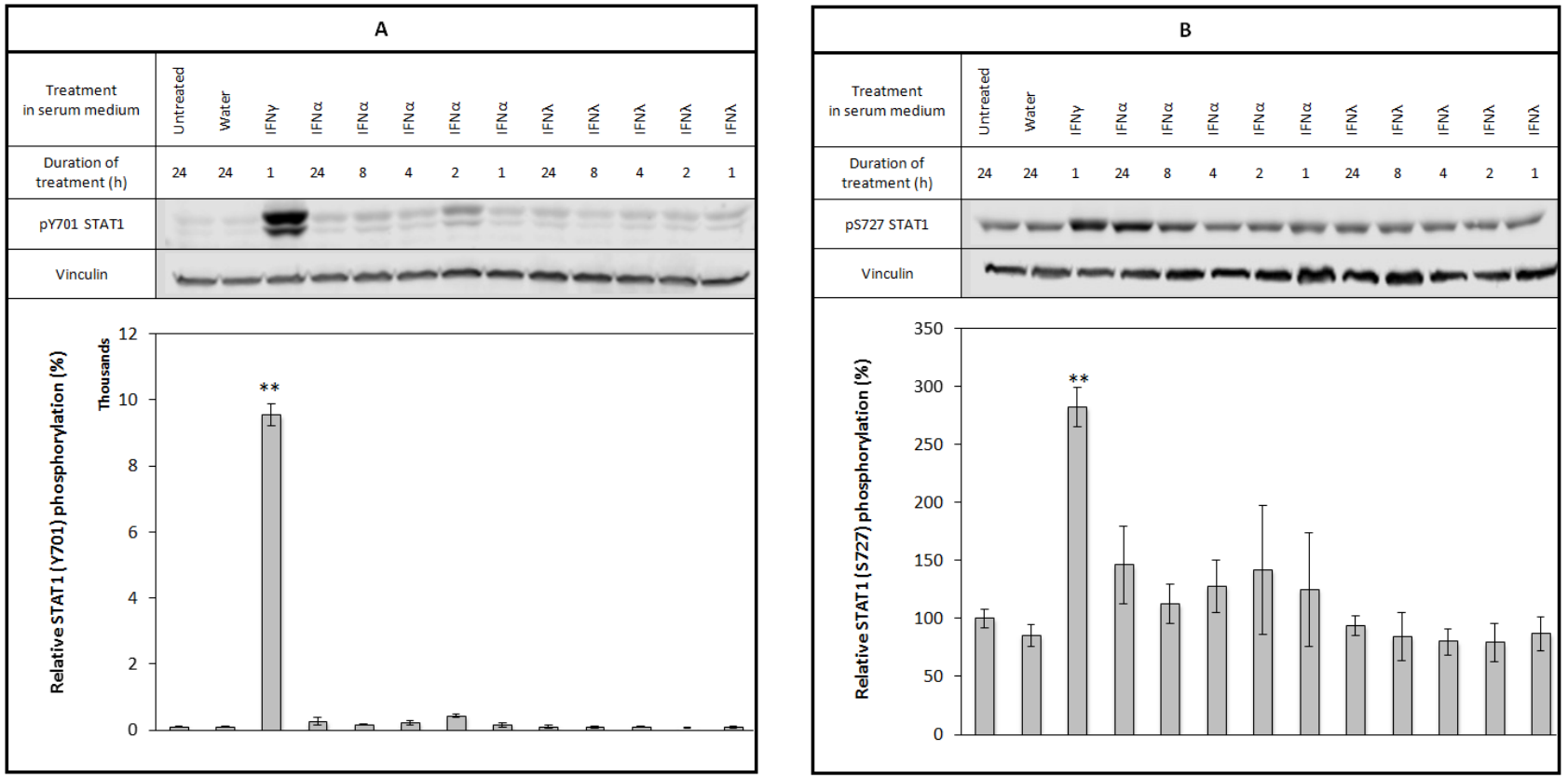

Figure 40. *Neither type I nor type III IFN induces the phosphorylation of STAT1 Tyr[701] (A) and STAT Ser[727] (B) in* ***3T3-L1 mature adipocytes***. For both *figures A* and *B*, 3T3-L1 mature adipocytes were treated with IFN-γ (20 ng/mL) (lane 3), IFN-α (lanes 4 to 8) and IFN-λ (lanes 9 to 13) in 10% FBS/DMEM (HG). An equivalent volume of MilliQ water was used as control for the IFN treatments (8 µL) (lane 2). Cells were lysed with 80 µL 1% TX-100 lysis buffer per well. 71 µg and 59 µg of protein were loaded per lane in *figures A* and *B*, respectively (10% SDS-acrylamide gel). ** denotes a treatment statistically different from all other treatments (p-value < 0.05). Data from three independent experiments.

III. 3. 5. 2. Using hMADS cell line

As previously, the experiments carried out in mice adipocytes were also performed in human fat cells. *Figures 41* and *42* present the data collected in hMADS pre-adipocytes. Neither type I nor type III IFN elicited a statistically significant increase in STAT3 phosphorylation, although p-STAT3 Tyr^{705} levels were increased 2.5-fold after a 1 h treatment with IFN-α (*Figure 41A*). Likewise, STAT1 activation is not enhanced by the cytokines beyond statistically significance (*Figure 42*).

Lastly, the experiment was performed in differentiated human adipocytes (*Figures 43* and *44*). Although IFN-γ does not induce the previously observed 2-fold increase in p-STAT3 Tyr^{705} after 1 h of treatment shown in *figure 24A*, IFN-α did stimulate phosphorylation in a comparable magnitude with a peak after 1 h treatment (*Figure 43A*). As expected, IFN-γ did not have an effect on the serine residue of STAT3 and neither did IFN-α (*Figure 43B*). IFN type I was also able to boost p-STAT1 Tyr^{701} levels with a 300-fold increase at the 2 h time point comparable to the IFN-γ-mediated induction (*Figure 44A*). Peaking after 24 h of treatment, the phosphorylation of the STAT1 serine residue was promoted to a lesser extent (30-fold) (*Figure 44B*). As for the mouse cells, type III IFN did not enhance the activity of either transcription factors in differentiated hMADS adipocytes.

In *table 12* are compiled the times at which each type of IFN elicit peak stimulation of STAT1 and STAT3 and *figures 45*, *46*, *47* and *48* superimpose the patterns of STAT phosphorylation induced by IFN-α, IFN-γ and IFN-λ in each cell type tested. For each cell type used (3T3-L1 pre-adipocytes in *figure 45*, 3T3-L1

mature adipocytes in *figure 46*, hMADS pre-adipocytes in *figure 47* and hMADS mature adipocytes in *figure 48*), the phosphorylation levels recorded for each residue is plotted against the duration of the treatment (p-STAT3 Tyr^{705} for the top left-hand side panel, p-STAT3 Ser^{727} for the top right-hand side panel, p-STAT1 Tyr^{701} for the bottom left-hand side panel and, lastly, p-STAT1 Ser^{727} for the bottom right-hand side panel). The blue, red and green plots reflect the variations in phosphorylation levels recorded following the IFN-α, IFN-γ and IFN-λ treatments, respectively. The first time point of these plots is 1 h as this is the shortest treatment duration performed in the time course experiments.

Table 12. *Summary of the effect of IFN-α, -γ and –λ on the phosphorylation of STAT1 Ser^{727}, STAT1 Tyr^{701}, STAT3 Ser^{727} and STAT3 Tyr^{705}.* Only statistically significant effects are recorded in this table.

Cell line	***3T3-L1 pre-adipocytes***			***3T3-L1 mature adipocytes***			***hMADS pre-adipocytes***			***hMADS mature adipocytes***		
IFN type	***α***	***γ***	***λ***	***α***	***γ***	***λ***	***α***	***γ***	***λ***	***α***	***γ***	***λ***
p-STAT1 Ser^{727}	+ 210 % (1 h)	+ 364 % (24 h)	✗	✗	+ 252% (2 h)	✗	✗	+ 413 % (1 h)	✗	+ 317 % (24 h)	+ 613 % (2 h)	✗
p-STAT1 Tyr^{701}	+ 15296 % (1 h)	+ 2259 % (1 h)	✗	✗	+ 34613% (2 h)	✗	✗	+ 15818 % (1 h)	✗	+ 3396 % (2 h)	+ 1188 % (1 h)	✗
p-STAT3 Ser^{727}	+ 94 % (1 h)	+ 141 % (24 h)	✗	✗	+ 105 % (1 h)	✗	✗	✗	✗	✗	✗	✗
p-STAT3 Tyr^{705}	+ 332 % (1 h)	+ 145 % (1 h)	✗	✗	+ 313 % (1 h)	✗	✗	+ 430 % (1 h)	✗	+ 129 % (1 h)	+ 112 % (1 h)	✗

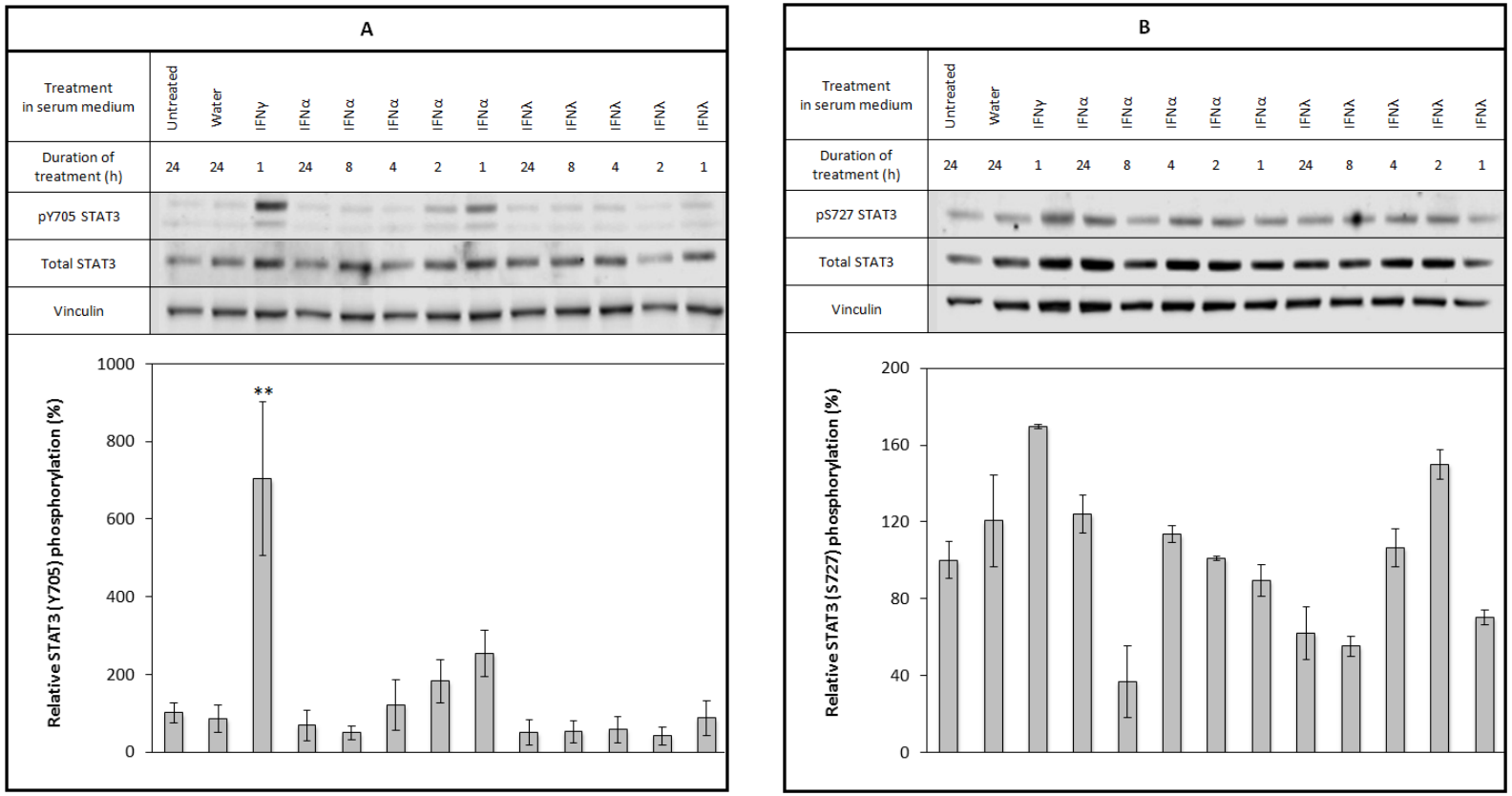

Figure 41. A. *Type I but not type III IFN induces the phosphorylation of STAT3 Tyr[705] in* ***hMADS pre-adipocytes*** *although this effect falls short of reaching statistical significance.* **B.** *Neither type I nor type III IFN induces the phosphorylation of STAT3 Ser[727] in hMADS pre-adipocytes.* For both *figures A* and *B*, hMADS pre-adipocytes were treated with IFN-γ (20 ng/mL) (lane 3), IFN-α (lanes 4 to 8) and IFN-λ (lanes 9 to 13) in complete DMEM (LG). An equivalent volume of MilliQ water was used as control for the IFN treatments (16 µL) (lane 2). Cells were lysed with 100 µL 1% TX-100 lysis buffer per 6 cm Ø dish. 4 µg and 14 µg of protein were loaded per lane for *figures A* and *B*, respectively (10% SDS-acrylamide gel). ** denotes a treatment statistically different from all other treatments (p-value < 0.05). Note that to avoid overcrowding *figure B*, only the differences between the treatments and the untreated control are considered, the result in full of the one-way ANOVA analysis can be found in *appendix VII. 10*. Data from three independent experiments.

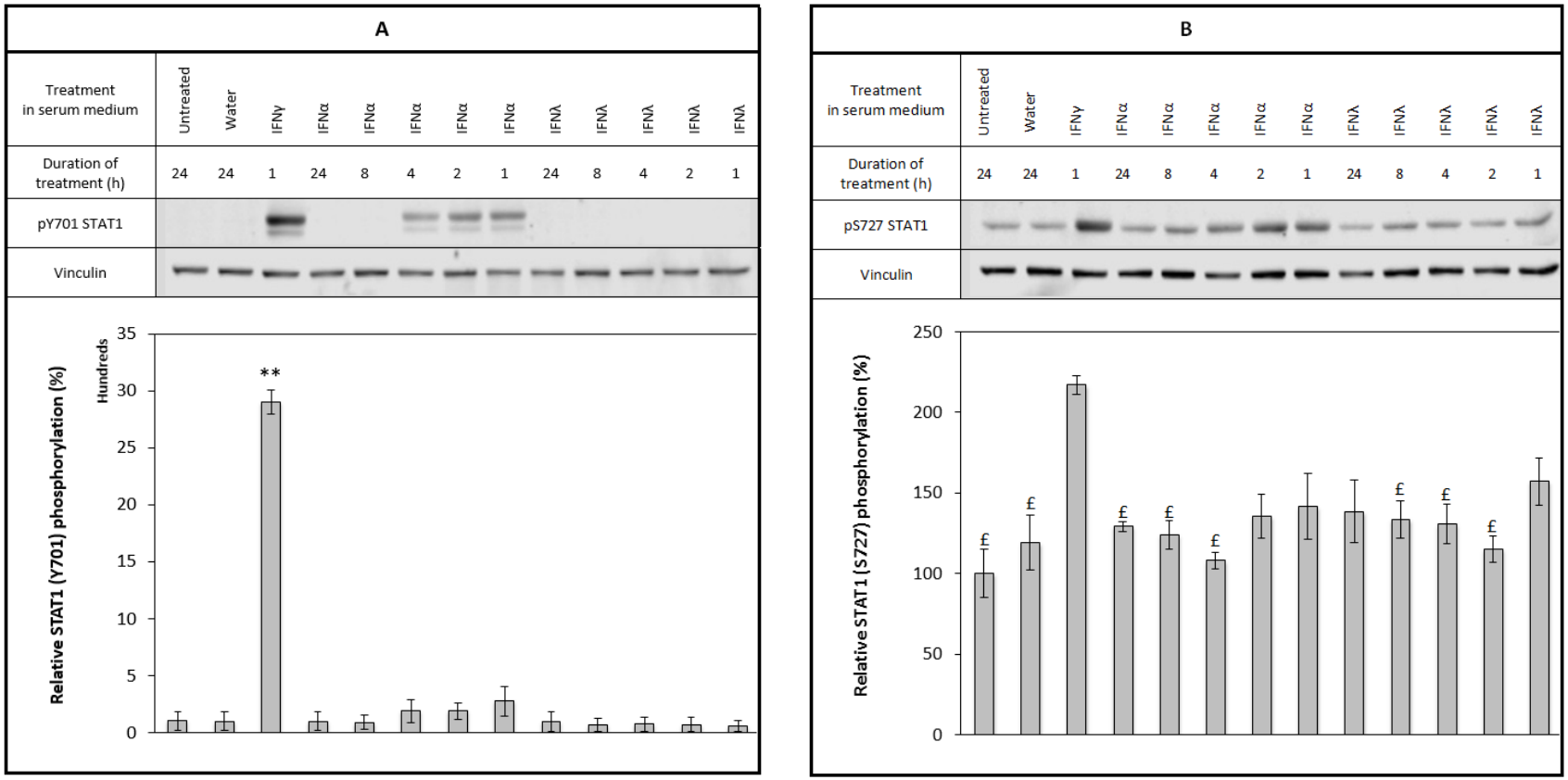

Figure 42. *Neither type I nor type III IFN induces the phosphorylation of STAT1 Tyr^{701} (A) and STAT1 Ser^{727} (B) in* ***hMADS pre-adipocytes***. For both *figures A* and *B*, hMADS pre-adipocytes were treated with IFN-γ (20 ng/mL) (lane 3), IFN-α (lanes 4 to 8) and IFN-λ (lanes 9 to 13) in complete DMEM (LG). An equivalent volume of MilliQ water was used as control for the IFN treatments (16 µL) (lane 2). Cells were lysed with 100 µL 1% TX-100 lysis buffer per 6 cm Ø dish. 8 µg of protein were loaded per lane (10% SDS-acrylamide gel). Statistical difference between the 1 h IFN-γ treatment and other treatments is indicated with £; ** denotes a treatment statistically different from all other treatments (p-value < 0.05). Data from three independent experiments.

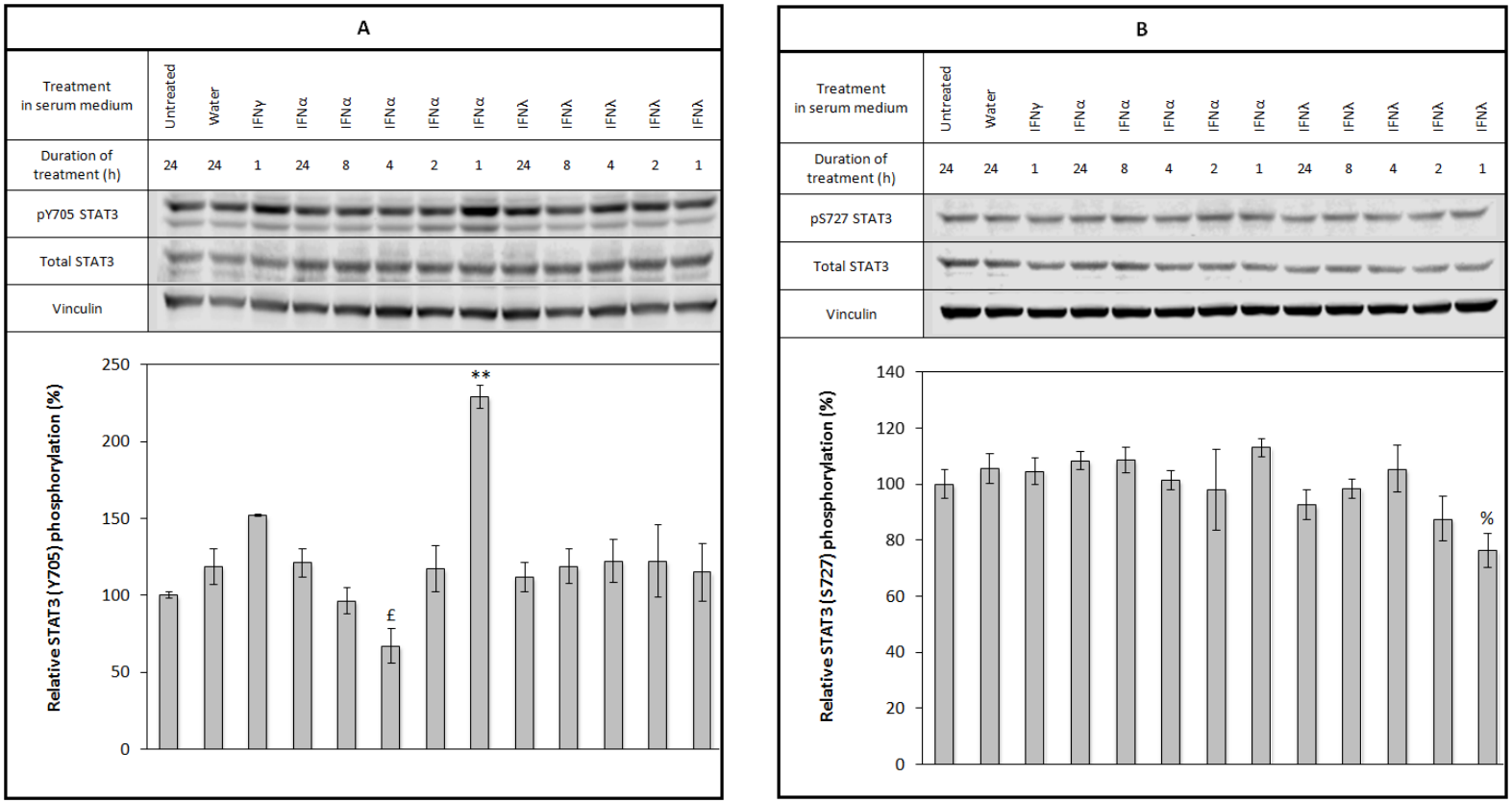

Figure 43. A. *Type I IFN but not type III IFN induces the phosphorylation of STAT3 Tyr[705] in* ***hMADS mature adipocytes***. **B.** Neither *Type I IFN nor type III IFN induces the phosphorylation of STAT3 Ser[727] in hMADS mature adipocytes.* For both *figures A* and *B*, hMADS mature adipocytes were treated with IFN-γ (20 ng/mL) (lane 3), IFN-α (lanes 4 to 8) and IFN-λ (lanes 9 to 13) in complete DMEM (LG). An equivalent volume of MilliQ water was used as control for the IFN treatments (8 µL) (lane 2). Cells were lysed with 80 µL 1% TX-100 lysis buffer per well. 51 µg of protein were loaded per lane (10% SDS-acrylamide gel). Statistical difference between the 1 h IFN-γ treatment and other treatments is indicated with £; statistical difference between the 1 h IFN-α treatment and other treatments is indicated with %; ** denotes a treatment statistically different from all other treatments (p-value < 0.05). Data from three independent experiments.

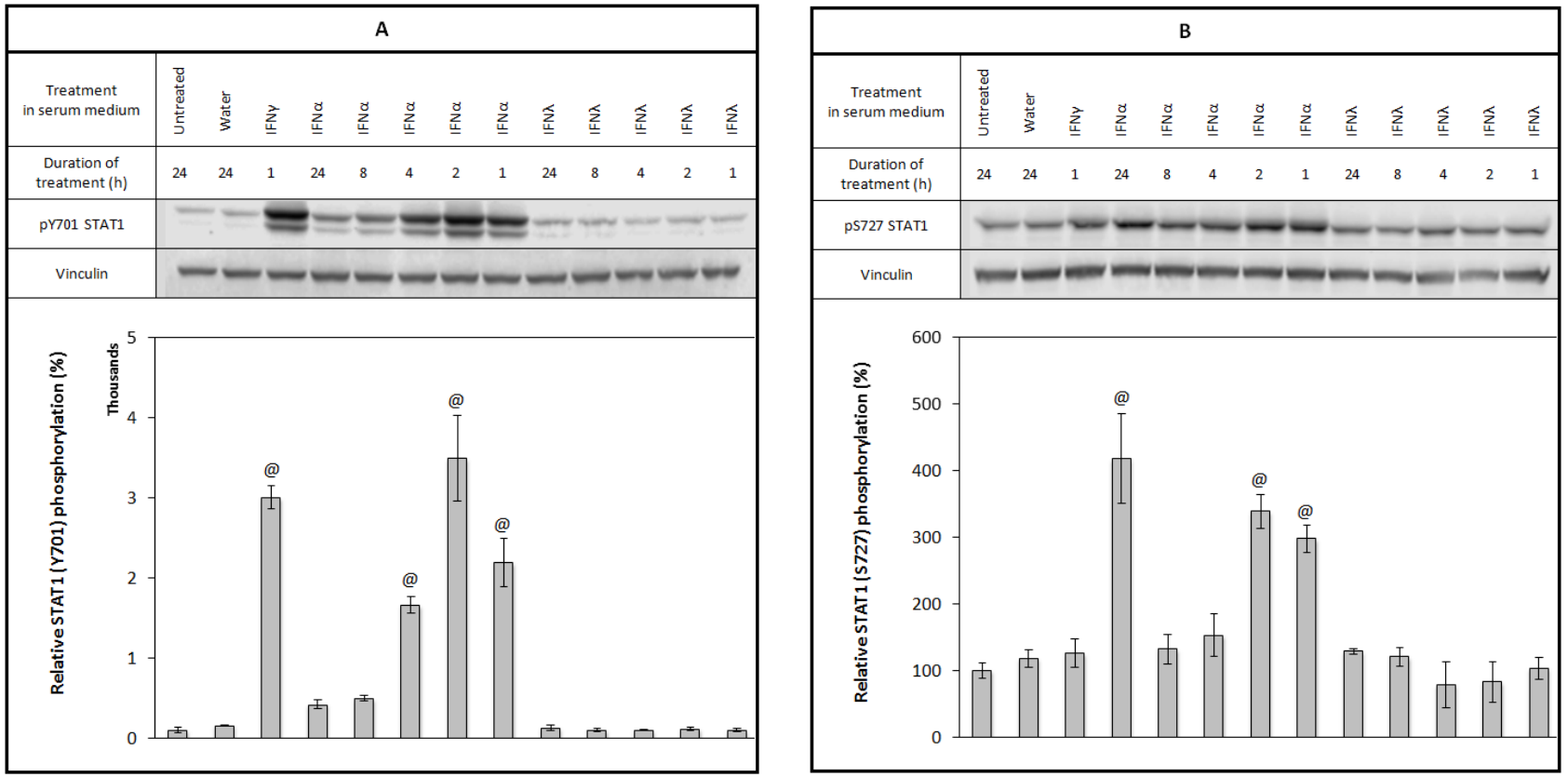

Figure 44. *Type I IFN but not type III IFN induces the phosphorylation of both STAT1 Tyr*^{705} *(A) and STAT1 Ser*^{727} *(B) in* ***hMADS mature adipocytes***. For both *figures A* and *B*, hMADS mature adipocytes were treated with IFN-γ (20 ng/mL) (lane 3), IFN-α (lanes 4 to 8) and IFN-λ (lanes 9 to 13) in complete DMEM (LG). An equivalent volume of MilliQ water was used as control for the IFN treatments (8 µL) (lane 2). Cells were lysed with 80 µL 1% TX-100 lysis buffer per well. 47 µg and 51 µg of protein were loaded per lane for *figures A* and *B*, respectively (10% SDS-acrylamide gel). Statistical difference between the untreated control and other treatments is indicated with @ (p-value < 0.05). Note that to avoid overcrowding both figures, only the differences relevant our analysis are shown, the result in full of the one-way ANOVA analysis can be found in *appendix VII. 10*. Data from three independent experiments.

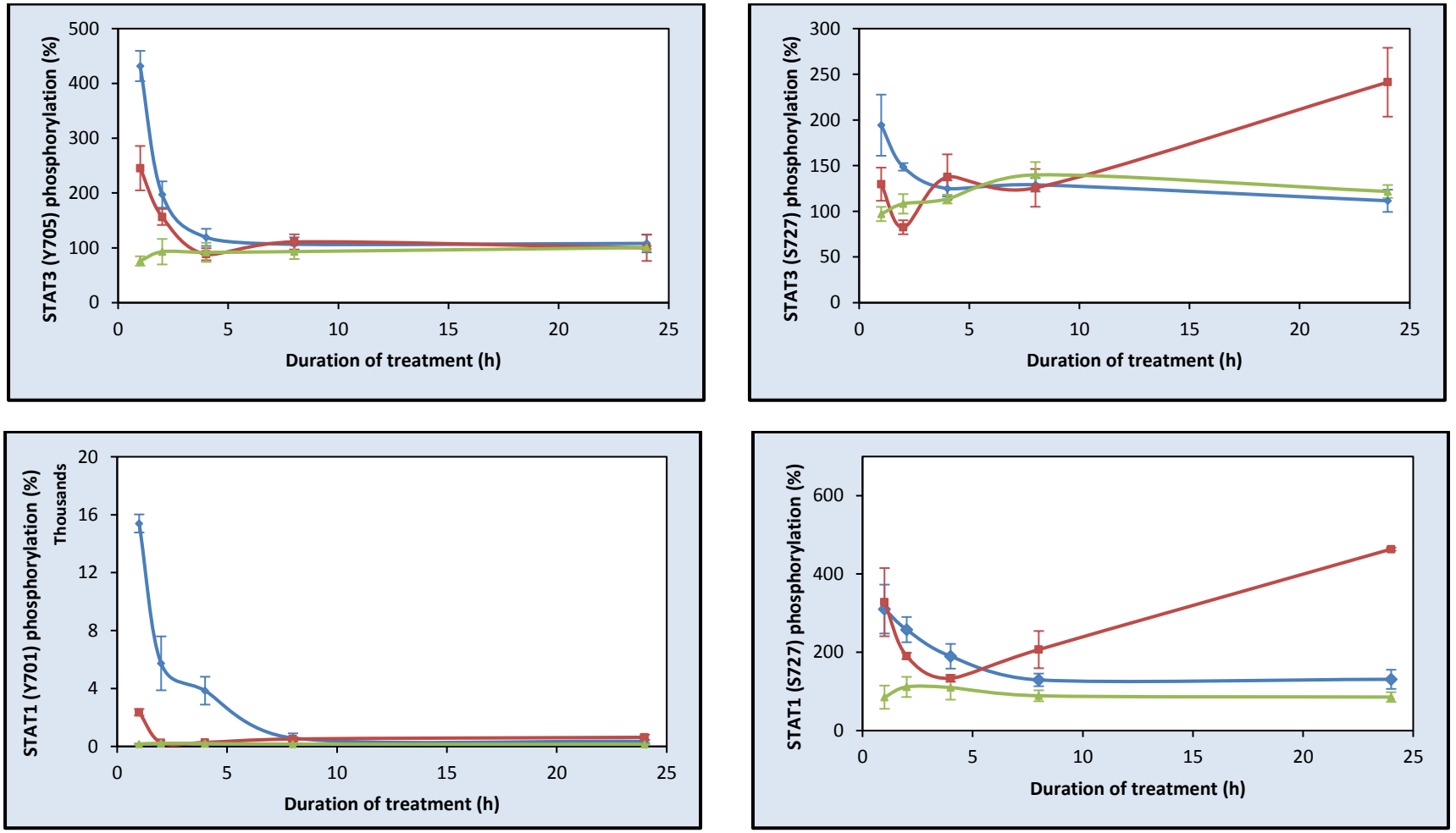

Figure 45. *Graph showing the induction of STAT3 Tyr^{705}, STAT3 Ser^{727}, STAT1 Tyr^{701} and STAT1 Ser^{727} by IFN-α (in blue), IFN-γ (in red) and IFN-λ (in green) in* ***3T3-L1 pre-adipocytes***. Cells were treated for 1, 2, 4, 8 and 24 h with the cytokines (20 ng/mL). Phosphorylation levels are compared to basal levels in untreated cells (100%).

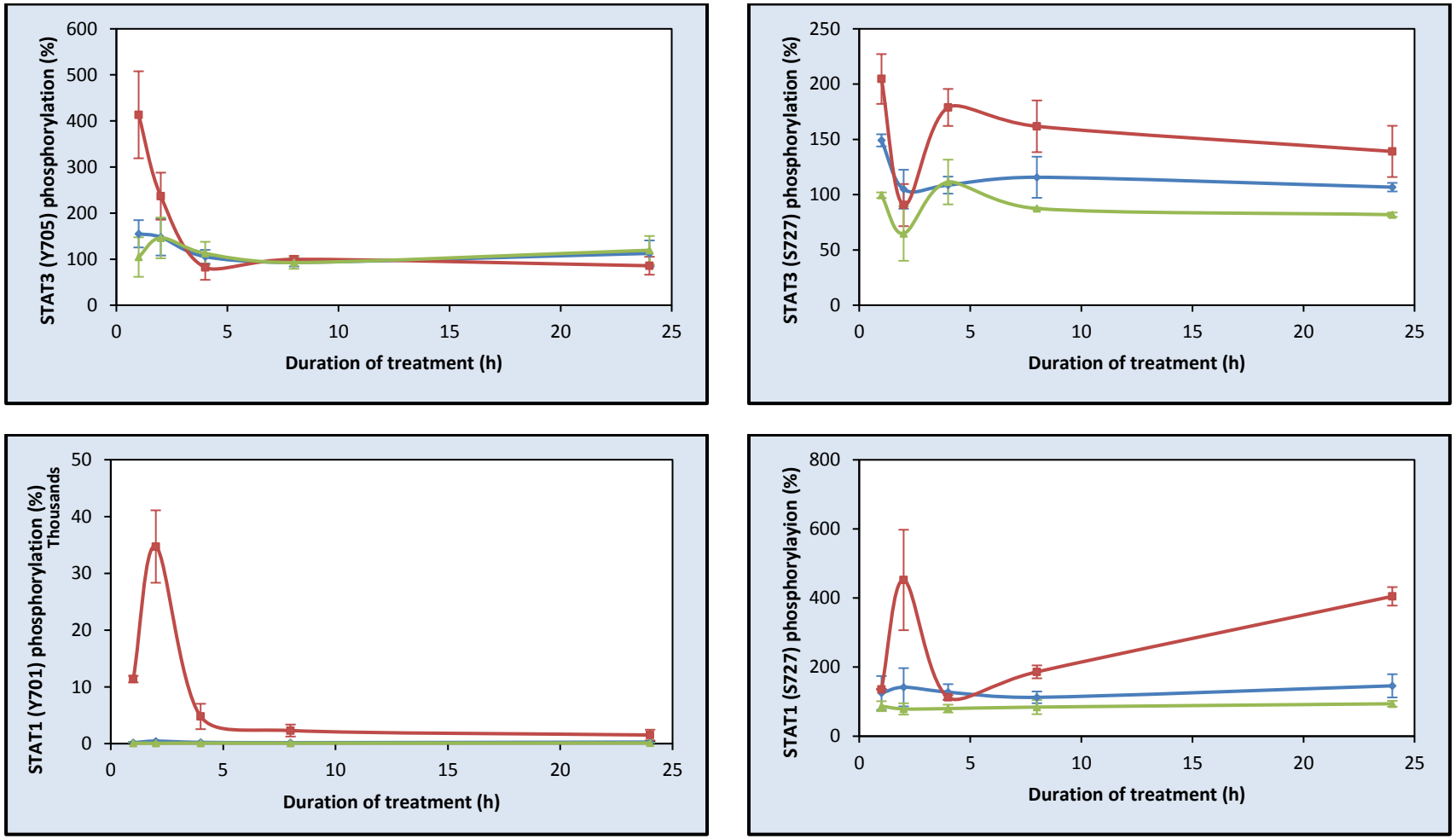

Figure 46. *Graph showing the induction of STAT3 Tyr^{705}, STAT3 Ser^{727}, STAT1 Tyr^{701} and STAT1 Ser^{727} by IFN-α (in blue), IFN-γ (in red) and IFN-λ (in green) in* ***3T3-L1 mature adipocytes***. Cells were treated for 1, 2, 4, 8 and 24 h with the cytokines (20 ng/mL). Phosphorylation levels are compared to basal levels in untreated cells (100%).

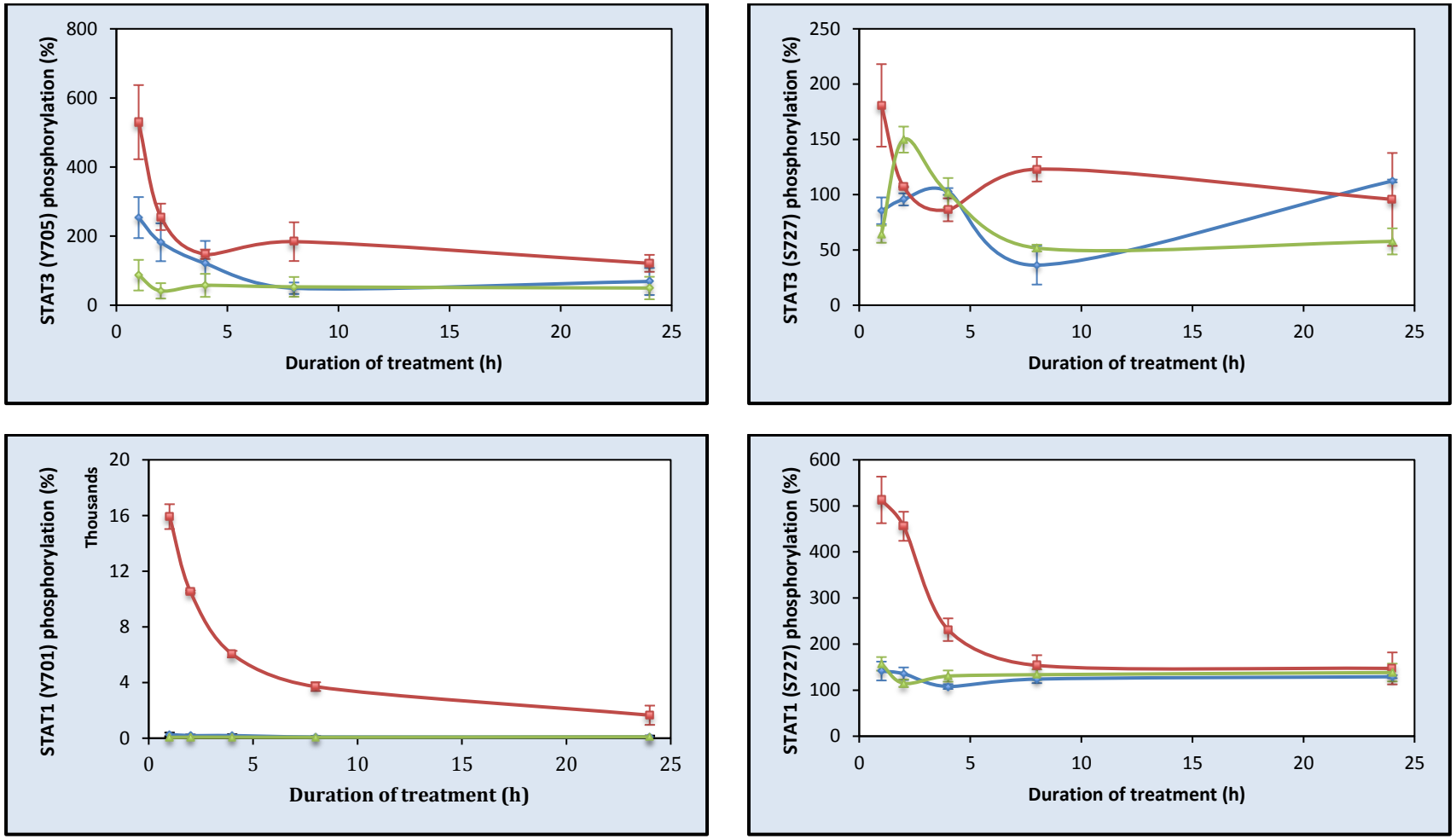

Figure 47. *Graph showing the induction of STAT3 Tyr^{705}, STAT3 Ser^{727}, STAT1 Tyr^{701} and STAT1 Ser^{727} by IFN-α (in blue), IFN-γ (in red) and IFN-λ (in green) in* ***hMADS pre-adipocytes***. Cells were treated for 1, 2, 4, 8 and 24 h with the cytokines (20 ng/mL). Phosphorylation levels are compared to basal levels in untreated cells (100%).

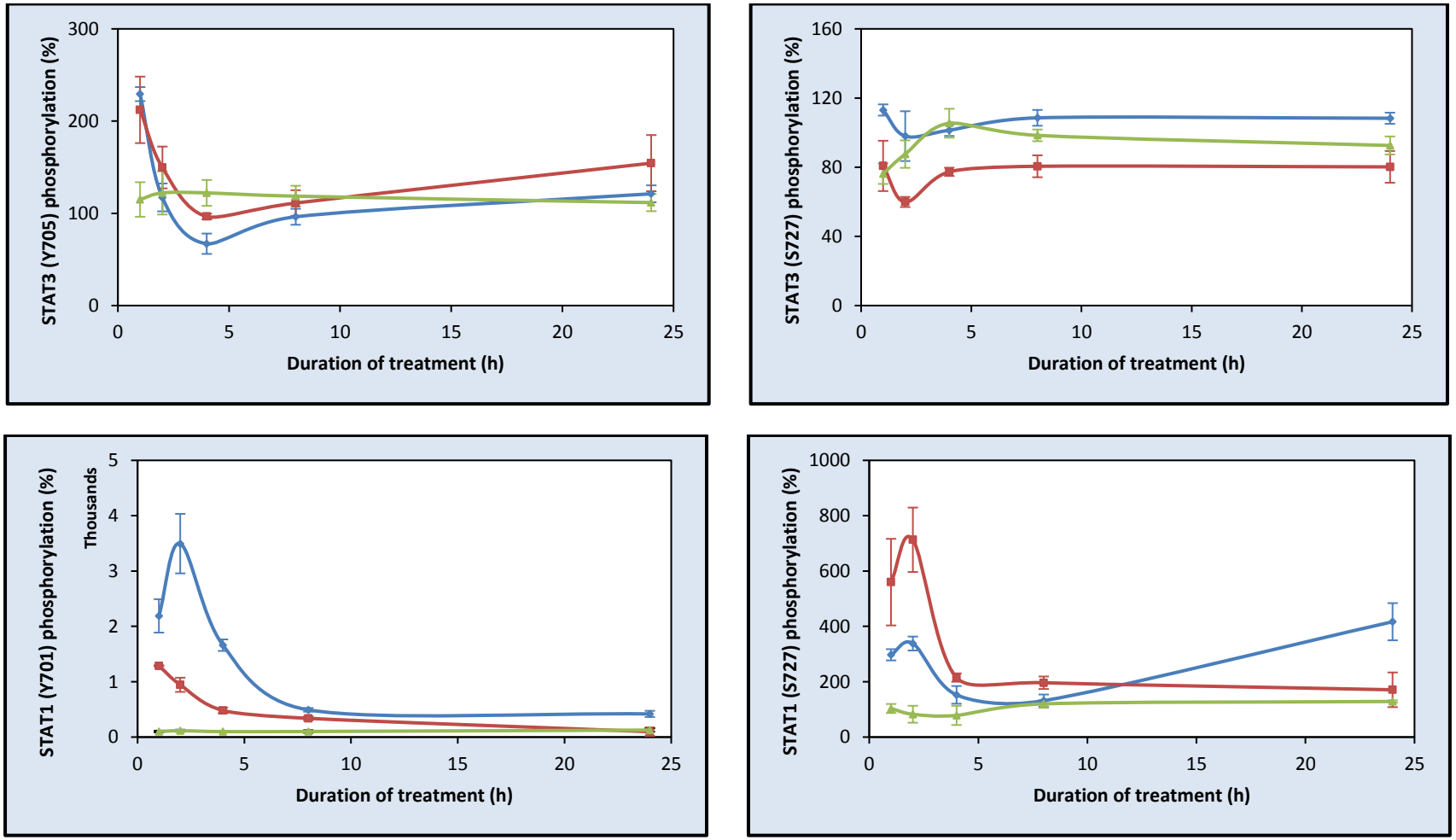

Figure 48. *Graph showing the induction of STAT3 Tyr^{705}, STAT3 Ser^{727}, STAT1 Tyr^{701} and STAT1 Ser^{727} by IFN-α (in blue), IFN-γ (in red) and IFN-λ (in green) in* ***hMADS mature adipocytes***. Cells were treated for 1, 2, 4, 8 and 24 h with the cytokines (20 ng/mL). Phosphorylation levels are compared to basal levels in untreated cells (100%).

III. 4. Discussion of Chapter 3

III. 4. 1. Models of palmitate- and IFN-γ-induced insulin resistance

Data from preliminary experiments on 3T3-L1 pre-adipocytes, where cells were treated either in absence or presence of serum, reveals a minor palmitate-induced increase in insulin-stimulated Akt phosphorylation relatively to insulin-stimulated control in both conditions tested (*Figure 13*). Yet, altering the experimental conditions to a 24 h treatment followed by a 3 h serum derivation resulted in a SFA-mediated attenuation of insulin-stimulated p-Akt signal in both pre-adipocytes and mature adipocytes (*Figures 14A* and *15A*). Such effect was rescued by adding A66 to the palmitate treatment, hence validating this cellular model of palmitate-induced insulin resistance as well as the positive metabolic impact of p110α inhibition. The beneficial effects of blocking this catalytic subunit of PI3K had indeed been reported Foukas *et al.* in 2006, when investigating the phenotypic traits of $p110\alpha^{D933A/WT}$ mice (L. C. Foukas 2006). Hence, the present results provide an understanding of this phenomenon at the cellular level in metabolic tissues. In human cells, the inhibitory effect of palmitate on insulin-stimulated Akt phosphorylation could only be reproduced in mature adipocytes. However, the response of the human pre- and mature adipocytes to the combined treatment of palmitate and A66 and A66 alone followed a similar trend as the response of murine cells (*Figures 16A* and *17A*).

IFN-γ treatment induced an unexpected increase in insulin-stimulated p-Akt in 3T3-L1 pre-adipocytes treated in presence of serum, while the opposite effect was recorded under SF conditions (*Figure 13*). This points to a potential interaction between the cytokine and serum-soluble receptors, which may act as competitive

inhibitors of IFN-γ activity by reducing its ability to bind cell-surface receptors (Oppenheim 1993). However, the inhibitory effect of the cytokine treatment in the absence of serum recorded in *figure 13* could not be reproduced in *figure 14B*.

In differentiated 3T3-L1 adipocytes, the cytokine treatment significantly inhibited insulin-stimulated phosphorylation of Akt, an effect abrogated with exposure to the p110α inhibitor (*Figure 15B*). A similar trend was observed in the mirror experiments carried out in pre- and mature hMADS adipocytes (*Figures 16B* and *17B*). Statistical significance of IFN-γ-mediated effect could not be achieved despite replicating the experimental conditions used by McGuillicuddy and colleagues, which they reported to significantly hinder the phosphorylation of Akt (McGillicuddy 2009). A likely explanation for this discrepancy is the difference in human adipocytes used: while they performed their experiments in SGBS cells, the present work was carried out in hMADS cells. Increasing the concentration of IFN-γ used might have allowed to statistically validate the inhibitory effect of the cytokine on insulin signalling.

III. 4. 2. STAT3, but not STAT1, is activated by palmitate

Focusing on the impact of palmitate on the phosphorylation of STAT1 and STAT3, our results indicate a stimulatory effect on p-STAT3 Tyr^{705} following an 8 h treatment in 3T3-L1 mature adipocytes solely (*Figure 20A*). The serine residues of STAT1 and STAT3, as well as the tyrosine residue of STAT1, were unaffected by palmitate treatment (*Figures 20B, 21A* and *21B*). In other cell types tested (3T3-L1 pre-adipocytes, hMADS pre- and mature adipocytes), the SFA failed to elicit a

reproducible effect on either p-STAT3 Tyr^{705}/ Ser^{727} or p-STAT1 Tyr^{701}/ Ser^{727} (*Figures 18, 19, 22, 23, 24* and *25*). A series of shorter time course experiments was performed confirming that neither STAT1 nor STAT3 was activated within an hour of the palmitate treatment (*Figures 26* to *33*). Collectively, these findings suggest that the observed palmitate-mediated phosphorylation of STAT3 Tyr^{705} occurs through a mechanism independent of IFN secretion, as STAT1 would have otherwise been induced by the SFA.

The induction of STAT3 by palmitate aligns with the studies discussed in the introduction of the present chapter. Indeed, Mashili and colleagues demonstrated the stimulatory effect of SFA on this tyrosine phosphorylation site of the transcription factor (Mashili 2013). Comparable to our findings, the palmitate-induced stimulation of STAT3 was associated with down-regulation of the insulin pathway. These results were corroborated by the study of Weigert and colleagues who evidenced the palmitate-mediated induction of pro-inflammatory IL-6, which in turn promoted the phosphorylation of STAT3 Tyr^{705} (Weigert 2004). These two studies were carried out in skeletal muscle cell and, to the best of our knowledge, no study has investigated the effect of palmitate on the phosphorylation of STAT3 or STAT1 in adipocytes.

Our experiments reveal that although palmitate induces STAT3, it has no effect on the phosphorylation of STAT1. Despite an overlap in the activating factors modulating the phosphorylation of the two STATs (e.g. IFN-γ, oncostatin-M, LIF) highlighted in the introduction of the present chapter, differences exist in their regulation and activity. These will now be explored in further detail to shed light on

the potential molecular mechanisms underlying the differential effect of palmitate on STATs 1 and 3. For instance, Vaisse *et al.* reported leptin to activate STAT3 but not STAT1 in the hypothalamus of *ob*/*ob* and WT mice (Vaisse 1996). Specific nutrients such as arginine were also found to induce the tyrosine phosphorylation of STAT3, without stimulating STAT1 in WAT (de Castro Barbosa 2009). McGillicuddy and colleagues evidenced that in human and murine adipocytes, IFN-γ down-regulates insulin signalling through STAT1 and to a lesser extent STAT3 (McGillicuddy 2009). This differential effect of the cytokine on STAT1 and STAT3 activation had been previously reported in human acute myelocytic leukemia cells (Sato 1997).

The differential pattern of activation described by McGillicuddy *et al.* and Sato *et al*. is characteristic of IFN-mediated STAT phosphorylation. As discussed in Chapter 1, IFN-γ promotes the phosphorylation of STATs through IFNGR, which interacts with JAK1 and JAK2. These kinases trigger the sustained activation of STAT1, while also inducing the activation of STAT3 in a weaker and more transient manner (Pensa 2013). As illustrated in *figure 8*, type I IFN drives the same activation pattern in STATs through binding IFNAR, which recruits and phosphorylate JAK1 and TYK2 (L. Platanias 2005). However, the opposite STAT activation pattern has been reported: a prolonged stimulation of STAT3 and transitory activation of STAT1 (Pensa 2013). Such pattern is associated with the glycoprotein 130 (gp130)-mediated induction of STAT.

Gp130 describes a family of cytokines, also known as the IL-6 family, which docks to the plasma membrane via receptor complexes characterised by a common signal transducing receptor chain, gp130 (P. B.-N. Heinrich 2003). In addition to

gp130, each cytokine interacts with another receptor component including the LIF receptor and an α receptor specific to each member of this family of proteins. For instance, IL-6 engages IL-6 receptor α and associated with a gp130 homodimer (P. B.-N. Heinrich 2003). Upon receptor activation, the tyrosine kinases of the JAK family (JAK1, JAK2 and TYK2) are induced and enable the binding of STATs to the receptor. The highly conserved SH2 domain of STATs mediates this interaction: STAT3 was reported to bind the phospho (p)YXXQ motif, while evidence indicates STAT1 to interact with the pYXPQ motif. The presence of the proline residue in the latter consensus sequence implicates that the interaction of STAT1 with the receptor is more restricted compared to STAT3. Thus IL-6 family cytokines were shown to be potent activators of STAT3 but minor inducers of STAT1 (A. Costa-Pereira 2014).

Illustrating the differential effect of IFN and IL-6 family cytokines on STATs induction, Costa-Pereira *et al*. observed that silencing STAT3 in mouse embryonic fibroblasts (MEFs) did not affect their IFN-γ response but altered the cellular response to IL-6 family cytokines (A. T. Costa-Pereira 2002). Surprisingly, the authors evidenced a switch from one cytokine signalling to the other triggered by the loss of the signalling component. Consistently with such findings, Hergovits *et al*. demonstrated that treating human fibroblasts with oncostatin-M induced a prolonged activation of STAT3 Tyr^{705}, while STAT1 Tyr^{701} was induced to a lesser extent and only transiently (Hergovits 2017). Interestingly, they evidenced that STAT3 acts as a negative regulator of STAT1 signalling following oncostatin-M stimulation. Indeed, silencing STAT3 was reported not only to inhibit STAT3 mRNA and protein expression, as well as pSTAT3 Tyr^{705}, but was also associated with a significant

increase in pSTAT1 Tyr^{701} levels in oncostatin-treated cells. Additional experiments indicate that the expression of STAT1 target genes was also altered. The authors identify SOCS3 as critical in the counter-regulatory activity of STAT3 (Hergovits 2017).

Therefore, it is likely that the palmitate-mediated phosphorylation of STAT3 Tyr^{705} reported in the present chapter is modulated through the secretion of gp130 cytokines rather than of IFN. Indeed, no evidence in the literature indicates that palmitate does stimulate the secretion of IFN or that adipocytes secrete IFN. Various studies, however, highlight the ability of the SFA to induce gp130 cytokines. As mentioned previously, both Weigert *et al.* and Oberbach *et al.* implicated palmitate in the expression of IL-6 in muscle cells (Weigert 2004, Oberbach 2010). The same observation was made in human coronary artery endothelial cells and in 3T3-L1 adipocytes (Staiger 2004, K. a. Ajuwon 2005). This link between palmitate and gp130 cytokines echoes the association between the latter and the onset of obesity and insulin resistance discussed in the introduction of the present chapter and reviewed by White and Stephens (U. a. White 2011).

III. 4. 3. The roles of STAT3 serine and tyrosine phosphorylation sites

To understand why only the tyrosine residue of STAT3 was phosphorylated in response to palmitate treatment, the individual roles of Ser^{727} and Tyr^{705} must be further investigated. As discussed by Heinrich *et al.*, the binding of STAT3 to the gp130 receptor is followed by the phosphorylation of the Tyr^{705} residue of the

transcription factor. This step is essential for the formation of active STAT3 dimers, which can then translocate from the cytoplasm to the nucleus where they modulate transcription (P. B.-N. Heinrich 2003). Located in the carboxyterminal, the Ser^{727} phosphorylation site, found in STAT1 too, also mediates the transcriptional activity of STAT3 but is not necessary for nuclear translocation. Moreover, this site is not required for the binding of STAT3 to the promoters of ISGs. Its role is limited to allowing full transcriptional activation (Wen 1995). It is unclear which kinase executes the phosphorylation of the Ser^{727} residue but p38 MAPK, MAPK/ERK kinase 1, ERK and c-Jun N-terminal kinase (JNK) have been implicated in this molecular event (P. B.-N. Heinrich 2003). The downstream effector of Akt, PKCδ, was also reported to be essential in the phosphorylation of STAT3 Ser^{727} in HepG2 cells. Evidence indicates that this event occurs within the nucleus following the phosphorylation of the tyrosine residue (Schuringa 2001).

The biological role of Ser^{727} phosphorylation is not as well understood as that of Tyr^{705}. Kramer and colleague postulated the involvement of the serine residue in a non-canonical mitochondrial translocation of STAT3 as a strategy to regulate adipogenesis (Kramer 2015). Alternatively, Chung *et al*. proposed that this site is implicated in the modulation of the Tyr^{705}-mediated STAT3 activity. Indeed, they provided evidence that STAT3 Ser^{727} phosphorylation inhibited STAT3 Tyr^{705} phosphorylation in COS cells (fibroblast-like) (Chung 1997). This seesaw regulation of STAT3 phosphorylation is also reflected by the study of Andersson and colleagues in 3T3-L1 adipocytes (Andersson 2007). The authors demonstrated the dual role of insulin, which, on the one hand, inhibited tyrosine phosphorylation, while simultaneously inducing phosphorylation at the serine position. Furthermore,

Andersson and colleagues reveal that the pancreatic hormone antagonises IL-6-induced STAT3 tyrosine phosphorylation and impairs STAT3 nuclear translocation.

The stimulatory effect of insulin on STAT3 Ser^{727} phosphorylation was later confirmed by Wada *et al.* in 3T3-L1 adipocytes (Wada, 2010). Similarly, Kim et *al.* reported that overexpressing STAT3-S727D sufficed to hinder insulin signalling in HepG2 cells (J. Y. Kim 2009). Together, these studies support the model proposed earlier by which gp130 cytokines rather than IFN-γ modulate palmitate-mediated phosphorylation of STAT3 Tyr^{705}. Indeed, as palmitate impairs the insulin sensitivity of the cell, STAT3 Ser^{727} phosphorylation is no longer induced and the inhibition of STAT3 Tyr^{705} phosphorylation mediated by both Ser^{727} phosphorylation and insulin is alleviated. Under these conditions, cytokines such as IL-6 would be able to freely influence transcription through STAT3 Tyr^{705} phosphorylation. In favour of this model, the phosphorylation of Ser^{727} was found to be critical in IFN-γ-dependent innate immune responses (L. Platanias 2005).

III. 4. 4. Palmitate-mediated induction of STAT3 Tyr^{705} phosphorylation is TLR4-independent

Various inhibitors were tested to probe the molecular mechanisms underlying palmitate-mediated stimulation of p-STAT3 Tyr^{705} in 3T3-L1 mature adipocytes. More specifically, A66, D030, TAK 242 and myriocin were used, targeting p110α, p110δ, TLR4 and SPT, respectively (*Figures 34*, *35* and *36*). However, none of these small molecules prevented the SFA-induced stimulation of STAT3. Here, the reason why inhibiting TLR4 failed to rescue the palmitate-mediated effect will be explored.

As discussed in the introduction of the present chapter, many studies indicate that TLR4 mediates palmitate signalling and has the ability to bind the SFA (Shi 2006, Holland 2011, Schilling 2013, Turpin 2014, Pal 2012, Nicholas 2017). The receptor, abundantly expressed in differentiated 3T3-L1 and adipose tissue, was also found to be a central modulator of the IFN response (Faure 2001, T. T. Kawai 2001, Noppert 2007, M. K. Song 2006). Furthermore, it was directly implicated in the up-regulation of STAT3 expression in bladder epithelial cells (Ying 2013). Collectively, these studies suggest that inhibiting TLR4 would likely affect palmitate-induced phosphorylation of STAT3 recorded in *figure 20A*. However, adding the inhibitor to the SFA treatment failed to rescue the palmitate-mediated effect (*Figure 34*). Pre-treating the cells with the TLR4 inhibitor (TAK 242) had no significant effect either (*Figure 35*). As TAK 242 successfully rescued the LPS-mediated induction of STAT3, the activity of the inhibitor could be verified.

A reason for this could be that in differentiated 3T3-L1, TLR4 mediates only the effect of palmitate through the stimulation of IFN secretion. Indeed, according to our model palmitate induction of STAT3 is likely to be modulated by gp130 cytokines, hence the absence of effect on STAT3 phosphorylation when inhibiting TLR4. The study of Song *et al*. supports this theory as they noted that palmitate did not significantly affect the expression of TLR4 target genes in mature 3T3-L1 (M. K. Song 2006). Therefore another receptor is likely to be mediating the effect of palmitate on STAT3. A potential candidate would be TLR2, a TLR homologue located at the cell surface which expression was found markedly elevated compared to that of TLR1 and TLR6 in both pre- and mature 3T3-L1 (Poulain-Godefroy 2010).

This receptor is induced by a range of ligands derived from bacteria (e.g. diacyl and triacyl lipopeptides, lipoteichoic acid and glycolipids), fungi (e.g. zymosan), protozoans (e.g. glycosylphosphatidylinositol anchor) and viruses (e.g. the envelope proteins of measles virus) (Uematsu 2008). Furthermore, similarly to TLR4, TLR2 is activated by SFA. For instance, in C2C12 myotubes, palmitate triggers the association of TLR2 with its adaptor protein MyD88, while also stimulating the downstream kinases JNK, PKC and p38 (J. Senn 2006). Various studies substantiated the importance of TRL2 in the development of obesity and its associated metabolic disorders. Indeed, Kim *et al.* report the expression of this receptor to be up-regulated in the adipose tissue of HFD-fed mice. In addition the expression of TLR2 was increased in both the visceral and subcutaneous fat depots of *ob*/*ob* mice *versus* lean control (S. C. Kim 2012). Ahmad *et al*. record the same observation when comparing the expression of the receptor in the subcutaneous adipose tissue of both obese and type 2 diabetic overweight subjects compared to lean individuals (Ahmad 2012).

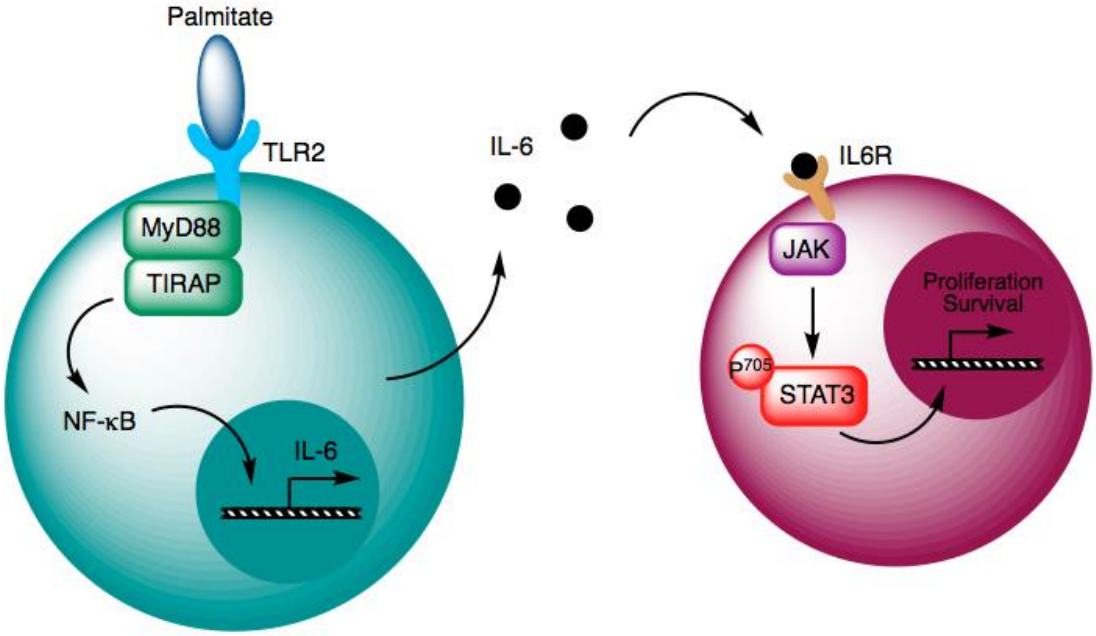

Figure 49. *Potential molecular mechanism mediating palmitate-induced activation of STAT3.* Palmitate binds TLR2 triggering NF-κB in a MyD88-dependent manner. This promotes the secretion of interleukin-6 (IL-6), which docks to its receptor (IL-6 receptor [IL6R] α associated to a glycoprotein 130 homodimer). Once activated, the receptor drives the phosphorylation of JAK and in turn STAT3 Tyr^{705}. STAT3 then translocates to the nucleus where it stimulates the transcription of pro-survival genes and promotes proliferation.

Poulain-Godefroy and colleagues demonstrated that TLR2 induction with Pam3CSK4, a TLR2 agonist, promotes the release of IL-6 form both pre- and mature 3T3-L1 adipocytes (Poulain-Godefroy 2010). Aligned with these findings, Ajuwon *et al*. reported that exposing 3T3-L1 cells to peptidoglycan stimulates the expression of both IL-6 and TLR2 (K. B. Ajuwon 2009). MyD88 is required for the secretion of IL-6 as MyD88-deficient mice fail to produce the gp130 cytokine when treated with TLR ligands (K. K. Takeda 2003). As illustrated in *figure 12*, TLR signalling can either be MyD88-dependent or MyD88-independent. Interestingly, TLR2 ligand-mediated activation of NF-κB is abolished in MyD88-deficient macrophages, while the NF-κB cascade is still activated by a TLR4 ligand. This reveals that TLR2

signalling requires MyD88, unlike TLR4 signalling which appears to rely on both MyD88-dependent and –independent pathways (T. A. Kawai 1999).

Exposure of MyD88-deficient macrophages to a TLR4 ligand (LPS) allowed further characterisation of the MyD88-independent cascade unveiling that although the expression of a range of ISGs was mediated by this cascade through the activation of IRF3, many pro-inflammatory cytokines such as IL-6 were not induced. On the contrary, exposure of these MyD88-deficient macrophages to a TLR2 ligand (macrophage-activating lipopeptide-2) failed to stimulate ISGs (T. T. Kawai 2001). Collectively, this data supports the model presented in *figure 49*, by which palmitate would induce IL-6 secretion through the TLR2/MyD88 cascade, resulting in the induction of STAT3 but not STAT1. Such model provides a mechanistic theory to the results discussed in Chapter 3.

III. 4. 5. Palmitate-mediated induction of STAT3 Tyr^{705} phosphorylation is a PI3K-independent

Aside from inhibiting TLR4, the effect of blocking both p110α and p110δ on palmitate-mediated induction of p-STAT3 Tyr^{705} was also investigated. As the inhibitory effect of the SFA on the phosphorylation of Akt could be rescued through the inhibition of p110α, it seemed plausible that this would also prevent the palmitate-induced stimulation of STAT3. However, as shown in *figure 34*, A66 had no effect on this endpoint. Having postulated that the effect of palmitate would be modulated via TLR4, an inhibitor of p110δ (D030) was also tested (*Figure 34*). Indeed, Aksoy *et al*. reported this isoform of PI3K to control the subcellular

compartmentalisation of TLR4 (Aksoy 2012). Yet, inhibiting p110δ also failed to rescue palmitate-mediated stimulation STAT3 Tyr^{705}.

In their review, Akira and Takeda discuss the interaction between PI3K and the TLR pathway (Akira 2004). They draw the reader's attention to the capacity of TLRs to bind the SH2 domain of the p85 regulatory subunit of PI3K. Upon binding, the catalytic subunit is recruited to the TLR-p85 complex allowing for the complete activation of PI3K. Furthermore, the authors note the presence of another PI3K binding site in the carboxyterminus of MyD88, which was also found to directly interact with Akt. Using a dominant negative mutant of p85 in human microvascular endothelial cells, Li *et al.* also provided evidence that PI3K is required for the transcriptional activity of NF-κB (X. T. Li 2003). In addition, they confirmed that inhibiting PI3K through this system hindered the production of IL-6 using an enzyme-linked immunosorbent assay. Together, these results seem to support that PI3K inhibition would alter palmitate-induced STAT3 activation if the latter were modulated through TLR2/MyD88/IL-6.

However, the effect of PI3K inhibition on IL-6 reported by Li *et al*. is mediated by LPS, which interacts with TLR4 rather than TLR2 (X. T. Li 2003). Therefore, the fact that A66/D030 does not rescue the effect of palmitate does not contradict our model presented in *figure 49* as the MyD88/PI3K interaction implicates TLR4. Consistent with such findings, Ortega-Molina *et al.* failed to observe a statistically significant decrease in IL-6 expression in the liver of HFD-fed mice treated with a pharmacological inhibitor of PI3K (CNIO-PI3Ki) *versus* mice on the same diet treated with vehicle (Ortega-Molina 2015). In addition, Ajuwon *et al.*

reported that exposing 3T3-L1 adipocytes to palmitate promotes NF-κB activity along with IL-6 production, but, importantly, the authors note that blocking PI3K using a non-specific, covalent inhibitor (wortmannin) magnified the response to palmitate alone (K. a. Ajuwon 2005).

The last inhibitor tested was myriocin, which targets SPT, an enzyme specialised in catalysing the first step of *de novo* ceramide synthesis. As with the other inhibitors tested, it had no effect on the palmitate-mediated stimulation of STAT3 Tyr^{705} phosphorylation (*Figure 35*). This result is consistent with the absence of effect of TAK 242, A66 and D030 on palmitate-induced activation of STAT3. Indeed, $C_{16:0}$-ceramides are associated to the onset of obesity and glucose intolerance through their effect on PI3K and TLR4 (Holland 2011, Schilling 2013, Hla 2014). If neither PI3K nor TLR4 is involved in modulating the stimulatory effect of palmitate on STAT3, it is to be expected that $C_{16:0}$- ceramides are not implicated in this molecular mechanism either.

III. 4. 6. Comparing the effect of the different types of IFN on STAT1 and STAT3

Time course experiments investigating the effect of three different types of IFN (IFN-α, IFN-γ and IFN-λ) on the phosphorylation of STAT1 Tyr^{701}, STAT1 Ser^{727}, STAT3 Tyr^{705} and STAT3 Ser^{727} were carried out in 3T3-L1 and hMADS pre- and mature adipocytes (*Figures 18* to *25* and *37* to *44*). For clarity, the data obtained was superimposed in four sets of graphs (*Figures 45* to *48*). In 3T3-L1 pre-adipocytes, IFN-α and IFN-γ to a lesser extent induced a rapid phosphorylation

(peaking at 1 h of treatment) of both STAT1 Tyr^{701} and STAT3 Tyr^{705}. The phosphorylation of STAT1 Tyr^{701} is significantly stronger than that of STAT3 Tyr^{705}. The serine residues of both STAT1 and STAT3 were stimulated by IFN-γ in the short and long term (weak induction after 1 h of treatment, stronger induction after 24 h of treatment) and by IFN-α only in the short term (peaking at 1 h of treatment) (*Figure 45*).

Comparing the response of pre-adipocytes to differentiated 3T3-L1 cells, we observe a considerable attenuation of IFN-α-mediated effect, which becomes comparable to that elicited by IFN-λ (*Figure 46*). Inversely, IFN-γ had a stronger effect on the phosphorylation of all residues in the mature murine adipocytes compared to pre-adipocytes. The trend previously recorded in pre-adipocytes can also be noted in mature cells: a short-term induction of the tyrosine residue is observed in both STAT1 and STAT3 with a stronger phosphorylation of STAT1 Tyr^{701}. Interestingly, IFN-γ-induced phosphorylation in the serine site followed an opposite pattern in STAT1 and STAT3. Indeed, after 1 h of treatment p-STAT3 Ser^{727} is stimulated, its level then dips after 2 h of treatment and rises back up after 4 h to gradually decrease again. The phosphorylation levels of STAT1 Ser^{727} respond to the IFN-γ treatment in the opposite manner.

In hMADS pre-adipocytes, IFN-γ had a significant impact on the phosphorylation of the four residues considered but IFN-α and IFN-λ did not. As for murine cells, the effect of the cytokine was stronger on STAT1 than STAT3. For all residues, the induction peaked after 1 h of treatment (*Figure 47*). In this cell line, differentiation down-regulated the IFN-γ mediated effect except for STAT1 Ser^{727}

(*Figure 48*). IFN-α significantly stimulated the phosphorylation of STAT1 Tyr^{701} as well as STAT1 Ser^{727} and STAT3 Tyr^{705} to a lesser extent. For both STAT1 phosphorylation sites, IFN-α-induced stimulation peaked after 2 h of treatment, while for STAT3 Tyr^{705} the peak was recorded after 1 h of treatment similarly to IFN-γ-induced activation. For STAT3 Ser^{727}, the three IFN tested only had a minor effect.

The pattern of activation of the tyrosine residue mediated by IFN-γ is consistent with the findings of McGillicuddy *et al.* who reported a strong induction of STAT1 Tyr^{701} and a milder activation of STAT3 Tyr^{705} in both murine and human adipocytes (McGillicuddy 2009). IFN-α has been reported to induce the formation of a range of STATs homo- and heterodimers including STAT1 and STAT3 homodimers, as well as STAT1-STAT3 heterodimers (L. Platanias 2005). However, to the best of our knowledge, no study has compared the effect of IFN-α on p-STAT1 Tyr^{701} and p-STAT3 Tyr^{705} levels over time in adipocytes. Tanabe *et al.* were able to demonstrate that IFN-β, another type I IFN, induces the phosphorylation of STAT1 Tyr^{701} after exposing murine T lymphocytes to the cytokine for 30 min. They report that STAT3 Tyr^{705} was also phosphorylated but to a lesser degree (Tanabe 2005). Such findings coincide with the observations reported in this chapter (*Figures 45* to *48*).

Interestingly, in 3T3-L1 pre-adipocyte cells the tyrosine phosphorylation of STAT1 and STAT3 induced by IFN-α was more significant than that elicited by IFN-γ (*Figure 45*). This trend was however reversed in mature 3T3-L1 adipocytes (*Figure 46*). This likely reflects the inhibitory effect of IFN-α on adipogenesis

recently described by Lee and colleagues in the same cell type (K. U. Lee 2016). They reported that both STAT1 expression and tyrosine phosphorylation were enhanced by the cytokine after 1 h of treatment, while inhibiting STAT1 prevented IFN-α from down-regulating the modulators of adipogenesis PPARγ and C/EBPα. STAT1 inhibition also rescued IFN-α-mediated cell cycle arrest. This anti-adipogenic property of IFN-α/STAT1 seems to corroborate the observation that STAT1 is more strongly activated in pre- rather than mature adipocytes.

Surprisingly, in hMADS cells, the opposite response can be observed, with IFN-γ having a more potent effect than IFN-α in pre-adipocytes and in mature cells IFN-γ-mediated effect being milder than that mediated by IFN-α (*Figures 47* and *48*). This result is supported by the study of McGillicuddy *et al.* demonstrating the anti-adipogenic effect of IFN-γ in human adipocytes (McGillicuddy 2009). Thus it seems that inhibition of the adipogenic process can be effected by either type I or type II IFN depending on the type of cell. Overall the pattern of serine phosphorylation was consistent with the current paradigm which supports that both type I and II IFN induce the phosphorylation of the serine residue of STAT1 and STAT3 (L. Platanias 2005). However, our data suggests a greater effect of type II IFN compared to type I IFN. Moreover, this effect is stronger in the long-term in murine cells but peaks in the short-term in human cells.

As illustrated by *figures 45* to *48*, IFN-λ treatment failed to produce any significant effect on the phosphorylation levels of STAT1 and STAT3 across cell types despite a trend towards a minor induction of serine phosphorylation most noticeable in hMADS pre-adipocyte STAT3 Ser^{727} (*Figure 47*). These results do not

rule out the implication of type III IFN in STAT1/3 activation all together. Indeed, as reported by Dickensheets *et al.* IFN-λ2 (used in this experiment) was found to have a milder effect on the phosphorylation of STAT1 Tyr^{701} compared to IFN-λ1 and IFN-λ3 (Dickensheets 2013). Moreover, the study investigated the IFN-λ-mediated induction of STAT1 in hepatocytes, lymphocytes and monocytes and recorded a striking variability of the cytokine-induced effect across cell types. Therefore, unlike IFN-λ2, IFN-λ1 or IFN-λ3 might have an effect on the phosphorylation of STAT in adipocytes. Further, an IFN-λ2-mediated effect might be observable at higher concentrations, as Dickensheets and colleagues recorded an effect at 50 and 500 ng/mL (Dickensheets 2013).

III. 4. 7. Limitations and future experiments

One limitation of the findings exposed in the present chapter was a model of IFN-γ-induced insulin resistance could only be established in differentiated 3T3-L1 cells, and even then the cytokine had only a mild inhibitory effect on p-Akt. IFN-γ failed to impair insulin signalling in 3T3-L1 and hMADS pre-adipocytes as well as in hMADS mature adipocytes. A higher concentration of IFN-γ might have induced a significant inhibition of Akt phosphorylation in these cells. Besides, future experiments could attempt to develop such model of insulin resistance in SGBS cells rather than hMADS and thus exactly reproduce the experimental design of McGillicuddy *et al*. (McGillicuddy 2009).

Another shortfall of this chapter was the inability to reproduce the palmitate-mediated induction of pSTAT3 Tyr^{705} observed in mature 3T3-L1 adipocytes in

mature hMADS cells. A potential reason for this could be that the basal levels of p-STAT3 Tyr^{705} is significantly higher in the latter cell line, thus subtle variations in phosphorylation might have gone undetected. Furthermore, we failed to successfully rescue the palmitate-mediated induction of pSTAT3 Tyr^{705} in mature murine cells. No positive control was included when testing the effect of A66, D030 or myriocin (*figures 34* and *36*) thus providing no guaranty that these worked efficiently. However, in the case of A66, experiments had been previously performed showing the inhibitor to successfully counteract the deleterious effect of palmitate on p-Akt levels. We were therefore confident that it efficiently inhibited p110α. Consequently, future experiments should seek to include appropriate positive controls for at least D030 and myriocin. These should also investigate whether inhibiting TLR2 would rescue palmitate-mediated induction of p-STAT3. If so this would validate the mechanistic model proposed in *figure 49*.

Lastly, future experiments could further explore the effect IFN-λ on STAT phosphorylation in adipocytes by comparing the effect of IFN-λ1, IFN-λ2 and IFN-λ3 side-by-side. These will need to include a valid positive control, the lack of which was another shortcoming of the data presented in the present chapter. Higher concentrations (comparable to the ones tested by Dickensheets and colleagues) might be required to observe a significant effect on the phosphorylation of the STAT transcription factors (Dickensheets 2013).

CHAPTER 4. EFFECTS OF SFA OVERLOAD ON LIPID METABOLISM IN ADIPOCYTES

IV. 1. Overview of Chapter 4

Having explored the impact of palmitate on the development of insulin resistance and investigated its effect on the downstream signalling of IFN, the present chapter focuses on the role of this lipid molecule in the modulation of other facets of adipocyte metabolism. Two processes disrupted in the obese insulin resistant state were studied: lipolysis and autophagy. While, the former describes the breakdown of stored lipids into FFAs, the latter is recognised as the cellular degradation of target cytosolic cargo through the activity of the autolysosome. Parallels can be drawn between such processes as both provide the cell with energy and molecular building blocks necessary for vital anabolic reactions to occur during nutrient deprivation. As both processes are sensitive to nutrient levels, it is unsurprising that crossovers exist in the molecular effectors in charge of their regulation: while insulin promotes the down-regulation of both lipolysis and autophagy, glucagon stimulates these two processes. Such similarities have led Singh and colleagues to coin the term "lipophagy" in reference to the type of autophagy targeting intracellular lipid stores (R. K. Singh 2009). Obesity-associated insulin resistance has been found to directly disrupt the lipophagic process by promoting low-grade systemic inflammation. The present chapter therefore investigates the effect of SFAs and IFN on the modulation of the lipophagic function in adipocytes.

IV. 1. 1. Aim of Chapter 4

In order to gather insight on the effect of palmitate and IFN on lipophagy, we assessed whether treating 3T3-L1 and hMADS adipocytes with the SFA and the cytokine affected markers of lipolysis, including the phosphorylation of HSL and of PKA. The activation of the autophagic pathways was also evaluated through quantifying the expression of protein kinase R (PKR) and microtubule-associated protein 1B-light chain 3-II (LC3B-II).

IV. 2. Introduction of Chapter 4

IV. 2. 1. The regulation of lipolysis by blood glucose concentration

Lipolysis, introduced in Chapter 1, describes the process by which TAG stores are hydrolysed to release FAs and glycerol into the circulation for endogenous use, thus allowing cells to cope with starvation. Having previously discussed its mechanisms and the critical role of key enzymes such as PKA and HSL, we will now focus on the implication of the glucagon/insulin tandem in its regulation. During fasting, glucagon elicits the pro-lipolytic activity of PKA through the stimulation of the cAMP pathway. Glucagon-mediated PKA activation also up-regulates the gluconeogenic programme via CREB phosphorylation. Indeed, through passive diffusion, the activated PKA catalytic subunits enter the nucleus where they phosphorylate CREB, thus promoting the transcription of its target gluconeogenic genes characterised by CRE-containing promoters.

As shown in *figure 50*, CREB-dependent transcription is promoted by association of CREB with CREB regulated transcription coactivators (CRTCs) (Altarejos 2011). Moreover, through the glucagon-mediated inhibition of salt-inducible kinase 2 (SIK2), CRTC2 is dephosphorylated and migrates to the nucleus where it further simulates the gluconeogenic program (Altarejos 2011). Gluconeogenesis is also amplified as a result of low insulin concentration driving the dephosphorylation of FOXO1. Indeed, as for CREB and CRTC2, the phosphorylation status of FOXO1 determines its subcellular localisation: the loss of its phosphate group at Ser^{316} induces the translocation of the transcription factor to the nucleus where it stimulates gluconeogenic genes (Oh 2013).

In the post-prandial state, insulin drives the down-regulation of the lipolytic process through inhibiting the cAMP/PKA signalling. Firstly, it promotes cAMP degradation through the activation of cyclic nucleotide phosphodiesterase 3B, thereby hindering PKA activity (Ahmed 2010). Furthermore, the hormone was shown to inhibit AC while also promoting the internalisation of β-ARs (J. a. Jocken 2008). Lastly, Strålfords and colleagues evidenced the insulin-induced dephosphorylation of HSL, attributed to the stimulation of a protein phosphatase (Stralfors 1989). It is therefore not unexpected that the obese insulin resistant state is associated with excessive basal lipolysis, as cells fail to respond to the anti-lipolytic effects of insulin (Duncan 2007). This leads to high levels of circulating FAs, which accumulate in the liver along with dietary FAs where they undergo esterification to TAGs. These can either accumulate in non-adipose tissues such as skeletal muscles, the pancreas and the liver (a process described as ectopic fat deposition), or be secreted into the blood as very low-density lipoproteins (Postic 2008). ER stress, cell death and mitochondrial dysfunction are additional consequences of unrestrained lipolysis. Together these metabolic disorders can seed life-threatening conditions such as T2D, liver steatosis and atherosclerosis (M. E. Schweiger 2014).

Unlike basal lipolysis, catecholamine-mediated lipolysis is blunted with obesity. Several mechanisms are thought to underlie the onset of this metabolic disruption, including a decrease in expression and activity of both β-ARs and HSL along with a diminished access of lipases to their substrate. Whether blunted catecholamine-induced lipolysis is the cause or the consequence of the disorder is the object of an on-going debate (J. a. Jocken 2008). Interestingly, CRTC3 was found to play a critical role in the attenuation of catecholamine signalling (Y. A.

Song 2010). Indeed, it appears that the CREB coactivator promotes obesity through the inhibition of AC in adipose tissues, with *Crtc3*$^{-/-}$ knockout mice protected from diet-induced obesity and from hepatic steatosis (Freson 2007). Overall, the data presented in this section emphasises the crosstalk between glucose and lipid metabolism and highlights the critical role of PKA/cAMP signalling in the modulation of these processes.

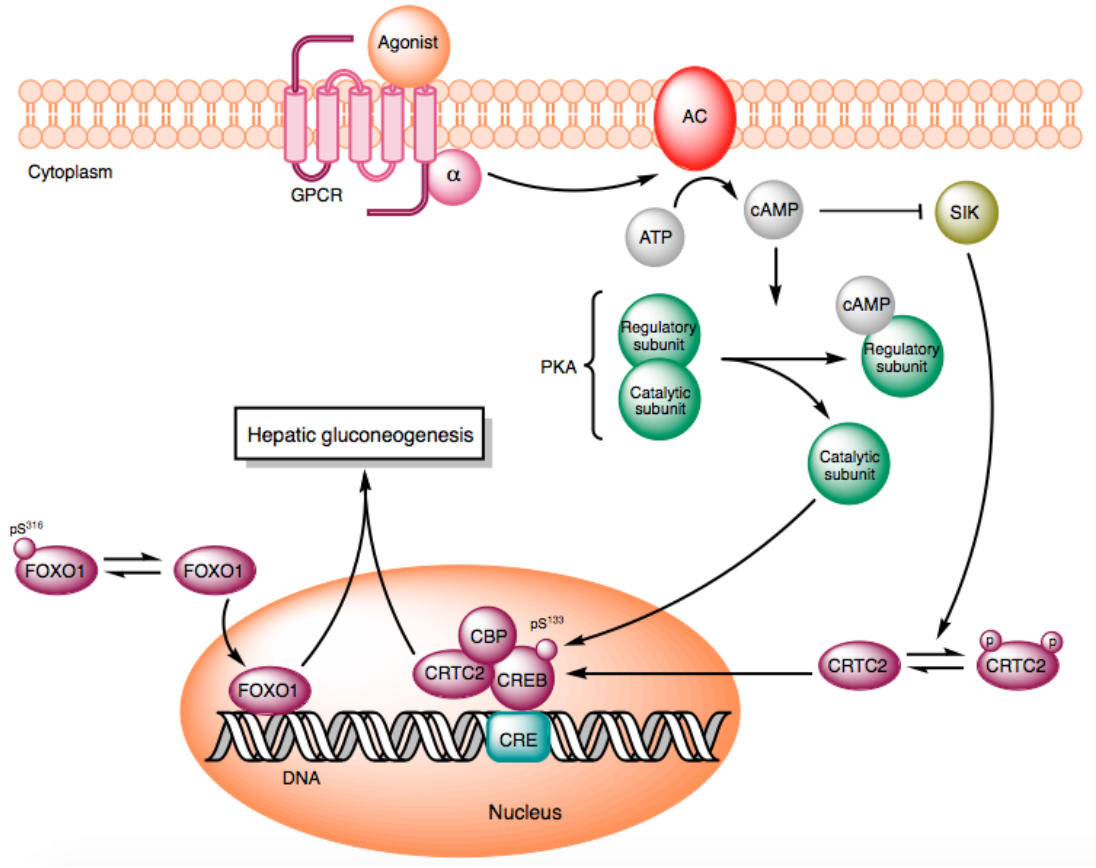

Figure 50. *The role of CREB phosphorylation in the regulation of hepatic gluconeogenesis.* Upon ligand engagement, the α-subunit of the stimulatory G-protein linked to the G protein-coupled receptor (GPCR) activates AC. This enzyme can then stimulate the synthesis of cAMP, which will promote the dissociation of the catalytic subunit of PKA. The latter will translocate to the nucleus where it enables the formation of the CREB-CBP-CRTC2 multi-protein complex through the phosphorylation of CREB. As a result of these molecular events along with the activation of FOXO1, the transcription of genes involved in hepatic gluconeogenesis will be up-regulated.

IV. 2. 2. The mechanisms of autophagy

The second aspect of lipophagy, which the present chapter will explore is autophagy. As mentioned in Chapter 1, it describes the catabolic process by which the cell degrades, through lysosomal activity, defective or threatening constituents such as intracellular pathogens and unfolded proteins (Cahova 2015). This process involves the formation of an autophagosome, which engulfs the components targeted for degradation. As illustrated by *figure 51*, two ubiquitin-like systems mark the synthesis of this double-membrane organelle. Firstly, the conjugation of the proteins encoded by autophagy related genes *Atg5* and *Atg12*, triggered by the ATG7-mediated activation of ATG12. Activated ATG12 then interacts with ATG10, which enables it to covalently bind ATG5 at Lys^{149} through its carboxyterminal glycine residue. Having recruited ATG16L, the resulting ATG5-ATG12-ATG16L complex associates with the phagophore to induce curvature in its structure through the asymmetric recruitment of LC3B. Once the autophagosome is formed, the complex dissociates from the membrane, thus making it a weak indicator of autophagy. In this system, parallels can be drawn between ATG7 and E1 ubiquitin-activating enzymes, on the one hand, and ATG10 and E2 ubiquitin-conjugating enzymes, on the other hand (Ohsumi 2001).

The second ubiquitin-like system required for autophagy is the ATG8 system, the yeast homologue of the mammalian LC3B, mentioned above. Upon induction of autophagy, the cytosolic unprocessed form of the protein (proLC3B) is cleaved by ATG4, thereby producing LC3B-I characterised by its exposed carboxyterminal glycine. Acting like an E1 ubiquitin-activating enzyme, ATG7 activates LC3B-I, which can consecutively be transferred to ATG3, thought to

assume the function of an E2-like enzyme. As illustrated by *figure 51,* conjugation of LC3B-I with the later enzyme precedes its interaction with phosphatidylethanolamine (PE), which produces LC3B-II. In an ATG5-ATG12 dependent manner, the lipophilic PE group drives the integration of LC3B-II into the phagophore membrane as well as the autophagosome membrane (Barth 2010). There, the ATG8 homologue has been implicated in the selection of cargo for degradation along with membrane fusion *in vitro*.

Following the expansion and fusion of the phagorphore membrane around the target cytosolic cargo, some LC3B-II is recycled and the maturation of the autophagosome unfolds (Glick 2010). This process involves the fusion for the outer membrane of the organelle with the endosome, which morphs into a lysosome, the resulting structure described as an "autolysosome". The elements contained in the inner membrane of the autophagosome are then digested by the lysosomic hydrolases and their building blocks are transported to the cytosol to be reused (Mizushima 2007).

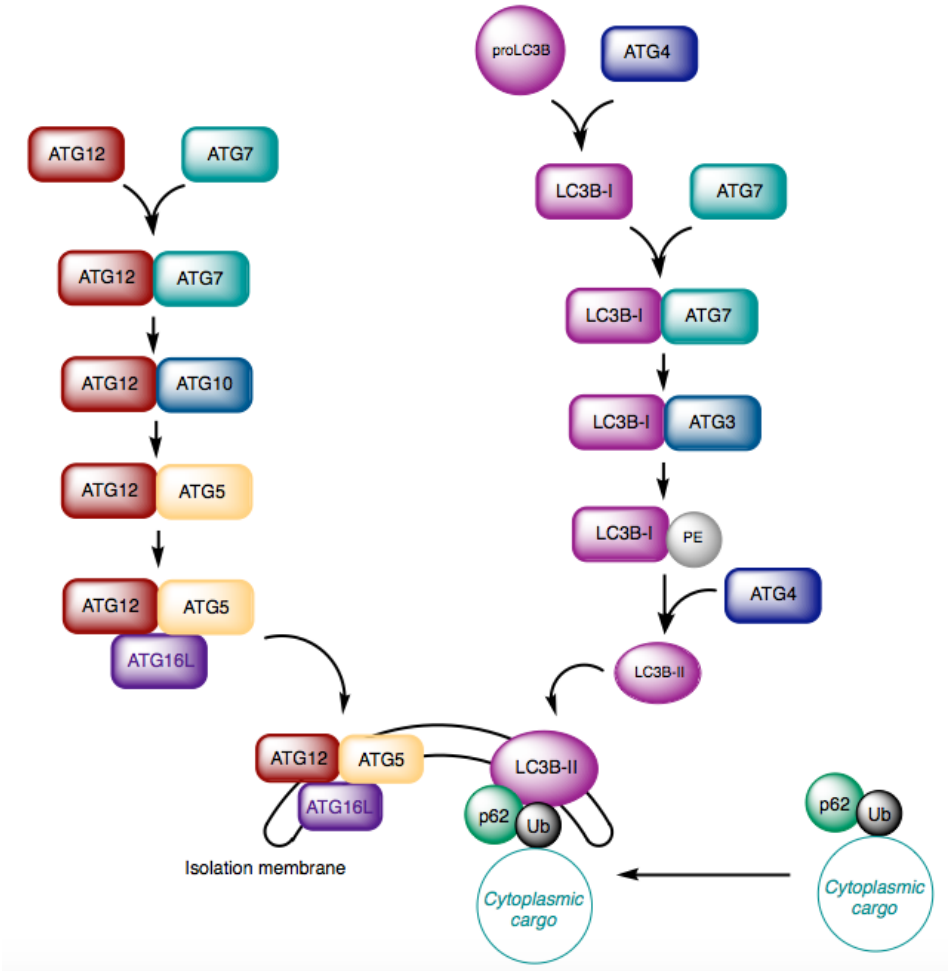

Figure 51. *The two ubiquitin-like systems necessary for the formation of the autophagosome.* The first ubiquitin-like system implicated in the formation of the autpohagic organelle is the ATG12-ATG5 complex. ATG7 (E1-like) activates ATG12, allowing for the activated enzyme to interact with ATG10 (E2-like). ATG12 is then conjugated to ATG5 and ATG16L. The resulting complex binds the isolation membrane and enables the recruitment of LC3B-II to the membrane as well. The latter is produced by the second ubiquitin-like system. Indeed, the cytosolic unprocessed form of LC3B-II, proLC3B, is initially cleaved by ATG4 to generate LC3B-I. Once activated by ATG7 (E1-like), this protein binds ATG3 (E2-like), which permits the conjugation of LC3B-I with phosphatidylethanolamine (PE). The protein complex is ruptured by ATG4, thereby producing LC3B-II, which binds the isolation membrane and recruits p62-bound ubiquitinated cytosolic cargo. *Ub*: ubiquitin.

Because LC3B-II does not dissociate from the membrane of the autophagic organelles, it has become a widely used marker of autophagy (Kirkin 2009). However, it is important to note that increased LC3B-II levels may indicate either an up-regulation of autophagosome synthesis or an impaired autophagosome turnover. Thus, in order to interpret fluctuations in this marker with less ambiguity, additional

controls should be included in the experimental design (Barth 2010). A commonly used control is the antibiotic bafilomycin A1, which inhibits of the vacuolar H^+ ATPase regulating the lysosomal pH and thereby blocking the autophagic flux. An up-regulation of LC3B-II levels occurring only in the absence of this antibiotic indicates a stimulation of a molecular event preceding autolysosme-mediated degradation, such as autophagosome synthesis. On the other hand, if a treatment induces the stimulation of LC3B-II levels both in the presence and absence of bafilomycin A1, it likely promotes the autophagic flux (Redmann 2017).

Aside from LC3B-II, alternative molecules can also be used to assess the rate of this process such as p62/sequestosome 1. This nucleoporin forms a complex with both LC3B and poly-ubiquitinated protein aggregates thus allowing the latter to be targeted for autophagosomal degradation (Barth 2010). Komatsu and colleagues were able to demonstrate that the homeostatic levels of p62 were inversely correlated to the rate of autophagy as they report an increase in the intracellular accumulation of these protein aggregates in autophagy/ATG7-deficient mice (Komatsu 2007).

IV. 2. 3. The importance of the endocrine system in the regulation of autophagy

Over the last decade many studies have investigated the impact of insulin resistance on the regulation of autophagy. Findings are far from unequivocal and appear to be dependent on the tissue and cell type investigated as well as the model of insulin resistance used. We will focus on the work carried out on adipose tissue and adipocytes as it is relevant to the model used in the present work. *Ex vivo*,

evidence from genetic experiments and the use of pharmacological inhibitors indicates a critical role of autophagy in adipogenesis. For example, Baerga and colleagues reported that knockdown of *Atg5* blocked the differentiation process in primary MEFs (Baerga 2009). The same year, similar results were obtained from knockdown experiments performed in 3T3-L1 pre-adipocytes targeting *Atg5* and *Atg7* (R. X. Singh 2009). *In vivo*, deletion of *Atg7* in murine models induced the development of singular adipocytes characterised by multiple lipid droplets and an abnormally high mitochondria count. These mice, significantly leaner than WT, displayed enhanced insulin sensitivity and were protected from diet-induced obesity (R. X. Singh 2009).

Insulin resistance appears to stimulate the rate of autophagy. Indeed, in obese patients both mRNA and protein levels of ATG5, LC3A and LC3B were increased compared to lean controls. In addition, elevated autophagosome numbers and a higher autophagic flux were associated with obesity (Kovsan 2011). In line with these findings, Nuñez and colleagues report that post-bariatric surgery weight loss in obese patients drove a reduction of the rate of autophagy in the subcutaneous adipose tissue. Such results are coherent with observations from a mouse model of diet-induced obesity and diabetes: restricting the caloric intake of the mice by 40% for two weeks induced a reduction in the expression of autophagy markers, elevated at baseline (Nunez 2013). Various hypotheses have been formulated to rationalise the effect insulin resistance on autophagy-mediated regulation of lipid metabolism. Ost and colleagues proposed that the increase in autophagy merely reflects the attenuation of mTORC1 signalling caused by insulin resistance. Indeed, in addition to up-regulated autophagy markers in the adipose tissue of obese diabetic patients,

they observed a decrease in phosphorylation of protein S6 kinase, the main mTORC1 substrate (Ost 2010).

Alternatively, insulin resistance may induce an increase in adipose tissue autophagy through ER stress. Such stress arises when the ER, where the bulk of protein synthesis occurs, fails to process misfolded proteins. These accumulate within the lumen of the organelle prompting a series of reactions known as the unfolded protein response (UPR), which either restores ER function or induces apoptosis (Cahova 2015). Autophagy is induced as part of the UPR in order to shield adipocytes from toxic protein aggregates. Lastly, Jansen and colleagues hypothesised that increased autophagic rates in the context of obesity allows to buffer inflammation in adipose tissue and avoid worsening of insulin resistance. Indeed, they revealed that inhibiting autophagy stimulated the expression of pro-inflammatory cytokines in both adipose tissue explants and adipocytes, an effect enhanced in obese mice *versus* lean control (Jansen 2012).

IV. 2. 4. The role of the IFN response in the regulation of autophagy

Although other cytokines such as IL-4 and -10 were reported to have an inhibitory effect on autophagy, IFN-γ has emerged as an inducer of the self-degradative process. Indeed, promoting autophagy is part of the immune strategy to facilitate clearance of intracellular bacterial pathogens. Despite the underlying mechanisms being only partially understood, it appears that IFN-γ-induced autophagy is mediated through both immunity-related GTPases (IRG) and members

of the 65 kDa guanylate binding protein family (Al-Zeer 2009). In the absence of infection, members of the IRG family are predominantly localised in the cytosol. However, some IRGs can be found at the ER, the Golgi or the endolysosomal membranes. Upon infection, IFN-induced proteins migrate to pathogen-containing vacuoles or phagosomes, where they are able to stimulate acidification and drive fusion with the lysosome permitting the elimination of the pathogen (Al-Zeer 2009). Interestingly, having investigated IFN-γ-induced autophagy in macrophages, Matsuzawa and colleagues concluded that this process required JAK1 and JAK2, PI3K and p38 MAPK but was independent of STAT1 (Matsuzawa 2012). Li and colleagues also identified IRF1 as a key modulator in this process in human hepatocellular carcinoma cells and demonstrate that, in this model, autophagy hinders growth and promotes cell death (P. D. Li 2012).

Type I IFN was also found to elicit autophagy in a range of cancer cells in a JAK1-, STAT1- and STAT2-dependent manner (Schmeisser 2014). Similarly, STAT3 has been implicated in the regulation of autophagy. On the one hand, nuclear STAT3 does so through modulating the transcription of a panel of genes involved in both up- and down-regulation autophagy. The direction of STAT3 mediation appears to be context-dependent, as the transcription factor responds to a wide range of cues. On the other hand, cytoplasmic STAT3 is a constitutive inhibitor of autophagy as it sequesters PKR (You 2015). The pro-autophagic role of this kinase is further explored in the following section.

IV. 2. 5. PKR, a key modulator of autophagy

The results of the transcription analysis, which originated the present project, drew the focus of our experimental work onto PKR, a critical modulator of the IFN-mediated antiviral response, also known as eukaryotic translation initiation factor 2 α (EIF2α) kinase 2. Indeed, RNA sequencing data evidenced that expression of this kinase was down-regulated in the presence of the PI3K inhibitor A66. PKR is part of a family of protein kinases that modulate protein synthesis in response to environmental stresses through the phosphorylation EIF2α. More specifically, as this reaction drives the sequestration of the guanine nucleotide exchange factor EIF2β, guanosine diphosphate is no longer recycled leading to the inhibition of translation. The cellular antiviral response can then be launched at the gene expression level (Sadler 2008).

Inactive PKR is constitutively expressed in all tissues at a basal level. However, upon viral infection, the kinase is induced by viral double-stranded RNA (dsRNA). Once activated, it dimerises to form a homodimer able to phosphorylate EIF2α. PKR induction by dsRNA is mediated through the two RNA-binding motifs found at the N-terminus of the kinase, which allows for the autophosphorylation of PKR through its intramolecular kinase domain (Sadler 2008). In addition to viral dsRNA, PKR can be activated by other pathogen-associated molecules. For instance, in bone-marrow-derived macrophages, Hsu and colleagues reported that the dsRNA-responsive kinase is promptly activated by LPS, a ligand of TLR4 found at the surface of gram-negative bacteria. This LPS-mediated induction of PKR was dependent on TRIF and did not appear to alter the expression of a large number of NF-κB target genes. Interestingly, knocking out PKR disrupted LPS-induced STAT1

phosphorylation and protected the cell from apoptosis in response to LPS treatment (Hsu 2004). The pro-apoptotic role of PKR had first been suggested ten years earlier by Lee and colleagues who over-expressed the kinase in HeLa cells (S. a. Lee 1994). Additional studies in virus-infected cells confirmed this finding in both HeLa and U937 cells (Kibler 1997, Takizawa 1996, Yeung 1999).

Further PKR activators have been identified such as protein activator of the IFN-induced protein kinase (PACT), a cellular protein which, unlike LPS, interacts directly with PKR. Along with its human homolog (retina and anterior neutral fold homeobox protein), PACT was shown to induce PKR in response to stressors including peroxide, sodium arsenite treatments and, relevantly to the present work, ceramides (Ruvolo 2001). This indirect ceramide-mediated stimulation of PKR hints to a role outside of it the immune response for the kinase. Indeed, studies are increasingly focussing on its involvement in nutrient sensing and inflammation in the context of obesity and insulin resistance. It was initially observed that the antiviral action of the kinase was linked with key inflammatory signalling pathway also involved in metabolic homeostasis such as IκB kinase and JNK (Lancaster 2016). Nakamura and colleagues then presented a series of interesting results pointing in this direction. Firstly, PKR activity was up-regulated in the liver and WAT of both *ob*/*ob* mice and mice fed with a HFD compared to lean control. Secondly, relevant to Chapter 5, *Isg15* mRNA levels were found to be increased in the adipocytes of mice on the HFD compared to the lean control. They were also able to demonstrate that PKR activity was induced by lipid infusion *in vivo* and more specifically, that palmitic acid drove the same effect in MEFs. Interestingly, such effect of the SFA did not seem to be mediated by the TLR4 pathway (T. F. Nakamura 2010).

The data of Nakamura *et al*. indicates a direct interaction between PKR and IRS1, involved in modulating insulin signalling at the IR (T. F. Nakamura 2010). Furthermore, comparing the response of a *Pkr*$^{-/-}$ knockout mice to a HFD to a WT control, they evidenced the functional significance of PKR in the development of metabolic disorders as the deletion of PKR protected against insulin resistance, inflammation and obesity. Consistent data was published two years later by Cavalho-Filho and colleagues who documented a similar role for PKR in human tissue (Carvalho-Filho 2012). Indeed, they noted that bariatric surgery resulted in a significant reduction of PKR activity in the liver, muscle and adipose tissues and that markers of ER stress, inflammation and insulin resistance were reduced following the procedure (Carvalho 2013).

In light of these findings, the results of Cho and colleagues are rather unexpected as they put forward an anti-apoptotic role for PKR, evidencing with biophysical assays that palmitate directly binds PKR near the ATP binding site, thus preventing its autophosphorylation (Cho 2011). It is important to note that their research was carried out in human hepatocellular carcinoma cells as additional studies performed in tumour-cells supported anti-apoptotic PKR activity (S. F. Kim 2000, Hiasa 2003). Also challenging the mainstream model of PKR function, the findings of Lancaster and colleagues suggest that PKR is not obligatory for HFD-induced obesity and its associated metabolic and inflammatory dysregulations (Lancaster 2016). Indeed, they were unable to notice any significant differences in the response of their genetic *Pkr*$^{-/-}$ knockout model and that of WT mice to HFD. Both groups experienced the same changes in body composition over the 16 weeks

of the dietary intervention.

Furthermore, Lancaster *et al*. reported that deleting PKR did not alter glucose tolerance and fasting plasma insulin concentrations, despite it lowering plasma insulin levels during oral glucose tolerance tests (Lancaster 2016). They reported that markers of HFD-induced hepatic steatosis (increased fasting plasma cholesterol levels, decreased fasting plasma FFA), found to be prevented by PKR loss by Nakamura and colleagues, was unaffected by the genetic knockout. Although the loss of PKR did moderately reduce adipose tissue inflammation in line with the results of the other studies, they were unable to attribute this observation to the protection against lipid-induced inflammation: palmitate treatment *ex vivo* produced comparable increases in JNK and EIF2α in both WT and $Pkr^{-/-}$ knockout bone marrow-derived macrophages and similar concentrations of pro-inflammatory cytokines were measured in the media of both cell lines.

Lancaster and colleagues argue that the discrepancies between their findings and the other two studies discussed can be explained by the genetic background of the mice used in the knockout model and the difference in cell types used. They also emphasised the lack of consistency in the phenotypes associated to PKR deletion from one study to another (Lancaster 2016). Interestingly, Flannery and colleagues produce results concurring with the finding of Lancaster and colleagues: using the same murine $Pkr^{-/-}$ knockout model, they reported that the genotype of the mice does not affect their HFD-induced weight gain (Flannery 2013). Therefore, further research is needed to validate the model by which PKR would integrate a cellular lipid sensing with the activation of inflammatory signalling pathways thus

connecting the nutrient-surplus and chronic hyperlipidaemia associated with obesity to the low-grade inflammation characteristic of this disease.

The metabolic role of PKR was recently extended to the modulation of autophagy. Indeed, a chemical screen aimed at establishing novel inducers of autophagy led Shen and colleagues to concentrate their research on STAT3. As mentioned in the previous section, they were able to demonstrate that through the interaction of its SH2 domain with the catalytic domain of PKR, cytoplasmic STAT3 disrupts the enzymatic activity of PKR. They reported that both pharmacological and genetic inhibition of the transcription factor promoted the activity of PKR and consequently EIF2α phosphorylation (Shen 2012). Such inhibition of STAT3 stimulated of autophagy in a PKR-dependent manner. This group then performed a chemical screen designed at identifying PKR-dependent autophagy inducers revealing palmitate as a key stimulator of this process (M. S. Niso-Santano 2013). Furthermore, their findings supported that the effect of the SFA relies on the disruption of the STAT3-PKR interaction and necessitates the activation of the pro-inflammatory kinases MAPK8 and JNK1 as well as IRS1. Together, the studies discussed in this section shed light on the crosstalk between IFN and insulin pathway and obesity.

IV. 3. Results of Chapter 4

IV. 3. 1. Investigating the effect of FA- and IFN-γ-treatments on lipolysis in adipocytes

The first metabolic response to starvation investigated in adipocytes was the process of lipolysis. To this end, two endpoints were considered: on the one hand the phosphorylation levels of HSL and on the other hand, that of PKA substrate. As mentioned in the introduction of this chapter, these enzymes are mediators of lipolysis. Indeed, PKA is activated in response to increases in cAMP cellular concentration. The liberated catalytic subunit of PKA phosphorylates HSL, enabling the lipase to translocate to the lipid droplet from the cytoplasm. There, HSL catalyses the second step of the lipolytic process, i.e. breakdown of DAG to MAG. In addition, PKA prompts the conformational change of perilipin, a protein found at the surface of the droplet, thereby increasing the exposure of the lipids within the droplet to lipases. Therefore, an increase in phosphorylation levels of HSL and PKA would manifest a stimulation of the lipolytic process. Note that, in order to assess the effect of palmitate and IFN-γ on lipolysis, this cellular process was activated through an acute treatment with the epinephrine analogue, isoproterenol, a β-AR agonist. As for previous experiments, results were produced in both mature and pre-adipocytes from the 3T3-L1 and hMADS cell lines.

IV. 3. 1. 1. Using 3T3-L1 cell line

Figure 52 investigates the effect of IFN-γ and palmitate in murine pre-adipocytes. Because previous experiments showed that the BSA used to solubilise palmitate-stimulated STAT phosphorylation, both BSA conjugated and

unconjugated palmitate was used. However, neither of the treatments tested compared to the corresponding controls induced a significant change in p-HSL S^{660} or p-PKA substrate in 3T3-L1 pre-adipocytes. Interestingly, both conjugated palmitate and its BSA control drove a 70% drop in phosphorylation levels of HSL Ser^{660} compared to the isoproterenol-stimulated control, suggesting a BSA-mediated down-regulation of lipolysis. Consistent with this finding, such treatments also inhibited PKA substrate (perilipin) phosphorylation by 55% compared to the isoproterenol-stimulated control. LPS - included as positive control as it was demonstrated to stimulate lipolysis in adipose tissue of healthy subjects, as well as in human adipocytes - failed to induce p-HSL or p-PKA (Rittig 2016, Grisouard 2012).

As pre-adipocytes have not yet undergone adipogenesis, the effect of isoproterenol acute stimulation on p-HSL and p-perilipin is rather weak compared to that in mature adipocytes (*Figure 53)*. Indeed, there is no statistically significant difference between the phosphorylation levels of HSL and PKA substrate in untreated *versus* isoproterenol-stimulated pre-adipocytes. As for the undifferentiated cells, the lipolytic process in mature 3T3-L1 adipocytes was not affected by either IFN-γ, conjugated and unconjugated palmitate or LPS. However, unlike the pre-adipocytes experiment, BSA did not appear to impact lipolysis in differentiated 3T3-L1.

Figure 52. *IFN-γ, conjugated and unconjugated palmitate and LPS affect neither HSL nor PKA substrate phosphorylation in **3T3-L1 pre-adipocytes***. For both *figures A* and *B*, 3T3-L1 pre-adipocytes were treated in with IFN-γ (20 ng/mL) (lane 4), palmitate 3:1 BSA (500 µM) (lane 6), unconjugated palmitate (500 µM) (lane 8) and LPS (100 ng/mL) (lane 10) in 10% FBS/DMEM (HG) for 24 h. Equivalent volumes of MilliQ water (16 µL) (lane 3), BSA (400 µL) (lane 5), DMEM (LG) (400 µL) (lane 7) and PBS (40 µL) (lane 9) were used as control for these treatments. Following a 3 h serum deprivation (SF DMEM, HG, 0.2% BSA), cells were stimulated with isoproterenol (1 µM for 20 min). Cells were lysed with 60 µL 1% TX-100 lysis buffer per 6 cm Ø dish. 30 µg of protein were loaded per lane (10% SDS-acrylamide gel). Statistical difference between the water control and other treatments is indicated with $; statistical difference between the BSA FAF control and other treatments is indicated with *; statistical difference between the palmitate 3:1 BSA treatment and other treatments is indicated with # (p-value < 0.05). The red arrow indicates p-perilipin (56 kDa). Data from three independent experiments.

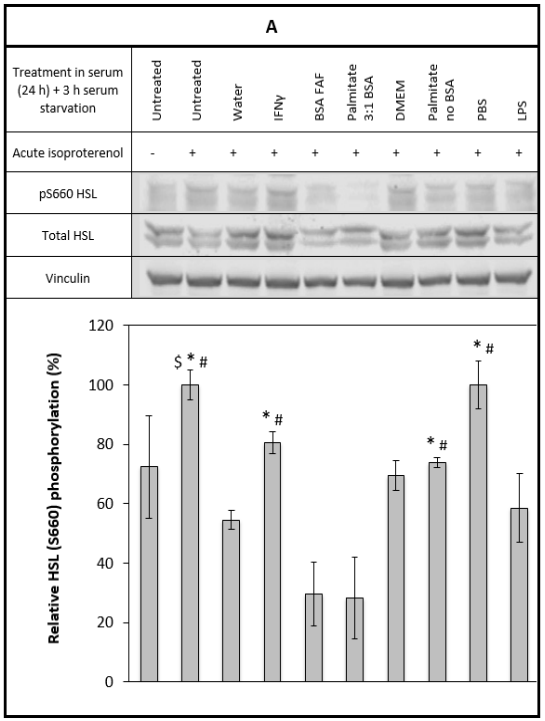

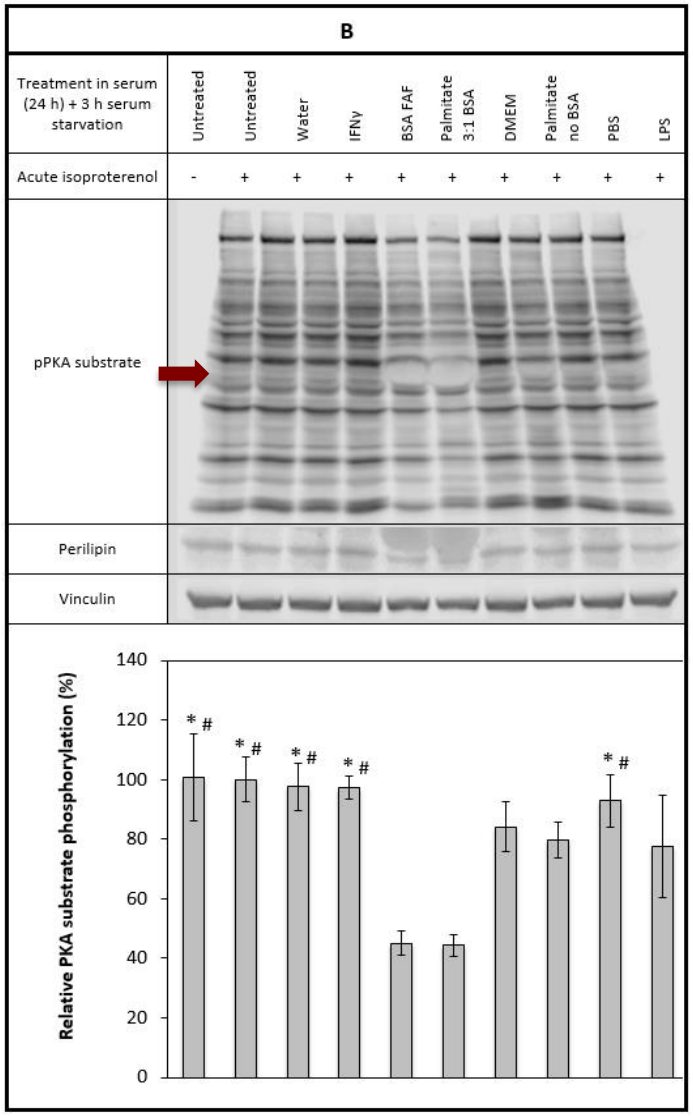

Figure 53. *IFN-γ, conjugated and unconjugated palmitate and LPS affect neither HSL nor PKA substrate phosphorylation in* ***3T3-L1 mature adipocytes***. For both *figures A* and *B*, 3T3-L1 mature adipocytes were treated in with IFN-γ (20 ng/mL) (lane 4), palmitate 3:1 BSA (500 µM) (lane 6), unconjugated palmitate (500 µM) (lane 8) and LPS (100 ng/mL) (lane 10) in 10% FBS/DMEM (HG) for 24 h. Equivalent volumes of MilliQ water (8 µL) (lane 3), BSA (200 µL) (lane 5), DMEM (LG) (200 µL) (lane 7) and PBS (20 µL) (lane 9) were used as control for these treatments. Following a 3 h serum deprivation (SF DMEM, HG, 0.2% BSA), cells were stimulated with isoproterenol (1 µM for 20 min). Cells were lysed with 80 µL 1% TX-100 lysis buffer per well. 44 µg of protein were loaded per lane (10% SDS-acrylamide gel). ** denotes a treatment statistically different from all other treatments (p-value < 0.05). The red arrow indicates p-perilipin (56 kDa). Data from three independent experiments.

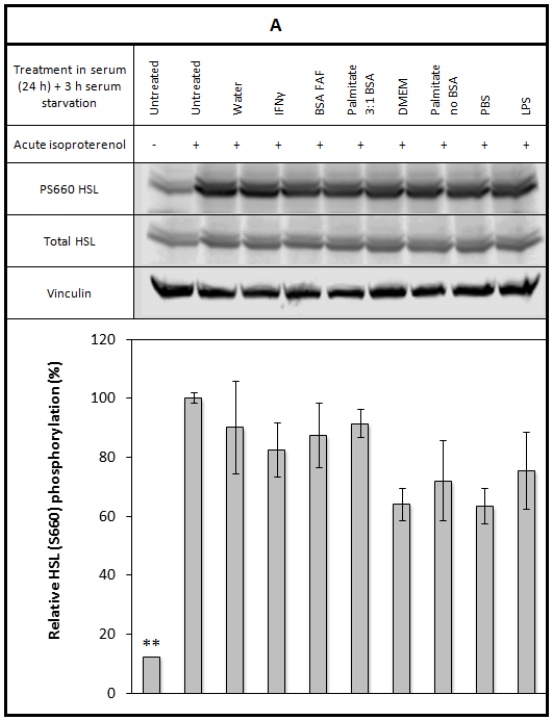

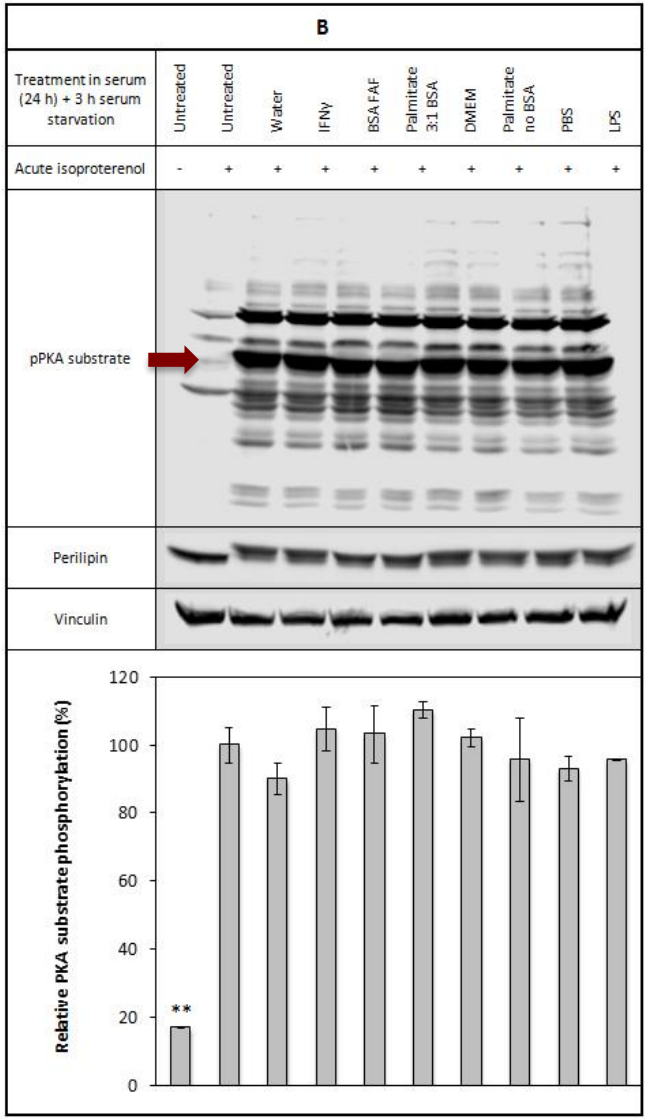

IV. 3. 1. 2. Using hMADS cell line

Figure 54 and *55* describe the experiments presented in the previous subsection in hMADS rather than 3T3-L1 cells. As for the murine cells, human pre-adipocytes were markedly less sensitive to isoproterenol stimulation compared to the differentiated cells. This is likely reflecting an increase in AR expression upon differentiation. While the p-HSL signal, although poor, seemed not to be affected by the acute isoproterenol treatment, the phosphorylation of PKA substrate was marginally stimulated by the epinephrine analogue with a 45% increase compared to the untreated control (*Figure 54*). Besides, it appears that BSA inhibits both HSL and PKA substrate activation to a lesser extent than in 3T3-L1 pre-adipocytes.

Figure 55 details the effect of the treatments on mature hMADS cells. As for differentiated 3T3-L1, isoproterenol induces a significant increase in lipolysis (even though the increase in PKA substrate phosphorylation observed in the isoproterenol-stimulated control fell short of statistical significance). Unlike previous experiments, none of the treatments tested effected a change in phosphorylation levels except for LPS which appears to promote the activation of both proteins: a 52% increase in p-HSL and a 45% increase in p-PKA substrate levels compared with the PBS-treated control. This result suggests LPS to be mildly enhancing lipolysis.

Figure 54. *IFN-γ, conjugated and unconjugated palmitate and LPS affect neither HSL nor PKA substrate phosphorylation in* ***hMADS pre-adipocytes***. For both *figures A* and *B*, hMADS pre-adipocytes were treated in with IFN-γ (20 ng/mL) (lane 4), palmitate 3:1 BSA (500 µM) (lane 6), unconjugated palmitate (500 µM) (lane 8) and LPS (100 ng/mL) (lane 10) in complete DMEM (LG) for 24 h. Equivalent volumes of MilliQ water (16 µL) (lane 3), BSA (400 µL) (lane 5), DMEM (LG) (400 µL) (lane 7) and PBS (40 µL) (lane 9) were used as control for these treatments. Following a 3 h serum deprivation (SF DMEM, LG, 0.2% BSA), cells were stimulated with isoproterenol (1 µM for 20 min). Cells were lysed with 100 µL 1% TX-100 lysis buffer per 6 cm Ø dish. 24 µg of protein were loaded per lane (10% SDS-acrylamide gel). Statistical difference between the untreated control and other treatments is indicated with %; statistical difference between the BSA FAF control and other treatments is indicated with *; statistical difference between the palmitate 3:1 BSA treatment and other treatments is indicated with # (p-value < 0.05). The red arrow indicates p-perilipin (56 kDa). Data from three independent experiments.

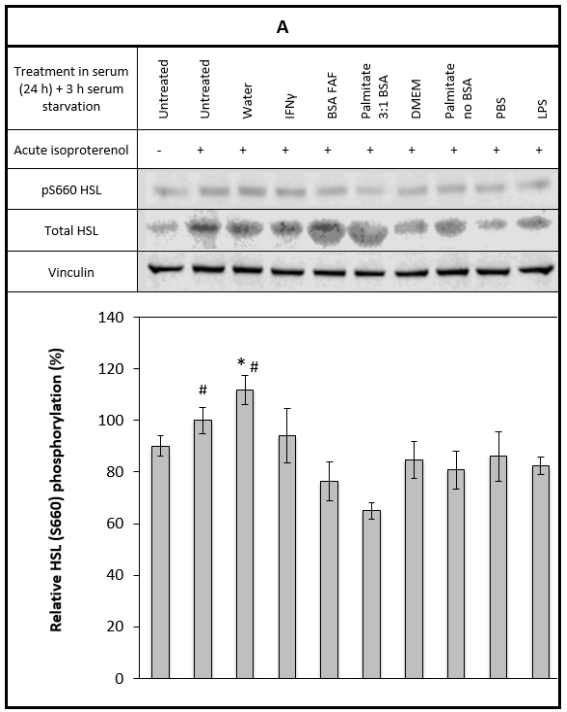

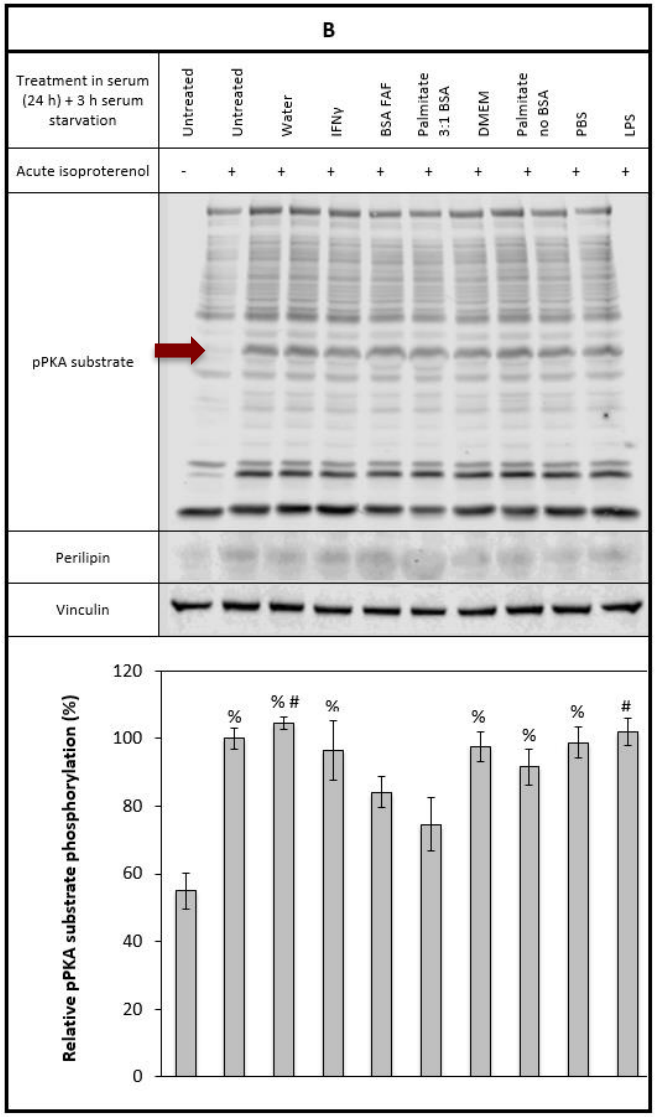

Figure 55. *IFN-γ, conjugated and unconjugated palmitate and LPS affect neither HSL nor PKA substrate phosphorylation in* ***hMADS mature adipocytes***. For both *figures A* and *B*, hMADS mature adipocytes were treated in with IFN-γ (20 ng/mL) (lane 4), palmitate 3:1 BSA (500 µM) (lane 6), unconjugated palmitate (500 µM) (lane 8) and LPS (100 ng/mL) (lane 10) in complete DMEM (LG) for 24 h. Equivalent volumes of MilliQ water (8 µL) (lane 3), BSA (200 µL) (lane 5), DMEM (LG) (200 µL) (lane 7) and PBS (20 µL) (lane 9) were used as control for these treatments. Following a 3 h serum deprivation (SF DMEM, LG, 0.2% BSA), cells were stimulated with isoproterenol (1 µM for 20 min). Cells were lysed with 80 µL 1% TX-100 lysis buffer per well. 68 µg of protein were loaded per lane (10% SDS-acrylamide gel). Statistical difference between the untreated control and other treatments is indicated with %; statistical difference between the LPS treatment and other treatments is indicated with &; ** denotes a treatment statistically different from all other treatments (p-value < 0.05). The red arrow indicates p-perilipin (56 kDa). Data from three independent experiments.

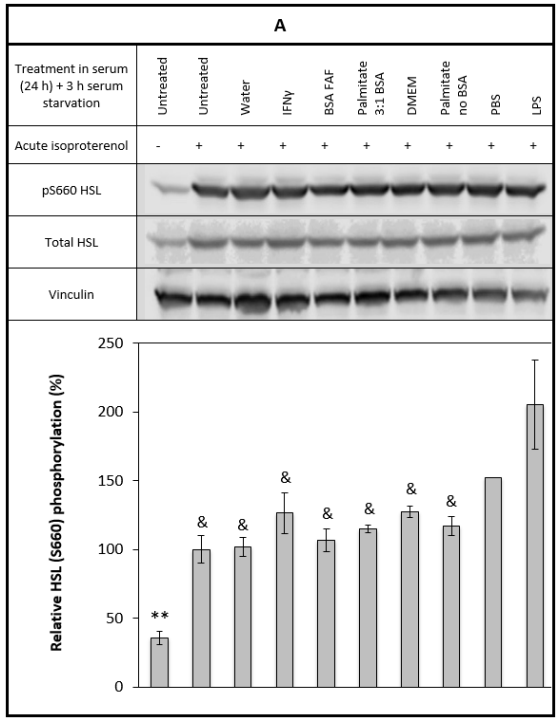

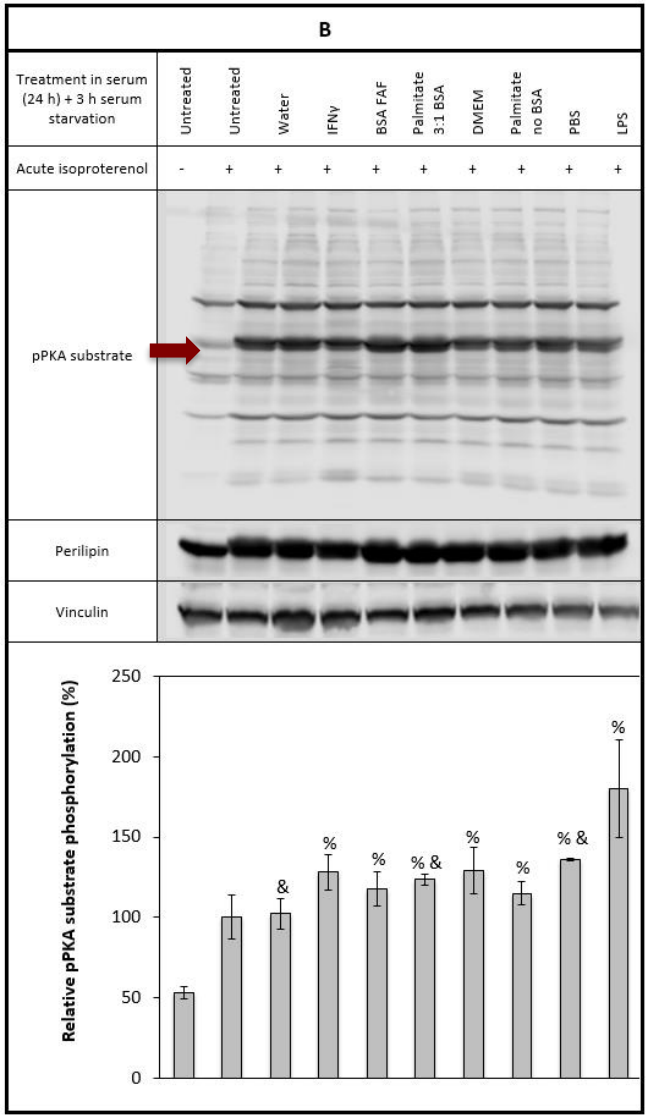

IV. 3. 2. Investigating the effect of palmitate on autophagy

Having investigated the effect of palmitate and IFN-γ on lipolysis, we focused our attention on the effect of the SFA on autophagy, the second cellular response to starvation that was explored in the introduction of this chapter. To this end, time course experiments were performed, treating both murine and human pre- and mature-adipocytes with unconjugated palmitate. The expression levels of LC3B-II were used as an indicator of the activity of the autophagic pathway. Having selected the time point at which the SFA had the strongest effect on LC3B-II, further experiments were performed including bafilomycin A1 treatment as an additional control. Indeed, as explained in section 2. 2. of the introduction, this antibiotic is known to inhibit the autophagic flux and thus provides a mean of better interpreting variations in LC3B-II levels.

IV. 3. 2. 1. Using 3T3-L1 cell line

Figure 56A presents the effect of palmitate on LC3B-II levels in 3T3-L1 pre-adipocytes. The SFA induces a significant up-regulation of this marker of autophagy, with a peak stimulation at 24 h of 484% compared to the 24 h DMEM-treated control. LPS treatment did not affect LC3B-II expression after 1 h of treatment but further time points should be tested to rule out an effect of LPS on autophagy as palmitate had not effect at this time point either. An analogous time course experiment was performed in murine differentiated adipocytes. As shown in *figure 56B*, the autophagic process of mature cells was not sensitive to palmitate. Indeed, at none of the time points tested did the SFA elicit an increase in the expression levels of LC3B-II compared to the controls. Interestingly, the basal expression levels of

this protein are considerable higher than those recorded in the pre-adipocytes.

In order to interpret palmitate-mediated induction autophagy in 3T3-L1 pre-adipocytes, bafilomycin A1 was included as a control in the experiment presented in *figure 57A*. Although the maximal induction of LC3B-II expression was recorded after 24 h of palmitate treatment, the cells were treated for 4 h. Indeed, at the 24 h time point, the effect of bafilomycin A1 was too strong to allow for the detection of a palmitate-mediated effect when combining the antibiotic and SFA treatments (*data not shown*). Comparing the LC3B-II expression levels following palmitate treatment (lane 3) to those following the SFA treatment supplemented with the antibiotic, one can see that bafilomycin A1 drives the induction of the autophagy marker even further than palmitate alone. As explained in the introduction, stimulation of LC3B-II levels in both the absence and presence of this antibiotic indicates that palmitate induces the autophagic flux. Having demonstrated that the SFA drives "true autophagy", A66 was added to the palmitate treatment (in the presence or absence of bafilomycin A1) in order to evaluate the role of PI3K catalytic subunit p110α in this process. As the levels of LC3B-II are unaffected by the inhibitor, we can conclude that palmitate-mediated induction of autophagy in 3T3-L1 pre-adipocytes is p110α-independent.

Figure 57B investigates the effect of the same treatments on p62 expression levels of 3T3-L1 pre-adipocytes. This nucleoporin stands as an alternative marker to LC3B-II as it forms a complex with LC3B and poly-ubiquitinated protein aggregates targeted for autophagosomal degradation (Barth 2010). p62 expression levels are expected to be inversely correlated to the rate of autophagy and therefore of LC3B-II

expression levels, which is coherent with the data presented in *figure 57B*. This validates the pro-autophagic activity of palmitate discussed in the previous paragraph.

In order, to further explore the signalling pathways involved in the regulation of palmitate-mediated induction of autophagy in 3T3-L1 pre-adipocytes, cells were treated with the SFA for 24 h in the presence or absence of A66, D030, TAK 242 and myriocin. To maximise the potential effect of the inhibitors, these were added to the media 1 h before the start of the palmitate treatment. As seen in *figure 58*, none of the inhibitors tested has a statistically significant effect on palmitate-mediated induction of autophagy, although there is a trend indicating that inhibiting p110α would rescue this effect. Indeed, analysing the data using a one-way ANOVA (F (11, 21) = 10.80) yields a p-value of 0.58 when comparing the palmitate-treated sample to the palmitate- plus A66-treated sample. A two-way ANOVA examining the interaction between the effects of the SFA and the inhibitor also falls short of statistical significance, F (1, 7) = 3.55, p-value = 0.10. Overall, the data points towards the pro-autophagic role of palmitate being independent of the PI3K, TLR4 and ceramide pathways.

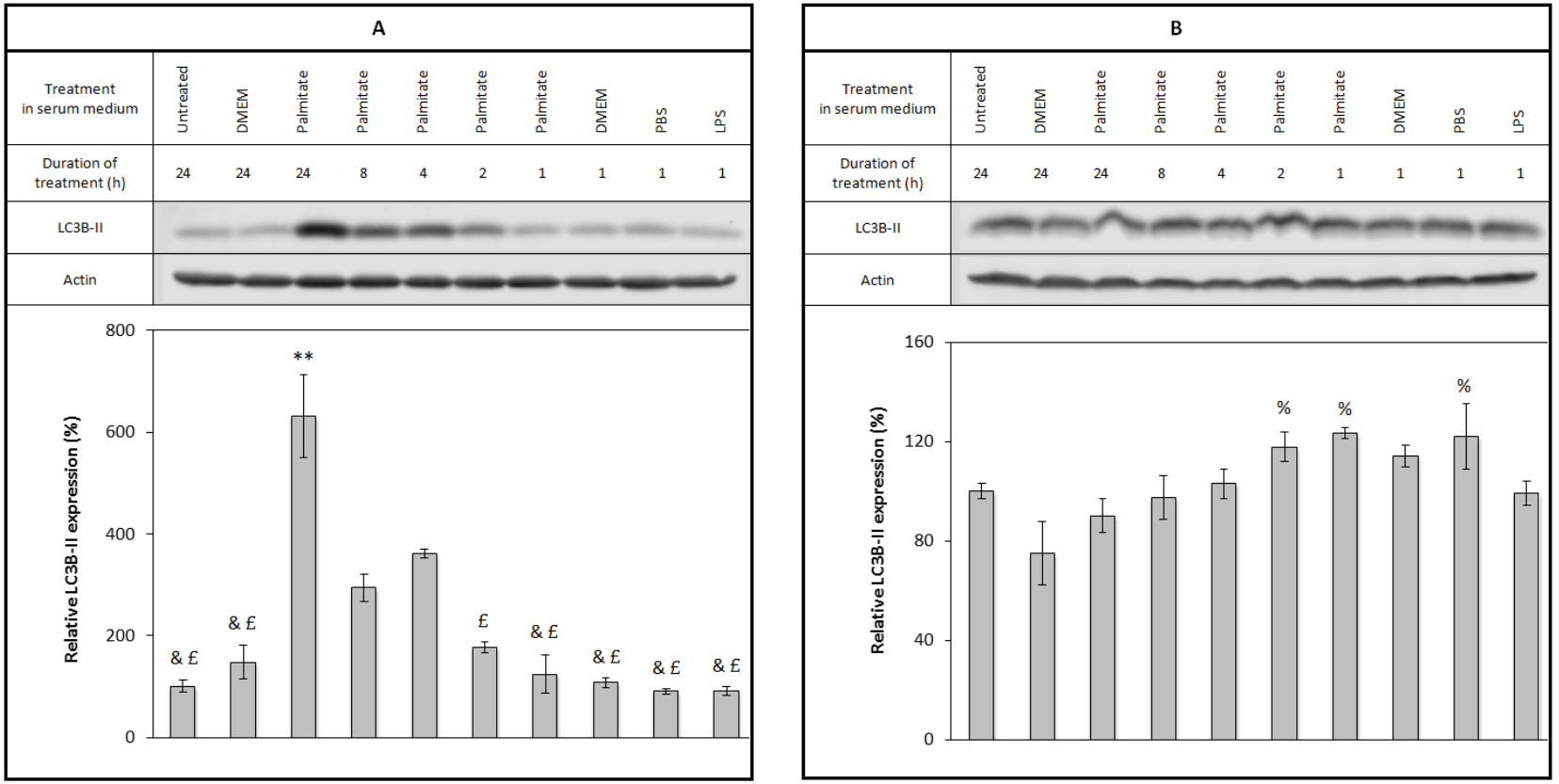

Figure 56. A. *Palmitate stimulates LC3B-II levels after 24 h of treatment in **3T3-L1 pre-adipocytes**.* **B.** *LC3B-II levels were not altered following palmitate or LPS treatment in **3T3-L1 mature adipocytes**.* For both *figures A* and *B*, cells were treated with unconjugated palmitate (500 µM) (lanes 3 to 7) and LPS (100 ng/mL) (lane 10) in 10% FBS/DMEM (HG). Equivalent volumes of DMEM (LG) (400 µL for *figure A* and 200 µL for *figure B*) (lanes 2 and 8) and PBS (40 µL for *figure A* and 20 µL for *figure B*) (lane 9) were used as control for the palmitate and LPS treatments, respectively. Cells were lysed with 100 µL 1% TX-100 lysis buffer per 6 cm Ø dish for *figure A* and with 80 µL 1% TX-100 lysis buffer per well for *figure B*. 34 µg and 54 µg of protein were loaded per lane in *figures A* and *B*, respectively (15% SDS-acrylamide gel). Statistical difference between the 24 h DMEM control and other treatments is indicated with %; statistical difference between the 8 h palmitate treatment and other treatments is indicated with &; statistical difference between the 4 h palmitate treatment and other treatments is indicated with £; ** denotes a treatment statistically different from all other treatments (p-value < 0.05). Data from three independent experiments.

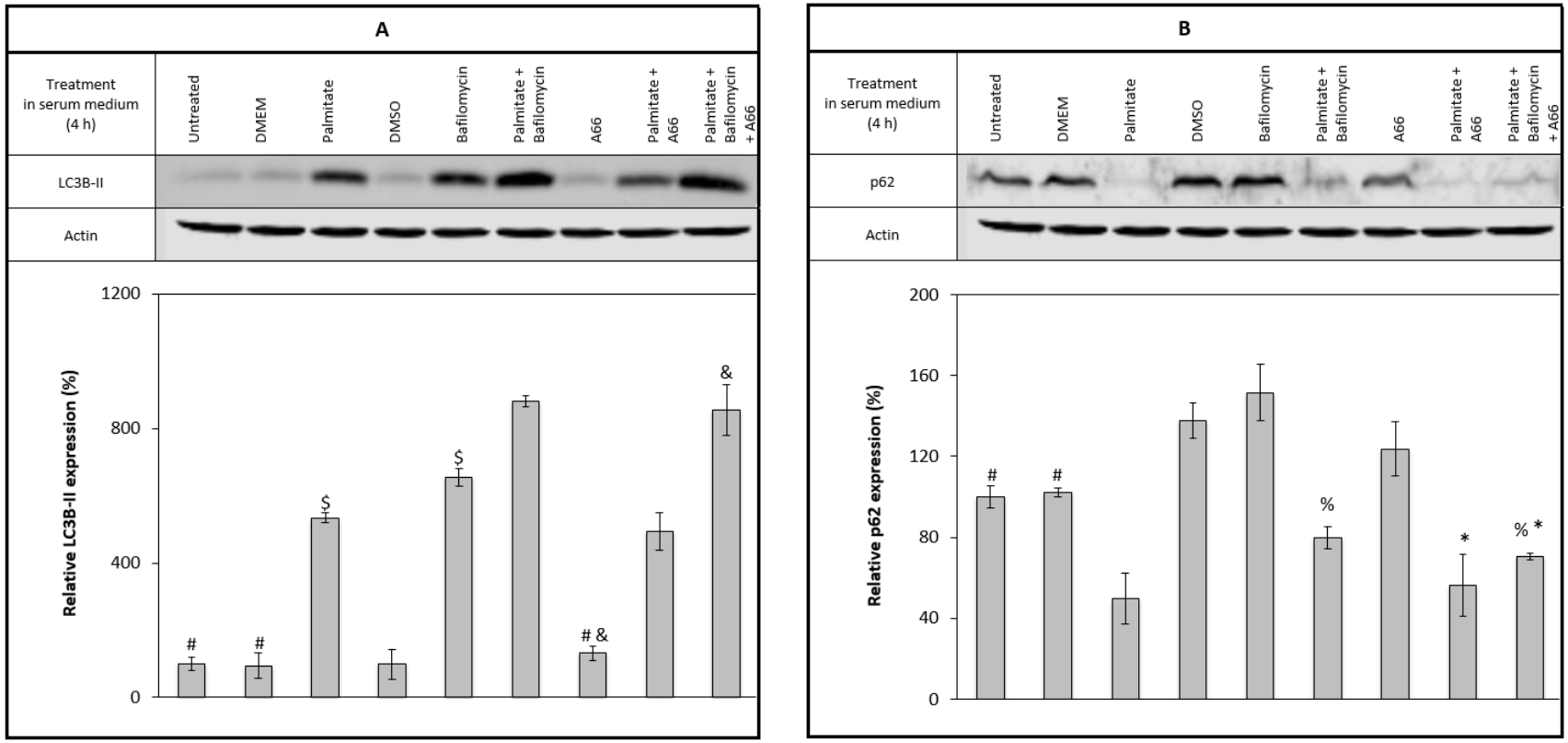

Figure 57. A. *Palmitate stimulates LC3B-II levels after 4 h of treatment in **3T3-L1 pre-adipocytes** and adding bafilomycin A1 to the SFA treatment enhances this effect.* **B.** *Palmitate inhibits p62 levels after 4 h of treatment in **3T3-L1 pre-adipocytes***. For both *figures A* and *B*, cells were treated with unconjugated palmitate (500 µM) (lanes 3, 6 and 9), bafilomycin A1 (10 nM) (lanes 5, 6 and 9) and A66 (2 µM) (lanes 7, 8 and 9) in 10% FBS/DMEM (HG) for 4 h. Equivalent volumes of DMEM (LG) (400 µL) (lane 2) and DMSO (8 µL) (lane 4) were used as control for the palmitate and bafilomycin A1/A66 treatments, respectively. Cells were lysed with 100 µL 1% TX-100 lysis buffer per 6 cm Ø dish. 30 µg of protein were loaded per lane (15% SDS-acrylamide gel). Statistical difference between the palmitate treatment and other treatments is indicated with #; statistical difference between the bafilomycin A1 treatment and other treatments is indicated with %; statistical difference between the "palmitate + bafilomycin A1" treatment and other treatments is indicated with $; statistical difference between the A66 treatment and other treatments is indicated with *; statistical difference between the "palmitate + A66" treatment and other treatments is indicated with & (p-value < 0.05). Note that to avoid overcrowding *figures A* and *B*, only differences relevant our analysis are shown, the results in full of the one-way ANOVA analyses can be found in *appendix VII. 10.* Data from three independent experiments.

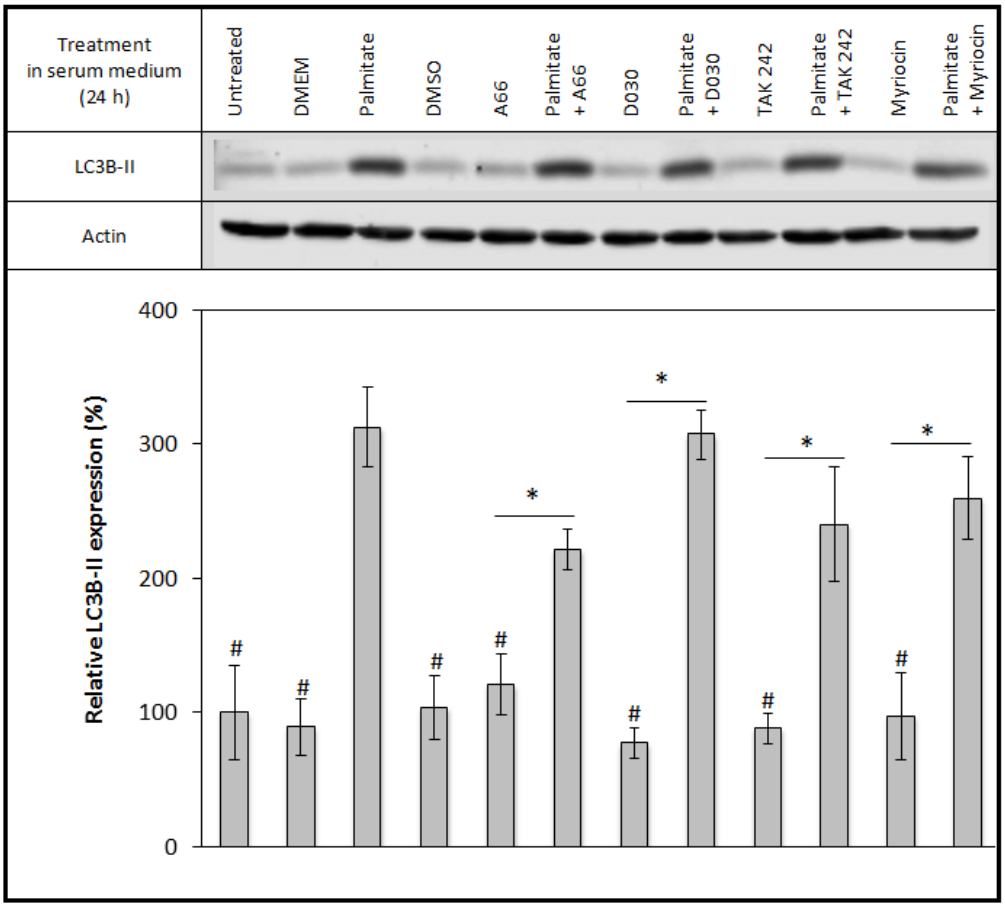

Figure 58. *None of the inhibitors tested rescue palmitate-mediated stimulation of LC3B-II levels after 24 h of treatment in **3T3-L1 pre-adipocytes**.* Cells were treated with unconjugated palmitate (500 µM) (lanes 3, 6, 8, 10 and 12), A66 (2 µM) (lanes 5 and 6), D030 (2 µM) (lanes 7 and 8), TAK 242 (2 µM) (lanes 9 and 10) and myriocin (2 µM) (lanes 11 and 12) in 10% FBS/DMEM (HG) for 24 h. Equivalent volumes of DMEM (LG) (400 µL) (lane 4) and DMSO (8 µL) (lane 4) were used as control for the palmitate and inhibitor treatments, respectively. Inhibitors and DMSO were added to the media 1 h prior to palmitate treatment. Cells were lysed with 100 µL 1% TX-100 lysis buffer per 6 cm Ø dish. 31 µg of protein were loaded per lane (15% SDS-acrylamide gel). Statistical difference between the palmitate treatment and other treatments is indicated with #; all other statistical differences between treatments is indicated with * (p-value < 0.05). Note that to avoid overcrowding the figure, only differences relevant our analysis are shown, the results in full of the one-way ANOVA analyses can be found in *appendix VII. 10.* Data from three independent experiments.

IV. 3. 2. 2. Using hMADS cell line

As for previous experiments, the experiments exploring autophagy in mouse adipocytes were reproduced in human cells. As shown in *figure 59*, human pre- and mature-adipocytes responded to the palmitate time course treated a similar fashion as mouse adipocytes: while LC3B-II expression in pre-adipocyte was significantly induced by the SFA with a peak at the 24 h time point (+395% compared to the 24 h

DMEM-treated control) (*Figure 59A*), the expression of this marker of autophagy was not altered by palmitate in mature hMADS adipocytes (*Figure 59B*). As for the mouse adipocytes, the hour-long LPS treatment did not elicit any effect on LC3B-II expression in hMADS adipocytes. However, the effect of palmitate on LC3B-II levels in hMADS pre-adipocytes could not be reproduced despite using the same aliquot of palmitate was used to produce the data in *figure 59*. Therefore, no further experiments investigating autophagy in hMADS were performed.

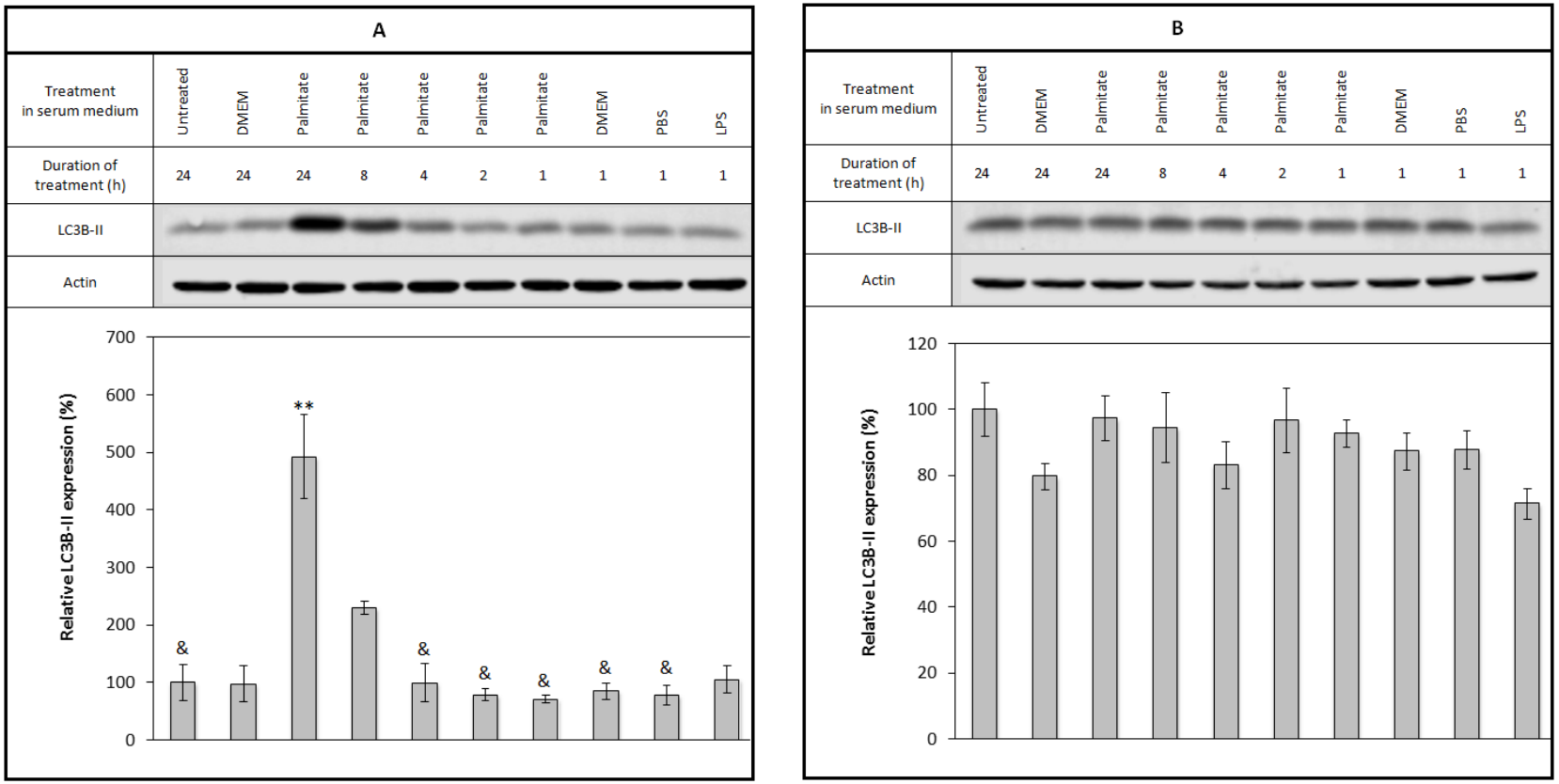

Figure 59. A. *Palmitate stimulates LC3B-II levels after 24 h of treatment in* ***hMADS pre-adipocytes***. **B.** *LC3B-II levels were not altered following palmitate or LPS treatment in* ***hMADS mature adipocytes***. For both *figures A* and *B*, cells were treated with unconjugated palmitate (500 µM) (lanes 3 to 7) and LPS (100 ng/mL) (lane 10) in 10% FBS/DMEM (HG). Equivalent volumes of DMEM (LG) (400 µL for *figure A* and 200 µL for *figure B*) (lanes 2 and 8) and PBS (40 µL for *figure A* and 20 µL for *figure B*) (lane 9) were used as control for the palmitate and LPS treatments, respectively. Cells were lysed with 100 µL 1% TX-100 lysis buffer per 6 cm Ø dish for *figure A* and with 80 µL 1% TX-100 lysis buffer per well for *figure B*. 12 µg and 30 µg of protein were loaded per lane in *figures A* and *B*, respectively (15% SDS-acrylamide gel). Statistical difference between the 8 h palmitate treatment and other treatments is indicated with &; ** denotes a treatment statistically different from all other treatments (p-value < 0.05). Data from three independent experiments.

IV. 3. 3. The effect of palmitate on PKR expression and activity

The following section investigates the effect of palmitate on both PKR expression and its activity in adipocytes. To this end, a time course experiment was performed exploring how palmitate treatment affects the expression levels of the kinase in all four cell models previously utilised (3T3-L1 and hMADS pre- and mature adipocytes). Additionally, we assessed the consequences of inhibiting PKR pharmacologically on the expression levels of LC3B-II following palmitate treatment in 3T3-L1 pre-adipocytes.

IV. 3. 3. 1. Using 3T3-L1 cell line

While *figure 60A* presents the result of the time course experiment carried out in mouse pre-adipocytes enquiring into the effect of palmitate on PKR expression levels, *figure 60B* does so in mouse mature adipocytes. In both types of cells, the SFA treatment (as well as the hour-long LPS treatment) had no significant effect on the expression of this kinase. Because palmitate was shown to induce the autophagic process in 3T3-L1 pre-adipocytes, the role of PKR activity was investigated in this context by using a PKR specific inhibitor named C16. While some cells were treated for 24 h with the SFA in the absence of C16, which resulted in an increase in LC3B-II expression consistent with previous results (+200% compared to the DMEM-treated control), other cells were treated with a combination of the SFA and the inhibitor (*Figure 61*). The inhibitor failed to rescue the palmitate-mediated induction of LC3B-II expression suggesting that the SFA regulates autophagy in a PKR-independent manner.

IV. 3. 3. 2. Using hMADS cell line

The experiments presented in *figure 60* were replicated in hMADS pre- and mature adipocytes (*Figure 62*). Similarly to the response of the mouse cells, the human cells were not affected by the palmitate treatment at any of the time points tested.

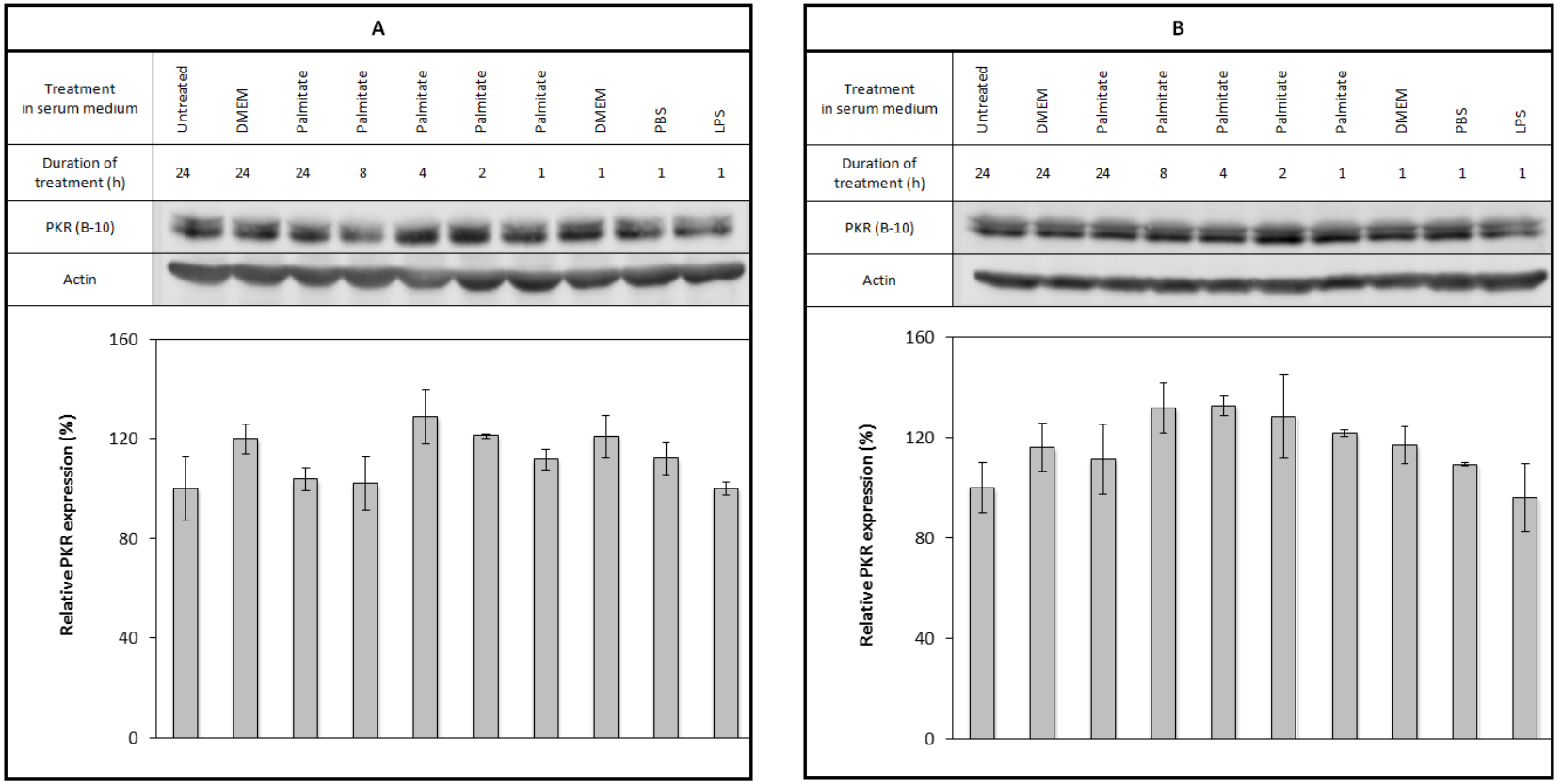

Figure 60. A. *PKR levels were not altered following palmitate or LPS treatment in **3T3-L1 pre-adipocytes***. **B.** *PKR levels were not altered following palmitate or LPS treatment in **3T3-L1 mature adipocytes***. For both *figures A* and *B*, cells were treated with unconjugated palmitate (500 µM) (lanes 3 to 7) and LPS (100 ng/mL) (lane 10) in 10% FBS/DMEM (HG). Equivalent volumes of DMEM (LG) (400 µL for *figure A* and 200 µL for *figure B*) (lane 2 and 8) and PBS (40 µL for *figure A* and 20 µL for *figure B*) (lane 9) were used as control for the palmitate and LPS treatments, respectively. Cells were lysed with 100 µL 1% TX-100 lysis buffer per 6 cm Ø dish for *figure A* and with 80 µL 1% TX-100 lysis buffer per well for *figure B*. 34 µg and 54 µg of protein were loaded per lane in *figures A* and *B*, respectively (10% SDS-acrylamide gel). Data from three independent experiments.

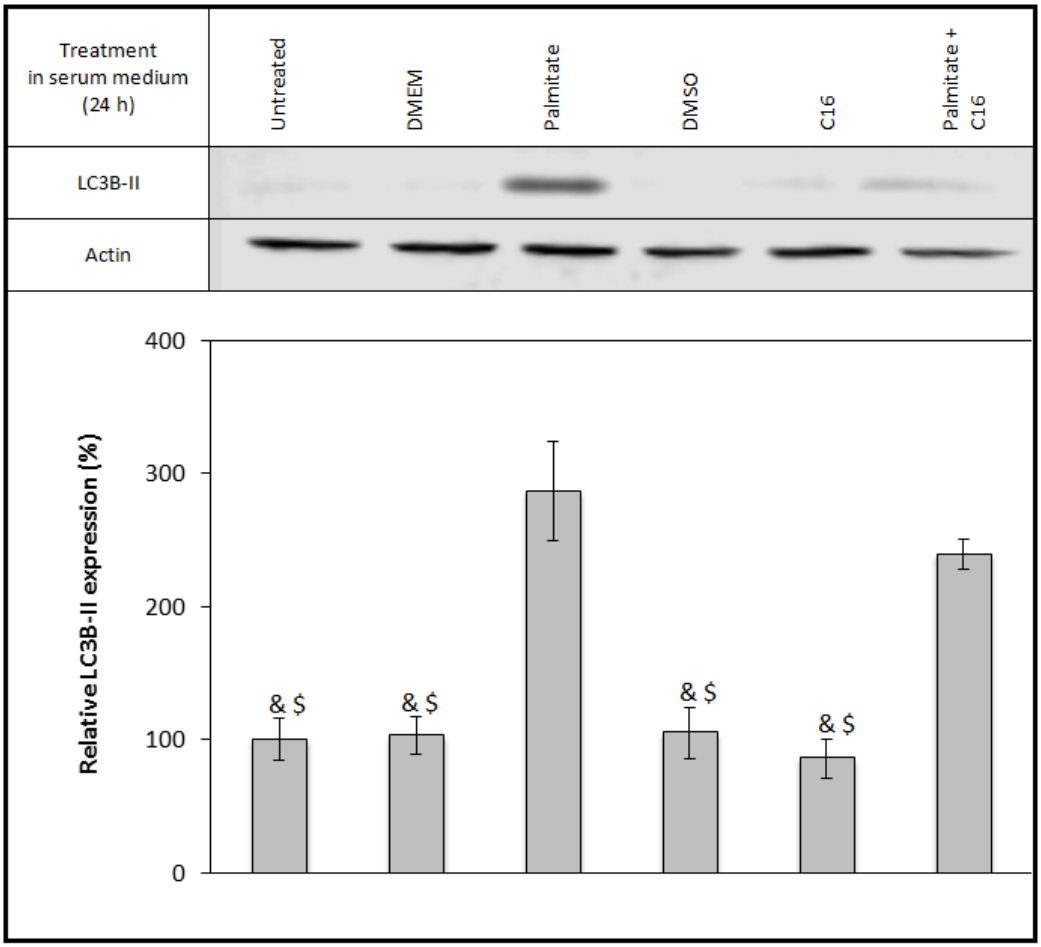

Figure 61. *Inhibiting PKR does not rescue palmitate-mediated induction of autophagy in **3T3-L1 pre-adipocytes**.* Cells were treated with unconjugated palmitate (500 µM) (lanes 3 and 6) and C16 (2 µM) (lanes 5 and 6) in 10% FBS/DMEM (HG). Equivalent volumes of DMEM (LG) (400 µL) (lane 2) and DMSO (8 µL) (lane 4) were used as control for the palmitate and C16 treatments, respectively. Cells were lysed with 100 µL 1% TX-100 lysis buffer per 6 cm Ø dish. 13 µg of protein were loaded per lane (15% SDS-acrylamide gel). Statistical difference between the palmitate treatment and other treatments is indicated with &; statistical difference between the palmitate treatment and other treatments is indicated with $ (p-value < 0.05). Data from four independent experiments.

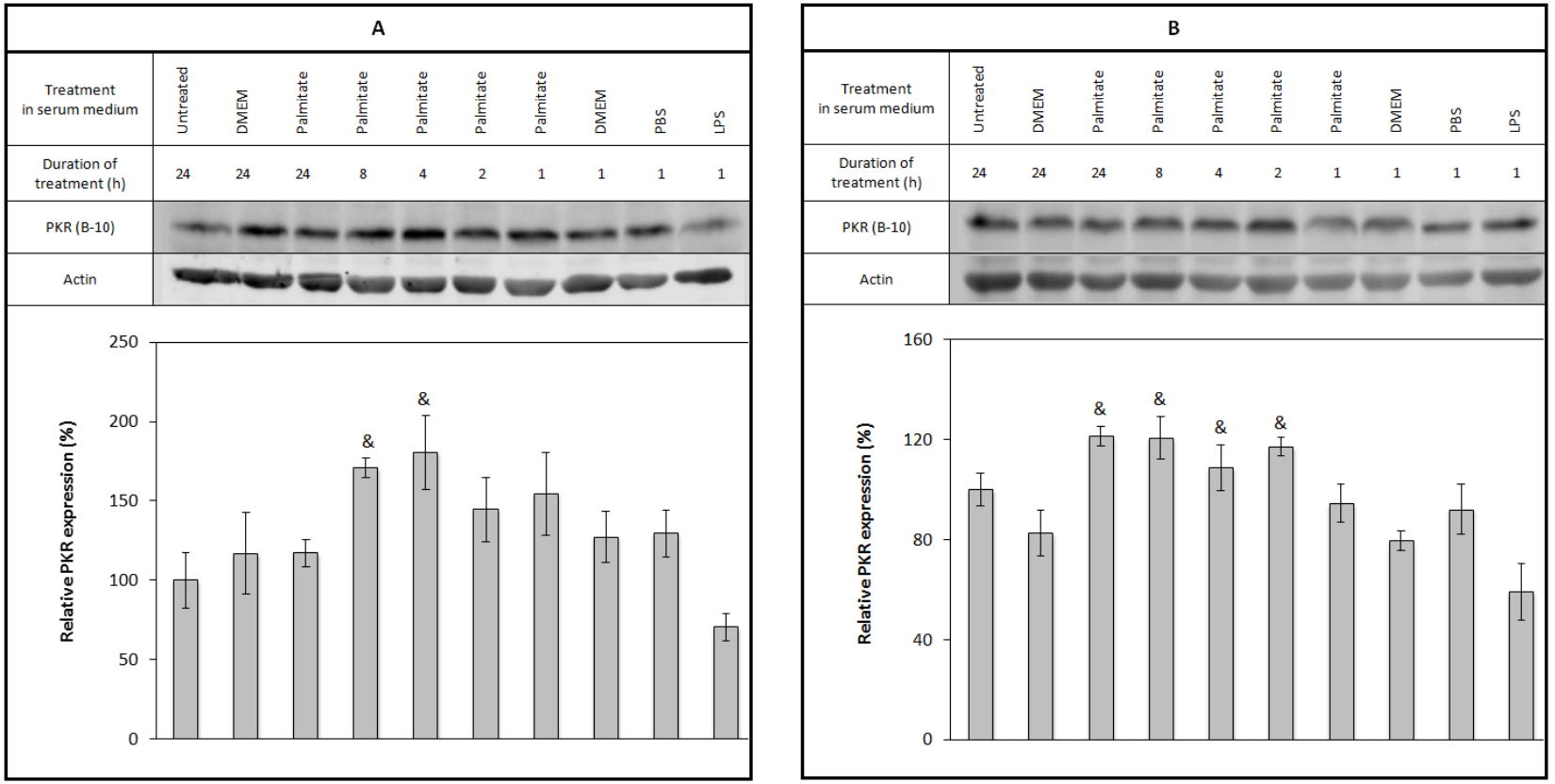

Figure 62. A. *PKR levels were not altered following palmitate or LPS treatment in* ***hMADS pre-adipocytes***. **B.** *PKR levels were not altered following palmitate or LPS treatment in hMADS mature adipocytes.* For both *figures A* and *B*, cells were treated with unconjugated palmitate (500 µM) (lanes 3 to 7) and LPS (100 ng/mL) (lane 10) in 10% FBS/DMEM (HG). Equivalent volumes of DMEM (LG) (400 µL for *figure A* and 200 µL for *figure B*) (lane 2 and 8) and PBS (40 µL for *figure A* and 20 µL for *figure B*) (lane 9) were used as control for the palmitate and LPS treatments, respectively. Cells were lysed with 100 µL 1% TX-100 lysis buffer per 6 cm Ø dish for *figure A* and with 80 µL 1% TX-100 lysis buffer per well for *figure B*. 11 µg and 47 µg of protein were loaded per lane in *figures A* and *B*, respectively (10% SDS-acrylamide gel). Statistical difference between the LPS treatment and other treatments is indicated with & (p-value < 0.05). Data from three independent experiments.

IV. 4. Discussion of Chapter 4

IV. 4. 1. Evidence supporting the anti-lipolytic effect of palmitate

In this chapter, the regulation of the so-called lipophagy was investigated, focusing firstly on lipolysis and then on autophagy. We report that neither palmitate nor IFN-γ affected the markers selected to assess lipolytic activity (p-HSL Ser^{660} and p-PKA) in 3T3-L1 and hMADS pre- and mature adipocytes (*Figures 52* to *55*). Because the experimental conditions and treatments used had proven to elicit insulin resistance in most of the cell types tested in Chapter 3, such models would have been expected to induce catecholamine resistance as well. Indeed, impaired catecholamine-induced lipolysis has been reported in the obese insulin resistant state (J. a. Jocken 2008). A number of studies have documented this metabolic disruption in the whole body of obese subjects (Horowitz 2000, Connacher 1991). At the level of subcutaneous adipose tissue, Jocken and colleagues evidenced *in vivo* blunted glycerol release in response to intravenous infusion of a non-selective β-adrenergic agonist isoprenaline in obese compared to lean subjects (J. G. Jocken 2008). This demonstrates without ambiguity impeded catecholamine-induced lipolysis in this type of tissue.

In vitro, Burns and colleagues were able to verify the effect of FFAs, including palmitate, on lipolysis rates in human adipose tissue cells as early as 1978 (Burns 1978). Using adipocytes isolated from human subcutaneous tissue samples, they measured the concentration of FAs released in the medium after incubating the cells with the SFA in the presence of isoproterenol (10^{-7} M). Following a 4 h-long incubation, they reported a 35% inhibition of FA release mediated by palmitate (500 μM). Thirty years later, Müller and colleagues published results supporting the data

of Burns and colleagues in adipocytes from rat origin (G. W. Muller 2008). Testing the same concentrations of isoproterenol (1 μM) and of palmitate (500 μM) used in the experiments presented in the results section of the present chapter, they treated the cells for 2 h with the SFA prior to the addition of the β-AR agonist. After a further 2 h-long incubation, they measured the release of glycerol and FA and assessed the effect of the SFA treatment on the expression levels of HSL and PKA. Consistently, Müller and colleagues were able to report an inhibitory effect of palmitate on these markers of lipolysis.

IV. 4. 2. Understanding the discrepancies between published data and the present results

To understand the reason why the data presented in this chapter does not support the anti-lipolytic role of palmitate evidenced in the literature reviewed above, one may compare the experimental designs used. Indeed, although identical concentrations of palmitate and isoproterenol were employed, our experiments included an acute treatment with the β-AR agonist. Instead, in the study of Burns and colleagues, isoproterenol was added to the media for the entire duration of the palmitate treatment. Muller *et al*. on the other hand stimulated the cells with isoproterenol for a total of 2 h. The rational for performing an acute isoproterenol treatment in the experiments reviewed in this chapter was to avoid the desensitisation of the β-AR reported to occur over time when 3T3-L1 adipocytes are treated with either isoproterenol or insulin (Hupfeld 2003). Furthermore, the duration of the treatment performed in our experiments was significantly greater than in the literature (27 h in total *versus* 4 h).

Aside from experimental design, it is possible that the choice of endpoint was not optimal to demonstrate the anti-lipolytic effect of palmitate under the conditions tested: the effect of the SFA may be mediated through another phosphorylation site of HSL than Ser^{660}. Indeed, this residue is one of five involved in HSL regulation in murine adipocytes, also including Ser^{563}, Ser^{565}, Ser^{600} and Ser^{659}. While Ser^{563}, Ser^{650} and Ser^{660} have been shown to be phosphorylated by PKA, the phosphorylation of Ser^{600} is mediated through Erk and finally that of Ser^{565} depends on AMPK and calcium/calmodulin-dependent kinase II (Watt 2006). However, Gaidhu and colleagues did report the decrease of p-HSL Ser^{660} in the WAT of mice fed a HFD for 8 weeks *versus* a control group on a standard chow diet (Gaidhu 2010). From quantifying glycerol release induced by epinephrine exposure, they were able to demonstrate that this difference in p-HSL Ser^{660} was associated with a blunted epinephrine-stimulated lipolysis in the HFD group.

Investigating the effect of palmitate on ATGL expression and phosphorylation levels could have been informative. This enzyme is pivotal in TAG hydrolysis as it catalyses 95% of reactions together with HSL in mice WAT (M. S. Schweiger 2006). However, Zimmermann and colleague evidenced that the phosphorylation of ATGL is independent of PKA (Zimmermann 2004). This may be of relevance to our results as neither p-HSL Ser^{660} nor p-PKA substrate was affected by the SFA treatment. Lastly, two additional factors could shed light on the discrepancy between our findings and the literature. Firstly, the type of cells used. Indeed, to the best of our knowledge the anti-lipolytic effect of palmitate has not been confirmed in 3T3-L1 adipocytes, instead, research has been carried out in primary adipocytes.

Secondly, the data published by Muller and colleagues as well as Burns and colleagues does not include a control for the palmitate treatment solubilised in a BSA solution. Therefore, the SFA-mediated effect reported in these studies could merely correspond to a BSA-mediated inhibition of lipolysis. This is plausible as in the experiments presented in *figures 52* to *55*, BSA significantly hinders the phosphorylation of HSL and PKA substrate. Alternatively, the effect associated with BSA observed in the present chapter might merely reflect an artifact arising from protein loading or electrophoresis. Indeed, irregularities can be observed around the molecular weight of BSA (66 kDa) in lanes of BSA and BSA conjugated palmitate suggesting that large quantities of BSA migrated through the gel. This phenomenon is particularly prevalent in the experiment performed in murine and human pre-adipocytes (*Figures 52* and *55*). As expression levels of HSL and perilipin are low in these cells relatively to differentiated adipocytes, this is likely to be a valid explanation.

IV. 4. 3. Palmitate stimulates autophagy in 3T3-L1 pre-adipocytes

In the second part of this chapter, the pro-autophagic effect of palmitate was demonstrated. Indeed, the SFA was found to stimulate LC3B-II both in the presence and the absence of bafilomycin A1 in 3T3-L1 pre-adipocytes but none of the other cell types tested (mature 3T3-L1 adipocytes, pre- and mature hMADS) (*Figure 57A*). Although initial results indicated the same effect in hMADS pre-adipocytes, these findings could not be reproduced (*Figures 59A*). This is consistent with *in vivo* experiments associating obesity and HFD with increased rates of autophagy in both murine and human models (Kovsan 2011, Nunez 2013). *In vitro,* Yin and colleagues

were able to demonstrate the pro-autophagic effect of palmitate (500 μM) in mature 3T3-L1 adipocytes (Yin 2015). Indeed, following 12 h of SFA treatment they report the stimulation of both LC3-II levels and autophagosome formation using immunoblot analysis and fluorescence microscopy, respectively. This does not align with our findings in mature murine adipocytes, although this specific time point was not tested in our time course experiments (*Figure 56B*). It appears no study has focused on the autophagic response of 3T3-L1 pre-adipocytes to palmitate treatment.

This difference in the response of pre- and mature 3T3-L1 adipocytes to palmitate treatment is likely to reflect cellular variations in lipid metabolism. Indeed, autophagy has been shown in various cell types to protect against palmitate-mediated induction of apoptosis. For instance, Cai *et al.* demonstrated that while palmitate induced both apoptosis and autophagy in hepatocytes, inhibiting autophagy stimulated the rate of cell apoptosis and, inversely, inducing autophagy down-regulated palmitate-induced apoptosis (Cai 2014). Similar findings were produced in podocytes, a type of cell found in the kidneys, and in bone marrow mesenchymal stem cells (X. C. Jiang 2017, Y. W. Liu 2018). As mature adipocytes have a significantly higher capacity for esterification and storage of FA as TAG compared to pre-adipocytes, the deleterious effect of palmitate is likely to be neutralised in mature adipocytes. Thus, the autophagic response is not necessary to protect mature adipocytes unlike pre-adipocytes, explaining our results of *figure 56.*

As PI3K is found upstream of the autophagic inhibitor mTORC1, it was expected to be pivotal in the modulation of the degradative process (*Figure 2*). To explore the potential role of this kinase in palmitate-mediated induction of

autophagy, 3T3-L1 pre-adipocytes were treated with pharmacological inhibitors targeting two catalytic subunits of PI3K (p110α and p110δ) (*Figure 58*). Although these treatments failed to statistically rescue the SFA-induced up-regulation of LC3B-II levels, a trend in this direction was observed following the inhibition of p110α. This is in line with the published evidence linking insulin resistance with increase autophagy in adipose tissue discussed above. Indeed, as shown in Chapter 3, A66 rescues palmitate-induced insulin resistance in 3T3-L1 and the data presented in this chapter suggests that this inhibitor might also block the pro-autophagic effect of the SFA. Emphasising the importance of PI3K in the regulation of palmitate-induced autophagy, a recent paper by Niso-Santano and colleagues reports the dependence of palmitate-stimulated autophagy on AMPK, an energy-sensing kinase shown to be induced by PI3K in mouse adipocytes (M. M.-S.-Y. Niso-Santano 2015). Nevertheless, Foukas *et al.* failed to observe any significant effect of p110α inactivation in the autophagic activity of MEFs derived from $p110\alpha^{D933A/WT}$ embryos (L. B. Foukas 2013).

The role of TLR4 in palmitate-induced autophagy was also investigated using TAK 242. As illustrated by *figure 58,* this inhibitor did not rescue the effect of the SFA. However, the findings of Xu and colleagues still point at a critical role of this receptor in the regulation of autophagy (Y. J. Xu 2007). Indeed, they evidenced that LPS was able to induce autophagy in a TLR4-dependent manner in both human and murine macrophages. This study emphasises the interconnectivity of the autophagic and immune programmes and proposes the former as a cellular strategy to clear bacterial infections. Similarly to TAK 242, myriocin failed to rescue the effect of palmitate on autophagy, clearing SPT from a regulatory role in this process

(*Figure 58*). Nonetheless, published studies still implicate ceramides in the induction of the autophagic programme as reviewed by Jiang and Ogretmen (W. a. Jiang 2014).

IV. 4. 4. The unclear role of PKR in autophagy

The last section of the present chapter focused on the role of PKR in the autophagic process. Quantitative immunoblot analysis revealed that over the time points tested, palmitate treatment failed to induce the expression level of this protein in 3T3-L1 and hMADS pre- and mature adipocytes. As highlighted in the introduction of the present chapter, Nakamura and colleagues were able to demonstrate that PKR activity was up-regulated in the liver and WAT of both *ob*/*ob* mice and mice fed with a HFD compared to lean control (T. F. Nakamura 2010). In addition, their findings suggest that palmitic acid infusion stimulated PKR activity both *in vivo* and in MEFs cultured for 2 h in the presence of the SFA (500 μM). Furthermore, they provide compelling evidence for physical interaction between PKR and IRS1, a downstream effector of insulin signalling. Emphasising the importance of PKR in cellular metabolism, the *Pkr*$^{-/-}$ knockout mice produced by Nakamura *et al*. was protected from HFD-induced metabolic disorders including insulin resistance, inflammation and obesity. Cavalho and colleagues, who compared the phosphorylation of PKR as well as the overall PKR content in visceral adipose tissues of obese and lean subjects, present concordant data (Carvalho 2013) (*see introduction IV. 2. 5.*).

In light of such findings, one could have expected *figures 60* to *62* to unveil a

palmitate-induced stimulation of PKR. However, our results indicate that the SFA does not affect the expression of kinase. This discrepancy could be due to a difference in endpoint considered: while Nakamura *et al.* focused on the phosphorylation levels of PKR, the experiments presented in the present chapter assess the protein content. Yet, Carvalho and colleagues did measure an up-regulation of PKR contents in the adipose tissue of obese subjects *versus* lean controls. Another factor to consider is the difference in cell types used to perform the experiments. Nakamura *et al.* report their findings in MEFs as well as WAT lysate, the same model chosen by Carvalho *et al*. When discussing the difference between our results and those of these two studies, it is important to stress that other studies failed to demonstrate the pro-apoptotic role of PKR defended by Nakamura and colleagues. For instance, Lancaster and colleagues report that PKR is not obligatory for HFD-induced obesity and its associated metabolic and inflammatory dysregulations (Lancaster 2016). Potential reasons for the heterogeneity of the literature examining the role of PKR have been discussed in further detail in the introduction of the present chapter (*see introduction IV. 2. 5*.).

To further investigate the role of PKR in the context of the autophagy, the activity of the kinase was blocked using C16, a pharmacological inhibitor. As mentioned in the introduction of this chapter, the findings of Niso-Santano and colleagues form a compelling argument in favour of a regulatory role of PKR in palmitate-induced autophagy. Indeed, they demonstrated that in a cancerous human cell line, the pro-autophagic effect of palmitate depended on this kinase (M. M.-S.-Y. Niso-Santano 2015). Having produced a *Pkr*$^{-/-}$ knockdown cell line, they reported that palmitate-mediated induction of green fluorescent protein (GFP)-LC3 dots in

cultured cells was hindered compared to the control cell line. Furthermore, an earlier study published by the same group, revealed that the pro-autophagic effect of palmitate was mediated by the disruption of the STAT3-PKR complex (M. S. Niso-Santano 2013). Therefore, one could have expected that inhibition of PKR to rescue the palmitate-induced up-regulation of autophagy, however C16 had no effect on the pro-autophagic effect of palmitate.

IV. 4. 5. Limitations and future experiments

A limitation of the data presented in Chapter 4 is that it fails to align with the consensus supporting the anti-lipolytic action of palmitate. As discussed in the present section, this inconsistency may reflect differences in the experimental design used in the present work versus published studies. Therefore, future experiments may involve adding isoproterenol for the entire duration of the palmitate treatment, as well as shortening the latter to 4 h. However, prolonged exposure to isoproterenol might lead to desensitisation of the receptor. Moreover, we may wish to consider alternative endpoints such as the expression and phosphorylation levels of HSL Ser^{563}, Ser^{565}, Ser^{600} and ATGL. Using primary adipocytes may yield more conclusive results. Finally, it is important to note that immunoblotting only allows for the quantitation of phosphorylation state of the enzymes of interest (e.g. PKA, HSL, ATGL), which does not necessarily represent lipolytic activity as lipolysis is regulated by a large number of lipolytic enzymes and regulatory proteins. Therefore an activity-based assay measuring the release of lipolytic products such as FFA or glycerol, would provide a more direct assessment of lipolytic activity.

Another shortfall of this chapter was that palmitate-induced autophagy could only be demonstrated in pre-adipocytes, not in mature adipocytes. This may constitute a limitation to our findings as they become less relevant to the topic of lipid metabolism. Indeed, in this type of cells, autophagy might be induced in response to molecular damage triggered by palmitate, rather than representing lipophagy. In addition, the inhibitors tested failed to significantly rescue the palmitate-induced stimulation of LC3B-II expression in 3T3-L1 adipocytes. Although a trend in this direction was recorded when treating the cells with A66, this effect fell short of achieving statistical significance. Moreover, no positive control was included to demonstrate that these inhibitors successfully blocked their targets. Therefore, future experiments could test higher concentration of inhibitors, while also including positive controls. A TLR2 inhibitor could also be tested in view of the model proposed in the discussion of Chapter 3 (*Figure 49*). Lastly, the role of PKR in the context of autophagy could be further explore by considering the effect of palmitate on the phosphorylation levels of PKR rather than its impact on protein expression. Again using primary adipocytes may produce more conclusive data.

CHAPTER 5. INVESTINGATING THE ROLE OF ISG15

V. 1. Overview of Chapter 5

Isg15 is one of the main effectors of IFN-α. It is of particular interest because the transcriptome analysis, which originated the present work, evidenced that the expression of this gene was affected by the A66 treatment in mouse adipocytes. Furthermore, due to the nature of the peptide encoded by *Isg15*, this ISG was identified as a potential key modulator of the pathways studied in Chapters 3 and 4. Indeed, ISG15 has the ability to conjugate to a large number of proteins via a reaction similar to ubiquitination, known as ISGylation (D. a. Zhang 2011). Thus, it is likely to affect the activity of various cellular processes including those mediated by palmitate. In addition, a cytokine role has emerged for unconjugated ISG15, which could be another way by which this peptide could alter SFA-dependent cellular processes. In order to investigate the role of ISG15, experiments were performed in both WT adipocytes and 3T3-L1 cells transduced with either an empty vector (used as a control) or an *Isg15*-targeting shRNA construct. This RNAi technique, detailed in the material and methods chapter, allowed for the sustained silencing of the gene of interest in the resulting cell line. We were therefore enabled to study the consequences of knocking down *Isg15* on cellular responses to palmitate treatment and infer the role of ISG15.

V. 1. 1. Aim of Chapter 5

The first step in understanding the role of ISG15 in relation to SFA-induced pathways was to assess whether palmitate had an effect on ISG15 expression levels in mouse and human adipocytes. Secondly, since palmitate was demonstrated to stimulate Tyr phosphorylation of STAT3 in mature 3T3-L1 (Chapter 3), we investigated whether recombinant ISG15 elicited the activation of this transcription factor. The consequences of knocking down *Isg15* were evaluated, considering the cellular response to palmitate-induced insulin resistance, palmitate-mediated induction of STAT3 and LC3B-II. Lastly, mass spectrometry was employed to evaluate the impact of palmitate on ISGylation. Together, these experiments revealed a new role of ISG15 in the modulation of the metabolic effect of palmitate.

V. 2. Introduction of Chapter 5

V. 2. 1. The molecular mechanisms of ISGylation

The process of ISGylation, by which ISG15 is attached to target proteins, relies on the coordinated activity of three enzymes also involved in ubiquitin conjugation (D. a. Zhang 2011). As described in *figure 63*, it is initiated by the E1-mediated activation of ISG15, which is then transferred to the active site of E2, the conjugating enzyme. The E3 enzyme then enables the ligation of activated ISG15 to the lysine residue of the substrate. Ubiquitin-activating enzyme E1-like (UBE1L) and ubiquitin-conjugating enzyme H8 are the two proteins ensuring the roles of E1 and E2 in human cells, respectively (D. a. Zhang 2011). Three human proteins have been identified as the E3 ligase including estrogen-responsive finger protein, homologous to E6-associated protein carboxyterminus and regulator of chromosome condensation 1 containing protein 5 and human homolog of drosophila Ariadne. USP18 ensures the deconjugation of ISG15 from its target proteins (D. a. Zhang 2011). Interestingly, USP18, which expression is highly induced by type I IFN, competes with JAK1 to bind IFNAR2 in a STAT2-dependent manner. This results in USP18 hindering the JAK/STAT pathway in a manner that is independent from deISGylation (Arimoto 2017). The protease is therefore a key effector of the negative-feedback loop down-regulating IFN signalling.

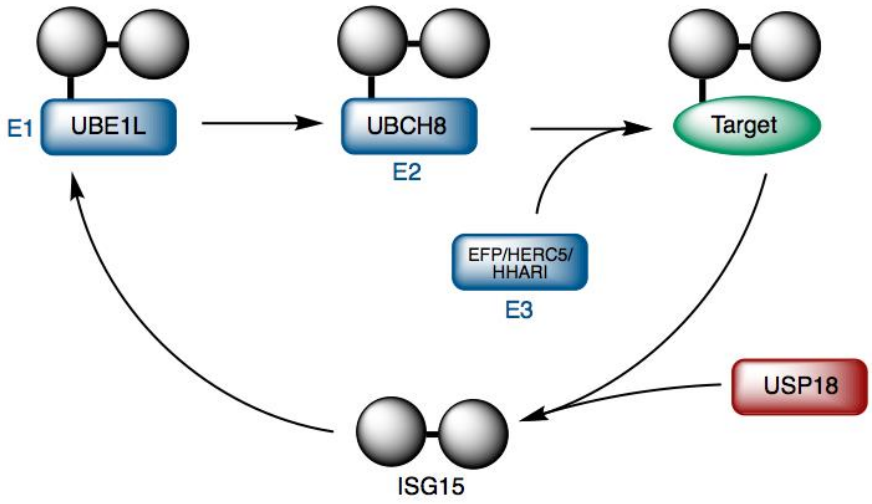

Figure 63. *Steps of the ISGylation process.* Free IFN-stimulated gene 15 (ISG15) is activated by E1 ubiquitin-activating enzyme E1-like (UBE1L) which catalyses adenylation and creates a thioester bond with ISG15. The activated protein then interacts with and covalently binds ubiquitin-conjugating enzyme H8 (UBCH8), the bona fide E2 enzyme for ISG15. Ligation to the lysine residue of the target substrate is capacitated by ligase E3. Ubiquitin-specific protease 18 (USP18) unconjugates ISG15 and its substrate thereby restoring the pool of free ISG15. *EFP*: estrogen-responsive finger protein; *HERC5*: HECT (homologous to E6AP carboxyterminus) and regulator of chromosome condensation 1 (RCC1) containing protein 5; *HHARI*: human homolog of drosophila Ariadne.

Although similar to ubiquitination, ISGylation has not been implicated in proteasomal degradation of its substrates. Rather, this process is thought to interfere with the ubiquitin system through competition for E2 and E3 or else the sequestration of ubiquitin in ISG15-ubiquitin mixed chains (Villarroya-Beltri 2017). The biological relevance of ISGylation has mainly been studied in the context of the cellular antiviral response. Evidence from *in vitro* studies and mice knockouts indicate a protective role of ISG15 against certain pathogens including influenza A and B virus and the Herpes simplex virus (Lenschow 2007). Interestingly, the antiviral effect of the protein is not systematically modulated via ISGylation. Indeed, Werneke and colleagues evidenced that susceptibility to chikunguya virus, enhanced in ISG15 knockout mice, is independent of UBE1L mediated conjugation. This

suggests that unconjugated ISG15 is likely to mediate the cellular response to this specific infection (Werneke 2011).

V. 2. 2. ISG15, a modulator of immunity

The biological function of unconjugated ISG15 is likely to be potentiated via its cytokine activity (*Figure 64*). Indeed, the protein was found to be secreted from a range of cells, including granulocytes, fibroblasts and epithelial cells, and was detected in the serum of healthy human treated with IFN-β (D'Cunha 1996, Bogunovic 2012). Sixteen years later, a study by Bogunovic and colleagues established ISG15 as an extracellular cytokine promoting the production of IFN-γ mainly from human natural killer cells, as well as from T cells, in response to mycobacterial disease (Bogunovic 2012). Although additional studies have focused on the topic of ISG15-regulated IFN-γ immunity, the cellular mechanisms involved remain unclear (Fan 2013). However, progress was made recently with the identification of leukocyte function-associated antigen-1 (LFA-1) as the receptor for extracellular ISG15 in natural killer cells. More specifically, Swaim and colleagues were able to evidence the interaction of the small peptide with CD11a, which combined with CD18, forms the LFA-1 integrin receptor (Swaim 2017). In addition, they evidenced that pharmacological inhibition of the receptor prevents ISG15-mediated stimulation of IFN-γ and IL-10 production.

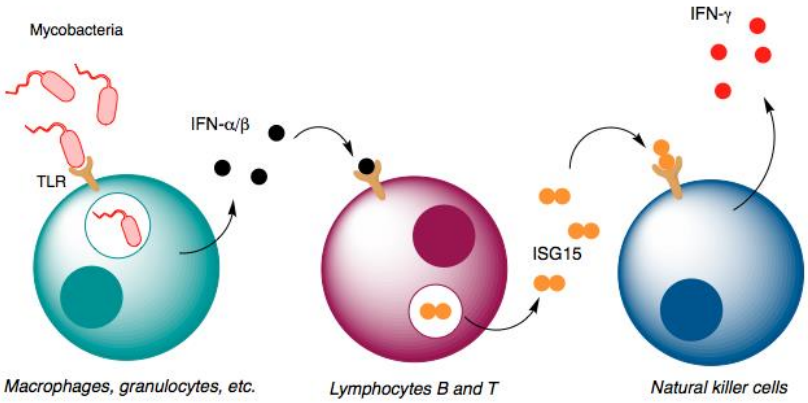

Figure 64. *ISG15 and its role as a cytokine.* Upon mycobacterial infection, cells implicated in the immune response system including macrophages and granulocytes secrete type I IFN, which is detected by lymphocytes B and T. These white blood cells in turn produce ISG15, which induce the secretion of IFN-γ by natural killer cells.

Importantly, the work of Bogunovic and colleagues revealed species-specific differences in the biological functions mediated by ISG15 (Bogunovic 2012). Indeed, patients bearing a genetic ISG15 deficiency did not display the expected enhanced susceptibility to viral infection recorded in ISG15-deficient mice. However, they were more susceptible to mycobacterial infections as their lymphocytes secreted less IFN-γ due to the lack of free ISG15. Furthermore, fibroblasts derived from ISG15-deficient patients not only failed to display enhanced susceptibility to viral infections but also demonstrated enhanced viral protection (Speer 2016). Meuwissen and colleagues explained this human-specific gain-of-function by a dip in levels of USP18, the protease involved in the down-regulation of IFN signalling (Meuwissen 2016). Indeed, in human but not mice, ISG15 is necessary to maintain USP18 cellular concentration. Lower USP18 activity therefore magnifies the antiviral IFN response in human ISG15-deficient cells. Therefore, in stark contrast with ISG15-deficient patients who exhibit increased type I IFN

immunity at both immunological and clinical levels, no sign of enhanced IFN response was described in the murine model (Villarroya-Beltri 2017).

V. 2. 3. The role of ISG15 in autophagy

With the IFN cascade playing such a critical role in autophagy, it is therefore unsurprising that ISG15 has also surfaced as a key player in this cellular process. Indeed, ISG15 was found to interact with both p62 and histone deacetylase 6 involved in the transport of misfolded proteins and the fusion of the autophagosome with the lysosome (Nakashima 2015). Furthermore, using ISG15-GFP fusion protein, Villarroya and colleagues provided evidence that ISGylation prompts protein aggregation and degradation by the lysosome (Villarroya-Beltri 2017). These findings indicate that protein ISGylation may enable selective autophagy. Recently, a study by Xu *et al.* substantiated the regulatory role of ISG15 in autophagy (D. Z. Xu 2015). The authors reported an anti-autophagic role of ISG15 inducer, type I IFN in human neuroglioma H4 cells and in HepG2 hepatoma cells. Such findings contrast with the results of Schmeisser and colleagues mentioned in Chapter 4, which supported a pro-autophagic role for type I IFN in a range of cancer cells in a JAK1-, STAT1- and STAT2-dependent manner (Schmeisser 2014).

Moreover, Xu *et al.* demonstrated that knocking down ISG15 or UBE1L restored autophagy in type I IFN-treated cells. They also showed that by competing with the ubiquitination process, ISGylation of the mammalian orthologue of yeast ATG6, beclin 1, down-regulates PIK3C3, a kinase necessary for autophagy. Inversely, they demonstrated a pro-autophagic effect of the enzyme involved in the

deISGylation process, USP18 (D. Z. Xu 2015). Such findings appear to be in contradiction with the data of Nakamura and colleagues. Indeed, they reported *Isg15* mRNA levels as well as pro-autophagic *Pkr* mRNA levels to be increased in the adipocytes of mice on a HFD compared to the standard chow-fed control (*supplementary material*) (T. F. Nakamura 2010).

V. 3. Results of Chapter 5

V. 3. 1. Investigating the effect of FA and IFN-γ on ISG15 expression in adipocytes

As explained in the introduction, ISG15 is likely to affect the activity of many proteins including those modulated by SFAs through its role as a cytokine and/or in protein ISGylation. To investigate these possibilities, the first experiment performed assessed whether palmitate induces expression of ISG15 and how it compared to the effect of IFN-γ. Two read-outs were considered: free ISG15 and total ISG15 (including the conjugated proteins).

V. 3. 1. 1. Using 3T3-L1 cell line

A time course experiment comparing the effect of IFN-γ and palmitate on ISG15 expression was initially performed in 3T3-L1 pre-adipocytes (*Figure 65*). Although IFN-γ stimulated ISG15 expression with a 121% increase in protein levels following a 24 h treatment compared to the untreated control, palmitate did not have an effect. Neither IFN-γ nor palmitate stimulated total ISG15 levels over the timeframe investigated. As illustrated by *figure 66*, the time course was reproduced in 3T3-L1 mature adipocytes. Compared to the undifferentiated cells, lower expression levels of ISG15 were detected in the mature adipocytes. In this cell type, IFN-γ nor palmitate prompted an increase in the levels of free ISG15 or total ISG15.

Figure 65. A. *IFN-γ but not palmitate stimulates ISG15 levels in* ***3T3-L1 pre-adipocytes*****. B.** *Neither IFN-γ nor palmitate enhances total ISG15 levels in 3T3-L1 pre-adipocytes.* For both *figures A* and *B*, 3T3-L1 pre-adipocytes were treated with IFN-γ (20 ng/mL) (lanes 3 to 7), unconjugated palmitate (500 µM) (lanes 9 to 13) and LPS (100 ng/mL) (lane 15) in 10% FBS/DMEM (HG). Equivalent volumes of MilliQ water (40 µL) (lane 2) and DMEM (LG) (1 mL) (lanes 8 and 14) were used as control for the IFN and palmitate treatments, respectively. Cells were lysed with 100 µL 1% TX-100 lysis buffer per 10 cm Ø dish. 65 µg of protein were loaded per lane (12% Tris-Tricine-SDS gel). Statistical difference between the 24 h IFN-γ treatment and other treatments is indicated with $; statistical difference between the 8 h IFN-γ treatment and other treatments is indicated with £ (p-value < 0.05). Data from three independent experiments.

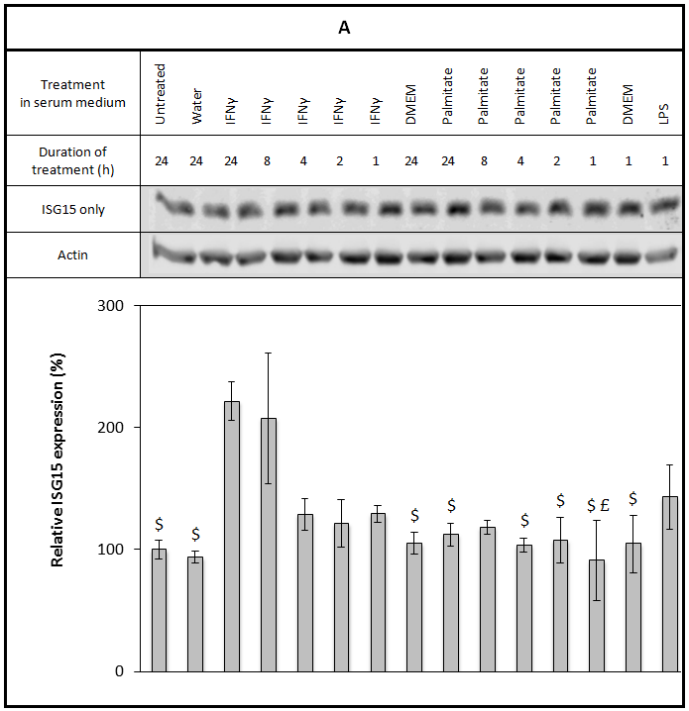

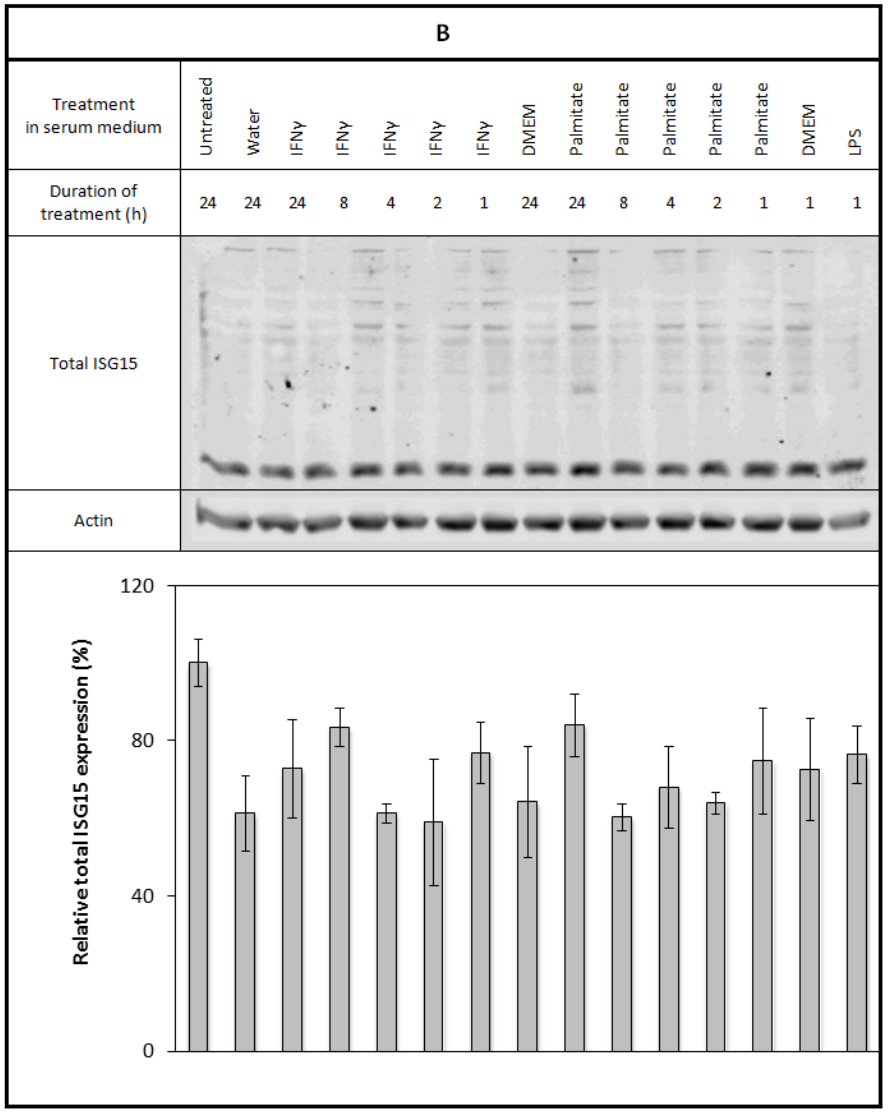

Figure 66. A. *Neither palmitate nor IFN-γ stimulates ISG15 levels in* ***3T3-L1 mature adipocytes*****. B.** *Neither IFN-γ nor palmitate enhances total ISG15 levels in 3T3-L1 mature adipocytes.* For both *figures A* and *B*, 3T3-L1 mature adipocytes were treated with IFN-γ (20 ng/mL) (lanes 3 to 7), unconjugated palmitate (500 µM) (lanes 9 to 13) and LPS (100 ng/mL) (lane 15) in 10% FBS/DMEM (HG). Equivalent volumes of MilliQ water (8 µL) (lane 2) and DMEM (LG) (200 µL) (lanes 8 and 14) were used as control for the IFN and palmitate treatments, respectively. Cells were lysed with 80 µL 1% TX-100 lysis buffer per well. 103 µg of protein were loaded per lane (12% Tris-Tricine-SDS gel).. Data from three independent experiments.

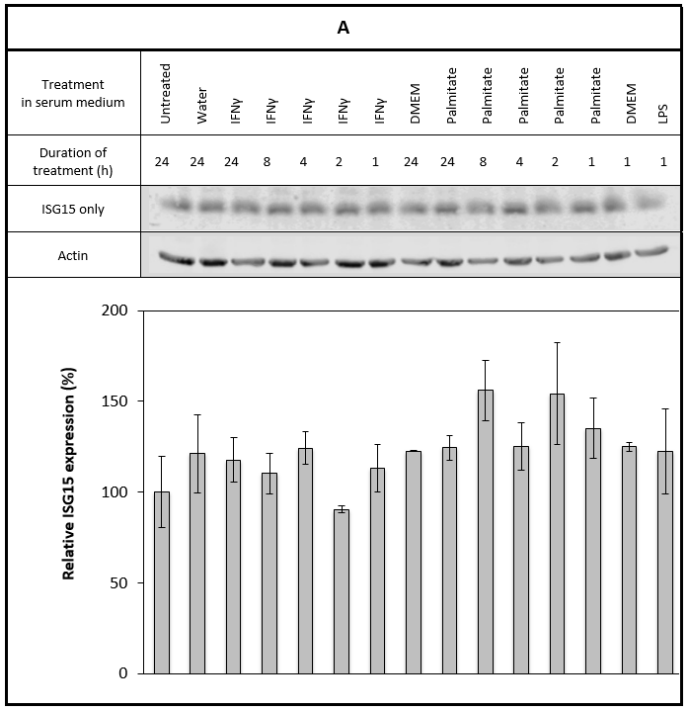

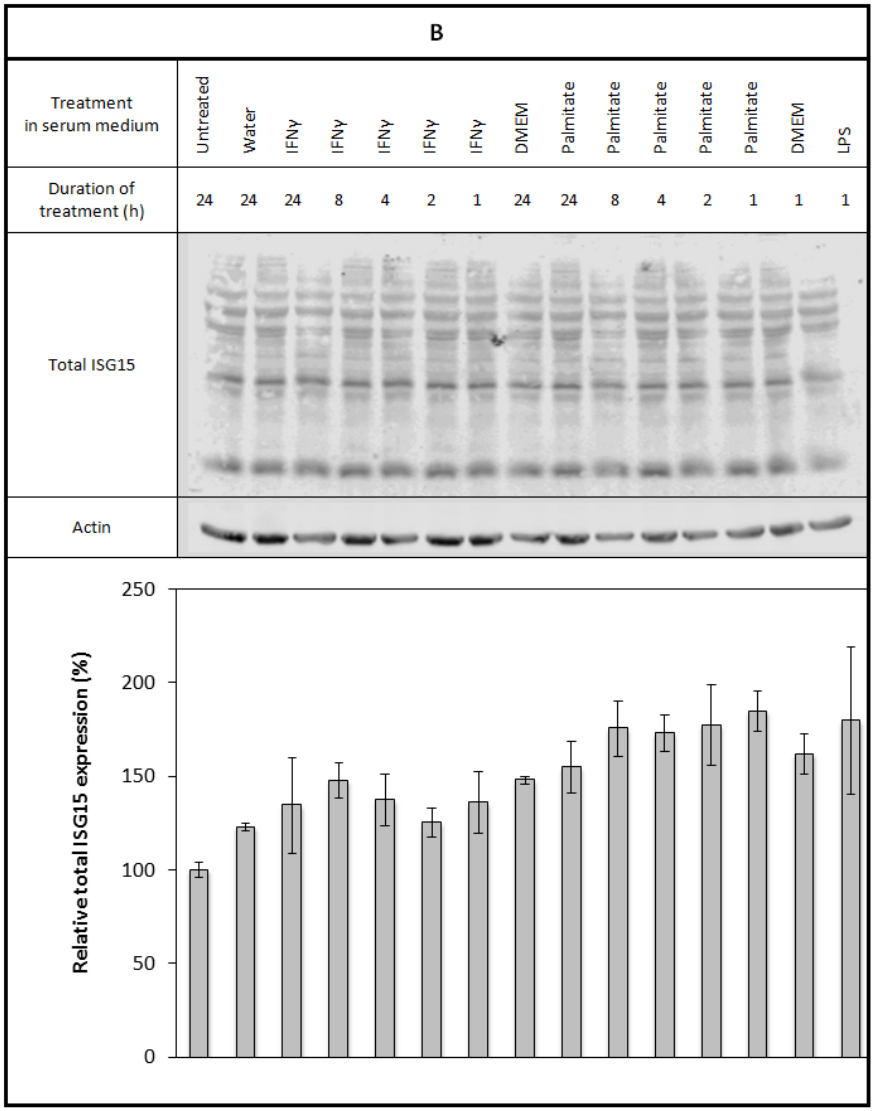

V. 3. 1. 2. Using hMADS cell line

The time course experiment presented in the previous subsection was also conducted in human pre- and mature adipocytes. *Figure 67* details the results of the former experiment. As for mouse cells, free-ISG15 expression peaked after treating the cells for 24 h with IFN-γ. A 123% increase in signal is recorded compared to untreated control. The cytokine did not alter the expression of total ISG15. Palmitate treatment affected neither endpoint. As shown in *figure 68*, ISG15 expression is considerably weaker in mature adipocytes as for murine cells. Therefore, the apparent inhibition of total ISG15 driven by both treatments is likely to be explained by the poor quality of the signal. Indeed, such effect could not be reproduced (*data not shown*).

Table 13. *Summary of the effect of IFN-γ and palmitate treatment on ISG15 and total ISG15 levels in mouse and human cell lines compared to the untreated control.* Effects recorded in this table achieved statistical significance when tested with a one-way ANOVA.

Cell line	*3T3-L1 pre-adipocytes*	*3T3-L1 mature adipocytes*	*hMADS pre-adipocytes*	*hMADS mature adipocytes*
IFN-γ-mediated ISG15 induction	✓ 121 % increase (24 h)	✗	✓ 123 % increase (24 h)	✓ 200 % increase (24 h)
IFN-γ-mediated total ISG15 induction	✗	✗	✗	✓ 78 % decrease (2 h)
Palmitate-mediated ISG15 induction	✗	✗	✗	✗
Palmitate-mediated total ISG15 induction	✗	✗	✗	✓ 82 % decrease (2 h)

Figure 67. A. *IFN-γ but not palmitate stimulates ISG15 levels in* ***hMADS pre-adipocytes*****. B.** *Neither IFN-γ nor palmitate enhances total ISG15 levels in* ***hMADS pre-adipocytes***. For both *figures A* and *B*, hMADS pre-adipocytes were treated with IFN-γ (20 ng/mL) (lanes 3 to 7), unconjugated palmitate (500 µM) (lanes 9 to 13) and LPS (100 ng/mL) (lane 15) in complete DMEM (LG). Equivalent volumes of MilliQ water (40 µL) (lane 2) and DMEM (LG) (1 mL) (lane 8 and 14) were used as control for the IFN and palmitate treatments, respectively. Cells were lysed with 100 µL 1% TX-100 lysis buffer per 10 cm Ø dish. 33 µg of protein were loaded per lane (12% Tris-Tricine-SDS gel). ** denotes a treatment statistically different from all other treatments (p-value < 0.05). Data from three independent experiments.

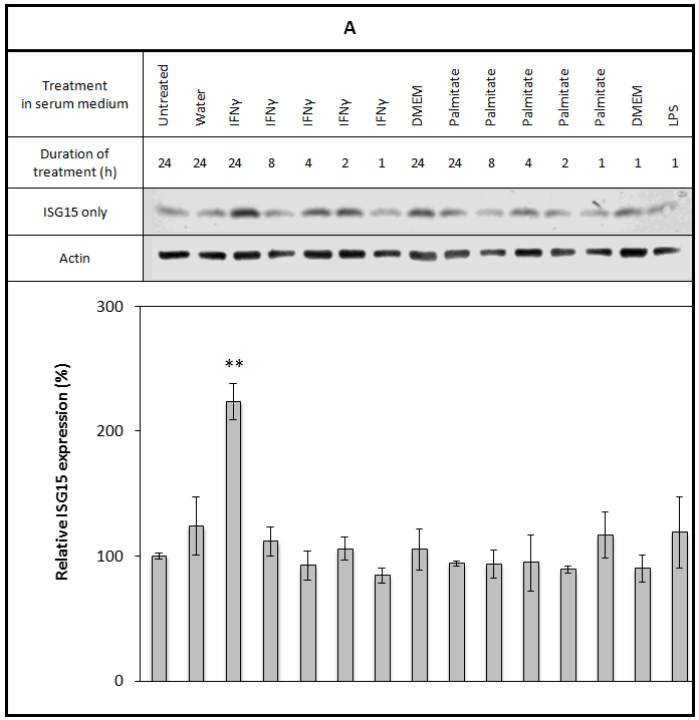

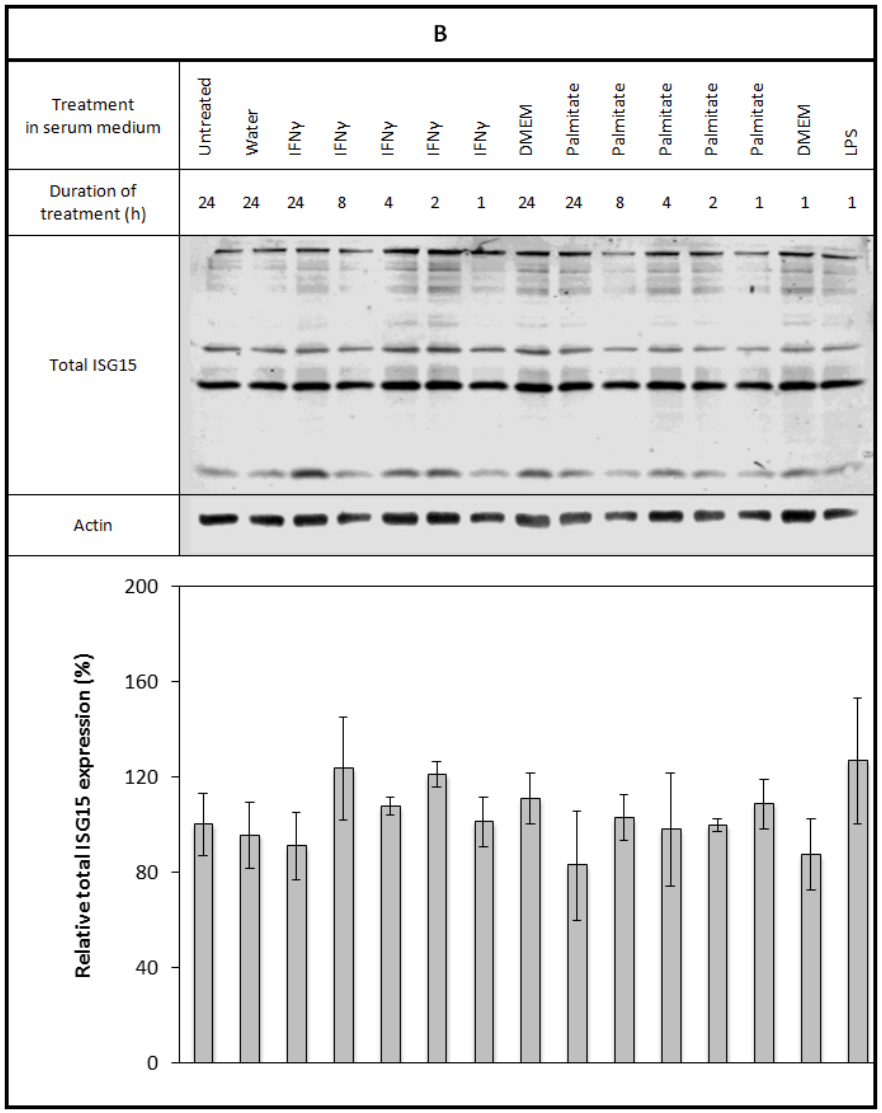

Figure 68. A. *IFN-γ but not palmitate stimulates ISG15 levels in* ***hMADS mature adipocytes***. **B.** *IFN-γ and palmitate reduce total ISG15 levels in* ***hMADS mature adipocytes***. For both *figures A* and *B*, hMADS mature adipocytes were treated with IFN-γ (20 ng/mL) (lanes 3 to 7), unconjugated palmitate (500 µM) (lanes 9 to 13) and LPS (100 ng/mL) (lane 15) in complete DMEM (LG). Equivalent volumes of MilliQ water (8 µL) (lane 2) and DMEM (LG) (200 µL) (lane 8 and 14) were used as control for the IFN and palmitate treatments, respectively. Cells were lysed with 80 µL 1% TX-100 lysis buffer per well. 116 µg of protein were loaded per lane (12% Tris-Tricine-SDS gel). Statistical difference between the untreated control and other treatments is indicated with £; statistical difference between the 24 h IFN-γ treatment and other treatments is indicated with $ (p-value < 0.05). Data from three independent experiments.

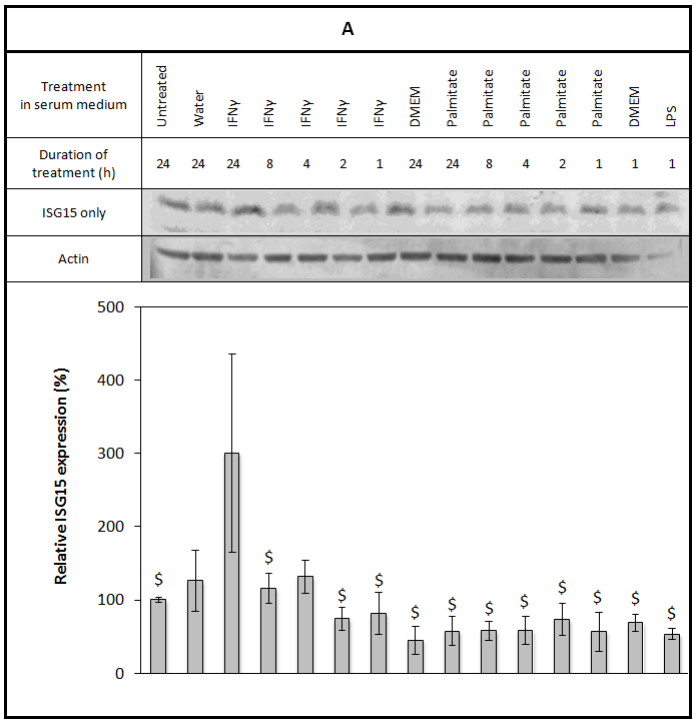

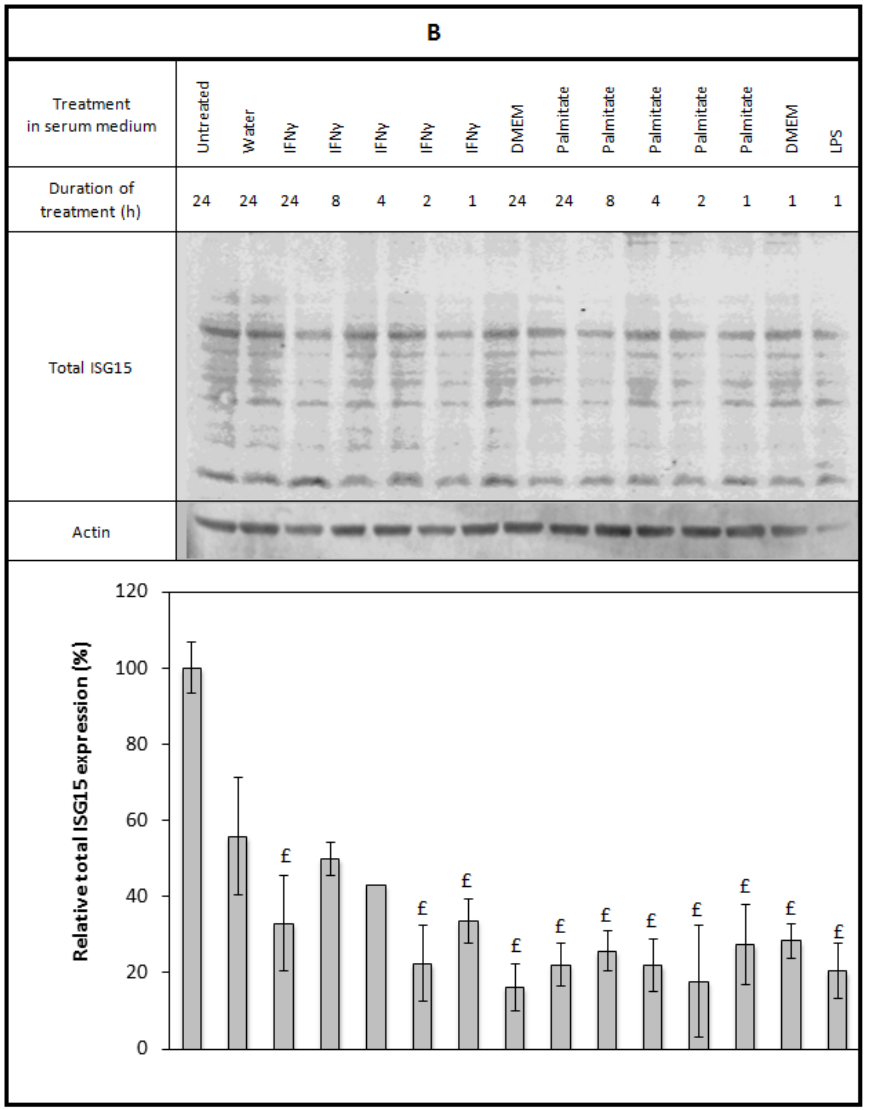

V. 3. 2. ISG15 induces STAT3 in mature 3T3-L1 adipocytes

Having investigated the effect of SFA on ISG15 expression, we sought to assess whether free ISG15 operating as a cytokine could mediate the effects of palmitate in adipocytes. To this end, we tested if recombinant ISG15 could induce the signalling pathways previously identified to be stimulated by palmitate. More specifically, we verified whether recombinant ISG15 could promote the phosphorylation of STAT3 Tyr^{705} in 3T3-L1 mature adipocytes. *Figure 69* presents the results of such time course experiment. ISG15 induced a time–dependent increase in STAT3 phosphorylation starting at approximately 2 h and up to the longest time point tested (48 h). After 48 h of treatment, the recombinant protein induces a statistically significant 117% increase in p-STAT3 Tyr^{705} compared to untreated control. The stimulation of the transcription factor gradually dampens as the length of the treatment reduces. After 1 hour of treatment, the effect of ISG15 is negligible. Another time course experiment should be performed over a shorter timeframe to dismiss a potential biphasic response similar to that induced by leptin in HEK 293T cells discussed in the introduction of Chapter 3 (C. W. Han 2016).

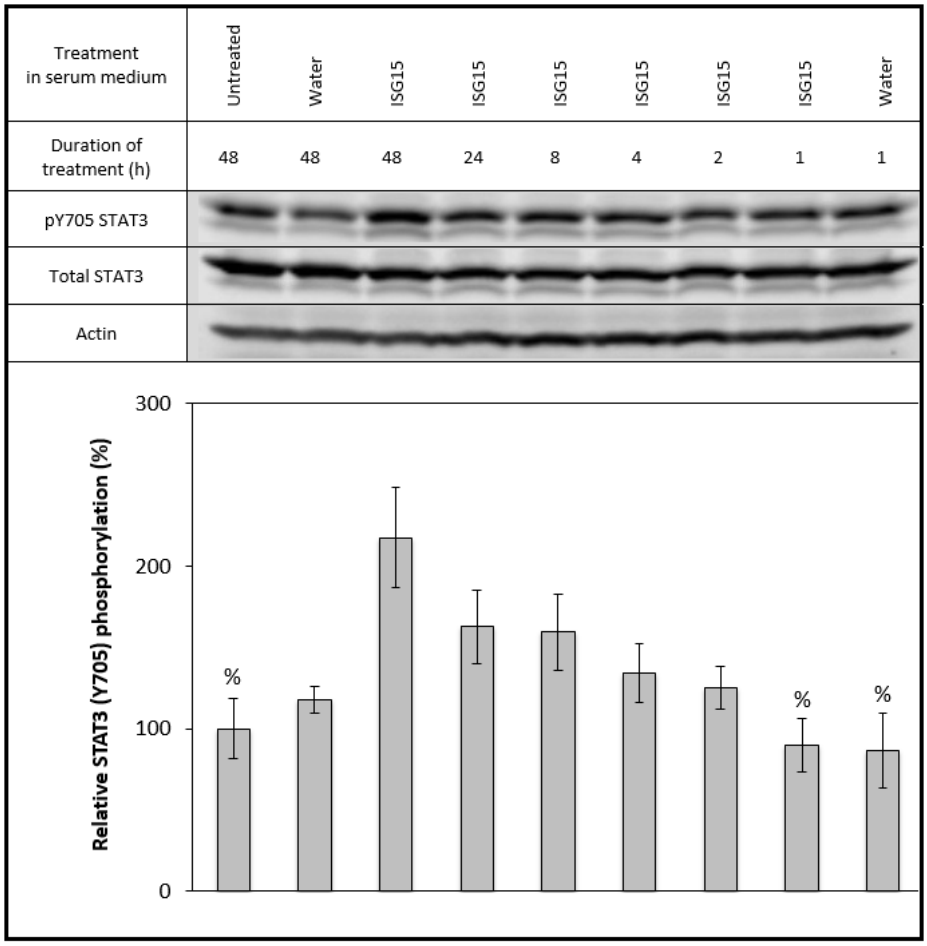

Figure 69. *ISG15 stimulates STAT3 tyrosine phosphorylation in 3T3-L1 mature adipocytes following prolonged treatment.* 3T3-L1 mature adipocytes were treated with recombinant human ISG15 (100 ng/mL) (lanes 3, 4, 5, 6, 7 and 8) in 10% FBS/DMEM (HG). Equivalent volumes of MilliQ water (4 µL) (lanes 2 and 9) were used as control for the ISG15 treatments, respectively. Cells were lysed with 80 µL 1% TX-100 lysis buffer per well. 147 µg of protein were loaded per lane (10% SDS-acrylamide gel). Statistical difference between the 48 h ISG15 treatment and other treatments is indicated with % (p-value < 0.05). Data from three independent experiments.

V. 3. 3. Use of RNAi experiments to study the potential role of ISG15 in palmitate-induced insulin resistance

This section presents the outcomes of RNAi experiments, aimed at establishing the role of the IFN pathway in palmitate-mediated insulin resistance by targeting a specific gene of the IFN cascade (*Isg15*) for knockdown. We developed as stable 3T3-L1 *Isg15* knockdown cell line (*Isg15*-KD) using an RNAi technique relying on the delivery of shRNA into the cells through viral infection. Such

approach has the benefit of producing long-term silencing of the gene and thus allows for experiments to be performed in both pre- and mature-adipocytes.

V. 3. 3. 1. Effects of silencing Isg15 *on insulin sensitivity in 3T3-L1 pre-adipocytes*

Figure 70 demonstrates the efficacy of the *Isg15*-KD. Indeed, it compares the expression levels of free ISG15 and total ISG15 of the adipocytes transduced with the empty pGIPZ and those transduced with the GIPZ containing the *Isg15*-targeting shRNA following stimulation with either IFN-α or IFN-γ. Although total ISG15 levels do not seem to differ from one cell line to the other, the expression of unconjugated ISG15 is four times higher in the cells transduced with the empty vector compared to the *Isg15*-KD pre-adipocytes. As expected, type I IFN drives a much more significant induction of ISG15 than type II. *Figure 71* compares the IFN-α-mediated induction of ISG15 in WT pre-adipocytes and in the two transduced cell lines. Consistent with the results presented in *figure 70*, levels of total ISG15 are not significantly affected by the treatment across cell lines. However, the expression of free ISG15 is up-regulated in both the WT pre-adipocytes and the cells transduced with the empty vector. The magnitude of this stimulation is comparable in both cell types. As noted in *figure 70*, the cytokine treatment fails to induce the expression of ISG15 in the *Isg15*-KD pre-adipocytes.

Figure 70. A. *IFN-α stimulates ISG15 levels in 3T3-L1 pre-adipocytes transduced with the empty vector but not the* Isg15*-KD cell line. IFN-γ has not effect on either cells lines.* **B.** *Neither IFN-α nor IFN-γ stimulates total ISG15 levels in 3T3-L1 pre-adipocytes transduced with the empty vector and the* Isg15*-KD cell line.* 3T3-L1 pre-adipocytes transduced with either the pGIPZ empty vector or with the pGIPZ-*Isg15* shRNA construct were treated for 24 h in SF DMEM (HG, 0.2% BSA) with IFN-α (20 ng/mL) (lanes 5 and 6) and IFN-γ (20 ng/mL) (lanes 7 and 8). Equivalent volumes of MilliQ water (40 µL) (lanes 3 and 4) were used as control. Cells were lysed with 100 µL 1% TX-100 lysis buffer per 10 cm Ø dish. 65 µg of protein were loaded per lane (12% Tris-Tricine-SDS gel). ** denotes a treatment statistically different from all other treatments (p-value < 0.05). Data from three independent experiments.

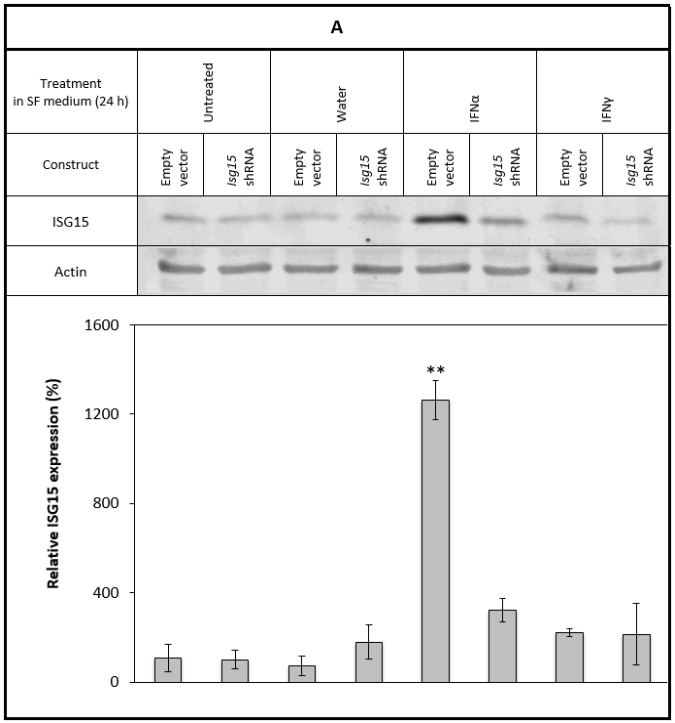

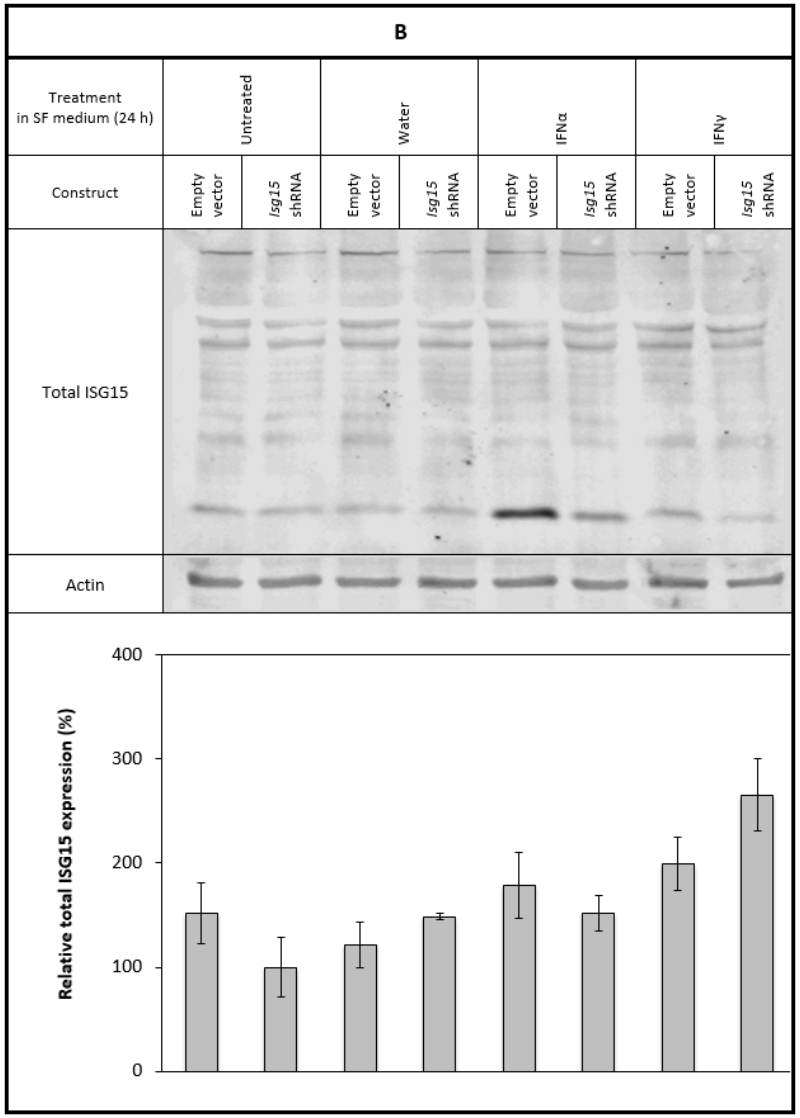

Figure 71. A. *IFN-α stimulates ISG15 levels in 3T3-L1 WT pre-adipocytes and 3T3-L1 pre-adipocytes transduced with the empty vector to similar levels but not the* Isg15*-KD cell line.* **B.** *IFN-α has no significant effect on total ISG15 levels in WT and transduced 3T3-L1 pre-adipocytes.* WT 3T3-L1 pre-adipocytes and 3T3-L1 pre-adipocytes transduced with either the pGIPZ empty vector or with the pGIPZ-*Isg15* shRNA construct were treated for 24 h in SF DMEM (HG, 0.2% BSA) with IFN-α (20 ng/mL) (lanes 3, 6 and 9). Equivalent volumes of MilliQ water (16 µL) (lanes 2, 5 and 8) were used as control. Cells were lysed with 100 µL 1% TX-100 lysis buffer per 6 cm Ø dish. 27 µg of protein were loaded per lane (12% Tris-Tricine-SDS gel). Statistical difference between the IFN-α treatment (WT cells) and other treatments is indicated with £; statistical difference between the IFN-α treatment (empty vector cells) and other treatments is indicated with % (p-value < 0.05). Data from three independent experiments.

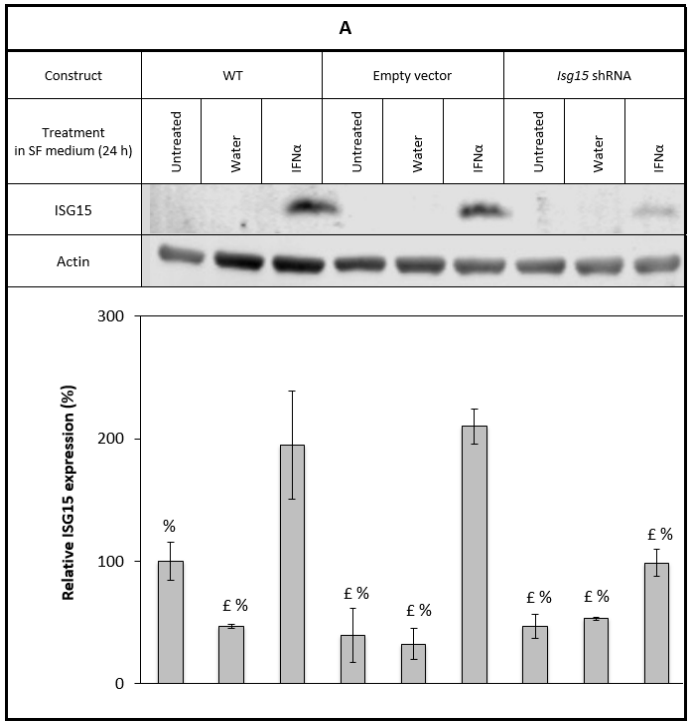

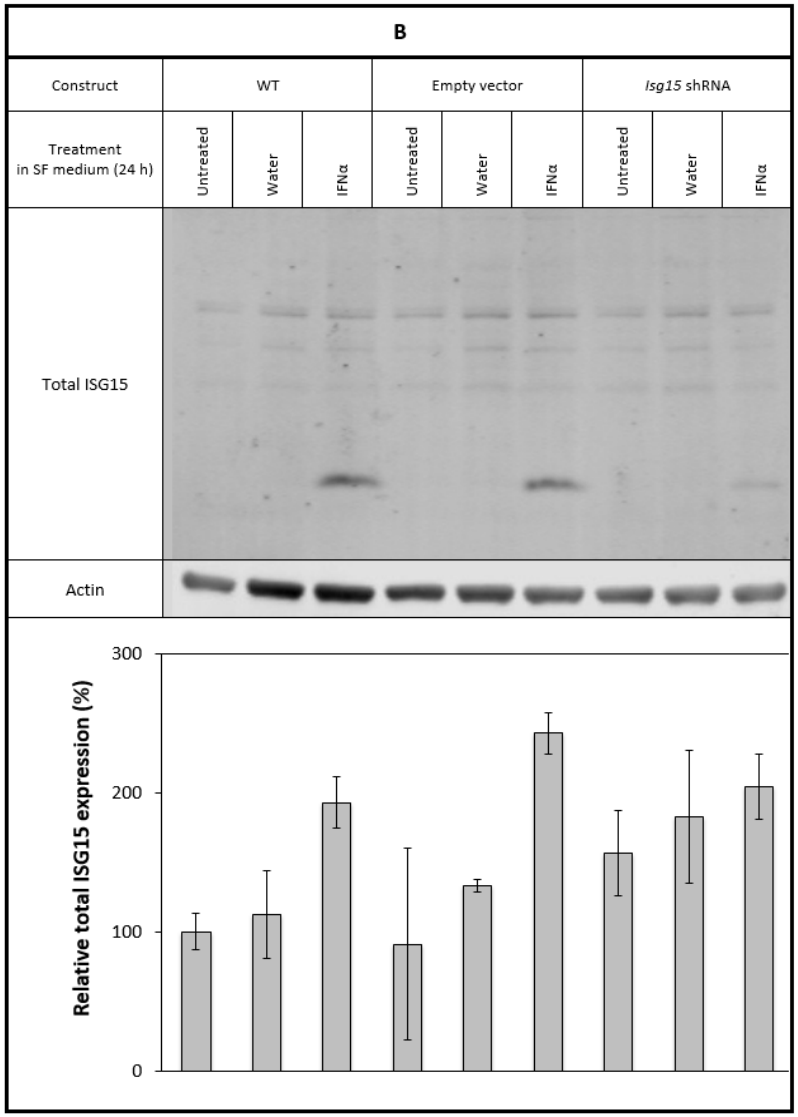

Having successfully produced a stable *Isg15*-KD cell line, we assessed whether conjugated or unconjugated palmitate affected ISG15 expression. As revealed by *figures 72* and *73*, neither types of SFA altered the expression levels of free ISG15 (or total ISG15) in either the cells transduced with the empty vector or those transduced with the pGIPZ-*Isg15* shRNA construct. This is consistent with the absence of palmitate-mediated effect on ISG15 expression levels recorded in WT 3T3-L1 pre-adipocytes detailed in *figure 65*. Investigating the phosphorylation of Akt Thr^{308}, it appears that silencing *Isg15* enhances cellular susceptibility to palmitate-induced insulin resistance (*Figure 74*). Indeed, following acute insulin stimulation, the *Isg15*-KD cell line treated with BSA-conjugated palmitate showed a statistically significant 63% and 58% decrease in p-Akt levels compared to the insulin-stimulated control and BSA-treated control, respectively. On the other hand, the control cell line was unresponsive to the deleterious effect of the SFA, suggesting it is more sensitive to insulin. Similarly to the WT strain of 3T3-L1 pre-adipocytes, IFN-α failed to induce insulin resistance in either type of transduced cell lines. As shown in panel C of *figure 75*, the difference in response to conjugated palmitate is quite substantial between the two transduced cell lines with p-Akt levels 68% lower for the *Isg15*-KD pre-adipocytes.

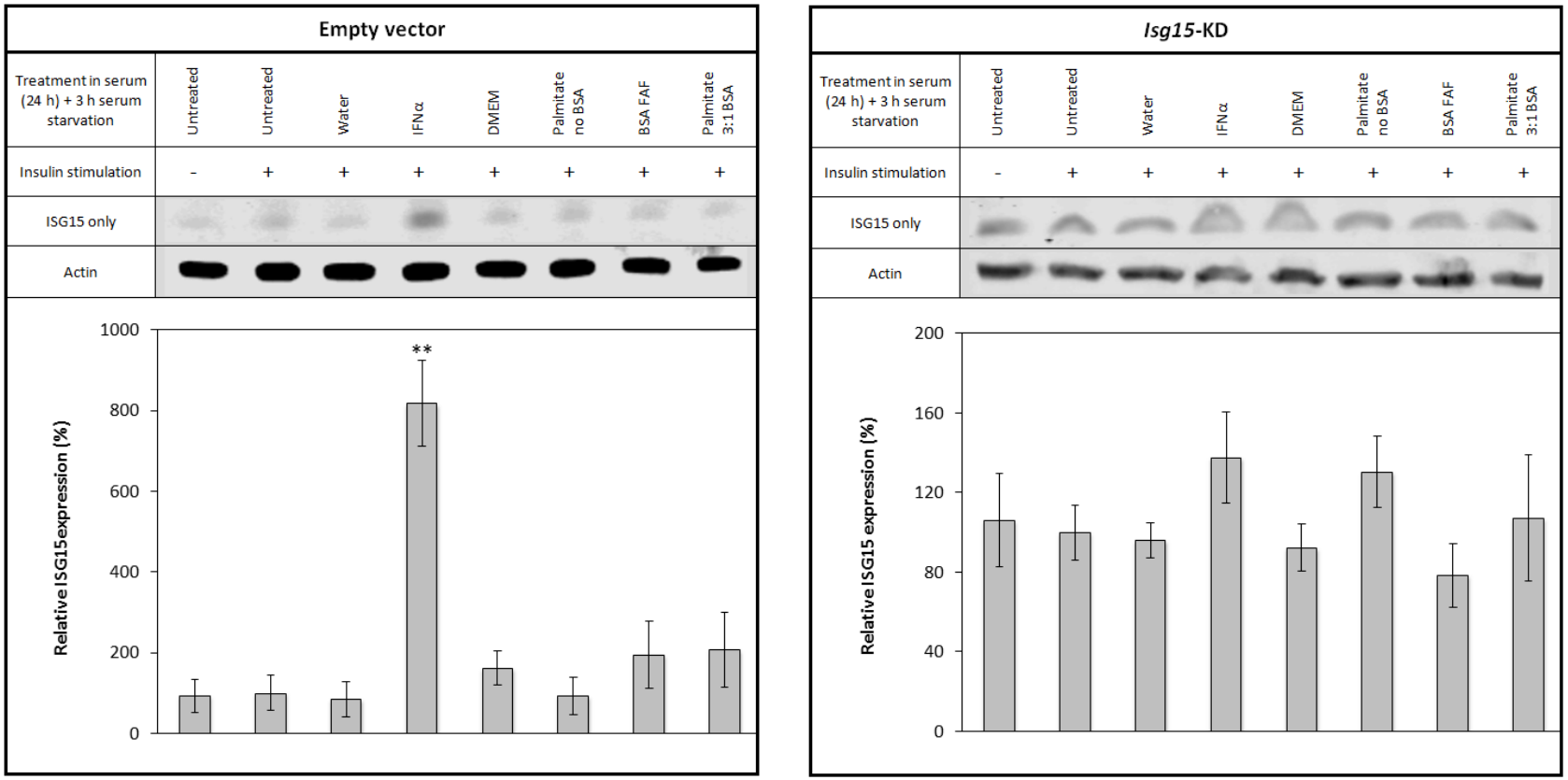

Figure 72. Empty vector. *IFN-α but not palmitate stimulates ISG15 expression in 3T3-L1 pre-adipocytes transduced with the empty vector.* ***Isg15*-KD.** *Both IFN-α and palmitate fail to stimulate ISG15 expression in* Isg15-*KD 3T3-L1 pre-adipocytes.* 3T3-L1 pre-adipocytes transduced with either the pGIPZ empty vector or with the pGIPZ-*Isg15* shRNA construct were treated with IFN-α (20 ng/mL) (lane 4), unconjugated palmitate (500 µM) (lane 6) and palmitate 3:1 BSA (500 µM) (lane 8) for 24 h in 10% FBS/DMEM (HG). Following a 3 h serum deprivation (SF DMEM, HG, 0.2% BSA), cells were stimulated with insulin (100 nM for 15 min) except for the first untreated control (lane 1). Equivalent volumes of MilliQ water (40 µL) (lane 3), DMEM (LG) (1 mL) (lane 5) and BSA FAF (1 mL) (lane 7) were used as control for the IFN-α, unconjugated and unconjugated palmitate treatments, respectively. Cells were lysed with 100 µL 1% TX-100 lysis buffer per 10 cm Ø dish. 87 µg of protein were loaded per lane in *Empty vector* (left) and 92 µg in *Isg15*-KD (right) (12% Tris-Tricine-SDS gel). ** denotes a treatment statistically different from all other treatments (p-value < 0.05). Data from four independent experiments.

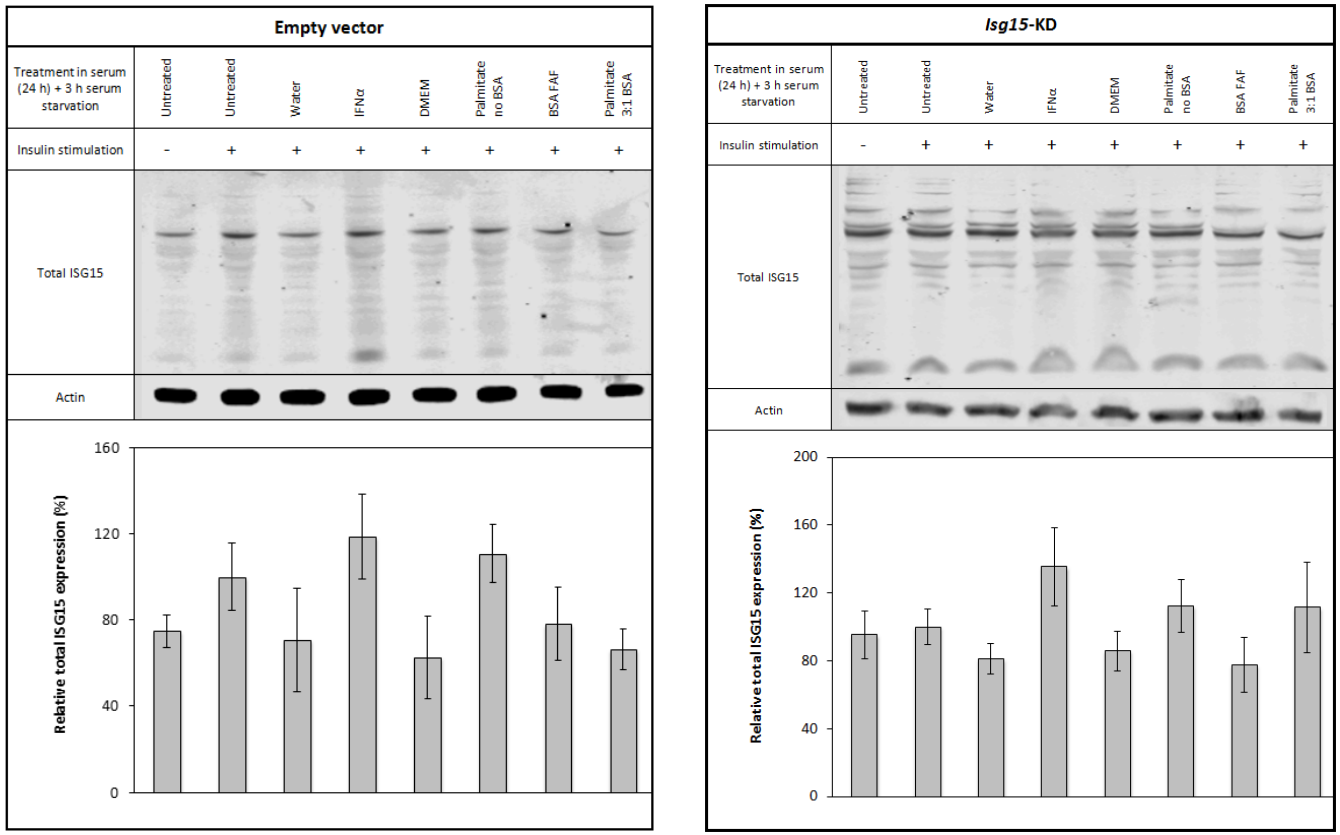

Figure 73. Empty vector. *Both IFN-α and palmitate fail to stimulate total ISG15 expression in 3T3-L1 pre-adipocytes transduced with the empty vector.* ***Isg15*-KD.** *Both IFN-α and palmitate fail to stimulate total ISG15 expression in* Isg15-*KD 3T3-L1 pre-adipocytes.* 3T3-L1 pre-adipocytes transduced with either the pGIPZ empty vector or with the pGIPZ-*Isg15* shRNA construct were treated with IFN-α (20 ng/mL) (lane 4), unconjugated palmitate (500 µM) (lane 6) and palmitate 3:1 BSA (500 µM) (lane 8) for 24 h in 10% FBS/DMEM (HG). Following a 3 h serum deprivation (SF DMEM, HG, 0.2% BSA), cells were stimulated with insulin (100 nM for 15 min) except for the first untreated control (lane 1). Equivalent volumes of MilliQ water (40 µL) (lane 3), DMEM (LG) (1 mL) (lane 5) and BSA FAF (1 mL) (lane 7) were used as control for the IFN-α, unconjugated and unconjugated palmitate treatments, respectively. Cells were lysed with 100 µL 1% TX-100 lysis buffer per 10 cm Ø dish. 87 µg of protein were loaded per lane in *Empty vector* (left) and 92 µg in *Isg15*-KD (right) (12% Tris-Tricine-SDS gel). Data from four independent experiments.

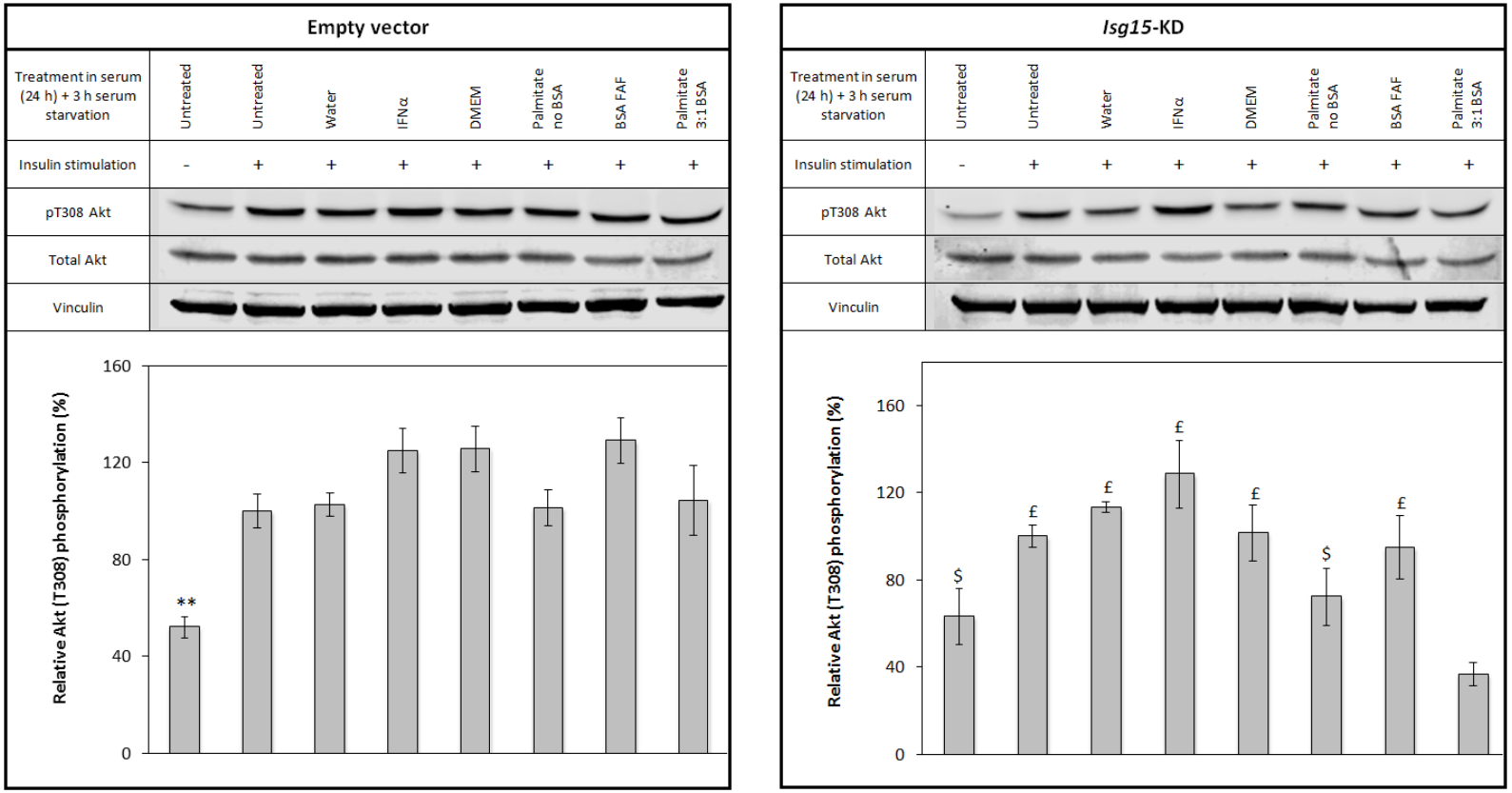

Figure 74. *Knockdown of ISG15 increases susceptibility to palmitate-induced insulin resistance in **3T3-L1 pre-adipocytes***. 3T3-L1 pre-adipocytes transduced with either the pGIPZ empty vector or with the pGIPZ-*Isg15* shRNA construct were treated with IFN-α (20 ng/mL) (lane 4), unconjugated palmitate (500 µM) (lane 6) and palmitate 3:1 BSA (500 µM) (lane 8) for 24 h in 10% FBS/DMEM (HG). Following a 3 h serum deprivation (SF DMEM, HG, 0.2% BSA), cells were stimulated with insulin (100 nM for 15 min) except for the first untreated control (lane 1). Equivalent volumes of MilliQ water (40 µL) (lane 3), DMEM (LG) (1 mL) (lane 5) and BSA FAF (1 mL) (lane 7) were used as control for the IFN-α, unconjugated and unconjugated palmitate treatments, respectively. Cells were lysed with 100 µL 1% TX-100 lysis buffer per 10 cm Ø dish. 87 µg of protein were loaded per lane in *Empty vector* (left) and 82 µg in *Isg15*-KD (right) (10% SDS-acrylamide gel). Statistical difference between the IFN-α treatment and other treatments is indicated with $; statistical difference between the palmitate 3:1 BSA treatment and other treatments is indicated with £; ** denotes a treatment statistically different from all other treatments (p-value < 0.05). Data from four independent experiments.

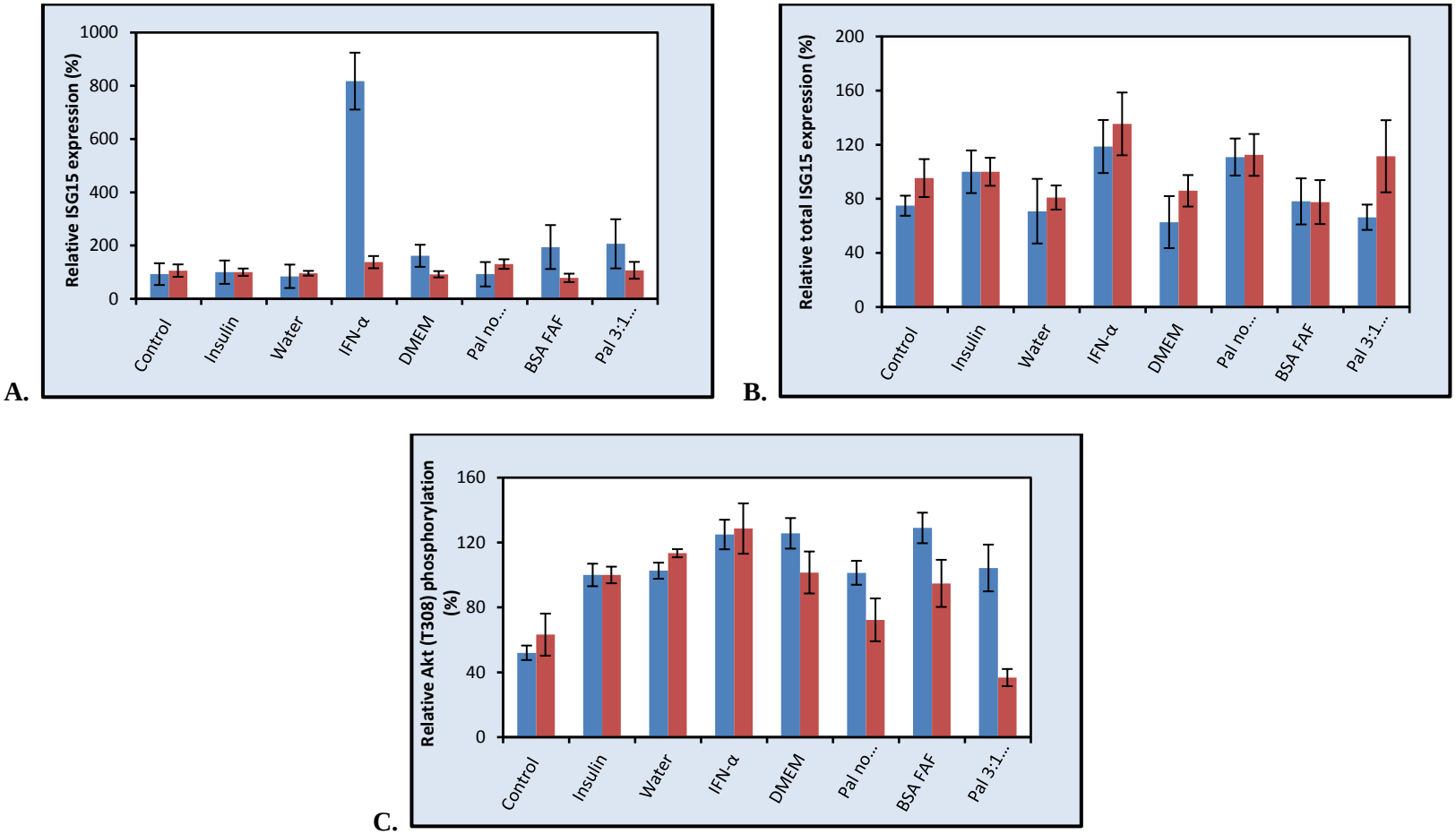

Figure 75. *Comparison of the effect of IFN-α, unconjugated and BSA-conjugated palmitate on* **A.** *ISG15 expression (top left),* **B.** *total ISG15 expression (top right) and* **C.** *insulin-stimulated Akt Thr^{308} phosphorylation (bottom) in 3T3-L1 pre-adipocytes transduced with the pGIPZ empty vector (blue) and the pGIPZ-*Isg15 *shRNA construct (red).* Cells were treated with IFN-α (20 ng/mL), unconjugated palmitate and palmitate 3:1 BSA (500 µM) for 24 h in 10% FBS/DMEM (HG). Following a 3 h serum deprivation (SF DMEM, HG, 0.2% BSA), cells were stimulated with insulin (100 nM for 15 min) except for the first untreated control. Equivalent volumes of MilliQ water (40 µL), DMEM (LG) (1 mL) and BSA FAF (1 mL) were used as control for the IFN-α, unconjugated and unconjugated palmitate treatments, respectively.

Figure 76 explores the effect of inhibiting p110α on palmitate-induced insulin resistance in the two transduced cell lines, using the phosphorylation levels of Akt as read-out. In line with the findings reported in *figure 74*, the pre-adipocytes transfected with the empty vector appear protected from palmitate-induced insulin resistance unlike the *Isg15*-KD cell line. Indeed, the p-Akt levels were not significantly affected by the SFA treatment compared to the p-Akt levels recorded in both the BSA-treated and the insulin-stimulated controls in pre-adipocytes transduced with the empty vector. In the *Isg15*-KD cells however, palmitate drove a 48% and 46% decrease in p-Akt *versus* the insulin-stimulated and the BSA-treated controls, respectively. The p-Akt levels recorded for the two controls are statistically different from the untreated control unlike those measured for cells treated with palmitate. As this is not the case in pre-adipocytes transduced with the empty vector (the p-Akt levels recorded for the two controls as well as for the SFA-treated cells are not statistically different from the untreated cells), we can conclude that the palmitate effect on Akt phosphorylation is greater in *Isg15*-KD pre-adipocytes.

Adding A66 to the palmitate treatment rescues the effect of the SFA in both cell lines although the difference in p-Akt levels between cells treated with palmitate alone and a combination of palmitate and A66 is only statistically significant in *Isg15*-KD pre-adipocytes. As shown in *figure 77*, the latter cell line seems less sensitive to the effect of A66 alone compared to pre-adipocytes transduced with the empty vector.

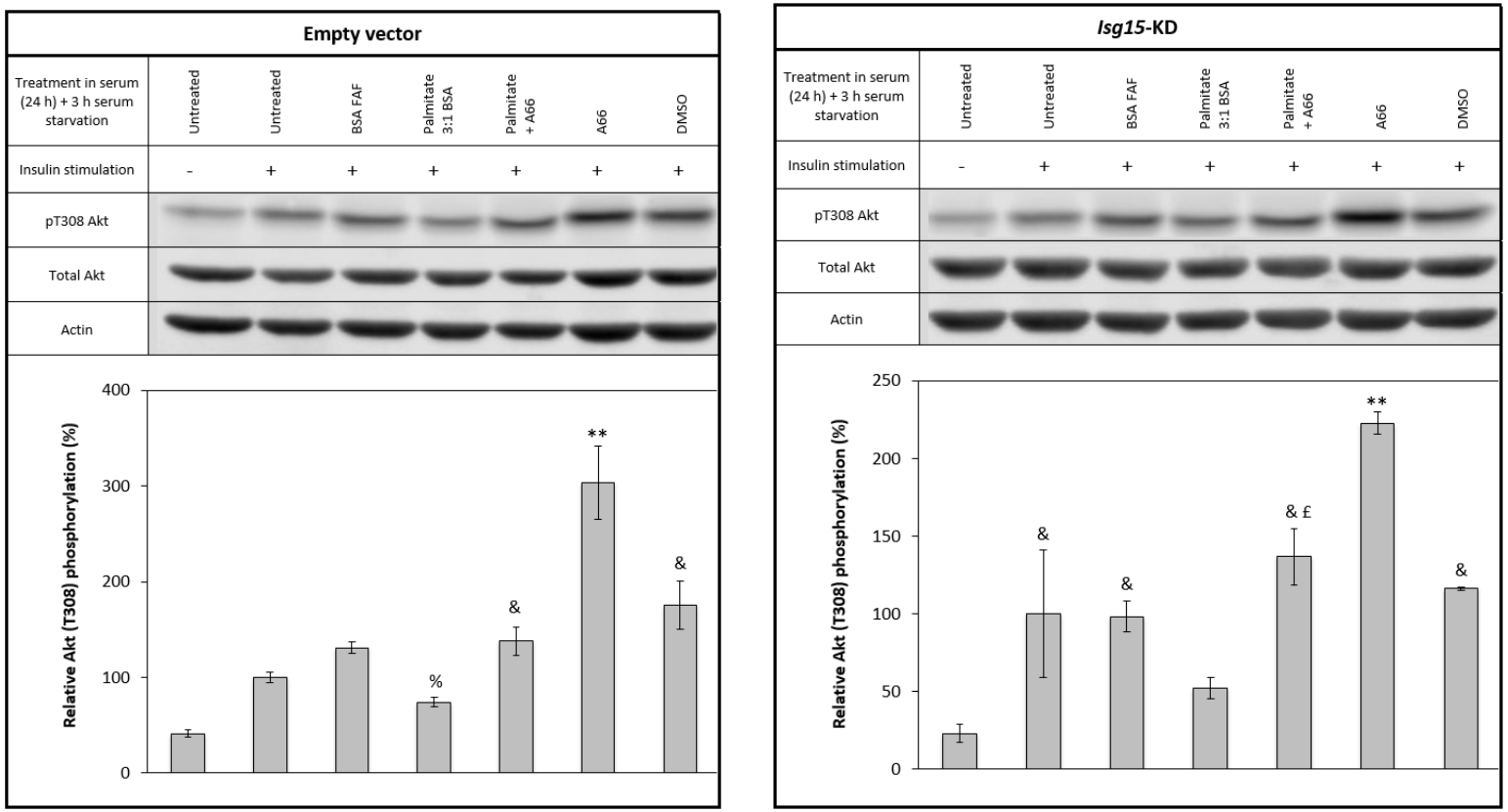

Figure 76. *A66 rescues the effect of palmitate on the phosphorylation of Akt in both 3T3-L1 pre-adipocytes transduced with the empty vector and* Isg15*-KD 3T3-L1 pre-adipocytes.* 3T3-L1 pre-adipocytes transduced with either the pGIPZ empty vector or with the pGIPZ-*Isg15* shRNA construct were treated with palmitate 3:1 BSA (500 µM) (lanes 4 and 5) and A66 (1 µM) (lanes 5 and 6) for 24 h in 10% FBS/DMEM (HG). Following a 3 h serum deprivation (SF DMEM, HG, 0.2% BSA), cells were stimulated with insulin (100 nM for 15 min) except for the first untreated control (lane 1). Equivalent volumes of BSA FAF (400 µL) (lane 3) and DMSO (40 µL) (lane 7) were used as control for the unconjugated palmitate treatment and A66 treatment, respectively. In both figures, cells were lysed with 100 µL 1% TX-100 lysis buffer per 6 cm Ø dish. 29 µg of protein were loaded per lane (10% SDS-acrylamide gel). Statistical difference between the untreated control and other treatments is indicated with &; statistical difference between the palmitate 3:1 BSA treatment and other treatments is indicated with £; statistical difference between the DMSO control and other treatments is indicated with %; ** denotes a treatment statistically different from all other treatments (p-value < 0.05). Data from three independent experiments.

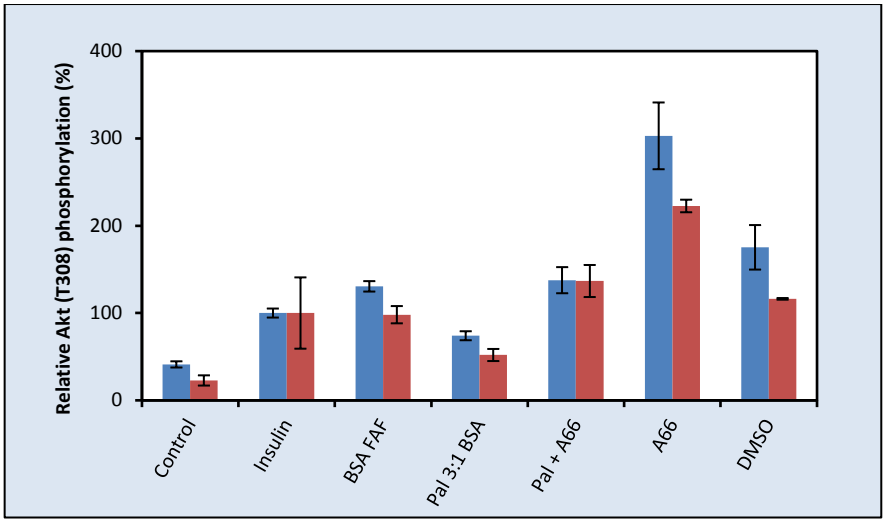

Figure 77. *Comparison of the effect of unconjugated palmitate and A66 on Akt Thr*^{308} *phosphorylation in* ***3T3-L1 pre-adipocytes*** *transduced with the pGIPZ empty vector (blue) and the pGIPZ-*Isg15 *shRNA construct (red).* Cells were treated with palmitate 3:1 BSA (500 µM) and A66 (1 µM) for 24 h in 10% FBS/DMEM (HG). Following a 3 h serum deprivation (SF DMEM, HG, 0.2% BSA), cells were stimulated with insulin (100 nM for 15 min) except for the first untreated control. Equivalent volumes of BSA FAF (400 µL) and DMSO (40 µL) were used as control for the unconjugated palmitate treatment and A66 treatment, respectively.

V. 3. 3. 2. Effects of silencing Isg15 *on palmitate-induced autophagy in 3T3-L1 pre-adipocytes*

Having investigated the consequences of silencing ISG15 on palmitate-mediated insulin resistance, we explored the effect of this manipulation on palmitate-induced stimulation of autophagy. In Chapter 4, the SFA was shown to elicit a significant increase in the expression levels of LC3B-II in 3T3-L1 pre-adipocytes. Therefore, the role of ISG15 in the modulation of the pro-autophagic effect of palmitate was evaluated in the same cell type. As illustrated by *figure 78A*, both the cells transduced with the empty vector and those transduced with the shRNA-*Isg15* construct responded to the palmitate treatment with a large increase in expression of the autophagy marker, LC3B-II. Interestingly, knocking down *Isg15* appeared to dull the palmitate-mediated induction: the SFA drove a 638% increase in LC3B-II levels compared to the DMEM-treated control in the control cell line, while only a 336%

increase was measured in the *Isg15*-KD cell line comparing the same conditions. The one-way ANOVA analysis confirms the statistical difference between the responses of the two cell lines to the palmitate treatment ($F(9,20) = 57.69$, p-value = 0.00; Tukey HSD *post hoc* test between "empty vector - palmitate treatment" and "*Isg15*-KD - palmitate treatment": p-value = 0.00).

Figure 78B explores the potential molecular mechanisms implicated in the modulation of palmitate-induced autophagy by ISG15. Indeed, in addition to the experimental conditions of *figure 78A*, C16 (PKR-selective inhibitor) was included in the presence or absence of palmitate. The effect of the SFA alone is consistent with *figure 78A*, with a more significant increase in LC3B-II expression in the control cells *versus* the knockdown cells following the palmitate treatment. Interestingly, blocking PKR partially rescues the pro-autophagic effect of the SFA in both cell types. This is rather unexpected as C16 had no effect on palmitate-induced autophagy in WT 3T3-L1 pre-adipocytes (*Figure 61*). When comparing the fold decrease in LC3B-II expression between the palmitate treatment and the palmitate treatment supplemented with C16, the ratios are the same for both cell lines (0.7), implying that this effect is irrespective of whether *Isg15* is silenced.

Figure 79A aims at confirming the nature of the effect of palmitate on autophagy by including bafilomycin A1 to the treatments. Treating the cells for 24 h with the antibiotic induced too large of a stimulation of LC3B-II expression to detect any cumulative effect of palmitate and bafilomycin A1 (*data not shown*). Therefore, the duration of the treatment was reduced from 24 h to 4 h. At this time point, the palmitate treatment does up-regulate LC3B-II levels, however no difference can be

observed in the responses of the cell lines. Nevertheless, the cells transduced with the empty vector are more sensitive to the effect of the antibiotic alone. In both cell lines, combining the bafilomycin A1 and palmitate treatments elicits an even greater stimulation of LC3B-II expression than does either treatment on its own. As explained in the previous chapter, an up-regulation of LC3B-II levels in both the absence and presence of bafilomycin A1 indicates a stimulation of the autophagic flux, inhibited by the antibiotic.

Considering another marker of autophagy, p62, we were able to verify the pro-autophagic effect of palmitate (*Figure 79B*). When comparing the expression of p62 of the DMEM-treated control cells with that of palmitate-treated control cells, the 65% decrease observed in the latter group is statistically significant. However, comparing these treatments in the knockdown cell line, the difference measure is smaller (52% decrease following palmitate treatment) and not statistically significant. This is in line with the data presented in *figure 78A*, which indicated that cells transduced with the empty vector were more sensitive to the pro-autophagic effect of palmitate.

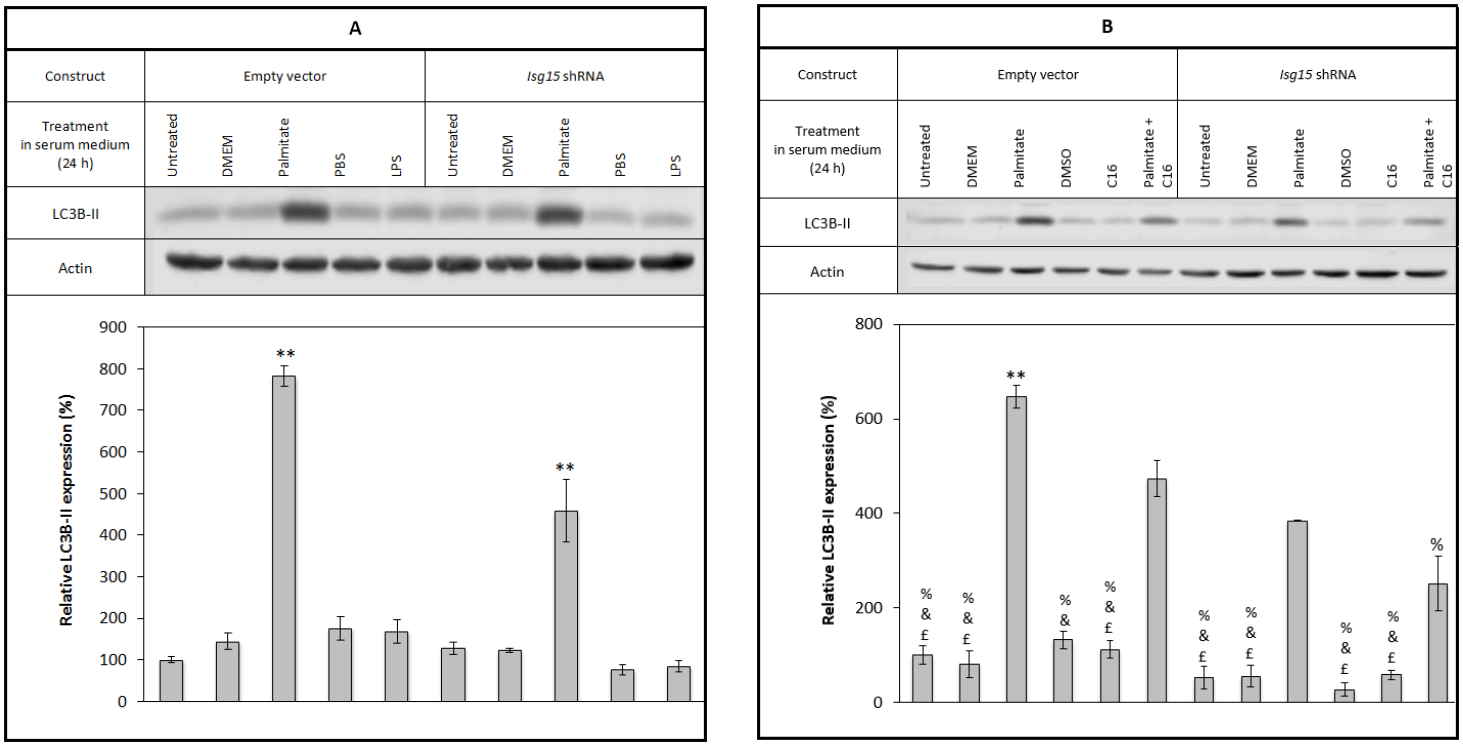

Figure 78. A. *Unconjugated palmitate stimulates the expression of LC3B-II in* ***3T3-L1 pre-adipocytes*** *transduced with the empty vector and to a lesser extent in* Isg15*-KD 3T3-L1 cells.* 3T3-L1 pre-adipocytes transduced with either the pGIPZ empty vector or with the pGIPZ-*Isg15* shRNA construct were treated with unconjugated palmitate (500 µM) (lanes 3 and 8) and LPS (100 ng/mL) (lanes 5 and 10) for 24 h in 10% FBS/DMEM (HG). Equivalent volumes of DMEM (LG) (400 µL) (lanes 2 and 7) and PBS (40 µL) (lanes 4 and 9) were used as control for the unconjugated palmitate and LPS treatments, respectively. **B.** *Inhibiting PKR in both cell type hinders the pro-autophagic effect of palmitate.* 3T3-L1 pre-adipocytes transduced with either the pGIPZ empty vector or with the pGIPZ-*Isg15* shRNA construct were treated with unconjugated palmitate (500 µM) (lanes 3, 6, 9 and 12) and C16 (2 µM) (lanes 5, 6, 11 and 12) for 4 h in 10% FBS/DMEM (HG). Equivalent volumes of DMEM (LG) (400 µL) (lanes 2 and 8) and DMSO (8 µL) (lanes 4 and 10) were used as control for the unconjugated palmitate and C16 treatments, respectively. For both *figures A* and *B*, cells were lysed with 100 µL 1% TX-100 lysis buffer per 6 cm Ø dish. 28 µg of protein were loaded per lane (15% SDS-acrylamide gel). Statistical difference between the "palmitate + C16" treatment (empty vector cells) and other treatments is indicated with %; statistical difference between the palmitate treatment (*Isg15*-KD cells) and other treatments is indicated with &; statistical difference between the palmitate + C16" treatment (*Isg15*-KD cells) and other treatments is indicated with £; ** denotes a treatment statistically different from all other treatments (p-value < 0.05). Data from three independent experiments.

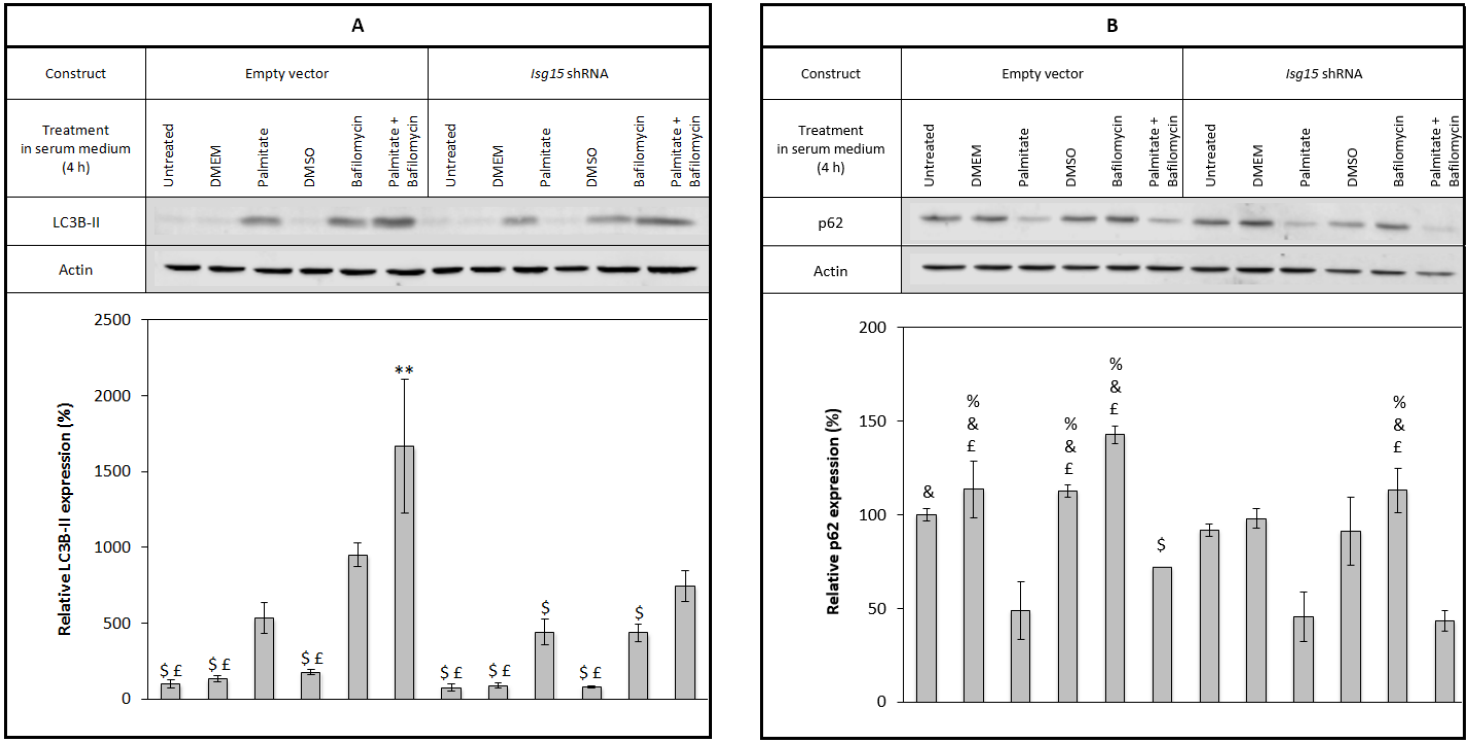

Figure 79. A. *Palmitate stimulates LC3B-II levels after 4 h of treatment in both* ***3T3-L1 pre-adipocytes*** *transduced with the empty vector and the* Isg15-*shRNA. Adding bafilomycin A1 to the SFA treatment enhances this effect to a greater extent in the cells transduced with the empty vector.* **B.** *Palmitate inhibits p62 levels after 4 h of treatment in both 3T3-L1 pre-adipocytes transduced with the empty vector and the* Isg15-*shRNA.* For both *figures A* and *B*, 3T3-L1 pre-adipocytes transduced with either the pGIPZ empty vector or with the pGIPZ-*Isg15* shRNA construct were treated with unconjugated palmitate (500 µM) (lanes 3, 6, 9 and 12) and bafilomycin A1 (10 nM) (lanes 5, 6, 11 and 12) for 4 h in 10% FBS/DMEM (HG). Equivalent volumes of DMEM (LG) (400 µL) (lanes 2 and 8) and DMSO (8 µL) (lanes 4 and 10) were used as control for the unconjugated palmitate and bafilomycin A1 treatments, respectively. Cells were lysed with 100 µL 1% TX-100 lysis buffer per 6 cm Ø dish. 25 µg and 33 µg of protein were loaded per lane in *figures A* and *B*, respectively (15% SDS-acrylamide gel). Statistical difference between the palmitate treatment (empty vector cells) and other treatments is indicated with %; statistical difference between the bafilomycin A1 treatment (empty vector cells) and other treatments is indicated with $; statistical difference between the palmitate treatment (*Isg15*-KD cells) and other treatments is indicated with &; statistical difference between the palmitate + bafilomycin A1" treatment (*Isg15*-KD cells) and other treatments is indicated with £; ** denotes a treatment statistically different from all other treatments (p-value < 0.05). Data from three independent experiments.

V. 3. 3. 3. Effects of silencing Isg15 *on insulin sensitivity in 3T3-L1 mature adipocytes*

The set of experiments presented in the previous section in transduced 3T3-L1 pre-adipocytes was reproduced in mature cells. As observed in WT 3T3-L1, ISG15 is less expressed in differentiated cells in the transduced cell lines. Nevertheless, a substantial decrease in ISG15 expression following IFN-α treatment can be noticed when comparing mature 3T3-L1 transduced with the empty vector *versus* the *Isg15*-KD cells (*Figure 80*). Indeed, while the type I cytokine drives a statistically significant increase in unconjugated ISG15 in the former cell line (+261% compared to the water treated control), no significant effect was recorded in the later cell line. As illustrated by panel A of *figure 83*, a 175% difference in IFN-α-induced stimulation of ISG15 expression was noted between the two types of cells. A more subtle stimulation of total ISG15 levels was also monitored in cells bearing the empty vector with a statistically significant increase of 44% compared to the water treated control. Such stimulation was absent in the *Isg15*-KD (*Figure 81*). Together these results indicate that the target gene was successfully silenced in differentiated cells. Note, as for pre-adipocytes, palmitate treatment did not promote free or conjugated ISG15 expression.

Considering the effect of knocking down *Isg15* on insulin sensitivity, the overall trend in mature adipocytes follows that noted in pre-adipocytes despite the differences between the two cell lines being milder in mature adipocytes. When comparing the phosphorylation of Akt Thr^{308} in the mature adipocytes transduced with the empty vector and the *Isg15*-KD cells, none of the variations in p-Akt levels

under the various treatments including with palmitate are statistically significant (*Figure 82*).

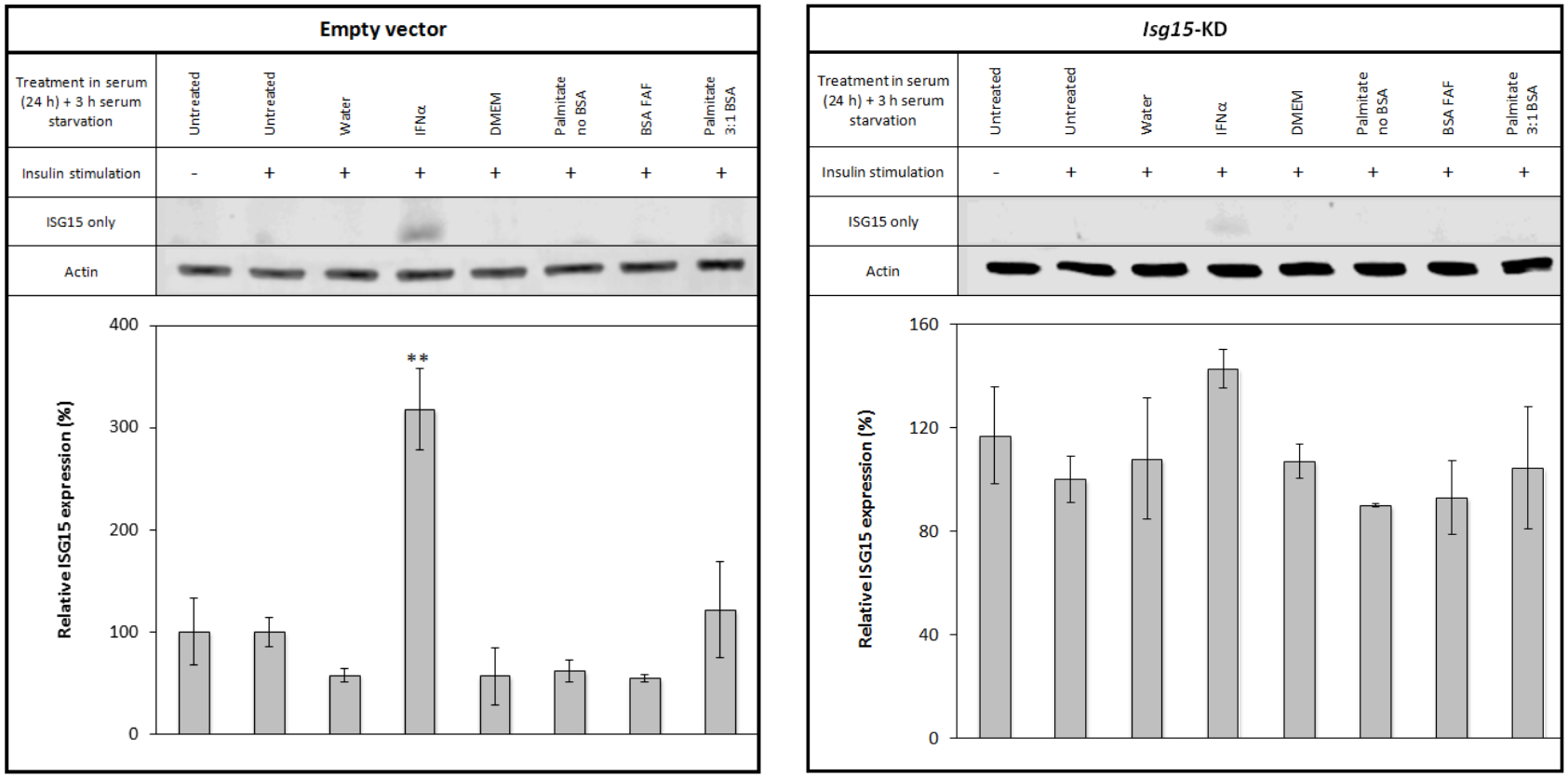

Figure 80. Empty vector. *IFN-α but not palmitate stimulates ISG15 expression in* ***3T3-L1 mature adipocytes*** *transduced with the empty vector.* ***Isg15*-KD.** *Both IFN-α and palmitate fail to stimulate ISG15 expression in* Isg15-*KD 3T3-L1 mature adipocytes.* 3T3-L1 mature adipocytes transduced with either the pGIPZ empty vector or with the pGIPZ-*Isg15* shRNA construct were treated with IFN-α (20 ng/mL) (lane 4), unconjugated palmitate (500 µM) (lane 6) and palmitate 3:1 BSA (500 µM) (lane 8) for 24 h in 10% FBS/DMEM (HG). Following a 3 h serum deprivation (SF DMEM, HG, 0.2% BSA), cells were stimulated with insulin (100 nM for 15 min) except for the first untreated control (lane 1). Equivalent volumes of MilliQ water (8 µL) (lane 3), DMEM (LG) (200 µL) (lane 5) and BSA FAF (200 µL) (lane 7) were used as control for the IFN-α, unconjugated and unconjugated palmitate treatments, respectively. Cells were lysed with 80 µL 1% TX-100 lysis buffer per well. 222 µg of protein were loaded per lane in *Empty vector* (left) and 185 µg in *Isg15*-KD (right) (12% Tris-Tricine-SDS gel). ** denotes a treatment statistically different from all other treatments (p-value < 0.05). Data from three independent experiments.

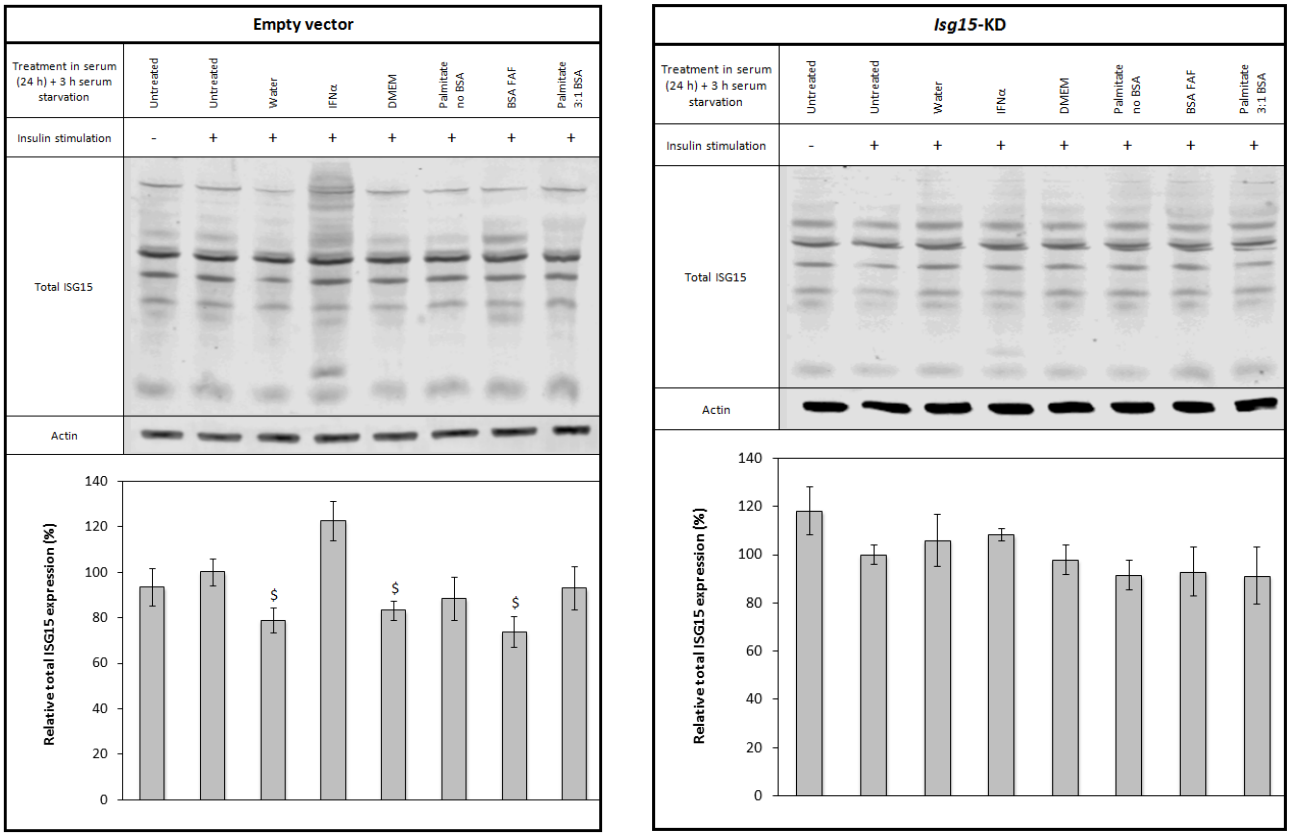

Figure 81. Empty vector. *IFN-α but not palmitate stimulates total ISG15 expression in* ***3T3-L1 mature adipocytes*** *transduced with the empty vector.* ***Isg15*-KD.** *Both IFN-α and palmitate fail to stimulate total ISG15 expression in* Isg15-*KD 3T3-L1 mature adipocytes.* 3T3-L1 mature adipocytes transduced with either the pGIPZ empty vector or with the pGIPZ-*Isg15* shRNA construct were treated with IFN-α (20 ng/mL) (lane 4), unconjugated palmitate (500 µM) (lane 6) and palmitate 3:1 BSA (500 µM) (lane 8) for 24 h in 10% FBS/DMEM (HG). Following a 3 h serum deprivation (SF DMEM, HG, 0.2% BSA), cells were stimulated with insulin (100 nM for 15 min) except for the first untreated control (lane 1). Equivalent volumes of MilliQ water (8 µL) (lane 3), DMEM (LG) (200 µL) (lane 5) and BSA FAF (200 µL) (lane 7) were used as control for the IFN-α, unconjugated and unconjugated palmitate treatments, respectively. Cells were lysed with 80 µL 1% TX-100 lysis buffer per well. 222 µg of protein were loaded per lane in *Empty vector* (left) and 185 µg in *Isg15*-KD (right) (12% Tris-Tricine-SDS gel). Statistical difference between the IFN-α treatment and other treatments is indicated with $ (p-value < 0.05). Data from three independent experiments.

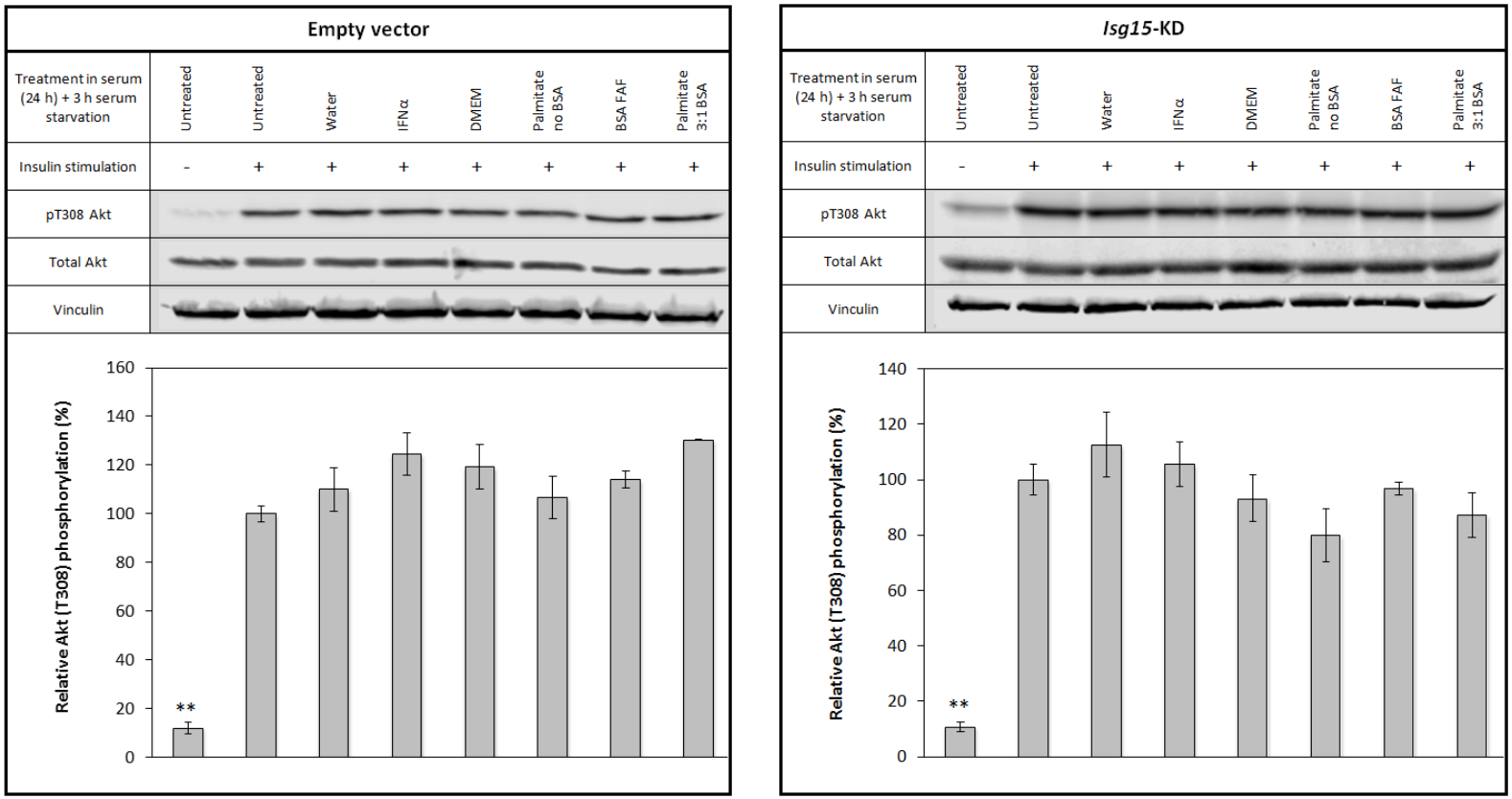

Figure 82. Empty vector. *Both IFN-α and palmitate fail to induce insulin resistance in* ***3T3-L1 mature adipocytes*** *transduced with the empty vector.* ***Isg15*-KD.** *Both IFN-α and palmitate fail induce insulin resistance in* Isg15-*KD 3T3-L1 mature adipocytes.* 3T3-L1 mature adipocytes transduced with either the pGIPZ empty vector or with the pGIPZ-*Isg15* shRNA construct were treated with IFN-α (20 ng/mL) (lane 4), unconjugated palmitate (500 µM) (lane 6) and palmitate 3:1 BSA (500 µM) (lane 8) for 24 h in 10% FBS/DMEM (HG). Following a 3 h serum deprivation (SF DMEM, HG, 0.2% BSA), cells were stimulated with insulin (100 nM for 15 min) except for the first untreated control (lane 1). Equivalent volumes of MilliQ water (8 µL) (lane 3), DMEM (LG) (200 µL) (lane 5) and BSA FAF (200 µL) (lane 7) were used as control for the IFN-α, unconjugated and unconjugated palmitate treatments, respectively. Cells were lysed with 80 µL 1% TX-100 lysis buffer per well. 224 µg of protein were loaded per lane in *Empty vector* (left) and 111 µg in *Isg15*-KD (right) (10% SDS-acrylamide gel). ** denotes a treatment statistically different from all other treatments (p-value < 0.05). Data from three independent experiments.

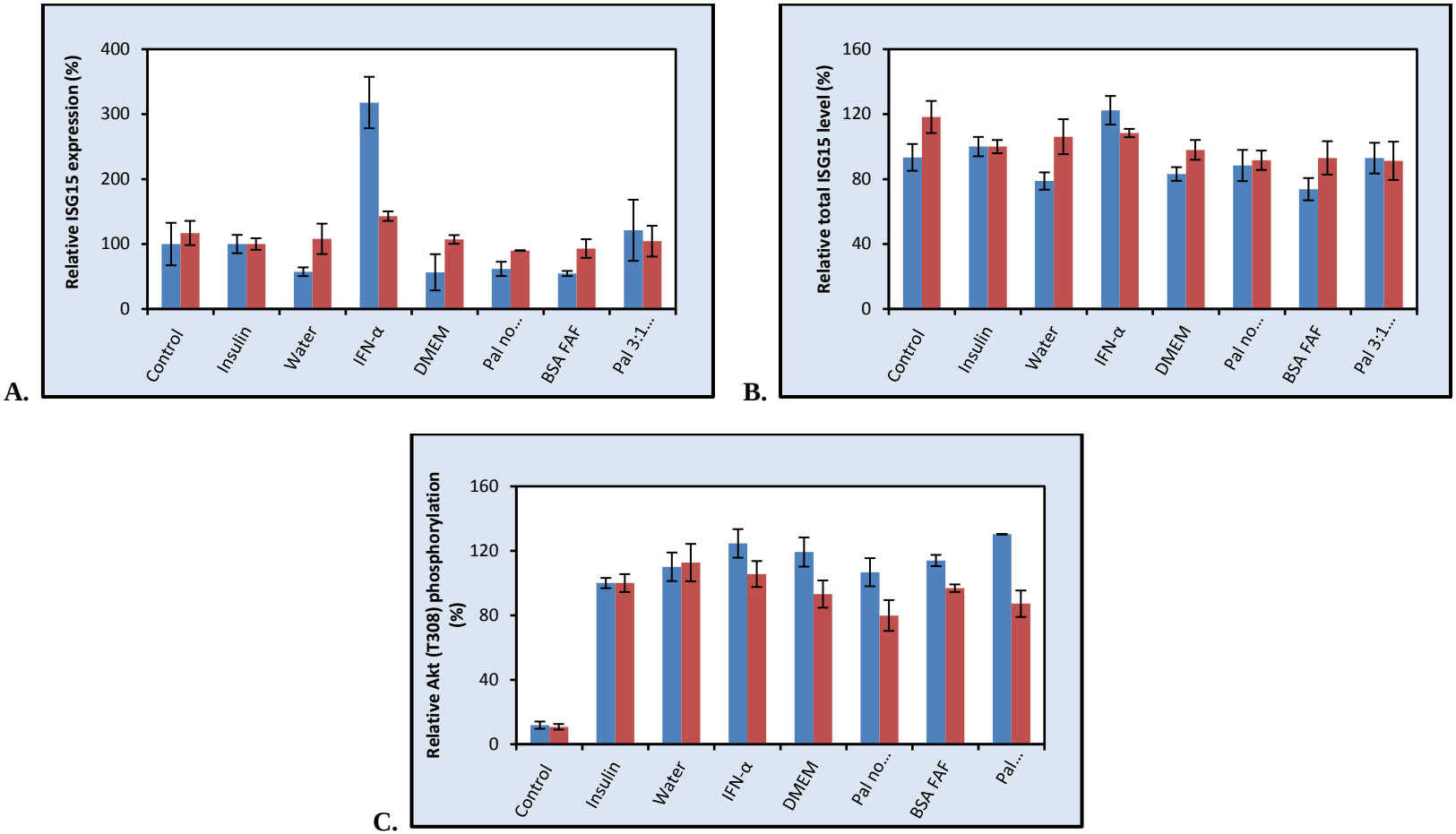

Figure 83. *Comparison of the effect of IFN-α, unconjugated and BSA-conjugated palmitate on* **A.** *ISG15 expression (top left),* **B.** *total ISG15 expression (top right) and* **C.** *Akt Thr^{308} phosphorylation (bottom) in* ***3T3-L1 mature adipocytes*** *transduced with the pGIPZ empty vector (blue) or with the pGIPZ-*Isg15 *shRNA construct (red).* Cells were treated with IFN-α (20 ng/mL), unconjugated palmitate and palmitate 3:1 BSA (500 µM) for 24 h in 10% FBS/DMEM (HG). Following a 3 h serum deprivation (SF DMEM, HG, 0.2% BSA), cells were stimulated with insulin (100 nM for 15 min) except for the first untreated control. Equivalent volumes of MilliQ water (8 µL), DMEM (LG) (200 µL) and BSA FAF (200 µL) were used as control for the IFN-α, unconjugated and unconjugated palmitate treatments, respectively.

Further experiments were performed to investigate the effect of A66 on the phosphorylation of Akt in the presence or absence of palmitate (*Figure 84*). The effect of the SFA recorded coincides with the results presented in *figure 82*, with a trend suggesting that the control cell line is more resistant to the effect of palmitate than the *Isg15*-KD cells are more susceptible to palmitate-induced insulin resistance compared to empty vector. Interestingly, the *Isg15*-KD cells are considerably less sensitive to the stimulatory effect of A66, which echoes the observations made in pre-adipocytes. The difference in response is clearly observable in *figure 85*. This suggests that the effect of A66 is mediated through ISG15 expression and points at an interaction between PI3K and ISG15. Overall our data indicates that ISG15 is a promoter of insulin signalling.

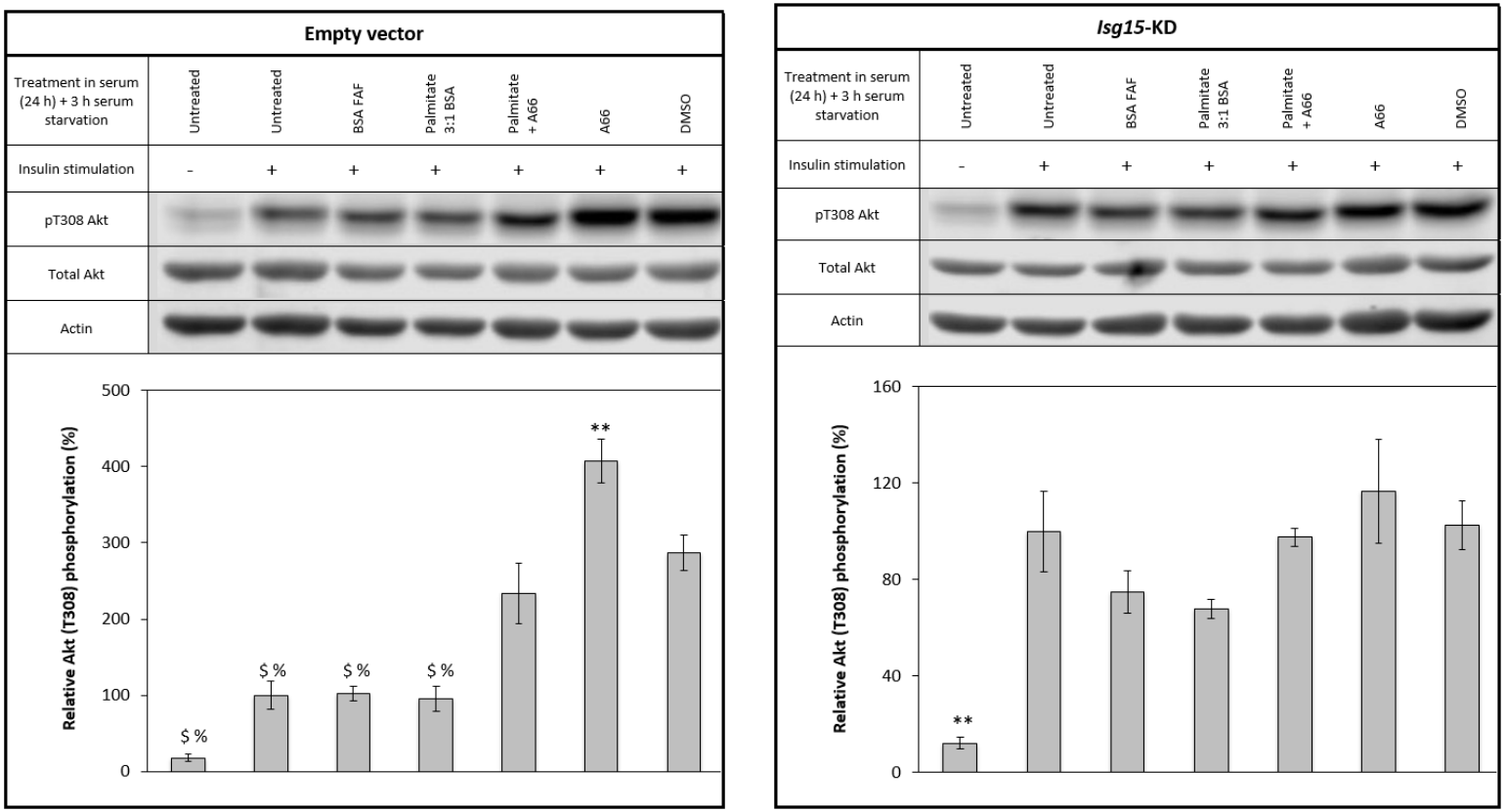

Figure 84. *A66 stimulates insulin-induced phosphorylation of Akt in **3T3-L1 mature adipocytes** transduced with the empty vector but not in* Isg15*-KD 3T3-L1 mature adipocytes.* 3T3-L1 mature adipocytes transduced with either the pGIPZ empty vector or with the pGIPZ-*Isg15* shRNA construct were treated with palmitate 3:1 BSA (500 μM) (lanes 4 and 5) and A66 (1 μM) (lanes 5 and 6) for 24 h in 10% FBS/DMEM (HG). Following a 3 h serum deprivation (SF DMEM, HG, 0.2% BSA), cells were stimulated with insulin (100 nM for 15 min) except for the first untreated control (lane 1). Equivalent volumes of BSA FAF (200 μL) (lane 3) and DMSO (20 μL) (lane 7) were used as control for the unconjugated palmitate treatment and A66 treatment, respectively. In both figures, cells were lysed with 80 μL 1% TX-100 lysis buffer per well. 25 μg of protein were loaded per lane (10% SDS-acrylamide gel). Statistical difference between the untreated control and other treatments is indicated with &; statistical difference between the "palmitate + A66" treatment and other treatments is indicated with $; statistical difference between the DMSO control and other treatments is indicated with %; ** denotes a treatment statistically different from all other treatments (p-value < 0.05). Data from three independent experiments.

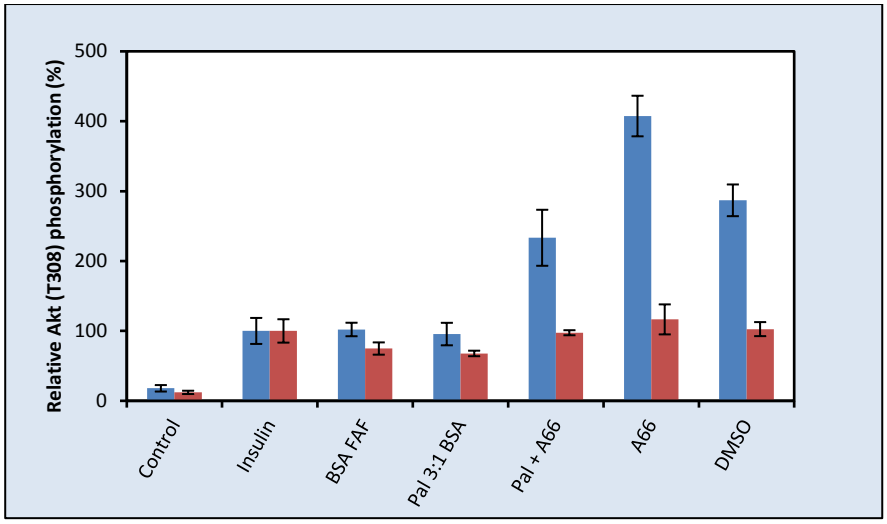

Figure 85. *A66 enhances the insulin-stimulated phosphorylation of Akt in* ***3T3-L1 mature adipocytes*** *transduced with the pGIPZ empty vector (blue) but not in* Isg15*-KD 3T3-L1 mature adipocytes (red).* Cells were treated with palmitate 3:1 BSA (500 µM) and A66 (1 µM) for 24 h in 10% FBS/DMEM (HG). Following a 3 h serum deprivation (SF DMEM, HG, 0.2% BSA), cells were stimulated with insulin (100 nM for 15 min) except for the first untreated control. Equivalent volumes of BSA FAF (200 µL) and DMSO (20 µL) were used as control for the unconjugated palmitate treatment and A66 treatment, respectively.

V. 3. 3. 4. Effects of silencing Isg15 *on lipid-induced stimulation of STAT3 Tyr^{705} in 3T3-L1 mature adipocytes*

Having investigated the effect of silencing *Isg15* on the insulin sensitivity of mature 3T3-L1 adipocytes, the effect of this knockdown on the phosphorylation of STAT3 Tyr^{705} was explored. As discussed in Chapter 3, palmitate was demonstrated to induce the phosphorylation of this residue in differentiated 3T3-L1 cells following 8 h of treatment. LPS was also found to elicit the activation of this transcription factor. *Figure 86* presents the response of the two transduced cell lines to palmitate and LPS treatments. In the control cells (lanes 1 to 5), both lipids stimulated the phosphorylation of STAT3, unlike in the *Isg15*-KD cells.

On the one hand, palmitate drove a 98% and 59% increase in p-STAT3 Tyr^{705} levels compared to untreated and DMEM-treated controls, respectively. On

the other hand, LPS prompted a 426% and 384% increase in the phosphorylation levels of STAT3 compared to untreated and PBS-treated controls, respectively. Unlike LPS, the effect of palmitate fell short of reaching statistical significance (one-way ANOVA $F(9,28) = 26.24$, p-value = 0.00; Tukey HSD *post hoc* test between "untreated control" and "palmitate treatment": p-value = 0.17; Tukey HSD *post hoc* test between "DMEM-treated control" and "palmitate treatment": p-value = 0.78). However, a paired 2-tailed student t-test associated difference in p-STAT3 levels measured in the untreated control and the palmitate-treated cells with a p-value of 0.00. Focussing on the response of the *Isg15*-KD cells, none of the treatments had an effect on the phosphorylation of STAT3 Tyr residue.

Comparing the effect of LPS in the two cell lines, silencing *Isg15* induced a drastic decrease in LPS-mediated stimulation of STAT3. The 398% difference between the two cell lines reaches statistical significance using a one-way ANOVA (Tukey HSD *post hoc* test between "LPS treatment" in control cells and "LPS treatment" in *Isg15*-KD cells: p-value = 0.00). The more modest 110% difference in the response of the two cell lines to palmitate treatment fell short of statistical significance when analysing the data using a one-way AONVA (Tukey HSD *post hoc* test between "palmitate treatment" in control cells and "palmitate treatment" in *Isg15*-KD cells: p-value = 0.16). Subjecting the data to an unpaired 2-tailed student t-test, the difference between the effect of the SFA in the two cell lines reaches a statistically significant p-value of 0.01.

Therefore, it seems that overall both palmitate and LPS stimulate the phosphorylation of STAT3 Tyr^{705} in the control cell line, but not in the Isg15-KD adipocytes, suggesting that the effect of the lipids is mediated by ISG15.

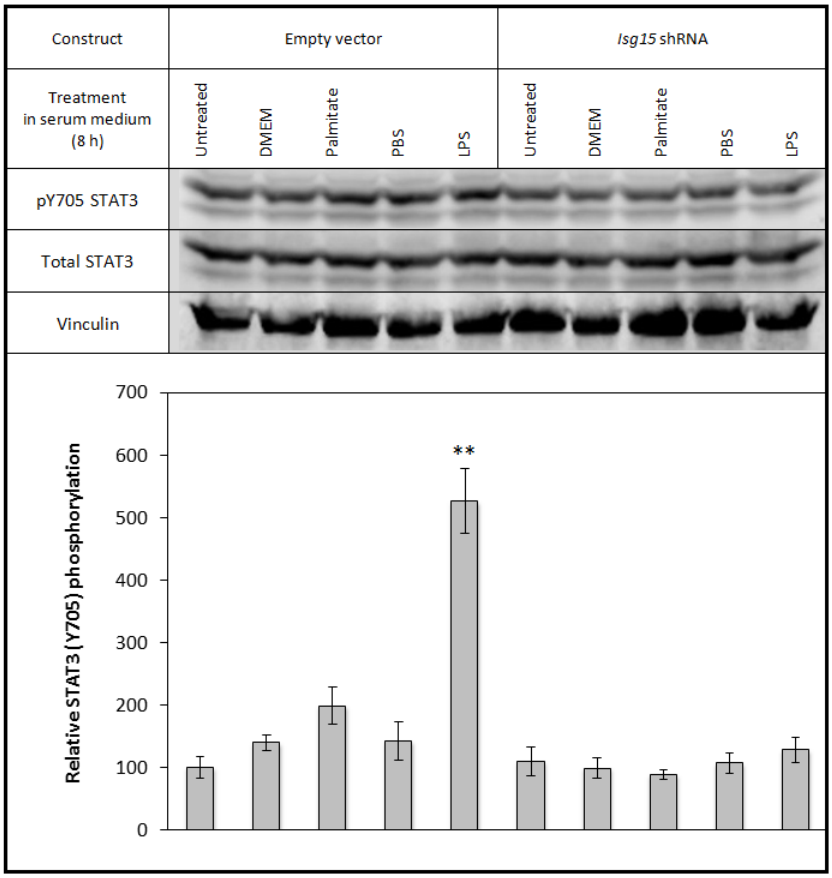

Figure 86. *LPS and to a lesser extent unconjugated palmitate stimulate the phosphorylation of STAT3 Tyr^{705} in* ***3T3-L1 mature adipocytes*** *transduced with the empty vector but not in* Isg15-*KD 3T3-L1 cells.* 3T3-L1 mature adipocytes transduced with either the pGIPZ empty vector or with the pGIPZ-*Isg15* shRNA construct were treated with unconjugated palmitate (500 µM) (lanes 3, 6, 9 and 12) and LPS (100 ng/mL) (lanes 5 and 10) for 8 h in 10% FBS/DMEM (HG). Equivalent volumes of DMEM (LG) (200 µL) (lanes 2 and 7) and PBS (20 µL) (lanes 4 and 9) were used as control for the unconjugated palmitate and LPS treatments, respectively. Cells were lysed with 80 µL 1% TX-100 lysis buffer per well. 171 µg of protein were loaded per lane (10% SDS-acrylamide gel). ** denotes a treatment statistically different from all other treatments (p-value < 0.05). Data from three independent experiments.

V. 3. 4. Insights from mass spectrometric analysis on the role of protein ISGylation

The last step of the present investigation was to perform a mass spectrometric analysis on anti-ISG15 immunoprecipitates derived from mature 3T3-L1 adipocytes treated with palmitate or IFN-α. This would allow the isolation of proteins conjugated to ISG15, a.k.a. ISGylated proteins. The aim of such experiment was to discover which ISGylated proteins would be induced or inhibited by the two treatments and whether some overlaps existed. *Figure 87* shows the western blot of IP samples derived from 3T3-L1 mature adipocytes treated with IFN-α or palmitate and incubated with or without an ISG15 specific antibody. The pattern observed validates that ISG15 and ISGylated proteins were successfully pulled-down with the applied IP protocol. A clear band at 17 kDa corresponding to ISG15 can be noticed in the lanes where IFN-α-treated cells were run. THP-1 cells treated with LPS were used as positive control.

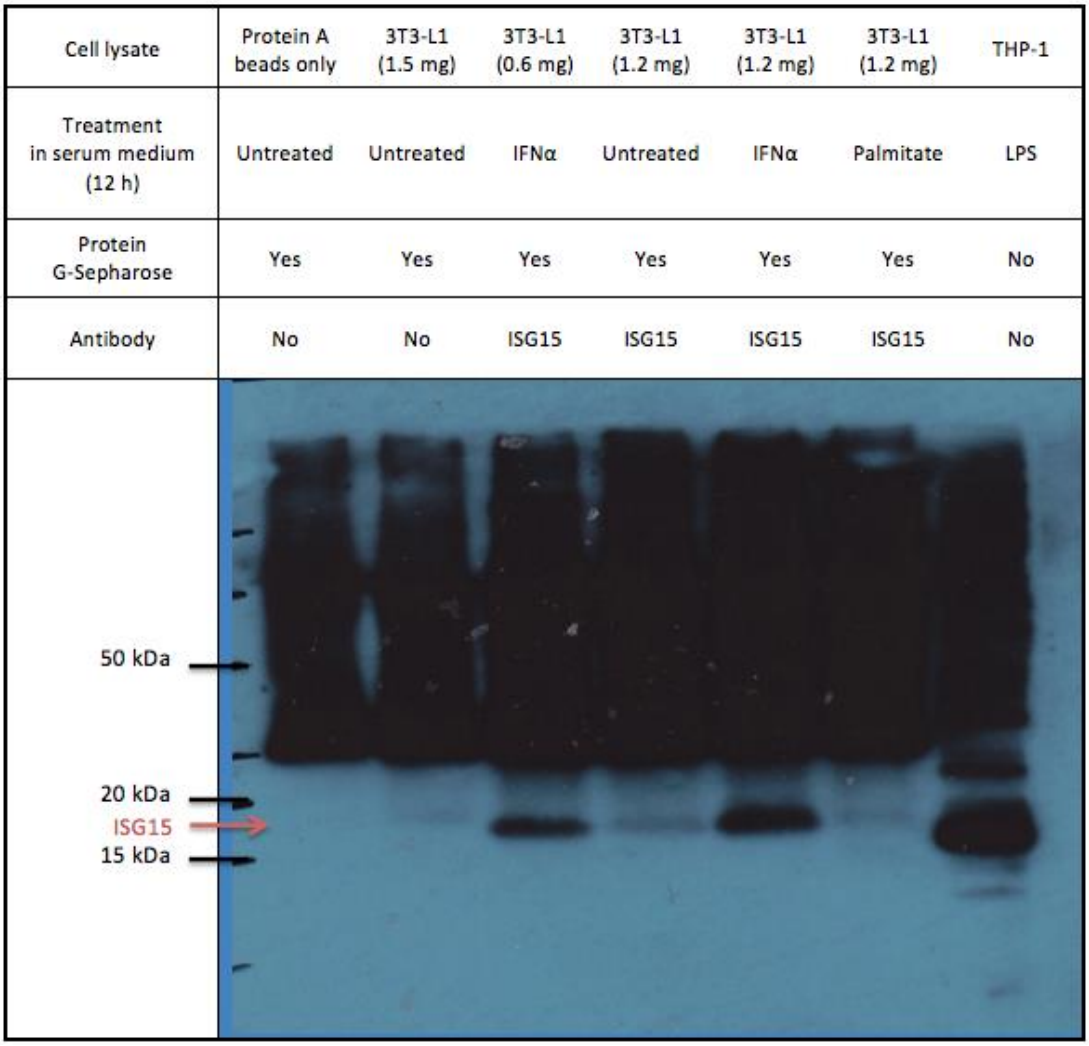

Figure 87. *ISG15 IP test following denaturation in 3T3-L1 mature adipocytes*. 3T3-L1 mature adipocytes were treated with IFN-α (20 ng/mL) (lanes 3 and 5) and palmitate 3:1 BSA (500 μM) (lane 6) for 12 h in 10% FBS/DMEM (HG). THP-1 cells were treated with LPS (100 ng/mL) (lane 7) for the same duration and in the same conditions. As additional controls, a sample containing only protein A beads in lysate buffer (lane 1) and a sample of untreated cells incubated with no antibody were ran (lane 2). Cells were lysed with 100 μL 2% SDS, 150 mM NaCl, Tris-HCl, pH 8.0 lysis buffer. After boiling the samples for 5 min, these were diluted 1:10 with 1% TX-100 lysis buffer. The samples were run on a 12% Tris-Tricine-SDS gel for 1 h. Detection: enhanced chemiluminescence (X-ray film).

As recorded in *table 14*, in total, the MS2 intensity (which can be used as a measure of the relative detection of a protein) of 264 proteins was down-regulated by IFN-α. That of 76 was stimulated by the same treatment. Levels of 322 and 108 proteins were inhibited and induced by the palmitate treatment, respectively. Levels of 42 proteins were up-regulated following the palmitate and IFN-α treatments

compared to the unstimulated control incubated in the ISG15 antibody. Levels of 174 proteins were down-regulated by both treatments; levels of 21 proteins were induced by IFN-α but inhibited by the SFA and, inversely, levels of 38 other proteins were induced by palmitate but inhibited by IFN-α. These hits were submitted to the DAVID database to derive biological themes (particularly gene ontology terms) and functionally-related gene groups of the lists of differentially expressed genes. The clusters identified are summarised in *table 14*.

Overall, there is a striking similarity between the gene clusters found to be down-regulated by palmiate and IFN-α, with the prevalence of genes involved in mitochondrial functions, ribosomal proteins, chaperonins, tubulin and heat shock proteins (HSP). For instance, the gene cluster down-regulated by palmitate with the third highest enrichment score (21.5) was also the one down-regulated by IFN-α with the highest enrichment score (22.2). This cluster included ribosomal proteins such as ribosomal proteins L13, S2 and S3A1. Another cluster down-regulated by both treatments included genes involved in mitochondrial functions such as cytochrome c oxidase subunit II and ubiquinol-cytochrome c reductase, Rieske iron-sulfur polypeptide 1, both implicated in the mitochondrial electron transport chain. Genes encoding the ATP synthase, proton transporting, mitochondrial F1 complex were also found in this cluster. Interestingly, one gene cluster down-regulated by both palmitate and IFN-α includes genes encoding the chaperonin containing T-complex protein 1 (CCT), which is key in the biogenesis of tubulin, a globular protein also encoded by genes found in a cluster inhibited by the two treatments (Yaffe 1992).

Lastly, the expression of glycerol-3-phosphate dehydrogenase 1 (GPD1), which ensures the reduction of dihydroxyacetone phosphate into glycerol-3-phosphate (G3P) was also down-regulated by both treatments. This reaction is critical for lipid biosynthesis as it enables glycerol production and in turn triglyceride synthesis (Yeh 2008). The expression of two other dehydrogenases are also inhibited by the palmitate and IFN-α treatments: malate dehydrogenase 1 (MDH1) and lactate dehydrogenase A (LDHA). The former, located in the cytoplasm similarly to GPD1, reversibly catalyses the oxidation of L-malate to oxaloacetate as part of the citric acid cycle (Minarik 2002). The latter guaranties the inter-conversion of L-lactate to pyruvic acid within the cytosol (Valvona 2016). The lactate and the G3P produced by LDHA and GPD1, respectively, feed into the citric acid cycle modulated by MDH1, thus connecting the three enzymes together.

Surprisingly, the list of genes induced by the IFN-α could not be classified into any gene cluster by the DAVID software (*Table 14*). Therefore no overlap could be identified in the biological functions of genes up-regulated by palmitate and IFN-α or between those of genes induced by IFN-α and inhibited by palmitate. As the mass spectrometric analysis identified *Isg15* as belonging to the latter category, further analyses were performed using an alternative software (STRING).

Table 14. *Overview of the gene clusters identified by the database for annotation, visualisation and integrated discovery (DAVID) software to be either up- or down-regulated by IFN-α and palmitate.* Mature 3T3-L1 cells were treated for 12 h with either palmitate (500 µM) or IFN-α (20 ng/mL) in 10% FBS/DMEM (HG). Cells were then lysed and the lysate was incubated with an ISG15-specific antibody. The samples were analysed using mass spectrometry. Information on the number of edges of the predicted network and the average node degree were derived from the Search Tool for the Retrieval of Interacting Genes/Protein (STRING) analysis performed on each gene list. Gene clusters are organised from highest to lowest enrichment score. The full DAVID analysis can be found in the *appendix V.II. 11. HSP*: heat shock protein; *NADH*: nicotinamide adenine dinucleotide.

	Up-regulated by IFN-α	***Down-regulated by IFN-α***	***Up-regulated by palmitate***	***Down-regulated by palmitate***	***Up-regulated by IFN-α and palmitate***	***Down-regulated by IFN-α and palmitate***	***Up-regulated by IFN-α and down-regulated palmitate***	***Down-regulated by IFN-α and up-regulated palmitate***
Number of genes	76	264	108	322	42	174	21	38
Number of edges*	254	2121	394	2681	89	1066	23	25
Average node degree*	6.8	16.2	7.4	16.9	4.3	12.4	2.2	1.3
Number of gene clusters in DAVID	0	14	4	14	0	9	0	1
General function of the gene clusters in DAVID	-	Ribosomal proteins; ATP synthase, H^+ transporting mitochondrial complex; Mitochondrial proteins; Tubulins; Chaperonins; Ribonucleoproteins; Histones; Malate/lactate dehydrogenases; Keratins; Coenzyme A enzymes; HSP	Ribonucleoproteins; Ribosomal protein; Histones; NADH dehydrogenases/cytochrome c oxidase and reducase	Keratins; Mitochondrial proteins; Ribosomal proteins; ATP synthase, H^+ transporting mitochondrial complex; tRNA synthetases; Malate/lactate dehydrogenases; Chaperonins; Tubulins; Ribonucleoproteins; Histones; HSP; Coenzyme A enzymes; Protein disulfide isomerases	-	Ribosomal proteins; Mitochondrial proteins; Chaperonins; ATP synthase, H^+ transporting mitochondrial complex; Pyruvate dehydrogenase; Tubulin; HSP; Malate/lactate dehydrogenases	-	Ribonucleoproteins

The STRING database was employed to derive known and predicted protein interactions, both physical and functional. This database compiles experimental data, computational prediction methods as well as public text collections. *Figures 87* and *88* represent the networks of predicted associations between proteins encoded by genes down-regulated and up-regulated by palmitate treatment of mature 3T3-L1 adipocytes, respectively. As these proteins were isolated by IP using an ISG15-specific antibody, one can assume that such proteins were either ISGylated or interact with ISGylated proteins. Only the hits with the largest and lowest fold increase are represented in order to avoid over-crowding the figures. The number of edges and the average node degree recorded in *table 14* provide an insight on how tightly knit these networks are when all hits are included. Overall, the palmitate-induced genes are fewer and showed lesser association than the palmitate-inhibited genes with 108 *versus* 322 nodes, 394 *versus* 2681 edges and 7.4 *versus* 16.9 average node degree (*table 14*).

As shown in *figure 88,* similar gene clusters can be identified with STRING and DAVID software, in the case of the genes down-regulated by palmitate. Circled in green are the coenzyme A dehydrogenases also recorded in *table 14;* circled in purple are proteins implicated in keratin production; circled in blue are ribosomal proteins; circled in orange are dehydrogenases critical for the critic acid cycle and in yellow are proteins important for molecular chaperones. The remaining clusters identified by the DAVID analysis are likely to be represented in the STRING network generated using the total hits obtained from mass spectrometric analysis, however such network was too dense for visualisation. ISG15, circled in red, is directly connected to HSP90αB1. Through its ATPase activity and its interaction

with various co-chaperones, this molecular chaperone ensures the maturation and the maintenance of the structural integrity of a range of protein targets involved in cell cycle control and signal transduction. It is able to modulate transcription via different strategies, including the regulation of epigenetic modifiers such are histone deacetylases and DNA methyl transferase, or else the removal of histones from the promoter of certain genes to permit their expression (Khurana 2015). Interestingly, Cheng *et al.* reported that the phosphorylation of STAT1 is indispensable for the activation of Hsp90β gene during heat shock response (Cheng 2010).

The STRING analysis also predicts the interaction of ISG15 with peptidylprolyl isomerase A (PPIA), also known as cyclophilin-A (*Figure 88*). Also implicated in protein folding, this enzyme accelerates the process by catalysing the cis-trans isomerisation of proline imidic peptide bonds in oligopeptides. It functions as a growth factor secreted upon oxidative stress to mitigate tissue damage. In endothelial cells, PPIA was shown to stimulate both the Akt and NF-κB pathways (Wei 2013). The following year, Ramachandran *et al*. evidenced increased concentration of PPIA in the plasma of T2D and coronary artery disease patients compared to healthy individuals (Ramachandran 2014). The network generated by the STRING software also indicates an association between ISG15 and the 40S subunit ribosomal proteins S2, S3, S4x and S19. Of these four ribosomal proteins, ribosomal protein S3 has the specificity of being involved in DNA repair.

Lastly, ISG15 appears to interact with phospholipase A2 (PLAA), an enzyme found in abundance in snake venom but also occurs in all organisms studied. It is specialised in the hydrolysis of the sn-2 position of glycerophospholipids thus

producing arachidonic acid as well as lysophospholipids (Harris 2013). This reaction has been implicated in various biological processes including inflammation as well as protein ubiquitination. Indeed, Hall *et al.* demonstrated that PLAA is necessary for ubiquitin-mediated sorting of membrane proteins targeted for lysosomal degradation in MEFs (Hall 2017). A recent study by Papadopoulos *et al*. also implicated PLAA in autophagy, more specifically, the clearance of ruptured ubiquitinated lysosomes (Papadopoulos 2016).

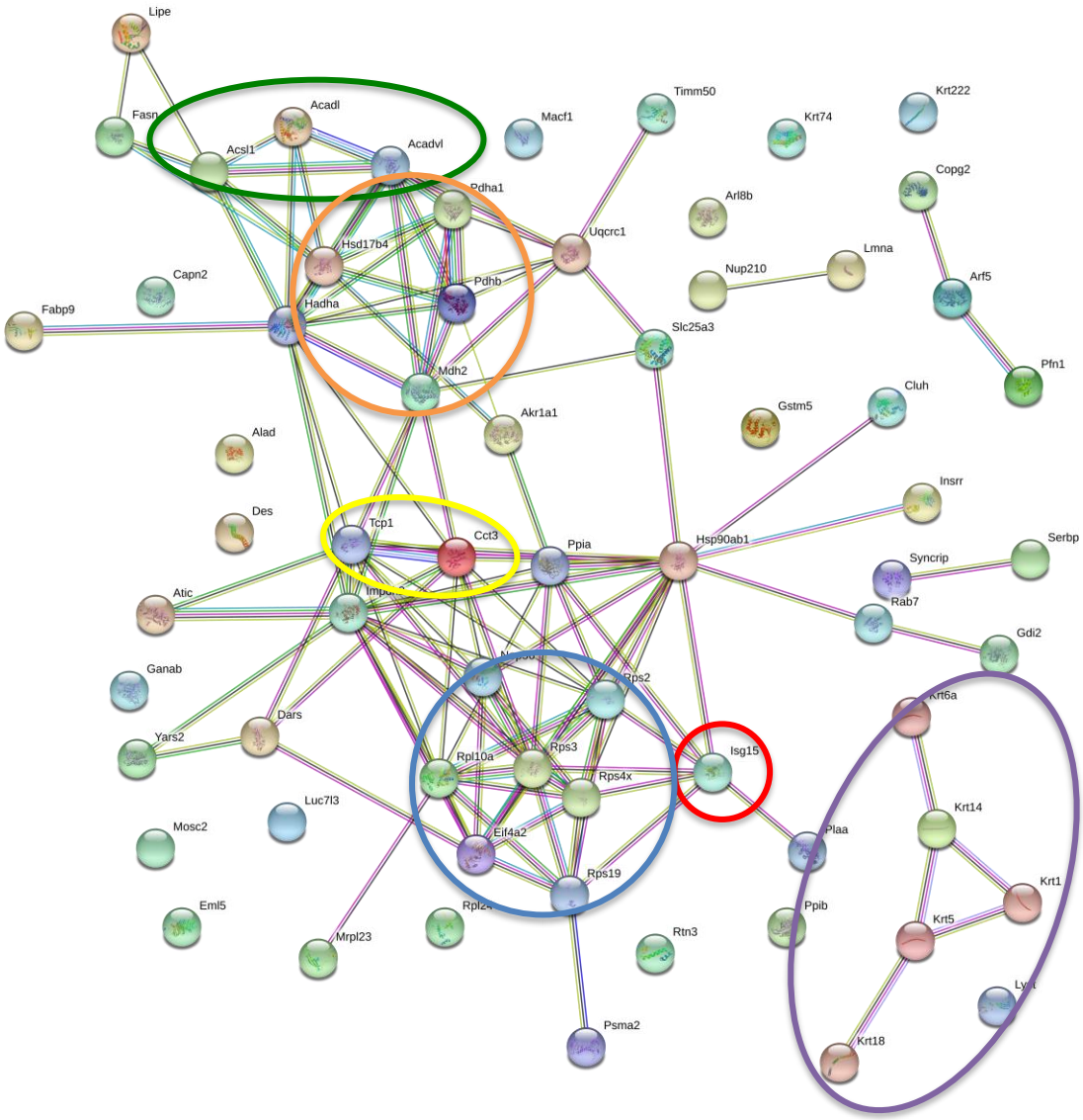

Figure 88. *Network view of predicted associations between proteins encoded by genes that were down-regulated following palmitate treatment (500 μM, 12 h) of mature 3T3-L1 in 10% FBS/DMEM (HG).* Each coloured line represents a specific type of evidence supporting the predicted functional association. A light blue line indicates a know interaction from curated databases; a pink line indicates a known interaction experimentally determined; a dark green line indicates a predicted interaction based on gene neighbourhood; a dark blue line indicates a predicted interaction based on the cooccurence of two genes across the genome; a light green line indicates that putative homologs are coexpressed in other species; a black line indicated that putative homologs are co-mentioned in PubMed abstracts; a purple line indicates protein homology (bit score > 60). Note that to avoid over-crowding the figure, this analysis only includes 66 of the 322 genes that were down-regulated by palmitate treatment. For this subset, the maximum fold increase compared to the untreated control was set to 0.1. ISG15, circled in red, was also included despite a fold increase of 0.2. Circled in green are the coenzyme A dehydrogenases; circled in purple are proteins implicated in keratin production; circled in blue are the ribosomal proteins; circled in orange the dehydrogenases critical for the critic acid cycle and in yellow are proteins important for molecular chaperones.

Figure 89 represents the network of predicted associations linking the proteins encoded by genes that were the most highly induced by palmitate (the full network is not represented because the high number of nodes made it illegible). The STRING software was able to identify gene clusters similar to those proposed by the DAVID software. The most noticeable one, circled in black, corresponds to ribonucloproteins, the cluster associated with the highest enrichment score in the DAVID analysis (*Table 14*). Circled in blue is the cluster of ribosomal proteins also recorded in *table 14*; circled in pink are the histone proteins; lastly, in grey is a cluster formed of two nicotinamide adenine dinucleotide dehydrogenases and a cytochrome c oxidase, the fourth cluster identified by the DAVID software to be induced by palmitate. Similarly to *figure 88*, only a portion of the mass spectrometric data was used to produce *figure 89* to avoid over crowding it. Nevertheless, all clusters recorded in *table 14* could be identified in the STRING network.

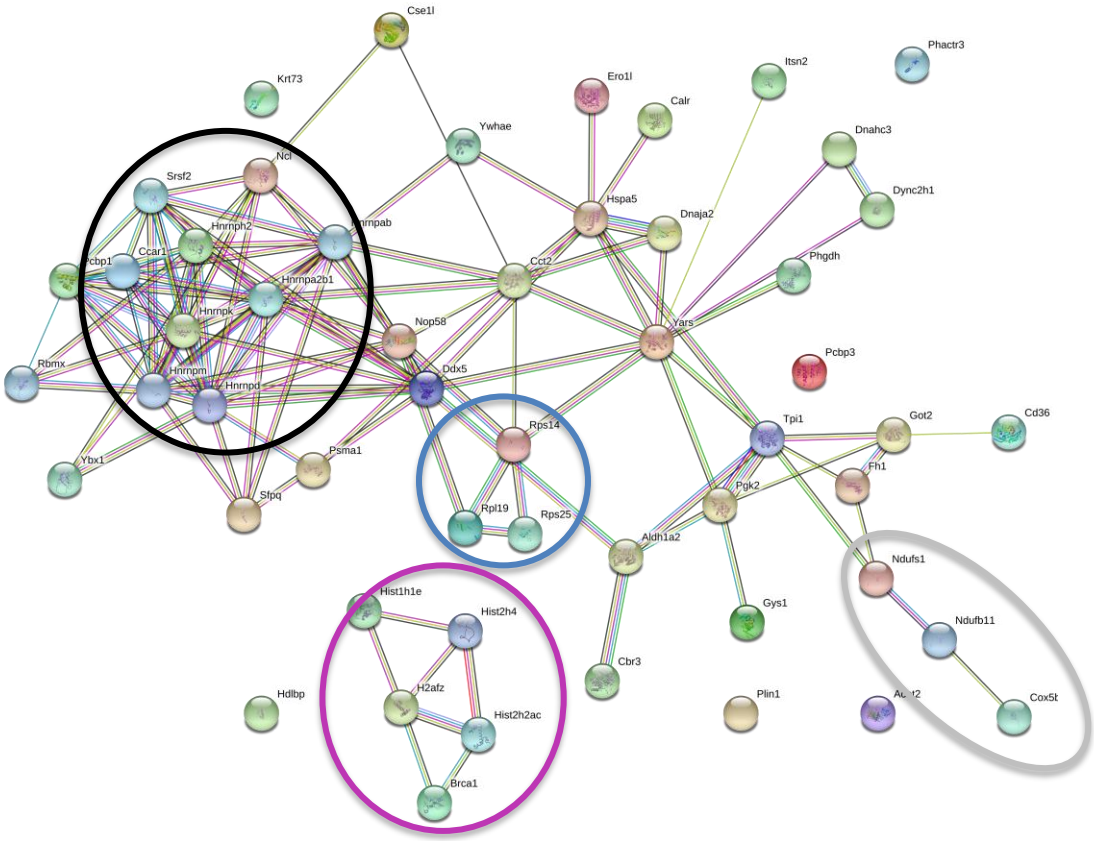

Figure 89. *Network view of predicted associations between proteins encoded by genes that were up-regulated following palmitate treatment (500 µM, 12 h) of mature 3T3-L1 in 10% FBS/DMEM (HG).* See *figure 88* for the code of the coloured lines. Note that to avoid over-crowding the figure, this analysis only includes 53 of the 108 genes that were up-regulated by palmitate treatment. For this subset, the minimum fold increase compared to the untreated control was set to 2. Circled in blue are the ribosomal proteins; circled in pink are the histone proteins; circled in black is a cluster of ribonucleoproteins; circled in grey is a cluster of NADH dehydrogenases.

Figure 90 presents the network of predicted associations between proteins encoded by genes that were simultaneously up-regulated by the IFN-α treatment and down-regulated by the palmitate treatment. This subgroup of protein is of particular interest as it includes ISG15, circled in red. Compared to the previous figures, this network is sparser with a total of only 21 nodes, 23 edges and an average node degree of 2.2 (*table 14*), which explains why no gene cluster was identified by the DAVID software. However, visualising the network produced by the STRING software, a cluster is clearly apparent and groups ISG15 with four other proteins

implicated in the ubiquitin proteasome system: ubiquitin C (UBC), ubiquitin-like modifier activating enzyme 1 (UBA1), proteasome 26S subunit protein (PSMC6) and USP14.

UBC is at the core of this system as it covalently binds target proteins and can link to other ubiquitin molecules to form polyubiquitin chains (Ryu 2007). UBA1, on the other hand, is implicated in catalysing ubiquitin conjugation of the proteins targeted for degradation (Groen 2015). PSMC6, component of the 26S proteasome, is critical in the ATP-dependent degradation of ubiquitinated protein (Rock 1994). The last player of the ubiquitin proteasome system found to directly interact with ISG15 was USP14, a proteasome-associated deubiquitinase involved in the release of ubiquitin from ubiquitinated proteins (B. L. Lee 2016). Collectively, these proteins are key in maintaining protein homeostasis as well as cellular levels of monomeric ubiquitin.

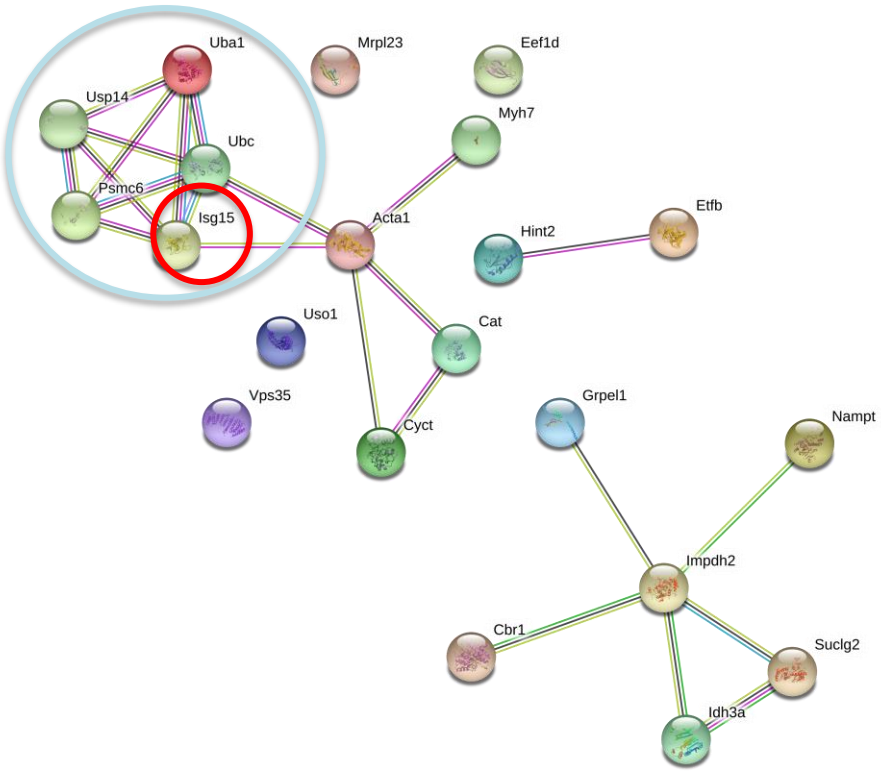

Figure 90. *Network view of predicted associations between proteins encodes by genes that were both up-regulated following IFN-α treatment (20 ng/mL, 12 h) of mature 3T3-L1 adipocytes and down-regulated following palmitate treatment (500 μM, 12 h) of the same cell type in 10% FBS/DMEM (HG).* See *figure 88* for the code of the coloured lines. Circled in blue is a cluster of proteins involved in the ubiquitin proteasome system; ISG15 is circled in red.

V. 4. Discussion of Chapter 5

V. 4. 1. ISG15 promotes insulin sensitivity

In this chapter, the importance of ISG15 in the pathways investigated so far was explored. Palmitate was found to have no effect on the expression of this protein (*Figures 65* to *68*). However, such finding does not rule out a SFA-mediated effect on ISGylation or the cytokine activity of ISG15. To gather a more thorough understanding of how this ISG may modulate the metabolic effects of palmitate, an *Isg15*-KD cell line was generated, using an RNAi technique to silence the gene of interest. Such technique relied on the intracellular delivery of shRNA via viral vector, which has the benefit of producing a sustained knockdown and thus differentiable KD cell line. We were able to reduce the expression of ISG15 induced by IFN-α by 83% and 55% in pre- and mature adipocytes, respectively (*Figures 75A* and *83A*). Interestingly, levels of ISG15 conjugated protein were only mildly affected by the knockdown (*Figures 75B* and *83B*).

Investigating whether silencing *Isg15* would affect the insulin sensitivity of the cells following palmitate treatment, the phosphorylation of Akt in *Isg15*-KD cells was compared to that of the control cell line (*Figures 75C* and *83C*). Overall, it seems that the adipocytes transfected with the empty vector failed to show signs of SFA-induced insulin resistance unlike the *Isg15*-KD cell line. The differences in the responses of the two cell lines were enhanced in pre-adipocytes *versus* mature adipocytes. This data thus indicates that silencing *Isg15* elicits a deleterious effect on cellular insulin sensitivity. Interestingly, similarly to the cellular response of WT 3T3-L1, exposing the adipocytes transfected with the empty vector to the p110α inhibitor rescues the inhibitory effect of the SFA on insulin sensitivity, especially in

mature adipocytes (*Figures 77* and *85*). The *Isg15*-KD cells, however, seem insensitive to the effect of A66.

This role of *Isg15* in the modulation of the metabolic effect of insulin is completely novel. It is therefore a limited endeavour to discuss it in the context of published literature. Nevertheless, a few studies have investigated the crosstalk between ISG15 and the PI3K/Akt pathway. For instance, Kaur and colleagues were the first to highlight the interaction between ISG15 and class I PI3K (S. S.-K. Kaur 2008). Indeed, using MEFs designed with a deletion of the regulatory subunits of PI3K (p85α and p85β), they established that IFN-α-induction of ISG15 expression required PI3K. Furthermore, they demonstrated that *Isg15* mRNA translation was impaired in the PI3K knockout cells in an Akt-dependent manner. Investigating the role of ISG15 in Akt-induced phagocytosis triggered by vaccinia virus infection, Yángüez *et al*. report that *Isg15*$^{-/-}$ macrophages displayed reduced p-Akt basal levels compared to *Isg15*$^{+/+}$ cells (Yanguez 2013). They concluded that the regulation of macrophagic antiviral response by ISG15 relies on the PI3K/Akt signalling cascade.

Such results are therefore consistent with the data presented in this chapter as silencing *Isg15* was shown to hinder Akt phosphorylation under the conditions tested. Moreover, we demonstrate that *Isg15*-KD cells did not benefit from the positive metabolic effect of inhibiting p110α, thus emphasising the interaction between ISG15 and PI3K and the importance of ISG15 in facilitating the downstream signalling of insulin. Also in line with our data, Tian and colleagues demonstrate in a recent study the dependence of mammalian reovirus replication on the PI3K/Akt pathway (Tian 2015). More specifically, they evidenced that the

reovirus-induced activation of PI3K/Akt stimulated the transcription of ISGs, including ISG15, and that both pharmacological and genetic inhibition of the kinase cascade down-regulated the expression of ISG15. Using the same PI3K inhibitor (LY294002) on human mammary epithelial MCF-10A cells, Tsai *et al.* also noted a reduction of ISG15 expression (Tsai 2011).

V. 4. 2. The pro-autophagic role of ISG15

The present chapter also evidenced that knocking down *Isg15* hinders the pro-autophagic effect of palmitate in 3T3-L1 pre-adipocytes (*Figure 78A*). Thus our data would indicate ISG15 to act as an inducer of autophagy in accordance with the findings of Nakamura and colleagues (T. F. Nakamura 2010). Indeed, as discussed in the introduction of this chapter, they revealed that both *Isg15* and pro-autophagic *Pkr* mRNA were stimulated on the adipocytes of mice on a HFD *versus* lean control. This aligns with the data reviewed by Schmeisser and colleagues advocating type I IFN, the main inducer of ISG15, as a promoter of autophagy in cancerous cells (Schmeisser 2014). Their model highlights the capacity of type I IFN to activate the PI3K/Akt axis, leading them to discuss the dichotomy by which the cytokine stimulates autophagy as well as the anti-autophagic PI3K/Akt pathway.

Such paradox is echoed in the data presented in the present chapter, as silencing *Isg15* is simultaneously associated with reduced p-Akt levels and an impaired autophagic response. To explain this potential contradiction, Schmeisser *et al*. postulate the existence of a negative feedback loop by which certain ISGs might inhibit the downstream signalling of PI3K/Akt allowing for the induction of

autophagy. In support of this theory, they examine the evidence suggesting that type I IFN hinders mTORC1 activity (induced by PI3K) thus triggering autophagy in tumour cells and lymphoblasts (Schmeisser 2014). Although, due to its pro-autophagic properties, *Isg15* would not be one of such ISGs, this stands for a compelling model.

An additional model tying the role of ISG15 in the modulation of autophagy and insulin signalling involves mTORC2. This multi-protein complex is activated by Akt and is critical for the optimal downstream signalling of the kinase (Tang 2016). Tang and colleagues recently demonstrated the mTORC2-mediated regulation of *de novo* lipogenesis and insulin sensitivity. Investigating the effects of HFD in mTORC2-deficient mice, they establish this complex as a critical element of the nutrient-sensing machinery regulating the metabolic effect of insulin and the onset of insulin resistance. mTORC2 is also involved in the regulation of autophagy. Indeed, it was found to down-regulate the pro-autophagic transcription factor FOXO3 through the stimulation of Akt at least in skeletal muscle cells (Jung 2010). Interestingly, Kaur and colleagues were able to establish a crosstalk between mTORC2 and ISG15 in MEFs (S. S.-K. Kaur 2012). By deleting elements of the complex, they revealed type I IFN-mediated activation of Akt to be dependent on mTORC2. Furthermore, they demonstrate that a fully functional complex is required for the downstream signalling of the cytokine, more specifically ISG15 expression.

V. 4. 3. The crosstalk between ISG15 and STAT3

As illustrated by *figure 79B*, inhibiting PKR hindered palmitate-induced stimulation of autophagy in both transduced cell types, although this could not be observed in WT 3T3-L1 pre-adipocytes (*Figure 61*). This reflects the findings of Shen *et al*., who report that PKR depletion down-regulated autophagy in MEFs (Shen 2012). Furthermore, in line with the study of Nakamura *et al*., the authors report that palmitate stimulates autophagy in a PKR-dependent manner. Relevantly to the present work, Nakamura and colleagues notice an elevation of *Isg15* mRNA expression in the adipocytes of HFD-fed mice *versus* a lean control (T. F. Nakamura 2010). Such observation supports the data presented in *figure 78B* as the palmitate-mediated induction of LC3B-II levels is reduced in the *Isg15*-KD cells compared to the control. Hence, the pro-autophagic effect of palmitate appears to be modulated by both PKR and ISG15.

Interestingly, Shen and colleagues provide evidence for a physical and functional STAT3-PKR interaction. Indeed, using published crystallographic structures along with computerised docking experiments, the authors identify the SH2 domain of the transcription factor as the binding site for the carboxyterminus of PKR (Shen 2012). In addition, they demonstrated that STAT3 coimmunoprecipitates with this moiety of the kinase but not with its N-terminus. Further point mutation experiments confirmed this model. Shen and colleagues also report a cytoplasmic STAT3-mediated anti-autophagic effect both in human osteosarcoma cells and MEFs *in vitro* and *in vivo*. This validates their initial findings demonstrating that STAT3 inhibitors stimulated the autophagic process. The data presented in that study indicated that the binding of cytoplasmic STAT3 to the catalytic site of PKR inhibits

the pro-autophagic activity of the kinase. Palmitate appears to have the same ability as STAT3 inhibitors to disrupt STAT3-PKR interaction, thus restoring PKR-mediated modulation of autophagy.

The link between STAT3, palmitate and ISG15 is investigated in *figure 86*. It shows that both palmitate- and LPS-mediated inductions of STAT3 Tyr^{705} phosphorylation are abrogated by silencing ISG15 in mature 3T3-L1 adipocytes. Moreover, treating the cells with recombinant ISG15 induced the phosphorylation of STAT3 Tyr^{705} (*Figure 69*). Putting such findings into perspective with the study of Shen *et al.*, it is likely that ISG15 promotes the phosphorylation of STAT3 through the stimulation of palmitate-PKR binding previously demonstrated by Cho *et al*. (Cho 2011). Indeed, this interaction between the SFA and the kinase prevents the binding of cytoplasmic STAT3 to PKR, therefore enabling the pro-autophagic effect of palmitate and PKR while also permitting free cytoplasmic STAT3 to be phosphorylated.

Such transcription-independent regulatory effect of cytoplasmic STAT3 on autophagy complements the model proposed in *figure 49* by which palmitate would regulate the expression of pSTAT3 Tyr^{705} through the TLR2-mediated secretion of gp130 cytokines such as IL-6. Indeed, Shen *et al.* note that PKR fails to bind STAT1, which would explain why palmitate was shown to induce the phosphorylation of STAT3 but not STAT1 in Chapter 3. Further, various elements of the model described in *figure 49* are known to stimulate autophagy. For instance, IL-6 was reported to promote autophagy in human $CD11b^{+}$ peripheral blood mononuclear cells (Roca 2009). Thus, palmitate and STAT3 may regulate autophagy

through the synergy of a transcription-dependent and a transcription-independent process. It is likely that enhanced autophagy has beneficial metabolic consequences, such as enhanced insulin sensitivity, and that this is facilitated by ISG15.

V. 4. 4. The impact of palmitate on ISGylation

The last part of the present investigation involved the mass spectrometric analysis of ISG15-immunoprecipitates derived for differentiated 3T3-L1 adipocytes treated overnight with either palmitate or IFN-α. The lysates were incubated with an antibody specific to ISG15, thus allowing for the isolation of ISGylated proteins and their binding partners. Mass spectrometric analysis allowed for identification of ISGylated proteins differentially expressed following the treatments. Using both DAVID and STRING software, we were able to cluster the genes identified by mass spectrometry and to compare those induced or inhibited by the treatments (*Figures 87*, *88* and *89* and *table 14*).

The results produced by the two softwares were consistent and revealed that palmitate down-regulates the expression of various 'ISGylated' (referring to both directly ISGylated and interacting with ISGylated proteins) mitochondrial proteins (*Figure 88*). This is of interest as mitochondrial dysfunction is a core element of insulin resistance. Indeed, the eukaryotic organelle is pivotal for generating the energy required for glucose and lipid metabolism. Kim *et al*. have reviewed the biological mechanisms associating mitochondrial failure to the onset of metabolic disorders and discussed the current evidence demonstrating that improving mitochondrial function can alleviate such symptoms (J. W. Kim 2008). In addition to

mitochondrial proteins, the SFA also inhibited the expression of ISGylated proteins involved in ribosomal structure and activity, tubulins, molecular chaperones, histones, proteins implicated in the citric acid cycle, keratins and HSP (*Figure 88*). The diversity of gene clusters identified highlights the importance of ISGylation and the wide range of biological processes regulated by it.

Interestingly, the molecular chaperone down-regulated by palmitate, i.e. CCT, was also inhibited by IFN-α. Its structure is characterised by eight homologous subunits, which mediate the folding of 10 to 15% of newly synthesised eukaryotic proteins as well as the refolding of other proteins, misfolded due to cellular stress (Cui 2015). CCT has been shown to mediate the folding of a variety of proteins implicated in cell growth and proliferation, including tubulins, another gene cluster simultaneously inhibited by palmitate and IFN-α (Cui 2015). Relevantly to the present work, Kasembeli *et al.* also evidenced the role of these chaperonins in the folding of STAT3 (Kasembeli 2014). Therefore, CCT might be the missing link explaining how ISG15 modulates the phosphorylation of STAT3 Tyr^{705} recorded in *figure 86*. We can postulate that palmitate induces the deISGylation of these chaperonins stimulating their activity, including the folding of STAT3, allowing for the palmitate-mediated up-regulation of p-STAT3 Tyr^{705} levels and autophagic rates.

Mass spectrometric analysis of human skeletal muscle revealed that the abundance of T-complex protein 1 (TCP1) - a member of the CCT complex identified in the DAVID analysis - was increased two-fold in obese and type 2 diabetic participant versus lean control (Hwang 2010). Besides, Guest *et al.* evidenced that pharmacological Akt inhibition resulted in the down-regulation of

TCP1 in a SUM breast cancer cell line (Guest 2015). Futher supporting the role of CCT in the regulation of insulin sensitivity through the PI3K/Akt pathway, CCT2, one of the eight subunits of CCT, has been identified as a substrate for ribosomal protein S6 kinase (S6K) 1, found downstream of mTORC1 (Jastrzebski 2011). This phospho-proteomic screen validated the ealier findings of Abe *et al*. who demonstrated that CCT2 was phosphorylated by S6K upon insulin stimulation of HEK 293T cells (Abe 2009). Furthermore, they confirmed that inhibiting PI3K using LY294002 rescued this effect. The modulation of CCP through ISGylation might explain the role of ISG15 in the regulation of insulin sensitivity.

Despite the findings of *figure 66*, which indicate the absence of a palmitate-mediated effect on ISG15 expression and on protein ISGylation, the mass spectrometric analysis shows that ISG15 expression was reduced following the palmitate treatment. This appears contradictory in the context of autophagy as both ISG15 and palmitate promote the same pro-autophagic effect. Therefore, if cells were exposed to the SFA, one might expect an increase in ISG15 expression. However, it is important to remember that the decrease evidenced by the mass spectrometric data only indicates a dip in the amount of free ISG15. Therefore, a stimulation of ISG15 expression might go undetected if the rate of protein ISGylation is also enhanced at the same time.

STRING analysis of ISGylated proteins down-regulated by palmitate identified seven direct associations between ISG15 and other proteins (*Figure 88*). One of them, HSP90αB1, is a molecular chaperone implicated in the maturation and the maintenance of the structural integrity of proteins involved in cell cycle control

and signal transduction (Khurana 2015). Interestingly, in the last few years, HSP90 has surfaced as a key modulator of insulin signalling and glucose homeostasis. Indeed, Lee *et al.* revealed that pharmacological inhibition of HSP90 could improve glucose homeostasis in *db*/*db* mice, while rescuing insulin sensitivity in diet-induced obese mice (J. G. Lee 2013). The role of isoform HSP90αB1 was further investigated this year by Jing *et al.*, who evidenced that its expression was up-regulated in skeletal muscle of diet-induced obese mice compared to lean control (Jing 2018). In addition, isoform specific knockdown of HSP90αB1 using siRNA in primary human skeletal muscle myotubes improved substrate metabolism, insulin sensitivity as well as mitochondrial respiration capacity. Therefore, the direct interaction between HSP90αB1 and ISG15 could explain the effect of the latter on insulin sensitivity reported in this chapter.

STRING analysis also predicts the interaction of ISG15 and PPIA (*Figure 88*). As mentioned in the results section of this chapter, this enzyme catalyses the cis-trans isomerisation of proline imidic peptide bonds in oligopeptide and was shown to significantly induce Akt phosphorylation in endothelial cells (Wei 2013). In diabetes, increased plasma concentration of PPIA was reported for T2D patients compared to healthy individuals (Ramachandran 2014). Indeed, the high glucose levels and reactive oxygen species characteristic of this condition stimulate monocytes to secrete PPIA, which acts as a pro-inflammatory cytokine (Tian-tian 2013). Considering the competition between ISGylation and ubiquitination, the decreased in ISGylated PPIA might reflect an increase in ubiquitinated PPIA. This would lead to the neutralisation of PPIA activity through proteasome degradation: PPIA-mediated stimulation of Akt would be hindered, thus contributing to palmitate-

induced insulin resistance.

A similar rationale could be applied to explain the down-regulation of ISGylated PLAA, another protein found to directly interact with ISG15, also shown to stimulate Akt phosphorylation. Indeed, this phospholipase was found to induce Akt phosphorylation in a p110α-dependent manner in macrophages (D. K. Park 2003). Recently, Kuefner *et al.* were able to demonstrate the critical role of a subset of PLAA, PLAA group IIA, in the modulation of insulin sensitivity and metabolism (Kuefner 2017). Having engineered a mouse expressing the human gene encoding this protein (mice do not express itdue to a frameshift mutation), the mice were fed either a HFD or a chow diet for 10 weeks, the former appear to have maintained their original weight and adiposity. In addition, the mutant mice were found to show increased insulin sensitivity and glucose tolerance (Kuefner 2017). Besides from its role in the Akt pathway, PLAA is directly linked with ubiquitination has surfaced for PLAA as it was evidenced to act within a multi-protein complex including the deubiquitinating enzyme YOD1, ubiquitin regulatory X domain-containing protein 1 and the AAA-ATPase p97 (Papadopoulos 2016). Interestingly, PLAA was also identified as a promoter of autophagy, which points at the same contradiction as that unveiled for ISG15: the phospholipase stimulates autophagy, while simultaneously benefiting insulin sensitivity through up-regulating the anti-autophagic PI3K/Akt pathway (Papadopoulos 2016).

This crosstalk between the ubiquitination and ISGylation systems is emphasised by the data presented in *figure 90*. Indeed, visualising the network of predicted associations between proteins encoded by genes that were up-regulated by

the IFN-α treatment and down-regulated by the palmitate treatment, one can identify ISG15 integrated within a cluster of four other proteins implicated in the ubiquitin proteasome system. It is interesting to note that the two treatments elicit opposite effects on the expression of ISGylated-ubiquitin related proteins. This might underlie the mechanistic differences in the onset of IFN- and palmitate-induced insulin resistance explored in Chapter 1.

V. 4. 5. Limitations and future experiments

A limitation of the findings presented in Chapter 5 could be that the response of the cell line bearing the empty vector to the palmitate treatment is rather different from that of the WT cell line. Indeed, the SFA does not inhibit Akt phosphorylation in the control cell line (*Figures 75C* and *83C*). This is unlikely to be due to variability in reagent preparation and experimental conditions as treatments of the control cell line and the Isg15-KD cell line were performed simultaneously. Issues such as differentiation variability or batch effects are also improbable as these would have also affected the results collected for the WT cell line as the same number of repeats were performed. Thus, this phenomenon might be associated with the process of having transduced the cells with the pGIPZ vector. However, because we were able to demonstrate that both the WT adipocytes and the cell line transfected with the empty vector expressed similar amount of ISG15, this does not undermine the conclusions drawn from the experiments presented in the present chapter (*Figure 71*).

Another limitation to the results discussed above is that mature adipocytes expressed considerably less ISG15 than pre-adipocytes. This is likely to explain why the differences between the two transduced cell lines is more noticeable in pre-adipocytes. Nevertheless, variations in the cellular responses to A66 are more detectable in mature cells (*Figure 85*) and the phosphorylation of STAT3 following palmitate exposure is still very different between the two differentiated cell lines (*Figure 86*). Reproducing the experiments presented in this chapter in *Isg15*-KD human cells would be very valuable to assert potential clinical significance. Therefore, knocking-down this ISG in hMADS could be the next experimental step to be taken.

It is common practice to use three different shRNA hairpins to validate results obtained with one. Indeed, effects observed can stem from partial complementarity of the strand to an unintended target gene, known as off-target effects. However, only one shRNA hairpin for *Isg15* was available from Dharmacon making this strategy inapplicable. However, future experiments might include a rescue experiment as another mean to exclude the possibility of off-target effects. This involves the co-transduction of the cells with an optimised version of the WT-Isg15 that is shRNA-resistant. An alternative and straight forward technique could also be considered in the future to confirm our findings such as clustered regularly interspaced short palindromic repeats (CRISPR)/ CRISPR-associated protein 9 (Cas9) gene inactivation of *Isg15*. This system would allow to edit-out our target gene and, therefore, permit to completely silence *Isg15* unlike RNAi techniques.

Regarding the mass spectrometry experiment, an obvious limitation would be the fact that no repeat was performed due to time limitations. In addition, only a small fraction of the detected protein was confirmed as ISGylated by detection of the characteristic Gly-Gly-Arg motif. Therefore for most hits, we are unsure whether the protein is truly ISGylated or if they interact with ISGylated proteins. Consequently, future experiments should focus on validating targets by IP of specific proteins and then confirm ISGylation through either mass spectrometry or by immunoblotting with anISG15-specific antibody. As not all hits would be able to be validated this way, proteins of interest would have to be selected beforehand. In addition, alternative biological readouts could be investigated such as mitochondrial function, which could be done through Seahorse analysis. Indeed, the mass spectrometric data revealed that both palmitate and IFN-α treatments potentially affected the ISGylation of mitochondrial and metabolic enzymes (*Table 14*).

CHAPTER 6. CONCLUSION

The present investigation aimed at identifying the molecular mechanisms underlying the onset of insulin resistance mediated by dietary FA and the impact of insulin pathway activity on this process. To this end, two cell-based models were employed: on one hand, the widely used murine 3T3-L1 adipocytes, and on the other hand, human hMADS adipocytes to ascertain the therapeutic potential of the findings. More specifically, the present work had the purpose of validating the findings of a transcriptome analysis performed on 3T3-L1 adipocytes treated with palmitate in the presence or absence of a p110α selective inhibitor. Sequencing analysis permitted the identification of an array of genes of expression was altered in response to the treatments, including genes known to be induced by type I IFN. These were up-regulated by palmitate in a p110α-dependent manner. This was of particular interest as IFN had been established in the literature to induce insulin resistance through the sustained activation of the downstream effectors of IFN, transcription factors STAT1 and STAT3.

The groundwork of the investigation was to propose models of palmitate- and IFN-mediated insulin resistance and examine the consequences of p110α inhibition in such models. This would enable further insight to be gathered on the findings of Foukas *et al.* regarding the beneficial phenotypic effect of such inhibition in the $p110\alpha^{D933A/WT}$ mice (L. C. Foukas 2006). In 3T3-L1 pre- and mature adipocytes and mature hMADS cells, palmitate was demonstrated to inhibit insulin-stimulated p-Akt

levels, an effect rescued by the p110α inhibitor, A66. Thereby, we could validate this cellular model of palmitate-induced insulin resistance as well as the positive metabolic impact of p110α inhibition. The model of IFN-γ-induced insulin resistance could only be established in mature 3T3-L1 adipocytes. In this case, adding A66 to the treatment also rescued the inhibition of Akt phosphorylation. Despite a similar trend observed in hMADS adipocytes, the effect was not statistically significant, likely due to cell line chosen. Indeed, IFN-γ-mediated insulin resistance had been described in SGBS cells (McGillicuddy 2009) before, but it has not been reported in hMADS.

In addition to these preliminary experiments, palmitate-induced phosphorylation of STAT1 and STAT3 was probed to confirm the interaction between the palmitate and the IFN pathway suggested by the transcriptome analysis data. Overall, it appears that the SFA prompts the phosphorylation of STAT3 Tyr^{705} after 8 h of treatment in mature 3T3-L1 (*Figure 20A*). The STAT1 Ser^{727}, STAT1 Tyr^{701} and STAT3 Ser^{727} were unaffected by palmitate treatment. Furthermore, the SFA elicited no reproducible effect in the other cell types tested (3T3-L1 pre-adipocytes, hMADS pre- and mature adipocytes). Collectively, these results indicate that palmitate-mediated phosphorylation of STAT3 Tyr^{705} occurs through a mechanism independent of IFN secretion, as STAT1 would have otherwise been induced by the SFA, as IFN is known to potently stimulate phosphorylation of this residue. To the best of our knowledge, no study so far has investigated the effect of palmitate on the phosphorylation of STAT3 or STAT1 in adipocytes.

The differential regulation of STAT1 and STAT3 activity had previously

been reported, implicating leptin, specific nutrients, IFN and gp130 cytokines as modulators (Vaisse 1996, de Castro Barbosa 2009, McGillicuddy 2009, Sato 1997, Pensa 2013). Evidence indicates that IFN triggers the sustained activation of STAT1, while also inducing the activation of STAT3 in a weaker and more transient manner. The opposite pattern of activation is promoted by gp130 cytokines (Pensa 2013). This observation led us to hypothesize that palmitate-mediated phosphorylation of STAT3 Tyr^{705} is modulated through the secretion of gp130 cytokines rather than of IFN. This inference is strengthened by the fact that no evidence in the literature indicates that palmitate stimulates the secretion of IFN or that adipocytes secrete IFN. Various studies, on the other hand, highlight the ability of SFA to induce gp130 cytokines in various cell types, including 3T3-L1 (Weigert 2004, Oberbach 2010, Staiger 2004, K. a. Ajuwon 2005)

From reviewing the studies published on this topic, it is probable that the reason why the tyrosine residue, but not the serine residue, of STAT3 was phosphorylated in response to palmitate treatment is the critical role of Tyr^{705} in enabling the transcriptional activity of STAT3 dimers (P. B.-N. Heinrich 2003). Moreover, it has been shown that the insulin signalling pathway stimulates serine phosphorylation while inhibiting IL-6 modulated tyrosine phosphorylation (Andersson 2007). In addition, phosphorylation of STAT3 Ser^{727} was also demonstrated to down-regulate p-STAT3 Tyr^{705} levels (Cheng 2010). Therefore, as palmitate impairs the insulin sensitivity of the cell, STAT3 Ser^{727} phosphorylation is no longer induced and inhibition of STAT3 Tyr^{705} phosphorylation mediated by both Ser^{727} phosphorylation and insulin is alleviated. Gp130 cytokines can then freely modulate transcription through STAT3 Tyr^{705} phosphorylation.

Various inhibitors (A66, D030, TAK 242 and myriocin) were tested to explore the molecular mechanisms underlying palmitate-mediated stimulation of p-STAT3 Tyr^{705} in 3T3-L1 mature adipocytes. Interestingly, none of these rescued the effect of SFA. TAK 242 was indeed expected to have an effect as a body of studies indicates that its target TLR4 mediates palmitate signalling and has the ability to bind the SFA (Shi 2006, Holland 2011, Schilling 2013, Turpin 2014, Pal 2012, Nicholas 2017). The receptor, abundantly expressed in differentiated 3T3-L1 and adipose tissue, was also found to be pivotal in the IFN response (Faure 2001, T. T. Kawai 2001, Noppert 2007, M. K. Song 2006). Furthermore, TLR4 was shown to stimulate STAT3 expression in bladder epithelial cells (Ying 2013). Yet, a study in mature 3T3-L1 demonstrated that palmitate did not significantly affect the expression of TLR4 target genes (M. K. Song 2006). We therefore postulate that another receptor is likely to be mediating the effect of palmitate on STAT3. TLR2 would be a probable candidate as it is highly expressed in 3T3-L1, activated by SFA and implicated in the pathogenesis of obesity (Poulain-Godefroy 2010, J. Senn 2006, S. C. Kim 2012). Besides, in line with the aforementioned model implicating gp130 cytokines in the palmitate-mediated phosphorylation of STAT3 Tyr^{705}, evidence suggests that TLR2 mediates the release of a gp130 cytokine, IL-6, in both pre- and mature 3T3-L1 adipocytes (Poulain-Godefroy 2010).

Palmitate-mediated regulation of STAT3 activity was also revealed to be p110α- and p110δ-independent despite strong evidence in the literature for a crosstalk between the PI3K and TLR pathways (Akira 2004, X. T. Li 2003). However, this interaction seems to be mainly mediated by TLR4, not TLR2, which

might explain why inhibiting PI3K did not affect palmitate-induced activation of STAT3. In light on such results, it was unsurprising to find that myriocin, which blocks *de novo* ceramide synthesis, failed to rescue SFA-mediated effect as $C_{16:0}$-ceramides are associated to the onset of obesity and glucose intolerance through their effect on PI3K and TLR4 (Holland 2011, Schilling 2013, Hla 2014). The final section of Chapter 3 investigated IFN-α- and IFN-λ2-mediated activation of STAT1 and STAT3 in order to confidently extend the statement that palmitate induces STAT3 activation without stimulating IFN-γ secretion to all types of IFNs. This could be done for IFN-α, which similar to IFN-γ induced both STAT1 and STAT3 phosphorylation. However, IFN-λ2 failed to stimulate these transcription factors. Additional experiments testing higher concentrations of IFN-λ2 and including a valid positive control would be required before drawing conclusions from this experiment. The phosphorylation of STAT1 and STAT3 following IFN-λ1 and IFN-λ3 treatment should also be explored.

Having explored the effect of SFA on the development of insulin resistance and investigated its effect on the downstream signalling of IFN, we went on to investigate the role of palmitate in the modulation of lipolysis and autophagy, two metabolic processes disrupted in the insulin resistant state. Two markers of lipolysis were considered: the phosphorylation of HSL and of perilipin, both substrates of PKA. Contrary to published data, we observed that palmitate did not affect either of these markers (Burns 1978, G. W. Muller 2008, Hupfeld 2003). Variations in experimental design may justify this discrepancy. Considering an alternative endpoint such as ATGL expression and phosphorylation levels, or else performing an activity-based assay measuring the release of lipolytic products such as FFA or

glycerol, could provide more conclusive results.

To assess the role of palmitate in autophagy, LC3B-II expression was monitored. In 3T3-L1 pre-adipocytes, the SFA triggered a significant increase in this marker, both in the presence and the absence of bafilomycin A1 indicating an induction of the autophagic flux. This is consistent with both *in vivo* and *in vitro* experiments associating obesity and HFD with impaired rates of autophagy and demonstrating the pro-autophagic effect of palmitate (Kovsan 2011, Nunez 2013, Ying 2013). Inhibiting PI3K and TLR4 failed to rescue the SFA-induced up-regulation of LC3B-II levels, although a trend in this direction was observed when treating the cells with the p110α inhibitor A66. Since, A66 also rescues palmitate-induced insulin resistance, such trend corroborates published evidence linking insulin resistance with increased autophagy in adipose tissue reviewed in the introduction of Chapter 4.

The last section of Chapter 4 focused on the role of PKR in the autophagic process, as according to prior reports, this kinase was expected to be a key player in this process in the context of insulin resistance and obesity (T. F. Nakamura 2010, Carvalho 2013, M. M.-S.-Y. Niso-Santano 2015). Palmitate did not alter the expression level of PKR in 3T3-L1 and hMADS pre- and mature adipocytes. The possible impact of PKR activity on autophagy was further explored using C16, a pharmacological inhibitor targeting the kinase, yet it had no effect on the pro-autophagic effect of the SFA. Such findings, although in opposition with the aforementioned literature, are consistent with the study of Lancaster and colleagues who report that PKR is not obligatory for HFD-induced obesity and its associated

metabolic and inflammatory dysregulations (Lancaster 2016). The heterogeneity of the data could be due to a difference in endpoint considered and the type of cells used. Therefore, future experiments might probe the phosphorylation levels of PKR rather than its expression in primary adipocytes rather than 3T3-L1 and hMADS. Considering the findings of Chapter 4, it is important to note that palmitate-induced autophagy could only be demonstrated in pre-adipocytes, not in mature adipocytes, reducing the relevance of our findings to regulation of lipid metabolism. Indeed, in pre-adipocytes, autophagy might be induced in response to molecular damage triggered by palmitate, rather than representing lipophagy.

The last chapter of this investigation explored the role of ISG15 in the cellular response to SFA. Due to its role as a cytokine and its ability to conjugate to a large number of proteins through ISGylation, this protein was likely to affect various cellular processes including those impacted by palmitate. Our first set of experiments revealed that palmitate had no effect on ISG15 expression levels in mouse and human adipocytes. Subsequently, the consequences of knocking down *Isg15* on palmitate-induced insulin resistance, palmitate-mediated induction of STAT3 and LC3B-II, were evaluated using an RNAi technique relying on the intracellular delivery of shRNA via viral vector. Overall, ISG15 seemed to promote insulin sensitivity as the insulin-stimulated Akt phosphorylation levels of the *Isg15*-KD cell were more affected by the palmitate treatment than the control cell line. In addition, the *Isg15*-KD cells failed to respond to the beneficial effect of A66 on insulin sensitivity. This role of ISG15 in the modulation of the metabolic effect of insulin is completely novel but echoes studies linking ISG15 to the PI3K/Akt pathway in MEFs and macrophages (S. S.-K. Kaur 2008, Yanguez 2013, Tsai 2011).

Another finding derived from the RNAi experiments was that silencing *Isg15* hindered the pro-autophagic effect of palmitate in 3T3-L1 pre-adipocytes, indicating that ISG15 has a positive role in autophagy. This raises the issue of a paradox by which ISG15 has a pro-autophagic effect despite stimulating the anti-autophagic PI3K/Akt pathway. Interestingly, inhibiting PKR hindered palmitate-induced stimulation of autophagy in both transduced cell types (*Isg15*-KD and empty vector control cell), although this could not be observed in WT 3T3-L1 pre-adipocytes. This suggests that at least in the transduced cells, the pro-autophagic effect of palmitate is modulated by both PKR and ISG15. This can explain why palmitate-mediated phosphorylation of STAT3 is abrogated by silencing *Isg15* in mature 3T3-L1 adipocytes, and why treating the cells with recombinant ISG15 induced the phosphorylation of STAT3 Tyr^{705}. Indeed, if ISG15 promotes the pro-autophagic effect of palmitate and PKR, it stimulates the formation of palmitate-PKR complexes. Such complexes prevent the binding of cytoplasmic STAT3 to PKR, thus permitting free cytoplasmic STAT3 to be phosphorylated.

Lastly, mass spectrometry was employed to evaluate the impact of palmitate on ISGylation. Analysing the data using the DAVID and the STRING software revealed a striking overlap between the 'ISGylated' proteins which expression was down-regulated by the palmitate and the IFN-α treatments. These included 'ISGylation' of various mitochondrial proteins, which is interesting as mitochondrial dysfunction is a core element of insulin resistance. The two treatments also inhibited the detection of 'ISGylated' CCT, involved in the folding of STAT3 (Kasembeli 2014). This protein might therefore be involved in ISG15-mediated regulation of

STAT3 phosphorylation. The STRING analysis also predicts the interaction of ISG15 with PPIA and PLAA, two proteins known to stimulate the Akt pathway (Wei 2013, D. K. Park 2003). In addition, PLAA was implicated in the ubiquitin system and autophagy (Papadopoulos 2016). It would therefore be interesting to validate these targets by investigating their role in the context of SFA-induced insulin resistance and autophagy and clarify the regulatory role of ISG15 in their downstream signalling. The results of the mass spectrometric analysis also emphasised the crosstalk between the ubiquitination and ISGylation systems, thus highlighting the importance of ISG15 in the regulation of protein homeostasis in the context of SFA-induced insulin resistance.

ACKNOWLDEGMENTS

I wish to thank Dr Lazaros Foukas for his supervision and guidance during this four year-long project. I would like to express my appreciation for Anqi Yan, who showed me around the laboratory during my first year and for her support. I would also like to thank the BBSRC for funding the research. Lastly, I extend my gratitude to my partner Mattias Broc, my family and friends for their love and constant encouragements.

REFERENCES

Abe, Y., Yoon, S., Kubota, K., Mendoza, M., Gygi, S. and Blenis, J. "p90 ribosomal S6 kinase and p70 ribosomal S6 kinase link phosphorylation of the eukaryotic chaperonin containing TCP-1 to growth factor, insulin, and nutrient signaling." *The Journal of Biological Chemistry* 284, no. 22 (2009): 14939-14948.

Ahmad, R., Al-Mass, A., Atizado, V., Al-Hubail, A., Al-Ghimlas, F., Al-Arouj, M., Bennakhi, A., Dermime, S. and Behbehani, K. "Elevated expression of the toll like receptors 2 and 4 in obese individuals: its significance for obesity-induced inflammation." *The Journal of Inflammation* 9 (2012): 48.

Ahmed, K., Tunaru, S., Tang, C., Muller, M., Gille, A., Sassmann, A., Hanson, J. and Offermanns, S. "An autocrine lactate loop mediates insulin-dependent inhibition of lipolysis through GPR81." *Cell Metabolism* 11, no. 7 (2010): 311-319.

Ajuwon, K. and Spurlock, M. "Palmitate activates the NF-kappa B transcription factor and induces IL-6 and TNF alpha expression in 3T3-L1 adipocytes." *The Journal of Nutrition* 135, no. 8 (2005): 1841-1846.

Ajuwon, K., Banz, W. and Winters, T. "Stimulation with peptidoglycan induces interleukin 6 and TLR2 expression and a concomitant downregulation of adiponectin receptors 1 and 2 in 3T3-L1 adipocytes." *The Journal of Inflammation* 6, no. 1 (2009): 8.

Akira, S. and Takeda, K. "Toll-like receptor signalling." *Nature Reviews Immunology* 4, no. 7 (2004): 499-511.

Aksoy, E., Taboubi, S., Torres, D., Delbauve, S., Hachani, A., Whitehead, M.A., Pearce, W.P., Berenjeno, I.M., Nock, G., Filloux, A., Beyaert, R., Flamand, V. and Vanhaesebroeck, B. "The p110 delta isoform of the kinase PI(3)K controls the subcellular compartmentalisation of TLR4 signaling and protects from endotoxic shock." *Nature Immunology* 13, no. 11 (2012): 1045-1054.

Altarejos, J. and Montminy, M. "CREB and the CRTC co-activators: sensors for hormonal and metabolic signals." *Nature Reviews Molecular Cell Biology* 12, no. 3 (2011): 141-151.

Al-Zeer, M., Al-Younes,H., Braun, P., Zerrahn, J. and Meyer, T. "IFN-gamma inducible Irga6 mediates host resistance against Chlamydia trachomatis via autophagy." *PLoS One* 4, no. 2 (2009): E4588.

Andersson, C., Sopasakis, K., Wallerstedt, E. and Smith, U. "Insulin antagonizes interleukin-6 signaling and is anti-inflammatory in 3T3-L1 adipocytes." *The Journal of Biological Chemistry* 282, no. 13 (2007): 9430-9435.

Arimoto, K., Lochte, S., Stoner, S.A., Burkart, C., Zhang, Y., Miyauchi, S., Wilmes, S., Fan, J., Heinisch, J., Li, Z., Yan, M., Pellegrini, S., Colland, F., Piehler, J. and Zhang, D. "STAT2 is an essential adaptor in USP18-mediated suppression of type I interferon signalling." *Nature Structural and Molecular Biology* 24, no. 3 (2017): 279-289.

Aronoff, S., Berkowitz, K., Shreiner, B. and Want, L. "Glucose metabolism and regulation: beyond insulin and glucagon." *Diabetes Spectrum* 17, no. 3 (2004): 183-190.

Aubert, J., Dessolin, S., Belmonte, N., Li, M., McKenzie, F., Staccini, L., Villageois, P., Barhanin, B., Vernallis, A., Smith, A., Ailhaud, G. and Dani, C. “Leukemia inhibitory factor and its receptor promote adipocyte differentiation via the mitogen-activated protein kinase cascade.” *The Journal of Biological Chemistry* 274, no. 35 (1999): 24965-24972.

Baerga, R., Zhang, Y., Chen, P., Goldman, S. and Jin, S. “Targeted deletion of autophagy-related 5 (atg5) impairs adipogenesis in a cellular model and in mice.” *Autophagy* 5, no. 8 (2009): 1118-1130.

Balhoff, J. and Stephens, J. “Highly specific and quantitative activation of STATs in 3T3-L1 adipocytes.” *Biochemical and Biophysical Research Communications* 247, no. 3 (1998): 894-900.

Barth, S., Glick, D. and Macleod, K. “Autophagy: assays and artifacts.” *The Journal of Pathology* 221, no. 2 (2010): 117-124.

Bates, S., Stearns, W., Dundon, T., Schubert, M., Tso, A., Wang, Y,, Banks, A., Lavery, H., Haq, A., Maratos-Flier, E., Neel, B., Schwartz, M. and Myers, M. “STAT3 signalling is required for leptin regulation of energy balance but not reproduction.” *Nature* 421, no. 6925 (2003): 856-859.

Biazik, J., Yla-Anttila, P., Vihinen, H., Jokitalo, E. and Eskelinen, E. “Ultrastructural relationship of the phagophore with surrounding organelles.” *Autophagy* 11, no. 3 (2015): 439-451.

Bluher, M., Michael, D., Peroni, O., Ueki, K., Carter, N., Kahn, B. and Kahn, R. “Adipose tissue selective insulin receptor knockout protects against obesity and obesity-related glucose intolerance.” *Developmental Cell* 3, no. 1 (2002): 25-38.

Bogunovic, D., Byun, M., Durfee, L.A., Abhyankar, A., Sanal, O., Mansouri, D., Salem, S., Radovanovic, I., Grant, A., Adimi, P., Mansouri, N., Okada, S., Bryant, V., Kong, X.-F., Kreins, A., Velez, M., Boisson, B., Khalilzadeh, S., Ozcelik, U., Darazam, I., Schoggins, J., Rice, C., Al-Muhsen, S., Behr, M., Vogt, G., Puel, A., Bustamante, J., Gros, P., Huibregtse, J., Abel, L., Boisson-Dupuis, S. and Casanova, J.-L. “Mycobacterial disease and impaired IFN-gamma immunity in humans with iherited ISG15 deficiency.” *Science* 337, no. 6102 (2012): 1684-1688.

Bolen, C., Ding, S., Robek, M. and Kleinstein, S. “Dynamic expression profiling of type I and type III interferon-stimulated hepatocytes reveals a stable hierarchy of gene expression.” *Hepatology* 59, no. 4 (2014): 1262-1272.

Bray, G. and Ryan, D. *Overweight and the metabolic syndrom: from bench to bedside.* Baton Rouge: Springer Science and buisness media, 2007.

Burns, T., Langley, P., Terry, B. and Robinson, G. “The role of free fatty acids in the regulation of lipolysis by human adipose tissue cells.” *Metabolism* 27, no. 12 (1978): 1755-1762.

Cahova, M. “Chapter 14 - Regulation of autophagy in insulin resistance and type 2 diabetes.” In *Autophagy: cancer, other pathologies, inflammation, immunity, infection and aging*, by M. Cahova, 213-235. Academic Press, 2015.

Cai, N., Zhao, X., Jing, Y., Sun, K., Jiao, S., Chen, X., Yang, H., Zhou, Y. and Wei, L. “Autophagy protects against palmitate-induced apoptosis in hepatocytes.” *Cell and Bioscience* 4, no. 28 (2014): 1-9.

Carvalho, B., Oliveira, A., Ueno, M., Araujo, T., Guadagnini, D., Carvalho-Filho, M,m Geloneze, B., Lima, M., Pareja, J., Carvalheira, J. and Saad, M. “Modulation of double-stranded RNA-activated protein kinase in insulin sensitive tissues of obese humans.” *Obesity* 21, no. 12 (2013): 2452-2457.

Carvalho-Filho, M., Carvalho, B., Oliveira, A., Guadagnini, D., Ueno, M., Dias, M., Tsukumo, D., Hirabara, S., Reis, L., Curi, R., Carvalheira, J. and Saad, M. “Double-stranded RNA-activated protein

kinase is a key modulator of insulin sensitivity in physiological conditions and in obesity in mice." *Endocrinology* 153, no. 11 (2012): 5261-5274.

Cernkovich, E., Deng, J., Bond, M., Combs, T. and Harp, J. "Adipose-specific disruption of signal transducer and activator of transcription 3 increases body weight and adiposity." *Endocrinology* 149, no. 4 (2008): 1581-1590.

Cheng, M., Zhang, Y., Zhong, X., Sutter, B., Cao, C., Chen, X., Cheng, X., Zhang, Y., Xiao, L. and Shen, Y. "Stat1 mediates an auto-regulation of hsp90b gene in heat shock response." *Cellular Signalling* 22 (2010): 1206-1213.

Cho, H., Mukherjee, S., Palasuberniam, P., Pillow, L., Bilgin, B., Nezich, C., Walton, P., Feig, M. and Chan, C. "Molecular mechanism by which palmitate inhibits PKR autophosphorylation." *Biochemistry* 50, no. 6 (2011): 1110-1119.

Choi, K. and Kim, Y-B. "Molecular mechanism of insulin resistance in obesity and type 2 diabetes." *The Korean Journal of Internal Medicine* 25, no. 2 (2010): 119-129.

Chung, J., Uchida, E., Grammer, T. and Blenis, J. "STAT3 serine phosphorylation by ERK-dependent and -independent pathways negatively modulates its tyrosine phosphorylation." *Molecular and Cellular Biology* 17, no. 11 (1997): 6508-6516.

Cinti, S., Mitchell, G., Barbatelli, G., Murano, I., Ceresi, E., Faloia, E., Wang, S., Fortier, M., Greenberg, A. and Obin, M. "Adipocyte death defines macrophage localization and function in adipose tissue of obese mice and humans." *The Journal of Lipid Research* 46, no. 11 (2005): 2347-2355.

Coe, N.R., Simpson, M.A. and Bernlohr, D.A. "Targeted disruption of the adipocyte lipid-binding protein (aP2 protein) gene impairs fat cell lipolysis and increases cellular fatty acid levels." *The Journal of Lipid Research*, no. 40 (1990): 967-972.

Coelho, M., Oliveira, T. and Fernandes, R. "Biochemistry of adipose tissue: an endocrine organ." *Archives of Medical Science* 9, no. 2 (2013): 191-200.

Combs, T., Pajvani, U., Berg, A., Lin, Y., Jelicks, L., Laplante, M., Nawrocki, A., Rajala, M., Parlow, A., Cheesebor, L., Ding, Y., Russell, R., Lindemann, D., Hartley, A., Baker, G., Obici, S., Deshaies, Y., Ludgate, M., Rossetti, L. and Scherer, P. "A transgenic mouse with a deletion in the collagenous domain of adiponectin displays elevated circulating adiponectin and improved insulin sensitivity." *Endocrinology* 145, no. 1 (2004): 367-383.

Connacher, A., Bennet, W., Jung, R., Bier, D., Smith, C., Scrimgeour, C. and Rennie, M. "Effect of adrenaline infusion of fatty acid and glucose turnover in lean and obese human subjects in the post-absorptive and fed states." *Clinical Science* 81, no. 5 (1991): 635-644.

Costa-Pereira, A. "Regulation of IL-6-type cytokine responses by MAPKs." *Biochemical Society Transactions* 42, no. 1 (2014): 59-62.

Costa-Pereira, A., Tininini, S., Strobl, B., Alonzi, T., Schlaak, J., Is'harc, H., Gesualdo, I., Newman, S., Kerr, I. and Poli, V. "Mutational switch of an IL-6 response to an interferon-gamma-like response." *Proceedings of the National Academy of Sciences of the USA* 99, no. 12 (2002): 8043-8047.

Cui, X., Hu, Z., Li, Z., Gao, P. and Zhu, J. "Overexpression of chaperonin containing TCP1, subunit 3 predicts poor prognosis in hepatocellular carcinoma." *World Journal of Gastroenterology* 21, no. 28 (2015): 8588-8604.

Dai, J., Pan, W. and Wang, P. “ISG15 facilitates cellular antiviral response to dengue and west nile virus infection in vitro.” *Virology Journal* 8, no. 1 (2011): 468-474.

Dasu, M., Devaraj, S., Zhao, L., Hwang, D. and Jialal, I. “High glucose induces Toll-like receptor expression in human monocytes: mechanism of activation.” *Diabetes* 57, no. 11 (2008): 3090-3098.

D'Cunha, J., Ramanujam, S., Wagner, R., Witt, P., Knight, E. Jr and Borden, E. “In vitro and in vivo secretion of human ISG15, an IFN-induced immunomodulatory cytokine.” *The Journal of Immunology* 157, no. 9 (1996): 4100-4108.

de Castro Barbosa, T., de Carvalho, J., Poyares, L., Bordin, S., Machado, U. and Nunes, M. “Potential role of growth hormone in impairment of insulin signaling in skeletal muscle, adipose tissue, and liver of rats chronically treated with arginine.” *Endocrinology* 150, no. 5 (2009): 2080-2086.

De Weerd, N., Samarajiwa, S. and Hertzog, P. “Type I interferon receptors: biochemistry and biological functions.” *The Journal of Biological Chemistry* 282, no. 28 (2007): 20053-20057.

Deb, D., Sassano, A., Lekmine, F., Majchrzak, B., Verma, A., Kambhampati, S., Uddin, S., Rahman, A., Fish, E. and Platanias, L. “Activation of protein kinase C delta by IFN-gamma.” *The Journal of Immunology* 171, no. 1 (2003): 267-273.

Delezie, J., Dumont, S., Dardente, H., Oudart, H., Grechez-Cassiau, A., Klosen, P., Teboul, M., Delaunay, F., Pevet, P. and Challet, E. “The nuclear receptor REV-ERBa is required for the daily balance of carbohydrate and lipid metabolism.” *The FASEB Journal* 26, no. 8 (2012): 3321-3335.

Deng, J., Hua, K., Caveney, E., Takahashi, N. and Harp, J. “Protein inhibitor of activated STAT3 inhibits adipogenic gene expression.” *Biochemical and Biophysical Research Communications* 339, no. 3 (2006): 923-931.

Dennis, G., Sherman, B., Hosack, D., Yang, J., Gao, W., Lane, C. and Lempicki, R. “DAVID: Database for Annotation, Visualization, and Integrated Discovery.” *Genome Biology* 4, no. 9 (2003): R60.

Dentin, R., Liu, Y., Koo, S., Hedrick, S., Vargas, T., Heredia, J., Yates, J. and Montminy, M. “Insulin modulates gluconeogenesis by inhibition of the coactivator TORC2.” *Nature* 449, no. 7160 (2007): 366-369.

Desai, S., Haas, A., Wood, L., Tsai, Y., Pestka, S., Rubin, E., Saleem, A., Nur-E-Kamal, A. and Liu, L. “Elevated expression of ISG15 in tumor cells interferes with the ubiquitin/26 S proteasome pathway.” *Cancer Research* 66, no. 2 (2006): 921-928.

Dickensheets, H., Sheikh, F., Park, O., Gao, B. and Donnelly, R. “Interferon-lambda induces signal transduction and gene expression in human hepatocytes, but not in lymphocytes or monocytes.” *The Journal of Leukocyte Biology* 93, no. 3 (2013): 377-385.

Duncan, R., Ahmadian, M., Jaworski, K., Sarkadi-Nagy, E. and Sul, H. “Regulation of lipolysis in adipocytes.” *Annual Review of Nutrition* 27 (2007): 79-101.

Engelman, J., Luo, J. and Cantley, L. “The evolution of phosphatidylinositol 3-kinases as regulators of growth and metabolism.” *Nature Reviews Genetics* 7, no. 8 (2006): 606-619.

Erion, D. and Shulman, G. “Diacylglycerol-mediated insulin resistance.” *Nature Medicine* 16, no. 4 (2010): 400-402.

Erridge, C. and Samani, N. “Saturated fatty acids do not directly stimulate Toll-like receptor signaling.” *Arterioscleriosis, Thrombosis, and Vascular Biology* 29, no. 11 (2009): 1944-1949.

Fan, J. and Zhang, D. “ISG15 regulates IFN-gamma immunity in human mycobacterial disease.” *Cell Research* 23, no. 2 (2013): 173-175.

Faure, E., Thomas, L., Xu, H., Medvedev, A., Equils, O. amd Arditi, M. “Bacterial liposaccharide and IFN-gamma induce Toll-Like Receptor 2 and Toll-Like Receptor 4 expression in human endothelial cells: role of NF-KB activation.” *The Journal of Immunology* 166, no. 3 (2001): 2018-2024.

Fioravante, M., Bombassaro, B., Ramalho, A., Dragano, N., Morari, J., Solon,C., Tobar, N., Ramos, C. and Velloso, L. “Inhibition of hypothalamic leukemia inhibitory factor exacerbates diet-induced obesity phenotype.” *The Journal of Neuroinflammation* 14, no. 1 (2017): 178.

Flannery, B., He, K. and Pestka, J. “Deoxynivalenol-induced weight loss in the diet-induced obese mouse is reversible and PKR-independent.” *Toxicology Letters* 221, no. 1 (2013): 9-14.

Foukas, L., Bilanges, B., Bettedi, L., Pearce, W., Ali, K., Sancho, S., Withers, D. and Vanhaesebroack, B. “Long-term p110 alpha PI3K inactivation exerts a benefical effect on metabolism.” *EMBO Molecular Medicine* 5, no. 4 (2013): 563-571.

Foukas, L., Claret, M., Pearce, W., Okkenhaug, K., Meek, S., Peskett, E., Snacho, S., Smith, A., Withers, D. and Vanhaesebroeck, B. “Critical role for the p110 alpha phosphoinositide-3-OH kinase in growth and metabolic regulation.” *Nature* 441, no. 7091 (2006): 366-370.

Freson, K., Stolarz, K., Aerts, R., Brand, E., Brand-Herrmann, S., Kawecka-Jaszcz, K., Kuznetsova, T., Tikhonoff, V., Thijs, L., Vermylen, J., Staessen, J. and Van Geet, C. “-391 C to G substitution in the regulator of G-protein signalling-2 promoter increases susceptibility to the metabolic syndrome in white European men: consistency between molecular and epidemiological studies.” *The Journal of Hypertension* 25, no. 1 (2007): 117-125.

Gaidhu, M., Anthony, N., Patel, P., Hawke, T., and Ceddia, R. “Dysregulation of lipolysis and lipid metabolism in visceral and subcutaneous adipocytes by high-fat diet: role of ATGL, HSL, and AMPK.” *The American Journal of Physiology-Cell Physiology* 298, no. 4 (2010): C961-C971.

Gil, J., Garcia, M., Gomez-Puertas, P., Guerra, S., Rullas, J., Nakano,H., Alcami, J. and Esteban, M. “TRAF family proteins link PKR with NF-kappa B activation.” *Molecular Cell Biology* 24, no. 10 (2004): 4502-4512.

GIPZ Lentiviral shRNA. www.dharmacon.gelifesciences.com/shrna/gipz-lentiviral-shrna/ (accessed February 22, 2018).

Glick, D., Barth, S. and Macleod, K. “Autophagy: cellular and molecular mechanisms.” *The Journal of Pathology* 221, no. 1 (2010): 3-12.

Graham, F. and van der Eb, A. “A new technique for the assay of infectivity of human adenovirus 5 DNA.” *Virology* 52, no. 2 (1973): 456-467.

Gregoire, F., De Broux, N., Hauser, N., Heremans, H., Van Damme, J. and Remacle, C. “Interferon-gamma and interleukin-1 beta inhibit adipoconversion in cultured rodent preadipocytes.” *The Journal of Cell Physiology* 151, no. 2 (1992): 300-309.

Grisouard, J., Bouillet, E., Timper, K., Radimerski, T., Dembinski, K., Frey, D., Peterli, R., Zulewski, H., Keller, U., Muller, B. and Christ-Crain, M. “Both inflammatory and classical lipolytic pathways are involved in lipopolysaccharide-induced lipolysis in human adipocytes.” *Inate Immunity* 18, no. 1 (2012): 25-34.

Groen, E. and Gillingwater, T. “UBA1: at the crossroads of ubiquitin homeostasis and neurodegeneration.” *Trends in Molecular Medicine* 21, no. 10 (2015): 622-632.

Guest, S., Kratche, Z., Bollig-Fischer, A., Haddad, R. and Ethier, S. “Two members of the TRiC chaperonin complex, CCT2 and TCP1 are essential forsurvival of breast cancer cells and are linked to driving oncogenes.” *Experimental Cell Research* 332, no. 2 (2015): 223-235.

Guo, S. “Insulin signaling, resistance, and the metabolic syndrome: insights from mouse models to disease mechanisms.” *The Journal of Endocrinology* 220, no. 2 (2014): T1-T23.

Halaas, J., Gajiwala, K., Maffei, M., Cohen, S., Chait, B., Rabinowitz, D., Lallone, R., Burley, S. and Friedman, J. “Weight-reducing effects of the plasma protein encoded by the obese gene.” *Science* 269, no. 5223 (1995): 543-456.

Hall, E., Nahorski, M., Murray, L., Shaheen, R., Perkins, E., Dissanayake, K., Kristaryanto, Y., Jones, R., Vogt, J., Rivagorda, M., Handley, M., Mali, G., Quidwai, T., Soares, D., Keighren, M., McKie, L., Mort, R., Gammoh, N., Garcia-Munoz, A., Davey, T., Vermeren, M., Walsh, D., Budd, P., Aligianis, I., Faqeih, E., Quigley, A., Jackson, I., Kulathu, Y., Jackson, M., Ribchester, R., Von Kriegsheim, A. Alkuraya, F., Woods, G., Maher, E. and Mill, P. “PLAA mutations cause a lethal infantile epileptic encephalopathy by disrupting ubiquitin-mediated endolysosomal degradation of synaptic proteins.” *The American Journal of Human Genetics* 100, no. 5 (2017): 706-724.

Han, C., Wu, W., Ale, A., Kim, M. and Cai, D. “Central leptin and tumor necrosis factor alpha in dirunal control of blood pressure and hypertension.” *The Journal of Biological Chemistry* 291, no. 29 (2016): 15131-15142.

Han, H., Kang, G., Kim, J., Choi, B. and Koo, S. “Regulation of glucose metabolism from a liver-centric perspective.” *Experimental and Molecular Medicine* 48, no. 3 (2016): e218.

Harp, J., Franklin, D., Vanderpuije, A. and Gimble, J. “Differential expression of signal transducers and activators of transcription during human adipogenesis.” *Biochemical and Biophysical Research Communications* 281, no. 4 (2001): 907-912.

Harris, J. and Scott-Davey, T. “Secreted phospholipases A2 of snake venoms: effects on the peripheral neuromuscular system with comments on the role of phospholipases A2 in disorders of the CNS and their uses in industry.” *Toxins (Basel)* 5, no. 12 (2013): 2533-2571.

Heinrich, P., Behrmann, I., Haan, S., Hermanns, H., Muller-Newen, G. and Schaper, F. “Principles of interleukin (IL)-6-type cytokine signalling and its regulation.” *The Biochemical Journal* 374, no. 1 (2003): 1-20.

Heinrich, P., Behrmann, I., Muller-Newen, G., Schaper, F. and Graeve, L. “Interleukin-6-type cytokine signalling through the gp130/Jak/STAT pathway.” *The Biochemical Journal* 334, no. 2 (1998): 297-314.

Hergovits, S., Mais, C., Hann, C., Costa-Pereira, A. and Hermanns, H. “Oncostatin M induces RIG-I and MDA5 expression and enhances the double-stranded RNA response in fibroblasts.” *The Journal of Cellular and Molecular Medicine* 21, no. 11 (2017): 3087-3099.

Hervas-Stubbs, S., Perez-Grcia, J., Rouzaut, A., Sanmamed, M., Le Bon, A. and Melero, I. “Direct effects of type I interferons on cells of the immune system.” *Clinical Cancer Research* 17, no. 9 (2011): 2619-2627.

Hiasa, Y., Kamegaya, Y., Nuriya, H., Onji, M., Kohara, M., Schmidt, E., Chung, R. “Protein kinase R is increased and is functional in hepatitis C virus-related hepatocellular carcinoma.” *The American Journal of Gastroenterology* 98, no. 11 (2003): 2528-2534.

Hla, T. and Kolesnick, R. “C16:0-Ceramide signals insulin resistance.” *Cell Metabolism* 20, no. 5 (2014): 703-705.

Hogan, J. and Stephens, J. “STAT1 binds to the LPL promoter in vitro.” *Biochemical and Biophysical Research Communications* 307, no. 2 (2003): 350-354.

Holland, W., Bikman, B., Wang, L., Yuguang, G., Sargent, K., Bulchand, S., Knotts, T., Shui, G., Clegg, D., Wenk, M., Pagliassotti, M., Scherer, P. and Summers, S. “Lipid-induced insulin resistance mediated by the proinflammatory receptor TLR4 requires saturated fatty acid-induced ceramide biosynthesis in mice.” *The Journal of Clinical Investigation* 121, no. 5 (2011): 1858-1871.

Hommelberg, P., Plat, J., Sparks, L., Schols, A., Essen, A., Kelders, M., Beurden, D., Mensink, R. and Langen, R. “Palmitate-induced skeletal muscle insulin resistance does not require NF-kB activation.” *Cellular and Molecular Life Sciences* 68, no. 7 (2011): 1215-1225.

Horowitz, J. and Klein, S. “Whole body and abdominal lipolytic sensitivity to epinephrine is suppressed in upper body obese women.” *The American Journal of Physiology-Endocrinology and Metabolism* 278, no. 6 (2000): E1144-1152.

Hotamisligil, G., Shargill, N. and Spiegelman, B. “Adipose expression of tumor necrosis factor-alpha: direct role in obesity-linked insulin resistance.” *Science* 259, no. 5091 (1993): 87-91.

Hsu, L., Park, J., Zhang, K., Luo, J., Maeda,S., Kaufman, R., Eckmann, L., Guiney, D. and Karin, M. “The protein kinase PKR is required for macrophage apoptosis after activation of Toll-like receptor 4.” *Nature* 428, no. 6980 (2004): 341-345.

Hupfeld, C., Dalle, S. and Olefsky, J. “Beta-arrestin 1 down-regulation after insulin treatment is associated with supersensitization of beta 2 adrenergic receptor Galpha s signaling in 3T3-L1 adipocytes.” *Proceedings of the National Academy of Sciences of the USA* 100, no. 1 (2003): 161-166.

Hwang, H., Bowen, B., Lefort, N., Flynn, C., De Filippis, E., Roberts, C., Smoke, C., Meyer, C.. Hojlund, K., Yi, Z. and Mandarino, L. “Proteomic analysis of human skeletal muscle reveals novel abnormalities in obesity and type 2 diabetes.” *Diabetes* 59, no. 1 (2010): 33-42.

Ivashki, L. and Donlin, L. “Regulation of type I interferon responses.” *Nature Reviews Immunology* 14, no. 1 (2014): 36-49.

Jamieson, S., Flanagan, J., Kolekar, S., Buchanan, C., Kendall, J., Lee, W., Rewcastle, G., Denny, W., Singh, R., Dickson, J., Baguley, B. and Shepherd, P. “A drug targeting only p110 alpha can block phosphoinositide 3-kinase signalling and tumour growth in certain cell types.” *The Biochemical Journal* 438 (2011): 53-62.

Jamieson, S., Flanagan, J., Kolekar, S., Buchanan, C., Kendall, J., Lee, W-J., Rewcastle, G., Denny, W., Singh, R., Dickson, J., Baguley, B. and Shepherd, P. “A drug targeting only p110 alpha can block phosphoinositide 3-kinase signalling and tumour growth in certain cell types.” *The Biochemical Journal* 438, no. 1 (2011): 53-62.

Jansen, H., Essen, P., Koenen, T., Joosten, L., Netea, M., Tack, C. and Stienstra, R. “Autophagy activity is up-regulated in adipose tissue of obese individuals and modulates proinflammatory cytokine expression.” *Endocrinology* 153, no. 12 (2012): 5866-5874.

Jarvis, R. *Low transfection efficiency and low cell viability are the most frequent causes of unsuccessful gene silencing experiments.* 31 10 Accessed 2016. www.thermofisher.com (accessed 06 29, 2016).

Jastrzebski, K., Hannan, K., House, C., Hung, S., Pearson, R. and Hannan, R. “A phospho-proteomic screen identifies novel S6K1 and mTORC1 substrates revealing additional complexity in the signaling network regulating cell growth.” *Cell Signalling* 23, no. 8 (2011): 1338-1347.

Jiang, C., Kim, J., Li, F., Qu, A., Gavrilova, O., Shah, Y. and Gonzalez, F. “Hypoxia-inducible factor 1 aplha regulates a SOCS3-STAT3-adiponectin signal transduction pathway in adipocytes.” *The Journal of Biological Chemistry* 288, no. 6 (2013): 3844-3857.

Jiang, W. and Ogretmen, B. “Autophagy paradox and ceramide.” *Biochimica et Biophysica Acta* 1841, no. 5 (2014): 783-792.

Jiang, X., Chen, X., Wan, J., Gui, H., Ruan, X. and Du, X. “Autophagy protectes against palmitic acid-induced apoptosis in podocytes in vitro.” *Scientific Reports* 7 (2017): 42764.

Jing, E., Sundararajan, P., Majumdar, I., Hazarika, S., Fowler, S., Szeto, A., Gesta, S., Mendez, A., Vishnudas, V., Sarangarajan, R. and Narain, N. “Hsp90b knockdown in DIO mice reverses insulin resistance and improves glucose tolerance.” *Nutrition and Metabolism*, 2018: 15:11.

Jocken, J. and Blaak, E. “Catecholamine-induced lipolysis in adipose tissue and skeletal muscle in obesity.” *Physiology and Behavior* 94, no. 2 (2008): 219-230.

Jocken, J., Goossens, G., Van Hees, A., Frayn, K., Van Baak, M., Stegen, J., Pakbiers, M., Saris, W. and Blaak, E. “Effect of beta-adrenergic stimulation on whole-body and abdominal subcutaneous adipose tissue lipolysis in lean and obese men.” *Diabetologia* 51, no. 2 (2008): 320-327.

Jung, C., Ro, S., Cao, J., Otto, N. and Kim, D. “mTOR regulation of autophagy.” *FEBS Letters* 584, no. 7 (2010): 1287-1295.

Kasembeli, M., Lau, W., Roh, S., Eckols, T., Frydman, J., Chui, W. and Tweardy, D. “Modulation of STAT3 folding and function by TRiC/CCT chaperonin.” *PLoS Biology* 12, no. 4 (2014): e1001844.

Kaur, S., Sassano, A., Joseph, A., Majchrzah-Kita, B., Eklund, E., Verma, A., Brachmann, S., Fish, E. and Platanias, L. “Dual regulatory roles of phosphatidylinositol 3-kinase in IFN signaling.” *The Journal of Immunology* 181, no. 10 (2008): 7316-7323.

Kaur, S., Sassano, A., Majchrzak-Kita, B., Baker, D., Su, B., Fish, E. and Platanias, L. “Regulatory effects of mTORC2 complexes in type I IFN signaling and in the generation of IFN responses.” *Proceedings of the National Academy of Sciences of the USA* 109, no. 20 (2012): 7723-7728.

Kawai, T., Adachi, O., Ogawa, T., Takeda, K. and Akira, S. “Unresponsiveness of MyD88-deficient mice to endotoxin.” *Immunity* 11, no. 1 (1999): 115-122.

Kawai, T., Takeuchi, O., Fujita, T., Inoue, J., Muhlradt, P., Sato, S., Hoshino, K. and Akira, S. “Lipopolysaccharide stimulates the MyD88-independent pathway and results in activation of IFN-regulatory factor 3 and the expression of a subset of lipopolysaccharide-inducible genes.” *The Journal of Immunology* 167, no. 10 (2001): 5887-5894.

Kennedy, A., Martinez, K., Chuang, C., LaPoint, K. and McIntosh, M. “Saturated fatty acid-mediated inflammation and insulin resistance in adipose tissue: mechanisms of action and implications.” *The Journal of Nutrition* 139, no. 1 (2009): 1-4.

Kershaw. E. and Flier, J. “Adipose tissue as an endocrine organ.” *The Journal of Clinical Endocrinology and Metabolism* 89, no. 6 (2004): 2548-2556.

Khurana, N. and Bhattacharyya, S. “Hsp90, the concertmaster: tuning transcription.” *Frontiers in Oncology* 5 (2015): 100.

Kibler, K., Shors, T., Perkins, K., Zeman, C., Banaszak, M., Biesterfeldt, J., Langland, J. and Jacobs, B. “Double-stranded RNA is a trigger for apoptosis in vaccinia virus-infected cells.” *The Journal of Virology* 71, no. 3 (1997): 1992-2003.

Kim, H., Kong, M., Kim, T., Suh, Y., Kim, W., Lim, J., Song, J. and Jung, M. “NFATc4 and ATF3 negatively regulate adiponectin gene expression in 3T3-L1 adipocytes.” *Diabetes* 55, no. 5 (2006): 1342-1352.

Kim, J., Fillmore, J., Chen, Y., Yu, C., Moore, I., Pypaert, M., Lutz, E., Kako, Y., Velez-Carrasco,W., Goldberg, I., Breslow, J. and Shulman, G. “Tissue-specific overexpression of lipoprotein lipase causes tissue-specific insulin resistance.” *Proceedings of the National Academy of Sciences of the USA* 98, no. 13 (2001): 7522-7527.

Kim, J., Wei, Y. and Sowers, J. “Role of mitochondrial dysfunction in insulin resistance.” *Circulation Research* 102, no. 4 (2008): 401-414.

Kim, J., Yoon, M. and Chen, J. “Signal transducer and activator of transcription 3 (STAT3) mediates amino ancid inhibition of insulin signaling through serine 727 phosphorylation.” *The Journal of Biological Chemistry* 284, no. 51 (2009): 35425-35432.

Kim, S., Choi, Y., Choi, Y. and Park, T. “Obesity activates toll-like receptor-mediated proinflammatory signaling cascades in the adipose tissue of mice.” *The Journal of Nutritional Biochemistry* 23, no. 2 (2012): 113-122.

Kim, S., Forman, A., Mathews, M. and Gunnery, S. “Human breast cancer cells contain elevated levels and activity of the protein kinase, PKR.” *Oncogene* 19, no. 27 (2000): 3086-3094.

Kirkin, V., McEwan, D., Novak, I. and Dikic, I. “A role for ubiquitin in selective autophagy.” *Molecular Cell Review* 34, no. 3 (2009): 259-269.

Kobayashi, K. “Role of catecholamine signaling in brain and nervous system functions: new insights from mouse molecular genetic study.” *The Journal Investigative Dermatology Symposium Proceedings* 6, no. 1 (2001): 115-121.

Koivisto, V., Pelkonen, R. and Cantell, K. “Effect of interferon on glucose tolerance and insulin sensitivity.” *Diabetes* 38, no. 5 (1989): 641-647.

Komatsu, M., Waguri, S., Koike, M., Sou, Y., Ueno, T., Hara, T., Mizushima, N., Iwata, J., Ezaki, J., Murata, S., Hamazaki, J., Nishito, Y., Iemura, S., Natsume, T., Yanagawa, T., Uwayama, J., Warabi, E., Yoshida, H., Ishii, T., Kobayashi. A., Yamamoto, M., Yue, Z., Uchiyama, Y, Kominami, E. and Tanaka, K. “Homeostatic levels of p62 control cytoplasmic inclusion body formation in autophagy-deficient mice.” *Cell* 131, no. 6 (2007): 1149-1163.

Kovsan, J., Bluher, M., Tarnovscki, T., Kloting, N., Kirshtein, B., Madar, L., Shai, I., Golan, R., Harman-Boehm, I., Schon, M., Greenberg, A., Elazar, Z., Bashan, N. and Rudich, A. “Altered autophagy in human adipose tissues in obesity.” *The Journal of Clinical Endocrinology and Metabolism* 96, no. 2 (2011): E268-E277.

Kramer, A., Kadye, R., Houseman, P. and Prinsloo, E. “Mitochondrial STAT3 and reactive oxygen species: a fulcrum of adipogenesis?” *JAKSTAT* 4, no. 2 (2015): e1084084.

Krotkiewski, M., Bjorntorp, P., Sjostrom, L. and Smith, U. “Impact of obesity on metabolism in men and women. Importance of regional adipose tissue distribution.” *The Journal of Clinical Investigation* 72, no. 3 (1983): 1150-1162.

Kuefner, M., Pham, K., Redd, J., Stephenson, E., Harvey, I., Deng, X., Bridges, D., Boilard, E., Elam, M. and Park, E. “Secretory phospholipase A2 group IIA modulates insulin sensitivity and metabolism.” *The Journal of Lipid Research* 58, no. 9 (2017): 1822-1833.

Kundrat, L. and Regan, L. “Identification of residues on Hsp70 and Hsp90 ubiquitinated by the cochaperone CHIP.” *The Journal of Molecular Biology* 395, no. 3 (2010): 587-594.

Laird, M., Rhee, S., Perkins, D., Medvedev, A., Piao, W., Fenton, M. and Vogel, S. “TLR4/MyD88/PI3K interactions regulate TLR4 signaling.” *The Journal of Leukocyte Biology* 85, no. 6 (2009): 966-977.

Lancaster, G., Kammoun, H., Kraakman, M., Kowalski, G., Bruce, C. and Febbraio, M. “PKR is not obligatory for high-fat died-induced obesity and its associated metabolic and inflammatory complications.” *Nature Communications* 7 (2016): 1038.

Lebovitz, H. “Insulin resistance: definition and consequences.” *Experimental and Clinical Endocrinology and Diabetes* 109, no. Suppl 2 (2001): S135-S148.

Lee, B., Lu, Y., Prado, M., Shi, Y., Tian, G., Sun, S., Elsasser, S., Gygi, S., King, R. and Finley, D. “USP14 deubiquitinates proteasome-bound substrates that are ubiquitinated at multiple sites.” *Nature* 532 (2016): 398-401.

Lee, J., Gao, J., Kosinski, P., Elliman, S., Hughes, T., Gromada, J. and Kemp, D. “Heat shock protein (HSP90) inhibitors activate the heat shock factor 1 (HSF1) stress response pathway and improve glucose regulation in diabetic mice.” *Biochemical and Biophysical Research Communications* 430, no. 3 (2013): 1109-1113.

Lee, K., Um, S., Rhee, D. and Pyo, S. “Interferon-alpha inhibits adiopgenesis via regulation of JAK/STAT1 signaling.” *Biochimica et Biophysica Acta* 1860, no. 11 (2016): 2416-2427.

Lee, S. and Esteban, M. “The interferon-induced double-stranded RNA-activated protein kinase induces apoptosis.” *Virology* 199, no. 2 (1994): 491-496.

Lenschow, D., Lai, C., Frias-Staheli, N., Giannakopoulos, N., Lutz, A., Wolff, T., Osiak, A., Levine, B., Schmidt, R., Garcia-Sastre, A., Leib, D., Pekosz, A., Knobeloch, K., Horak, I. and Virgin, H. “IFN-stimulated gene 15 functions as a critical antiviral molecule against influenza, herpes, and Sindbis viruses.” *Proceedings of the National Academy of Sciences of the USA* 104, no. 4 (2007): 1371-1376.

Li, B., Shin, J. and Lee, K. “Interferon-stimulated gene ISG12b1 inhibits adipogenic differentiation and mitochondrial biogenesis in 3T3-L1 cells.” *Endocrinology* 150, no. 3 (2009): 1217-1224.

Li, P., Du, Q., Cao, Z., Guo, Z., Evankovich, J., Yan, W., Chang, Y., Shao, L., Stolz, D., Tsung, A. and Geller, D. “Interferon-gamma induces autophagy with growth inhibition and cell death in human hepatocellular carcinoma (HCC) cells through interferon-regulatory factor-1 (IRF-1).” *Cancer Letter* 314, no. 2 (2012): 213-222.

Li, X., Tupper, J., Bannerman, D., Winn, R., Rhodes, C. and Harlan, J. “Phosphoinositide 3 kinase mediates toll-like receptor 4-induced activation of NF-kappa B in endothelial cells.” *Infection and Immunity* 71, no. 8 (2003): 4414-4420.

Liu, H., Han, J., Cao, S., Hong, T., Zhuo, D., Shi, J., Liu, Z. and Cao, W. “Hepatic autophagy is suppressed in the presence of insulin resistance and hyperinsulinemia: inhibition of FoxO1-dependent expression of key autophagy genes by insulin.” *The Journal of Biological Chemistry* 284, no. 45 (2009): 31484-31492.

Liu, Y., Wand, N., Zhang, S. and Liang, Q. “Autophagy protects bone marrow mesenchymal stem cells from palmitate-induced apoptosis through the ROS-JNK/p38 MAPK signaling pathways.” *Molecular Medicine Reports*, 2018: 1485-1494.

LoPiccolo, J., Blumenthal, G., Bernstein, W. and Dennis, P. “Targeting the PI3K/Akt/mTOR pathway: effective combinations and clinical consifderations.” *Drug Resistance Updates* 11, no. 1-2 (2008): 32-50.

Lundgren, M. and Eriksson, J. “No in vitro effects of fatty acids on glucose uptake, lipolysis or insulin signalling in rat adipocytes.” *Hormone and Metabolic Research* 36, no. 4 (2004): 203-209.

Marshall, M., Doerrler, W., Feingold, K. and Grunfeld, C. “Leukemia inhibitory factor induces changes in lipid metabolism in cultured adipocytes.” *Endocrinology* 135, no. 1 (1994): 141-147.

Mashili, F., Chibalin, A., Krook, A. and Zierath, J. “Constitutive STAT3 phosphorylation contributes to skeletal muscle insulin resistance in type 2 diabetes.” *Diabetes* 62, no. 2 (2013): 457-465.

Matsunaga, N., Tsuchimori, N., Matsumoto, T. and Li, M. “TAK-242 (Resatorvid), a small-molecule inhibitor of Toll-like receptor (TLR) 4 signaling, binds selectively to TLR4 and interferes with interactions between TLR4 and its adaptor molecules.” *Molecular Pharmacology* 79, no. 1 (2011): 34-41.

Matsuzawa, T., Kim, B., Shenoy, A., Kamitani, S., Miyake, M. and MacMicking, J. “IFN-gamma elicits macrophage autophagy via the p38 MAPK signaling pathway.” *The Journal of Immunology* 189, no. 2 (2012): 813-818.

McGillicuddy, F., Chiquoine, E., Hinkle, C., Kim, R., Shah, R., Roche, H., Smyth, E. and Reilly, M. “Interferon gamma attenuates insulin signaling, lipid storage, and differenciation in human adipocytes via activation of the JAK/STAT pathway.” *The Journal of Biological Chemistry* 284, no. 46 (2009): 31936-31944.

Meuwissen, M., Schot, R., Buta, S., Oudesluijs, G., Tinschert, S., Speer, S., Li, Z., van Unen, L., Heijsman, D., Goldmann, T., Lequin. M., Kros, J., Stam, W., Hermann, M., Willemsen, R., Brouwer, R., van Ijcken, W., Martin-Fernandez, M., de Coo, I., Dudink, J., de Vries, F.A., Bertoli Avella, A., Prinz, M., Crow, Y.J., Verheijen, F.W., Pellegrini, S., Bogunovic, D. and Mancini, G.M. “Human USP18 deficiency underlies type 1 interferonopathy leading to severe pseudo-TORCH syndrom.” *The Journal of Experimental Medicine* 213, no. 7 (2016): 1163-1174.

Minarik, P., Tomaskova, N., Kollarova, M. and Antalik, M. “Malate dehydrogenases - structure and function.” *General Physiology and Biophysics* 21 (2002): 257-265.

Mizushima, N. “Autophagy: process and function.” *Genes and Development* 21, no. 22 (2007): 2861-2873.

Moller, D. and Kaufman, K. “Metabolic syndrome: a clinical and molecular perspective.” *Annual Review of Medicine* 56 (2005): 45-62.

Moon, H., Dalamaga, M., Kim, S., Polyzos, S., Hamnvik, O., Magkos, F., Paruthi, J. and Mantzoros, C. “Leptin's role in lipodystrophic and nonlipodystrophic insulin-resistant and diabetic individuals.” *Endocrine Reviews* 34, no. 3 (2013): 377-412.

Moore, C., Guthrie, E., Huang, M. and Taxman, D. “Short hairpin RNA (shRNA): design, delivery and assessment of gene knockdown.” *Methods in Molecular Biology* 629 (2010): 141-158.

Moreno-Aliaga, M., Romero-Lozano, A., Castano, D., Prieto, J. and Bustos, M. “Role of cardiotrophin-1 in obesity and insulin resistance.” *Adipocyte* 1, no. 2 (2012): 112-115.

Muller, G., Wied, S., Over, S. and Frick, W. “Inhibition of lipolysis by palmitate, H2O2 and sulfonylureadrug, glimepiride,in rat adipocytes depends on cAMP degradation by lipid droplets.” *Biochemistry* 47, no. 5 (2008): 1259-1273.

Muller, M. and Geisler, C. “Defining obesity as a disease.” *Nature* 71 (2017): 1256-1258.

Nakamura, S., Takamura, T., Matsuzawa-Nagata, N., Takayama, H., Misu, H., Noda, H., Nabemoto, S., Kurita, S., Ota, T., Ando, H., Miyamoto, K. and Kaneko, S. “Palmitate induces insulin resistance in H4IIEc3 hepatocytes through reactive oxygen species produced by mitochondria.” *The Journal of Biological Chemistry* 284, no. 22 (2009): 14809-14818.

Nakamura, T., Furuhashi, M., Li, P., Cao, H., Tuncman, G., Sonenberg, N., Gorgun, C. and Hotamisligil, G. “Double-stranded RNA-dependent protein kinase links pathogen sensing with stress and metabolic homeostasis.” *Cell* 140, no. 3 (2010): 338-348.

Nakashima, H., Nguyen, T., Goins, W. and Chiocca, E. “Interferon-stimulated gene 15 (ISG15) and ISG15-linked proteins can associate with members of the selective autophagic process, histone deacetylase 6 (HDAC6) and SQSTM1/p62.” *The Journal of Biological Chemistry* 290, no. 3 (2015): 1485-1495.

Narasimhan, J., Wang, M., Fu, Z., Klein, J., Haas, A. and Kim, J. “Crystal structure of the Interferon-induced ubiquitin-like protein ISG15.” *The Journal of Biological Chemistry* 280, no. 29 (2005): 27356-27365.

Nguyen, H., Ramana, C., Bayes, J. and Stark, G. “Roles of phosphatidylinositol 3-kinase in interferon-gamma-dependent phosphorylation of STAT1 on serine 727 and activation of gene expression.” *The Journal of Biological Chemistry* 276, no. 36 (2001): 33361-33368.

Nicholas, D., Zhang, K., Hung, C., Glasgow, S., Aruni, A., Unternaehrer, J., Payne, K., Langridge, W. and De Leon, M. “Palmitic acid is a toll-like receptor4 ligand that induces human dendritic cell secretion of IL-1beta.” *PLoS One* 12, no. 5 (2017): e0176793.

Nigro, E., Scudiero, O., Monaco, M., Palmieri, A., Mazzarella, G., Costagliola, C., Bianco, A. and Daniele, A. “New insight into adiponectin role in obesity and obesity-related diseases.” *Biomedical Research International*, 2014: 658913.

Niso-Santano, M., Malik, S., Pietrocola, F., Bravo-San Pedro, J., Marino, G., Cianfanelli, V., Ben-Younes, A., Troncoso, R., Markaki, M., Sica, V., Izzo, V., Chaba, K., Bauvy, C., Dupont, N., Kepp, O., Rockenfeller, P., Wolinski, H., Madeo, F., Lavandero, S., Codogno, P., Harper, F., Pierron, G., Tavernarakis, N., Cecconi, F., Maiuri, M., Galluzzi, L. and Kroemer, G. “Unsaturated fatty acids induce non-canonical autophagy.” *The EMBO Journal* 34, no. 8 (2015): 1025-1041.

Niso-Santano, M., Shen, S., Adjemian, S., Malik, S., Marino, G., Lachkar, S., Senovilla, L., Kepp, O., Galluzzi, L., Maiuri, M. and Kroemer, G. “Direct interaction between STAT3 and EIF2AK2 controls fatty acid-induced autophagy.” *Autophagy* 9, no. 3 (2013): 415-417.

Noppert, S., Fitzgerald, K. and Hertzog, P. “The role of type I interferons in TLR responses.” *Immunology and Cell Biology* 85, no. 6 (2007): 446-457.

Nunez, C., Rodrigues, V., Gomes, F., de Moura, R., Victorio, S., Bombassaro, B., Chaim, E., Pareja, J., Geloneze, B., Velloso, L. and Araujo, E. “Defective regulation of adipose tissue autophagy in obesity.” *The International Journal of Obesity* 37, no. 11 (2013): 1473-1480.

Oberbach, A., Schlichting, N., Bluher, M., Kovacs, P., Till, H., Stolzenburg, J. and Neuhaus, J. “Palmitate induced IL-6 and MCP-1 expression in human bladder smooth muscle cells provides a link between diabetes and urinary tract infections.” *PLoS One* 5, no. 5 (2010): e10882.

Oh, K., Han, H., Kim, M. and Koo, S. “CREB and FoxO: two transcription factors for the regulation of hepatic gluconeogenesis.” *BMB Reports* 46, no. 12 (2013): 567-574.

Ohsumi, Y. “Ubiquitin and proteasomes: molecular dissection of autophagy: two ubiquitin-like systems.” *Nature Reviews Molecular Cell Biology* 2, no. 3 (2001): 211-216.

Ojaniemi, M, Glumoff, V., Harju, K., Liljeroos, M., Vuori, K. and Hallman, M. “Phosphatidylinositol 3-kinase is involved in Toll-like receptor 4-mediated cytokine expression in mouse macrophages.” *The European Journal of Immunology* 33, no. 3 (2003): 597-605.

O'Neill, L., Golenbock, D. and Bowie, A. “The history of Toll-like receptors - redefining innate immunity.” *Nature Reviews Immunology* 13, no. 6 (2013): 453-460.

Oppenheim, J., Rossio, J. and Gearing, A. *Clinical applications of cytokines, role in pathogenesis, diagnosis and therapy.* New York: Oxford University Press, 1993.

Ortega-Molina, A., Lopez-Guadamillas, E., Mattison, J., Mitchell, S., Munoz-Martin, M., Iglesias, G., Gutierrez, V., Vaughan, K., Szarowicz, M., Gonzalez-Gracia, I., Lopez, M., Cebrian, D., Martinez, S., Pastor, J., De Cabo, R. and Serrano, M. “Pharmacological inhibition of PI3K reduces adiposity and metabolic syndrome in obese mice and rhesus monkeys.” *Cell Metabolism* 21, no. 4 (2015): 558-570.

Ost, A., Svensson, K., Ruishalme, I., Brannmark, C., Franck, N., Krook, H., Sandstrom, P., Kjolhede, P. and Stralfors, P. “Attenuated mTOR signaling and enhanced autophagy in adipocytes from obese patients with type 2 diabetes.” *Molecular Medicine* 16, no. 7-8 (2010): 235-246.

Owen, J., Zhang, Y., Bae, S., Farooqi, M., Liang, G., Hammer, R., Goldstein, J. and Brown, M. “Insulin stimulation of SREBP-1c processing in transgenic rat hepatocytes requires p70 S6-kinase.” *Proceedings of the National Academy of Sciences of the USA* 109, no. 40 (2012): 16184-16189.

Pal, D., Dasgupta, S., Kundu, R., Maitra, S., Das, G., Mukhopadhyay, S., Ray, S., Majumdar, S. andBhattacharya, S. “Fetuin-A acts as an endogenous ligand of TLR4 to promote lipid-induced insulin resistance.” *Nature Medicine* 18, no. 8 (2012): 1279-1290.

Papadopoulos, C., Kirchner, P., Bug, M., Grum, D., Koerver, L., Schulze, N., Poehler, R., Dressler, A., Fengler, S., Arhzaouy, K., Lux, V., Ehrmann, M., Weihl, C. and Meyer, H. “VCP/p97 cooperates with YOD1, UBXD1 and PLAA to drive clearance of ruptured lysosomes by autophagy.” *The EMBO Journal* 36, no. 2 (2016): 135-150.

Park, B. and Lee, J. “Recognition of lipopolysaccharide pattern by TLR4 complexes.” *Experimental and Molecular Medicine* 45, no. 12 (2013): e66.

Park, D., Kim, J., Kim, S., Sonn, J., Bang, O., Kang, S., Kim, J. and Baek, S. “Akt a mediator ofsecretory phospholipase A2 receptor-involved inducible nitric oxide synthase expression.” *The Journal of Immunology* 170, no. 4 (2003): 2093-2099.

Pensa, S., Regis, G., Boselli, D., Novelli, F. and Poli, V. “STAT1 and STAT3 in tumorigenesis: two sides of the same coin?” *Madame Curie Bioscience Database*, 2013.

Platanias, L. “Mechanisms of type-I- and type-II-interferon-mediated signalling.” *Nature Reviews Immunology* 5, no. 5 (2005): 375-386.

Platanias, L., Uddin, S., Yetter, A., Sun, X. and White, M. “Type I interferon receptor mediates tyrosine phosphorylation of insulin receptor substrate 2.” *The Journal of Biological Chemistry* 271, no. 1 (1996): 278-82.

Pohl, C. and Dikic, I. “Fighting mycobacteria through ISGylation.” *EMBO Reports* 13, no. 10 (2012): 872-873.

Postic, C. and Girard, J. “Contribution of de novo fatty acid synthesis to hepatic steatosis and insulin resistance: lessons from genetically engineered mice.” *The Journal of Clinical Investigation* 118, no. 3 (2008): 829-838.

Poulain-Godefroy, O., Le Bacquer, O., Plancq, P., Lecoeur, C., Pattou, F., Fruhbeck, G. and Froguel, P. “Inflammatory role of Toll-like receptors in human and murine adipose tissue.” *Mediators of Inflammation* 823486 (2010).

Qi, L., Saberi, M., Zmuda, E., Wang, Y., Altarejos, J., Zhang, X., Dentin, R., Hedrick, S., Bandyopadhyay, G., Hai, T., Olefsky, J. and Montminy, M. “Adipocyte CREB promotes insulin resistance in obesity.” *Cell Metabolism* 9, no. 3 (2009): 277-286.

Rafols, E. “Adipose tissue: cell heterogeneity and functional diversity.” *Endocrinologia y Nutricion* 61, no. 2 (2014): 100-112.

Ramachandran, S., Venugopal, A., Kutty, V., Vinitha, A., Divya, G., Chitrasree, V., Mullassari, A., Pratapchandran, N., Santosh, K., Radhakrishna, P. and Kartha, C. “Plasma level of cyclophilin A is increased in patients with type 2 diabetes mellitus and suggests presence of vascular disease.” *Cardiovascular Diabetology* 13 (2014): 38.

Reaven, G. “Role of insulin resistance in human disease.” *Diabetes* 37, no. 12 (1988): 1595-1607.

Redmann, M., Benavides, G., Berryhill, T., Wani, W., Ouyang, X., Johnson, M., Ravi, S., Barnes, S., Darley-Usmar, V. and Zhang, J. “Inhibition of autophagy with bafilomycin and chloroquine decreases mitochondrial quality and bioenergetic function in primary neurons.” *Redox Biology* 11 (2017): 73-81.

Rhee, S., Jones, B., Toshchakov, V., Vogel, S. and Fenton, M. “Toll-like receptors 2 and 4 activate STAT1 serine phosphorylation by distinct mechanisms in macrophages.” *The Journal of Biological Chemistry* 278, no. 25 (2003): 22506-22512.

Richard, A. and Stephens, J. “The role of JAK-STAT signaling in adipose tissue function.” *Biochimica et Biophysica Acta* 1842, no. 3 (2014): 431-439.

Rittig, N., Bach, E., Thomsen, H., Pedersen, S., Nielsen, T., Jorgensen, J., Jessen, N. and Moller, N. “Regulation of lipolysis and adipose tissue signaling during acute endotoxin-induced inflammation: a human randomised crossover trial.” *PLoS One* 11, no. 6 (2016): e0162167.

Roca, H., Varsos, Z., Sud, S., Craig, M., Ying, C. and Pienta, K. “CCL2 and interleukin-6 promote survival of human CD11b+ peripheral blood mononuclear cells and induce M2-type macrophage polarization.” *The Journal of Biological Chemistry* 284, no. 49 (2009): 34342-34354.

Rock, K., Gramm, C., Rothstein, L., Clark, K., Stein, R., Dick, L., Hwang, D. and Goldberg, A. “Inhibitors of the proteasome block the degradation of most cell proteins and the generation of peptides presented on the MHC class I molecules.” *Cell* 78, no. 5 (1994): 761-771.

Roder, P., Wu, B., Liu, Y. and Han, W. “Pancreatic regulation of glucose homeostasis.” *Experimental and Molecular Medicine* 48, no. 3 (2016): 6413-6416.

Rodriguez, A., Pisani, D., Dechesne, C., Turc-Carel, C., Kurzenne, J., Wdziekonski, B., Villageois, A., Bagnis, C., Brettmayer, J., Groux, H., Ailhaud, G. and Dani, C. “Transplantation of a multipotent cell population from human adipose tissue induces dystrophin expression in the immunocompetent mdx mouse.” *The Journal of Experimental Medicine* 201, no. 9 (2005): 1327-1405.

Rosen, E. and Spiegelman, B. “What we talk about when we talk about fat.” *Cell* 156, no. 1-2 (2014): 20-44.

Ruan, H. and Lodish, H. “Insulin resistance in adipose tissue: direct and indirect effects of tumor necrosis factor-alpha.” *Cytokine and Growth Factor Reviews* 14, no. 5 (2003): 447-455.

Ruan, H., Miles, P., Ladd, C., Ross, K., Golub, T.,Olefsky, J. and Lodish, H. “Profiling gene transcription in vivo reveals adipose tissue as an immediate target of tumor necrosis factor-alpha: implications for insulin resistance.” *Diabetes* 51, no. 11 (2002): 3176-3188.

Ruvolo, P., Gao, F., Blalock, W., Deng, X. and Stratford May, W. “Ceramide regulates protein synthesis by a novel mechanism involving the cellular PKR activator RAX.” *The Journal of Biological Chemistry* 276, no. 15 (2001): 11754-11758.

Ryu, K., Maehr, R., Gilchrist, C., Long, M., Bouley, D., Mueller, B., Ploegh, H. and Kopito, R. “The mouse polyubiquitin gene Ubc is essential for fetal liver development, cell-cycle progression and stress tolerance.” *The EMBO Journal* 26, no. 11 (2007): 2693-2706.

Sadler, A. and Williams, B. “Interferon-inducible antiviral effectors.” *Nature Reviews Immunology* 8, no. 7 (2008): 559-568.

Sanchez-Infantes, D., White, U., Elks, C., Morrison, R., Gimble, J., Considine, R., Ferrante, A., Ravussin, E. and Stephens, J. “Oncostatin M is produced in adipose tissue and is regulated in conditions of obesity and type 2 diabetes.” *The Journal of Clinical Endocrinology and Metabolism* 99, no. 2 (2014): E217-E225.

Sarbassov, D., Ali, S., Sengupta, S., Sheen, J.-H., Hsu, P., Bagley, A., Markhard, A. and Sabatini, D. “Prolonged rapamycin treatment inhibits mTORC2 assembly and Akt/PKB.” *Molecular Cell* 22, no. 2 (2006): 159-168.

Sarjeant, K. and Stephens, J. “Adipogenesis.” *Cold Spring Harbor Perspective in Biology* 4, no. 9 (2012): a008417.

Sato, T., Selleri, C., Young, N. and Maciejewski, J. “Inhibition of interferon regulatory factor-1 expression results in predominance of cell growth stimulatory effects of interferon-gamma due to phosphorylation of STAT1 and STAT3.” *Blood* 90, no. 12 (1997): 4749-4758.

Schilling, J., Machkovech, H., He, L., Sidhu, R., Fujiwara, H., Weber, K., Ory, D. and Schaffer, J. “Palmitate and lipopolysaccharide trigger synergistic ceramide production in primary macrophages.” *The Journal of Biological Chemistry* 288, no. 5 (2013): 2923-2932.

Schmeisser, H., Bekisz, J. and Zoon, K. “New function of Type I IFN: induction of autophagy.” *The Journal of Interferon and Cytokine Research* 34, no. 2 (2014): 71-79.

Schoggins, J., Wilson, S., Panis, M., Murphy, M., Jones, C., Bieniasz, P. and Rice, C. “A diverse range of gene products are effectors of the type I interferon antiviral response.” *Nature* 472, no. 7344 (2011): 481-485.

Schraw, T., Wang, Z., Halberg, N., Hawkins, M. and Scherer, P. “Plasma adiponectin complexes have distinct biochemical characteristics.” *Endocrinology* 149, no. 5 (2008): 2270-2282.

Schuringa, J., Dekker, L., Vellenga, E. and Kruijer, W. “Sequential activation of Rac-1, SEK-1/MKK-4, and protein kinase Cdelta is required for interleukin-6-induced STAT3 Ser-727 phosphorylation and transactivation.” *The Journal of Biological Chemistry* 276, no. 29 (2001): 27709-27715.

Schweiger, M., Eichmann, T., Taschler, U., Zimmermann, R., Zechner, R. and Lass, A. “Measurement of lipolysis.” *Methods in Enzymology* 538 (2014): 171-193.

Schweiger, M., Schreiber, R., Haemmerle, G., Lass, A., Fledelius, C., Jacobsen, P., Tornqvist, H., Zechner, R. and Zimmermann, R. "Adipose triglyceride lipase and hormone-sensitive lipase are the major enzymes in adipose tissue triacylglycerol catabolism." *The Journal of Biological Chemistry* 281, no. 52 (2006): 40236-40241.

Sengupta, S., Peterson, T. and Sabatini, D. "Regulation of the mTOR complex 1 pathway by nutrients, growth factors and stress." *Molecular Cell* 40, no. 2 (2010): 310-322.

Senn, J. "Toll-like receptor-2 is essential for the development of palmitate-induced insulin resistnace in myotubes." *The Journal of Biological Chemistry* 281, no. 37 (2006): 26865-26875.

Senn, J., Klover, P., Nowak, I., Zimmers, T., Koniaris, L., Furlanetto, R. and Mooney, R. "Suppressor of cytokine signaling-3 (SOC-3), a potential mediator of interleukin-6-dependent insulin resistance in hepatocytes." *The Journal of Biological Chemistry* 278, no. 16 (2003): 13740-13746.

Shaw, R. "LKB1 and AMPK control of mTOR signalling and growth." *Acta Physiologica* 196, no. 1 (2009): 65-80.

Shen, S., Niso-Santano, M., Adjemian, S., Takehara, T., Malik, S., Minoux, H., Souquere, S., Marino, G., Lachkar, S., Senovilla, L., Galluzzi, L., Kepp, O., Pierron, G., Maiuri, M., Hikita, H., Kroemer, R. and Kroemer, G. "Cytoplasmic STAT3 represses autophagy by inhibiting PKR activity." *Molecular Cell* 48, no. 5 (2012): 667-680.

Shi, H., Kokoeva, M., Inouye, K., Tzameli, I., Yin, H. and Flier, J. "TLR4 links innate immunity and fatty acid-induced insulin resistance." *The Journal of Clinical Investigation* 116, no. 11 (2006): 3015-3025.

Singh, R., Kaushik, S., Wang, Y., Xiang, Y., Novak, I., Komatsu, M., Tanaka, K., Cuervo, A., Czaja, M. "Autophagy regulates lipid metabolism." *Nature* 458, no. 7242 (2009): 1131-1135.

Singh, R., Xiang, Y., Wang, Y., Baikati, K., Cuervo, A., Luu, Y., Tang, Y., Pessin, J., Schwartz, G. and Czaja, M. "Autophagy regulates adipose mass and differentiation in mice." *The Journal of Clinical Investigation* 119, no. 11 (2009): 3329-3339.

Sisler, J., Morgan, M., Raje, V., Grande, R., Derecka, M., Meier, J., Cantwell, M., Szczepanek, K., Korzun, W., Lesnefsky, E., Harris, T., Croniger, C. and Larner, A. "The signal transducer and activator of transcription 1 (STAT1) inhibits mitochondrial biogenesis in liver and fatty acid oxidation in adipocytes." *PLoS One* 10, no. 12 (2015): e0144444.

Song, M., Kim, K., Yoon, J. and Kim, J. "Activation of Toll-like receptor 4 is associated with insulin resistance in adipocytes." *Biochemical and Biophysical Research Communications* 346, no. 3 (2006): 739-745.

Song, Y., Altarejos, J., Goodarzi, M., Inoue, H., Guo, X., Berdeaux, R., Kim, J., Goode, J., Igata, M., Paz, J., Hogan, M., Singh, P., Goebel, N., Vera, L., Miller, N., Cui, J., Jones, M., CHARGE Consortium, Chen, Y., Taylor, K., Hsueh, W., Rotterm J. and Montminy, M. "The CREB coactivator CRTC3 links catecholamine signalling to energy balance." *Nature* 468, no. 7326 (2010): 933-939.

Speer, S., Li, Z., Buta, S., Payelle-Brogard, B., Qian, L., Vigant, F., Rubino, E., Gardner, T., Wedeking, T., Hermann, M., Duehr, J., Sanal, O., Tezcan, I., Mansouri, N., Tabarsi, P., Mansouri, D., Francois-Newton, V., Daussy, C., Rodriguez, M., Lenschow, D., Freiberg, A., Tortorella, D., Piehler, J., Lee, B., Gracia-Sastre, A., Pellegrini, S. and Bogunovic, D. "ISG15 deficiency and increased viral resistance in human but not mice." *Nature Communications* 7 (2016): 11496.

Spiller, S., Elson, G., Ferstl, R., Dreher, S., Mueller, T., Freudenberg, M., Daubeuf, B., Wagner, H. and Kirschning, C. "TLR4-induced IFN-gamma production increases TLR2 sensitivity and drives Gram-negative sepsis in mice." *The Journal of Experimental Medicine* 205, no. 8 (2008): 1747-1754.

Staiger, H., Staiger, K., Stefan, N., Wahl, H., Machicao, F., Kellerer, M. and Haring, H. "Palmitate-induced interleukin-6 expression in human coronary artery endothelial cells." *Diabetes* 53, no. 12 (2004): 3209-3216.

Stephens, J., Lumpkin, S. and Fishman, J. "Activation of signal transduces and activators of transcription 1 and 3 by leukemia inhibitory factor, oncostatin-M, and interferon-gamma in adipocytes." *The Journal of Biological Chemistry* 273, no. 47 (1998): 31408-31416.

Stephens, J., Morrison, R. and Plich, P. "The expression and regulation of STATs during 3T3-L1 adipocyte differentiation." *The Journal of Biological Chemistry* 271, no. 18 (1996): 10441-10444.

Steppan, C., Bailey, S., Bhat, S., Brown, E., Banerjee, R., Wright, C. Patel, H., Ahima, R. and Lazar, M. "The hormone resistin links obesity to diabetes." *Nature* 409, no. 6818 (2001): 307-312.

Stern, J., Rutkowski, J. and Scherer, P. "Adiponectin, leptin and fatty acids in the maintenance of metabolic homeostasis through adipose tissue crosstalk." *Cell Metabolism* 23, no. 5 (2016): 770-784.

Stralfors, P. and Honnor, R. "Insulin-induced dephosphorylation of hormone-sensitive lipase." *The European Journal of Biochemistry* 182, no. 2 (1989): 379-385.

Swaim, C., Scott, A., Canadeo, L. and Huibregtse, J. "Extracellular ISG15 signals cytokine secretion through the LFA-1 integrin receptor." *Molecular Cell* 68, no. 3 (2017): 581-590.

Szklarczyk, D., Franceschini, A., Wyder, S., Forslund, K., Heller, D., Huerta-Cepas, J., Simonovic, M., Roth, A., Santos, A., Tsafou, K., Kuhn, M., Bork, P., Jensen, L. and Von Mering, C. "STRING v10: protein-protein interaction networks, integrated over the tree of life." *Nucleic Acids Research* 43 (2015): D447-452.

Takeda, K., Kaisho, T. and Akira, S. "Toll-like receptors." *Annual Review of Immunology* 21 (2003): 335-376.

Takeda, K., Noguchi, K., Shi, W., Tanaka, T., Matsumoto, M., Yoshida, N., Kishimoto, T. and Akira, S. "Targeted disruption of the mouse Stat3 gene leads to early embryonic lethality." *Proceedings of the National Academy of Science of the USA* 94, no. 8 (1997): 3801-3804.

Takizawa, T., Ohashi, K. and Nakanishi, Y. "Possible involvement of double-stranded RNA-activated protein kinase in cell death by influenza virus infection." *The Journal of Virology* 70, no. 11 (1996): 8128-8132.

Tanabe, Y., Nishibori, T., Su, L., Arduini, R., Baker, D. and David, M. "Cutting edge: role of STAT1, STAT3, and STAT5 in IFN-alpha/beta responses in T lymphocytes." *The Journal of Immunology* 174, no. 2 (2005): 609-613.

Tang, Y., Wallace, M., Sanchez-Gurmaches, J., Hsiao, W., Li, H., Lee, P., Vernia, S., Metallo, C. and Guertin, D. "Adipose tissue mTORC2 regulates ChREBP-driven de novo lipogenesis and hepatic glucose metabolism." *Nature Communications* 7 (2016): 11365.

Tao, R., Gong, J., Luo, X., Zang, M., Guo, W., Wen, R. and Luo, Z. "AMPK exerts dual regulatory effects on the PI3K pathway." *The Journal of Molecular Signaling* 5, no. 1 (2010): 1-9.

Taylor, J., D'Cunha, J., Tom, P., O'Brien, W. and Borden, E. "Production of ISG-15, an interferon-inducible protein, in human corneal cells." *The Journal of Interferon and Cytokine Research* 16, no. 11 (1996): 937-940.

Tchoukalova, Y., Votruba, S., Tchkonia, T., Giorgadze, N., Kirkland, J. and Jensen, M. "Regional differences in cellular mechanisms of adipose tissue gain with overfeeding." *Proceedings of the National Academy of Science of the USA* 107, no. 42 (2010): 18226-18231.

Thong, F., Dugani, C. and Klip, A. "Turning signals on and off: GLUT4 traffic in the insulin-signaling highway." *Physiology* 20, no. 4 (2005): 271-284.

Tian, J., Zhang, X., Wu, H., Liu, C., Li, Z., Hu, X., Su, S., Wang, L. and Qu, L. "Blocking the PI3K/Akt pathway enhances mammalian reovirus replication by repressing IFN-stimulated genes." *Frontiers in Microbiology* 6 (2015): 886.

Tian-tian, Z., Zhang Jun-feng, M. and Ge Heng, M. "Functions of cyclophilin A in atherosclerosis." *Experimental and Clinical Cardiology* 18, no. 2 (2013): e118-e124.

Tsai, Y., Pestka, S., Wang, L., Runnels, L., Wan, S., Lyu, Y. and Liu, L. "Interferon-B signaling contributes to Ras transformation." *PLoS One* 6, no. 8 (2011): e24291.

Turpin, S., Nicholls, H., Willmes, D., Mourier, A., Brodesser, S., Wunderlich, C., Mauer, J., Xu, E., Hammerschmidt, P., Bronneke, H., Trufunovic, A., LoSasso, G., Wunderlich, F., Kornfeld, J-W., Bluher, M., Kronke, M. and Bruning, J. "Obesity-induced CerS6-dependent C16:0 ceramide production promotes weight gain and glucose intolerance." *Cell Metabolism* 20, no. 4 (2014): 678-686.

Uddin, S., Majchrzak, B., Wang, P., Modi, S., Khan, M., Fish, E. Platanias, L. "Interferon-dependent activation of the serine kinase PI 3-kinase requires engagement of the IRS pathway but not the Stat pathway." *Biochemical and Biophysical Research Communications* 270, no. 1 (2000): 158-162.

Uddin, S., Sassano, A., Deb, D., Verma, A., Majchrzak, B., Rahman, A., Malik, A., Fish, E. and Platanias, L. "Protein kinase C-delta is activated by type I interferons and mediates phosphorylation of Stat1 on serine 727." *The Journal of Biological Chemistry* 277, no. 17 (2002): 14408-14416.

Uddin, S., Yenush, L., Sun, X., Sweet, M., White, M. and Platanias, L. "Interferon-alpha engages the insulin receptor substrate-1 to associate with the phosphatidylinositol 3-kinase." *The Journal of Biological Chemistry* 270, no. 27 (1995): 15938-15941.

Uematsu, S. and Akira, S. *Toll-like receptors (TLRs) and their ligands.* Vol. 183, in *Handbook of Experimental Phamacology* . 2008.

Uthaiah, R., Praefcke, G., Howard, J. and Herrmann, C. "IIGP1, an interferon-gamma-inducible 47-kDa GTPase of the mouse, showing cooperative enzymatic activity and GTP-dependent multimerisation." *The Journal of Biological Chemistry* 278 (2003): 29336-29343.

Vaisse, C., Halaas, J., Horvath, C., Darnell, J., Stoffel, M. and Friedman, J. "Leptin activation of STAT3 in the hypothalamus of wild-type and ob/ob mice but not bd/bd mice." *Nature Genetics* 14, no. 1 (1996): 95-97.

Valvona, C., Fillmore, H., Nunn, P. and Pilkington, G. "The regulation and function of lactate dehydrogenase A: therapeutic potential in brain tumor." *Brain Pathology* 26 (2016): 3-17.

Van Boxel-Dezaire, A., Rani, M. and Stark, G. "Complex modulation of cell type-specific signaling in response to type I interferons." *Immunity* 25, no. 3 (2006): 361-372.

Van den Berghe, G. “How does blood glucose control with insulin save lives in intensive care?” *The Journal of Clinical Investigation* 114, no. 9 (2004): 1187-1195.

Vanhaesebroeck, B., Guillermet-Guibert, J., Graupera, M. and Bilanges, B. “The emerging mechanisms of isoform-specific PI3K signalling.” *Nature Reviews Molecular Cell Biology* 11, no. 5 (2010): 329-341.

Vilcek, J. “Novel interferons.” *Nature Immunology* 4, no. 1 (2003): 8-9.

Villarroya-Beltri, C., Guerra, S. and Sanchez-Madrid, F. “ISGylation - a key to lock the cell gates for preventing the spread of threats.” *The Journal of Cell Science* 130, no. 18 (2017): 2961-2969.

Vogt, P. and Hart, J. “PI3K and STAT3: a new alliance.” *Cancer Discovery* 1, no. 6 (2011): 481-486.

Wack, A., Terczynska-Dyla, E. and Hartmann, R. “Guarding the frontiers: the biology of type III interferons.” *Nature Immunology* 16 (2015): 802-809.

Wada, T., Hoshino, M., Kimura, Y., Ojima, M., Nakano, T., Koya, D., Tsuneki, H. and Sasaoka, T. “Both type I and II IFN induce insulin resistance by inducing different isoforms of SOCS expression in 3T3-L1 adipocytes.” *The American Journal of Physiology-Endocrinology and Metabolism* 300, no. 6 (2011): E1112-E1123.

Wang, D., Zhou, Y. Lei, W., Zhang, K., Shi, J., Hu, Y., Shu, G. and Song, J. “Signal transducer and activator of transcription 3 (STAT3) regulates adipocyte differentiatioin via peroxisome-proliferator-activated receptor gamma (PPARgamma).” *Biology of the Cell* 102, no. 1 (2009): 1-12.

Watt, M., Holmes, A., Pinnamaneni, S., Garnham, A., Steinberg, G., Kemp, B. and Febbraio, M. “Regulation of HSL serine phosphorylation in skeletal muscle and adipose tissue.” *The American Journal of Physiology-Endocrinology and Metabolism* 290, no. 3 (2006): E500-E508.

Wei, Y., Jinchuan, Y., Yi, L., Jun, W., Zhongqun, W. and Cuiping, W. “Antiapoptotic and proapoptotic signaling of cyclophilin A in endothelial cells.” *Inflammation* 36, no. 3 (2013): 567-572.

Weigert, C., Brodbeck, K., Staiger, H., Kausch, C., Machicao, F. Haring, H. and Schleicher, E. “Palmitate, but not unsaturated fatty acids, induces the expression of interleukin-6 in human myotubes through proteasome-dependent activation of nuclear factor-kappaB.” *The Journal of Biological Chemistry* 279, no. 23 (2004): 23942-23952.

Wen, Z., Zhong, Z. and Darnell, J. “Maximal activation of transcription by Stat1 and Stat3 requires both tyrosine and serine phosphorylation.” *Cell* 82, no. 2 (1995): 241-250.

Werneke, S., Schilte, C., Rohatgi, A., Monte, K., Michault, A., Arenzana-Seisdedos, F., Vanlandingham, D., Higgs, S., Fontanet, A., Albert, M. and Lenschow, D. “ISG15 is critical in the control of chikungunya virus infection independent of UBE1L mediated conjugation.” *PLoS Pathogenes* 7, no. 10 (2011): e1002322.

White, U. and Stephens, J. “The gp130 receptor cytokine family: regulators of adipocyte development and function.” *Current Pharmaceutical Design* 17, no. 4 (2011): 340-346.

White, U., Stewart, W., Mynatt, R. and Stephens, J. “Neuropoietin attenuates adipogenesis and induces insulin resistance in adipocytes.” *The Journal of Biological Chemistry* 283, no. 33 (2008): 22505-22512.

World Health Organisation. http://www.who.int/mediacentre/factssheets/fs311/en/ (accessed June 2016).

World Health Organisation. “Definition and diagnosis of diabetes mellitus and intermediate hyperglycemia: report of a WHO/IDF consultation.” Geneva, 2006.

World Health Organisation. “Global report on diabetes.” Geneva, 2016.

Xu, D., Zhang, T., Xiao, J., Zhu, K., Wei, R., Wu, Z., Meng, H., Li, Y. and Yuan, J. “Modification of BECN1 by ISG15 plays a crucial role in autophagy regulation by type I IFN/interferon.” *Autophagy* 11, no. 4 (2015): 617-628.

Xu, Y., Jagannath, C., Liu, X., Sharafkhaneh, A., Kolodziejska, K. and Eissa, T. “Toll-like receptor 4 is a sensor for autophagy associated with innate immunity.” *Immunity* 27, no. 1 (2007): 135-144.

Yaffe, M., Farr, G., Miklos, D., Horwich, A., Sternlicht, M. and Sternlicht, H. “TCP1 complex is a molecular chaperone in tubulin biogenesis.” *Nature* 358, no. 6383 (1992): 245-248.

Yanguez, E., Garcia-Culebras, A., Frau, A., Llompart, C., Knobeloch, K., Gutierrez-Erlandsson, S., Garcia-Sastre, A., Esteban, M. and Nieto, A. “ISG15 regulates peritoneal macrophages functionality against viral infection.” *PLoS pathogens* 9, no. 10 (2013): e1003632.

Yeh, J., Chinte, U. and Du, S. “Structure of glycerol-30phosphate dehydrogenase, an essential monotopic membrane enzyme involved in respiration and metabolism.” *The Proceedings of the National Academy of Sciences of the USA* 105, no. 9 (2008): 3280-3285.

Yeung, M., Chang, D., Camantigue, R. and Lau, A. “Inhibitory role of the host apoptogenic gene PKR in the establishment of persistent infection by encephalomyocarditis virus in U937 cells.” *Proceedings of the National Academy of Sciences of the USA* 96, no. 21 (1999): 11860-11865.

Yin, J., Wang, Y., Gu, L., Fan, N., Ma, Y. and Peng, Y. “Palmitate induces endoplasmic reticulum stress and autophagy in mature adipocytes: implications for apoptosis and inflammation.” *The International Journal of Molecular Medicine* 35, no. 4 (2015): 932-940.

Ying, H., Da, L., Yu-xiu, S., Yu, X., Li-xia, L., Li-mei, X. and Wei-dong, R. “TLR4 mediates MAPK-STAT3 axis activation in bladder epithelial cells.” *Inflammation* 36, no. 5 (2013): 1064-1074.

You, L., Wang, Z., Li, H., Shou, J., Jing,Z., Xie, J., Sui,X., Pan, H. and Han, W. “The role of STAT3 in autophagy.” *Autophagy* 11, no. 5 (2015): 729-739.

Zaragosi, L., Ailhaud, G. and Dani, C. “Autocrine fibroblast growth factor 2 signaling is critical for self-renewal of human multipotent adipose-derived stem cells.” *Stem Cells* 24, no. 11 (2006): 2412-2419.

Zhang, D. and Zhang, D. “Interferon-stimulated gene 15 and the protein ISGylation system.” *The Journal of Interferon and Cytokine Research* 31, no. 1 (2011): 119-130.

Zhang, K., Guo, W., Yang, Y. and Wu, J. “JAK2/STAT3 pathway is involved in early stage of adipogenesis through regulating C/EBPB transcription.” *The Journal of Cellular Biochemistry* 112, no. 2 (2011): 488-497.

Zhang, Y., Proenca, R., Maffei, M., Barone, M., Leopold, L. and Friedman, J. “Positional cloning of the mouse obese gene and its human homologue.” *Nature* 372, no. 6505 (1994): 425-432.

Zhou, Z., Hamming, O., Ank, N., Paludan, S., Nielsen, A. and Hartmann, R. “Type III interferon (IFN) induces a type I IFN-like response in a restricted subset of cells through signaling pathways involving both the Jak-STAT pathway and the mitogen-activated protein kinases.” *The Journal of Virology* 81, no. 14 (2007): 7749-7758.

Zimmermann, R., Strauss, J., Haemmerle, G., Schoiswohl, G., Birner-Gruenberger, R., Riederer, M., Lass, A., Neuberger, G., Eisenhaber, F., Hermetter, A. and Zechner, R. “Fat mobilisation in adipose tissue is promoted by adipose triglyceride lipase.” *Science* 306, no. 5700 (2004): 1383-1386.

Zvonic, S., Hogan, J., Arbour-Reily, P., Mynatt, R. and Stephens, J. “Effects of cadiotrophin on adipoctes.” *The Journal of Biological Chemistry* 279, no. 46 (2004): 47572-47579.

Zwick, R., Guerrero-Juarez, C., Horsley, V. and Plikus, M. “Anatomical, physiological, and functional diversity of adipose tissue.” *Cell Metabolism* 27, no. 1 (2018): 68-83.

VII. 1. Genes identified by the transcriptome analysis

Table 15. *List of genes identified by the transcriptome analysis*. The name of the genes is followed by their symbol, their NCBI ID and their Ensembl ID in brackets.

	Down-regulated by palmitate	*Up-regulated by palmitate*	*Down-regulated by A66*	*Up-regulated by A66*
Effect abrogated by A66	MLX interacting protein-like, *Mlxipl* (58805) [ENSMUSG00000005373] Carboxypeptidase M, *Cpm* (70574) [ENSMUSG00000020183] Pellino 3, *Peli3* (240518) [ENSMUSG00000024901] Haptoglobin, *Hp* (15439) [ENSMUSG00000031722] Kinesin family member 15, *Kif15* (209737) [ENSMUSG00000036768] DNA replication helicase 2 homolog, *Dna2* (327762) [ENSMUSG00000036875] Apolipoprotein C-I, *Apoc1* (11812) [ENSMUSG00000040564] Glucokinase, *Gck* (103988) [ENSMUSG00000041798] Excision repair cross-complementing rodent repair deficiency complementation group 6 like, *Ercc6l* (76251) [ENSMUSG00000051220] Predicted gene 5460, *Gm5460* (432838) [ENSMUSG00000072624] Homeobox B3 and homeobox B2, opposite	Nucleolar protein 3, *NoI3* (78688) [ENSMUSG00000014776] Lipin 3, *Lpin3* (64899) [ENSMUSG00000027412] Secreted frizzled-related protein 2, *Sfrp2* (20319) [ENSMUSG00000027996] Interferon-induced protein with tetratricopeptide repeats 1, *Ifit1* (15957) [ENSMUSG00000034459] Growth differentiation factor 15, *Gdf15* (23886) [ENSMUSG00000038508] RIKEN cDNA I830012O16 gene, *I830012O16Rik* (667370) [ENSMUSG00000062488] Shroom family member 4, *Shroom4* (208431) [ENSMUSG00000068270] Immunity-related GTPase family M member 2, *Irgm2* (54396) [ENSMUSG00000069874] Jun D proto-oncogene, *Jund* (16478) [ENSMUSG00000071076] Interferon-induced protein with tetratricopeptide repeats 3, *Ifit3* (15959) [ENSMUSG00000074891	-	-

	strand, *Hoxb3os* (102632302) [ENSMUSG00000084844]	6] Predicted gene 36963, *Gm36963* [ENSMUSG00000103932]		
Effect sustained in presence of A66	Ring finger protein 145, *Rnf145* (74315) [ENSMUSG00000019189] AarF domain containing kinase 3, *Adck3* (67426) [ENSMUSG00000026489] Adenylate cyclase activating polypeptide 1 receptor 1, *Adcyap1r1* (11517) [ENSMUSG00000029778] Integrin α L, *Itgal* (16408) [ENSMUSG00000030830] Phospholipase C, β 2, *Plcb2* (18796) [ENSMUSG00000040061]	Cytochrome P450, family 51, *Cyp51* (13121) [ENSMUSG00000001467] Mevalonate diphosphodecarboxylase, *Myd* (192156) [ENSMUSG00000006517] Chemokine (C-C motif) ligand 9, *Ccl9* (20308) [ENSMUSG00000019122] ATP citrate lyase, *Acly* (104112) [ENSMUSG00000020917] Farnesyl diphosphate farnesyl transferase 1, *Fdft1* (14137) [ENSMUSG00000021273] Fatty acid desturase 2, *Fads2* (56473) [ENSMUSG00000024665] Aldehyde dehydrogenase family 1, subfamily A7, *Aldh1a7* (26358) [ENSMUSG00000024747] Transmembrane 7 superfamily member 2, *Tm7sf2* (73166) [ENSMUSG00000024799] Hydroxysteroid (17-β) dehydrogenase 7, *Hsd17b7* (15490) [ENSMUSG00000026675] Acyl-CoA synthetase short-chain family member 2, *Acss2* (60525) [ENSMUSG00000027605] Low density lipoprotein receptor-related protein 8, apolipoprotein e receptor, *Lrp8* (16975) [ENSMUSG00000028613] NAD(P) dependent steroid dehydrogenase-like, *Nsdhl* (18194) [ENSMUSG00000031349] Methylsterol monoxygenase 1, *Msmo1* (66234)	-	-

		[ENSMUSG00000031604] Lanosterol synthase, *Lss* (16987) [ENSMUSG00000033105] Insulin induced gene 1, *Insig1* (231070) [ENSMUSG00000045294] 7-dehydrocholesterol reductase, *Dhcr7* (13360) [ENSMUSG00000058454] Farnesyl diphosphate synthetase, *Edps* (110196) [ENSMUSG00000059743] GRAM domain containing 2, *Gramd2* (546134) [ENSMUSG00000074259]		
Effect abrogated by palmitate	-	-	Interferon regulatory factor 9, *Irf9* (16391) [ENSMUSG00000002325] Proline dehydrogenase, *Prodh* (19125) [ENSMUSG00000003526] Hypoxia inducible factor 3, α subunit, *Hif3a* (53417) [ENSMUSG00000004328] Synapsin II, *Syn2* (20965) [ENSMUSG00000009394] Stanniocalcin 1, *Stc1* (20855) [ENSMUSG00000014813] DEXH (Asp-Glu-X-His) box polypeptide 58, *Dhx58* (80861) [ENSMUSG00000017830] Radcal S-adenosyl methionine domain containing 2, *Rsad2* (58185) [ENSMUSG00000020641] MX dynamin-like GTPase 2, *Mx2* (17858) [ENSMUSG00000023341] Calcium/calmodulin-dependent protein kinase II α, *Camk2a* (12322) [ENSMUSG00000024617] Interferon regulatory	Matric metallopeptidase 11, *Mmp11* (17385) [ENSMUSG00000009001] Immediate early response 3, *Ier3* (15937) [ENSMUSG00000003541] Transcription factor AP4, *Tfap4* (83383) [ENSMUSG00000005718] Nuclear receptor subfamily 1, group D, member 2, *Nr1d2* (353187) [ENSMUSG00000021775] Proviral integration site 1, *Pim1* (18712) [ENSMUSG00000024014] Ankyrin repeat domain 1, *Ankrd1* (107765) [ENSMUSG00000024803] Regulator of G-protein signaling 16, *Rgs16* (19734) [ENSMUSG00000026475] Cysteine rich protein 61, *Cyr61* (16007) [ENSMUSG00000028195] Sialic acid binding Ig-like lectin G, *Siglecg* (243958) [ENSMUSG00000030468] Transgelin, *Tagln*

			factor 7, *Irf7* (54123) [ENSMUSG00000025498] Neuronal PAS domain protein 2, *Npas2* (18143) [ENSMUSG00000026077] Interferon-induced protein 44, *Ifi44* (99899) [ENSMUSG00000028037] Guanylate binding protein 3, *Gbp3* (55932) [ENSMUSG00000028268] Hect domain and RLD 6, *Herc6* (67138) [ENSMUSG00000029798] Ubiquitin specific peptidase 18, *Usp18* (24110) [ENSMUSG00000030107] Apolipoprotein C-III, *Apoc3* (11814) [ENSMUSG00000032081] 2'-5' oligoadenylate synthetase 2, *Oas2* (246728) [ENSMUSG00000032690] Ring finger protein, transmembrane 2, *Rnft2* (269695) [ENSMUSG00000032850] Receptor transporter protein 4, *Rtp4* (67775) [ENSMUSG00000033355] Interferon-induced protein with tetratricopeptide repeats 1, *Ifit1* (15957) [ENSMUSG00000034459] Schlafen 8, *Slfn8* (276950) [ENSMUSG00000035208] Interferon stimulated gene 15, *Isg15* (100038882) [ENSMUSG00000035692] DEAD (Asp-Glu-Ala-Asp) box polypeptide 60, *Ddx60* (234311) [ENSMUSG00000037921] Olfactomedin-like 2B, *Olfml2b* (320078) [ENSMUSG00000038465]	(21345) [ENSMUSG00000032085] Ubiquitin D, *Ubd* (24108) [ENSMUSG00000035186] Lipid phosphate phosphatase-relate protein type 3, *Lppr3* (216152) [ENSMUSG00000035835] Ectonucleotide pyrophosphatase/ phosphodiesterase 1, *Enpp1* (18605) [ENSMUSG00000037370] Ribosomal protein S21, *Rps21* (66481) [ENSMUSG00000039001] Von Willebrand factor A domain containing 1, *Vwa1* (246228) [ENSMUSG00000042116] Coiled-coil domain containing 141, *Ccdc141* (545428) [ENSMUSG00000044033] Calcium/calmodulin-dependent protein kinase II inhibitor 1, *Camk2n1* (66259) [ENSMUSG00000046447] DEPP1 autophagy regulator, *Depp1* (213393) [ENSMUSG00000048489] Phosphatidylinositol-3, 4, 5-trisphosphate-dependent Rac exchange factor 2, *Prex2* (109294) [ENSMUSG00000048960] Nyctalopin, *Nyx* (236690) [ENSMUSG00000051228] Granzyme M (lymphocyte met-ase 1), *Gzmm* (16904) [ENSMUSG00000054206] Predicted gene 7536, *Gm7536* (665189) [ENSMUSG00000057036] D site albumin promoter binding protein, *Dbp* (13170) [ENSMUSG00000059824]

			3] Interferon activated gene 203, *Ifi203* (15950) [ENSMUSG00000039997] Flavin containing monooxygenase 1, *Fmo1* (14261) [ENSMUSG00000040181] DEAD (Asp-Glu-Ala-Asp) box polypeptide 58, *Ddx58* (230073) [ENSMUSG00000040296] XIAP associated factor 1, *Xaf1* (327959) [ENSMUSG00000040483] Phosphoglucomutase 5, *Pgm5* (226041) [ENSMUSG00000041731] Interferon inducible GTPase 1, *Iigp1* (60440) [ENSMUSG00000054072] Apolipoprotein L 9a, *Apol9a* (223672) [ENSMUSG00000057346] Interferon induced protein with tetratricopeptide repeats 1B like 2, *Ifit1bl2* (112419) [ENSMUSG00000067297] Lysophosphatidic acid receptor 5, *Lpar5* (381810) [ENSMUSG00000067714] PHD finger protein 11D, *Phf11d* (219132) [ENSMUSG00000068245] Schlafen 9, *Slfn9* (237886) [ENSMUSG00000069793] Immunity-related GTPase family M member 2, *Irgm2* (54396) [ENSMUSG00000069874] Predicted gene 11966, *Gm11966* [ENSMUSG00000080904] Predicted gene 20645, *Gm20645* [ENSMUSG00000093470] RIKEN cDNA	Mitochondrially encoded 12S rRNA, *Mt-Rnr1* [ENSMUSG00000064337] RNA, 7SK, nuclear, *Rn7sk* (19817) [ENSMUSG00000065037] Ribonuclease L (2', 5'-oligoisoadenylate synthetase-dependent), *Rnasel* (24014) [ENSMUSG00000066800] Collagen, type XXVIII, α1, *Col28a1* (213945) [ENSMUSG00000068794] Acyl-CoA thioesterase 1, *Acot1* (26897) [ENSMUSG00000072949] Lymphocyte antigen 6 complex, locus C1, *Ly6c1* (17067) [ENSMUSG00000079018] Predicted gene 10177, *Gm10177* (100042561) [ENSMUSG00000090136] Ribonuclease P RNA component H1, *Rpph1* (85029) [ENSMUSG00000092837] RIKEN cDNA F830112A20, *F839112A20Rik* (100038576) [ENSMUSG00000103159]

			2610528A11 gene, *2610528A11Rik* (70045) [ENSMUSG00000096001]	
Effect sustained in presence of palmitate	-	-	2'-5' oligoadenylate synthetase-like 2, *Oasl2* (23962) [ENSMUSG00000029561]	*Solute carrier family 7, member 7, Slc7a7* (20540) [ENSMUSG00000000958]

VII. 2. Media preparation

Table 16. *Media used in the culture of 3T3-L1 cells*. All DMEM, sera and antibiotics used were from *Life Technologies, Gibco*.

	10% Calf serum/DMEM	***10% FBS/DMEM***	***SF DMEM***
Media	500 mL 1X DMEM + GlutaMAX™ (4.5 g/L D-Glucose)	500 mL 1X DMEM + GlutaMAX™ (4.5 g/L D-Glucose)	500 mL 1X DMEM + GlutaMAX™ (4.5 g/L D-Glucose)
Serum	50 mL Newborn Calf Serum Heat Inactivated	FBS 50 mL	-
Antibiotics	5 mL 100X P/S	5 mL 100X P/S	5 mL 100X P/S

Table 17. *Media used in the culture of hMADS cells.* All DMEM and additional supplements were purchased from *Lonza, BioWhittaker* while sera and antibiotics were from *Life Technologies, Gibco*.

	hMADS complete media	***hMADS SF media***	***Ham's F12***
Media	500 mL 1X DMEM (1 g/L glucose)	500 mL 1X DMEM (1 g/L glucose)	Ham's F12 with L-Glutamine
Serum	50 mL FBS	-	-
Antibiotics	5 mL 100X P/S	5 mL 100X P/S	5 mL 100X P/S
Additional supplements	5 mL Hepes buffer (1 M)	5 mL Hepes buffer (1 M)	-
	5 mL L-Glutamine (200 mM)	5 mL L-Glutamine (200 mM)	-

VII. 3. Recipes for cell differentiation

VII. 3. 1. 3T3-L1 differentiation

1. *IBMX solution:* dissolve IBMX (*Sigma-Aldrich*) in a solution made of 0.1 N potassium hydroxide to a final concentration of 0.0111 g/mL. Filter sterilise through a 0.22 μm syringe filter.

2. *Insulin stock solution:* 1 mM in 0.02 M HCl. Filter sterilise through a 0.22 μm syringe filter and store at 4ºC.

3. *Dexamethasone stock solution (Sigma-Aldrich):* make up 10 mM in 100% ethanol. Filter sterilise through a 0.22 μm syringe filter and store at 4ºC.

4. *Rosiglitazone (Cayman Chemical):* make up 10 mM in dimethyl sulfoxide

(DMSO). Keep in aliquots at -20ºC.

5. *MDI Induction Media:*

To required volume of 10% FBS/DMEM supplemented with P/S add:

- 1:100 IBMX (final concentration: 0.5 mM);
- 1:1,000 insulin (final concentration: 1 μM);
- 1:10,000 dexamethasone (final concentration: 1 μM);
- 1:10,000 rosiglitazone (final concentration: 1 μM).

6. *Insulin media:* to required volume of 10% FBS/DMEM supplemented with P/S add insulin diluting 1:5,000 (200 nM).

VII. 3. 2. hMADS differentiation

1. *Transferrin (Sigma-Aldrich):* dilute 100 mg in 10 mL PBS and sterile filter the solution (10 mg/mL). Dilute 1:10 in PBS to get 1 mg/mL aliquots.

2. *Triiodothyronine (T3) (Sigma-Aldrich):* dissolve 1.346 mg in 1 mL DMSO to get 2 mM. Dilute 1:1,000 in DMSO to get 2 μM.

3. *Differentiation media:* to the required volume of a solution made up of equal volumes of SF DMEM supplemented with P/S and Ham's F12 supplemented with P/Sadd:

- 1:100 IBMX (final concentration: 0.5 mM);
- 1:1,000 human insulin (*Sigma-Aldrich*) (final concentration: 1.74 μM);
- 1:10,000 dexamethasone (final concentration: 1 μM);

- 1:10,000 rosiglitazone (final concentration: 1 μM);
- 1:10,000 T3 (final concentration: 0.2 nM);
- 1:100 Transferrin (final concentration: 10 μg/mL).

VII. 4. Stock solutions for treatments

VII. 4. 1. 5 mM stock palmitate – 10% BSA:

1. *75 mM palmitate solution:* weigh 19.2 mg palmitic acid (*Sigma-Aldrich*) in a 1.5 mL eppendorf tube. Dissolve in 1 mL 0.1N NaOH by heating at 70^{o}C in heating block and vortexing.

2. *Coupling to BSA (palmitate to BSA molar ratio ~3:1):* prepare 14.5 mL 10% FFA free-BSA (*Sigma-Aldrich*) (1.5 mM) in antibiotics-free SF DMEM (low glucose [LG]) (*Life Technologies, Gibco*). Place 9.5 mL of the BSA solution in a water bath at 40^{o}C (the remaining 5 mL are used as control). Add 670 μL of the palmitate solution dropwise into the BSA solution while stirring at 40^{o}C and stir the solution for 30 min. Filter sterilize through 0.45 μm filter and make 1 mL aliquots which are stored at -20^{o}C.

VII. 4. 2. 5 mM unconjugated stock palmitate

The same protocol at the palmitate 3:1 BSA was used to make unconjugated palmitate except plain SF DMEM (LG) was used instead of the BSA solution.

VII. 5. 1% TX-100 lysis buffer

1. To make 400 mL 2X lysis buffer, the final molarity is in brackets:

Tris base (*Sigma-Aldrich*) (50 mM)	*4.8 g*
Sodium chloride (*Fisher Scientific*) (100 mM)	*4.7 g*
Sodium fluoride (*Sigma-Aldrich*) (50 mM)	*1.7 g*
EDTA (*Sigma-Aldrich*) (5 mM)	*1.2 g*
Ethylene glycol tetraacetic acid (*Sigma-Aldrich*) (2 mM)	*0.61 g*
Sodium β-glycerophosphate pentahydrate (*Alfa Aesar*) (40 mM)	*9.8 g*
Sodium pyrophosphate (*Alfa Aesar*) (10 mM)	*2.1 g*
1% TX-100 (*Alfa Aesar*)	*8 mL (drop-wise)*

- Adjust pH to 7.4 with concentrated HCl;
- Add deionised water up to 400 mL.

2. On ice add inhibitors to 5 mL of 2X lysis buffer diluted in 4.8 mL of deionised water. The concentration of the stock solutions is in brackets:

Phenylmethylsulfonyl fluoride (100 mM in ethanol) (*Thermo Scientific*)	*100 μL*
Sodium orthovanadate (*Sigma-Aldrich*) (100 mM)	*100 μL*
Aprotinin (*Sigma-Aldrich*) (10 mg/mL in MilliQ water)	*10 μL*
Leupeptin (*Sigma-Aldrich*) (10 mg/mL MilliQ water)	*10 μL*
Pepstatin A (*Sigma-Aldrich*) (1 mg/mL in methanol)	*10 μL*

- Vortex.

VII. 6. Electrophoresis sample buffer 4X

- 250 mM Tris-HCl, pH 6.8
- 8 % SDS (*Fisher Scientific*)
- 40 % glycerol (*Fisher Scientific*)
- 0.04 % bromophenol blue sodium salt (*Sigma-Aldrich*)

Mix 25 mL 1M DTT with 75 mL buffer just before use.

For 75 mL (prepare as for 100 mL – this takes into account the dilution from the addition of the DTT solution), heat and stir (50C):

1M Tris-HCl pH 6.8	*25 mL*
SDS	*8 g*
Glycerol	*40 mL*
Bromophenol blue	*40 mg*

VII. 7. SDS-PAGE gel preparation (two mini gels – 10% SDS-acrylamide)

1. *Separating gel:*

1.5 M Tris-HCl pH 8.8 (375.6 mM)	*4.5 mL*
Deionised water	*7.1 mL*
30% acrylamide solution (*Sigma-Aldrich*) (1.4 M)	*6.0 mL*
10% SDS (3.5 mM)	*180 µL*
10% ammonium persulfate (*Sigma-Aldrich*) (4.4 mM)	*180 µL*

Tetramethylethylenediamine (TEMED) (*Sigma-Aldrich*) (~ 99%) *10 μL*

- Mix and pour between plates.
- Layer deionised water on top.
- Allow to set for 30 min.

Note: for a 15% SDS-acrylamide the volumes of water and acrylamide are switched to 4.1 and 9.0 mL, respectively.

2. *Stacking gel:*

1 M Tris-HCl pH 6.8 (125.5 mM)	*1.25 mL*
Deionised water	*6.8 mL*
30% acrylamide solution (720.4 mM)	*1.7 mL*
10% SDS (3.5 mM)	*100 μL*
10% ammonium persulfate (4.4 mM)	*100 μL*
TEMED	*10 μL*

- Mix and pour between plates on top of the separating gel after removing the layer of deionised water.
- Place a 1.5 mm comb into each gel.
- Allow to set for 30 min.
- When set submerge with 1X running buffer.

3. *Running buffer 10X:*

Glycine (*VWR International*) (1.9 M)	*144 g*
Tris base (247.6 mM)	*30 g*
SDS (34.7 mM)	*10 g*

- Mix and make up a total volume of 1L with deionised water. Store at room

temperature.

4. *Transfer buffer 10X:*

Glycine (1.9 M)	*144 g*
Tris base (247.6 mM)	*30 g*

- Mix and make up a total volume of 1L with deionised water. Store at room temperature.

Transfer buffer 1X:

10X transfer buffer stock solution	*100 mL*
Methanol	*200 mL*
Deionised water	*700 mL*

- Store at 4ºC.

5. *TBS-T buffer 10X:*

Tris base (199.9 mM)	*24.22 g*
NaCl (*VWR International*) (1.5 M)	87.66 *g*

- Add 900 mL deionised water and dissolve;
- Adjust pH to 7.4 with HCl 37%;
- Add 10 mL Tween-20 while stirring;
- Make up a total volume of 1L with deionised water. Store at room temperature.

VII. 8. Tris-Tricine gel

1. *Separating gel:*

Deionised water	*5.4 mL*
30% acrylamide solution (1.7 M)	*9 mL*
Gel buffer	*8 mL*
10% ammonium persulfate (3.9 mM)	*200 µL*
TEMED	*20 µL*

- Mix and pour between plates.
- Layer deionised water on top.
- Allow to set for 30 min.

2. *Stacking gel:*

Deionised water	*5.56 mL*
30% acrylamide solution (539.5 mM)	*1.3 mL*
Gel buffer	*3.2 mL*
10% ammonium persulfate (4.3 mM)	*100 µL*
TEMED	*10 µL*

- When set submerge with anode buffer under the tank and cathode buffer between the gel.

3. *Anode buffer 10X (pH 8.9):*

Tris base (2 M)	*242 g*

- Adjust pH to 8.9 with 37% HCl and make up a total volume of 1L with deionised

water. Store at room temperature.

4. *Cathode buffer 10X:*

Tricine (*VWR International*) (1 M)	*179 g*
Tris base (1 M)	*121g*
SDS (34.7 mM)	*10 g*

- Mix and make up a total volume of 1L with deionised water. Store at room temperature.

5. *Gel buffer (pH 8.45):*

Tris base (3 M)	*72.66 g*
SDS (2.1 mM)	0.6 *g*

- Adjust pH to 8.45 with 37% HCl and make up a total volume of 200 mL with deionised water. Store at room temperature.

VII. 9. Primary antibody solution

- Dissolve 1.5 g of BSA in 50 mL TBS-T.
- Add 50 µL 1:1,000 NaN_2 (20%) to the BSA solution.
- Add the chosen primary antibody according to the dilution factor specified by the manufacturer.

VII. 10. 2X HBS buffer

Hepes	*50 mM*
NaCl	*280 mM*
Na_2HPO_4 (*Sigma-Aldrich*)	*1.5 mM*

- Adjust pH to 7.0 using 37% HCl and filter sterilise. Store at -20°C.

VII. 11. One-way ANOVA analyses

For *figure 41B*:

One-way ANOVA:

	Sum of Squares	df	Mean Square	F	Sig.
Between Groups	3.793	12	.316	8.674	.000
Within Groups	.692	19	.036		
Total	4.485	31			

Multiple comparison: Tukey HSD *post hoc* test

(I) Treatment		*Mean Difference (I-J)*	*Std. Error*	*Sig.*	*95% Confidence Interval*	
					Lower Bound	Upper Bound
1.00	*2.00*	-.20451	.17426	.990	-.8593	.4503
	3.00	-.69594	.19089	.062	-1.4133	.0214
	4.00	-.24224	.19089	.981	-.9596	.4751
	5.00	.63186	.19089	.117	-.0855	1.3492
	6.00	-.13416	.19089	1.000	-.8515	.5832
	7.00	-.01005	.17426	1.000	-.6649	.6448
	8.00	.10621	.17426	1.000	-.5486	.7610
	9.00	.38077	.17426	.611	-.2741	1.0356
	10.00	.44897	.17426	.384	-.2059	1.1038
	11.00	-.06575	.17426	1.000	-.7206	.5891
	12.00	-.49977	.19089	.362	-1.2171	.2176

	13.00	.29596	.19089	.925	-.4214	1.0133
2.00	*1.00*	.20451	.17426	.990	-.4503	.8593
	3.00	-.49143	.17426	.269	-1.1463	.1634
	4.00	-.03773	.17426	1.000	-.6926	.6171
	5.00	.83637*	.17426	.006	.1815	1.4912
	6.00	.07035	.17426	1.000	-.5845	.7252
	7.00	.19445	.15586	.983	-.3912	.7802
	8.00	.31072	.15586	.725	-.2750	.8964
	9.00	.58528	.15586	.050	-.0004	1.1710
	10.00	.65347*	.15586	.021	.0678	1.2392
	11.00	.13876	.15586	.999	-.4469	.7245
	12.00	-.29526	.17426	.874	-.9501	.3596
	13.00	.50047	.17426	.248	-.1544	1.1553
3.00	*1.00*	.69594	.19089	.062	-.0214	1.4133
	2.00	.49143	.17426	.269	-.1634	1.1463
	4.00	.45370	.19089	.496	-.2636	1.1710
	5.00	1.32780*	.19089	.000	.6105	2.0451
	6.00	.56178	.19089	.221	-.1556	1.2791
	7.00	.68589*	.17426	.035	.0311	1.3407
	8.00	.80215*	.17426	.009	.1473	1.4570
	9.00	1.07671*	.17426	.000	.4219	1.7315
	10.00	1.14491*	.17426	.000	.4901	1.7997
	11.00	.63019	.17426	.066	-.0246	1.2850
	12.00	.19617	.19089	.997	-.5212	.9135
	13.00	.99190*	.19089	.003	.2746	1.7092
4.00	*1.00*	.24224	.19089	.981	-.4751	.9596
	2.00	.03773	.17426	1.000	-.6171	.6926
	3.00	-.45370	.19089	.496	-1.1710	.2636
	5.00	.87410*	.19089	.009	.1568	1.5914
	6.00	.10808	.19089	1.000	-.6093	.8254
	7.00	.23219	.17426	.973	-.4227	.8870
	8.00	.34845	.17426	.722	-.3064	1.0033
	9.00	.62301	.17426	.071	-.0318	1.2778
	10.00	.69121*	.17426	.033	.0364	1.3460
	11.00	.17649	.17426	.997	-.4783	.8313
	12.00	-.25753	.19089	.970	-.9749	.4598
	13.00	.53820	.19089	.269	-.1791	1.2555
5.00	*1.00*	-.63186	.19089	.117	-1.3492	.0855
	2.00	-.83637*	.17426	.006	-1.4912	-.1815
	3.00	-1.32780*	.19089	.000	-2.0451	-.6105
	4.00	-.87410*	.19089	.009	-1.5914	-.1568
	6.00	-.76601*	.19089	.030	-1.4834	-.0487
	7.00	-.64191	.17426	.058	-1.2967	.0129

	8.00	-.52565	.17426	.196	-1.1805	.1292
	9.00	-.25109	.17426	.953	-.9059	.4038
	10.00	-.18289	.17426	.996	-.8377	.4719
	11.00	-.69761*	.17426	.031	-1.3524	-.0428
	12.00	-1.13162*	.19089	.001	-1.8490	-.4143
	13.00	-.33590	.19089	.847	-1.0532	.3814
6.00	*1.00*	.13416	.19089	1.000	-.5832	.8515
	2.00	-.07035	.17426	1.000	-.7252	.5845
	3.00	-.56178	.19089	.221	-1.2791	.1556
	4.00	-.10808	.19089	1.000	-.8254	.6093
	5.00	.76601*	.19089	.030	.0487	1.4834
	7.00	.12410	.17426	1.000	-.5307	.7789
	8.00	.24037	.17426	.965	-.4145	.8952
	9.00	.51493	.17426	.217	-.1399	1.1698
	10.00	.58312	.17426	.110	-.0717	1.2380
	11.00	.06841	.17426	1.000	-.5864	.7232
	12.00	-.36561	.19089	.769	-1.0829	.3517
	13.00	.43012	.19089	.570	-.2872	1.1475
7.00	*1.00*	.01005	.17426	1.000	-.6448	.6649
	2.00	-.19445	.15586	.983	-.7802	.3912
	3.00	-.68589*	.17426	.035	-1.3407	-.0311
	4.00	-.23219	.17426	.973	-.8870	.4227
	5.00	.64191	.17426	.058	-.0129	1.2967
	6.00	-.12410	.17426	1.000	-.7789	.5307
	8.00	.11626	.15586	1.000	-.4694	.7020
	9.00	.39083	.15586	.421	-.1949	.9765
	10.00	.45902	.15586	.220	-.1267	1.0447
	11.00	-.05570	.15586	1.000	-.6414	.5300
	12.00	-.48971	.17426	.273	-1.1445	.1651
	13.00	.30601	.17426	.848	-.3488	.9608
8.00	*1.00*	-.10621	.17426	1.000	-.7610	.5486
	2.00	-.31072	.15586	.725	-.8964	.2750
	3.00	-.80215*	.17426	.009	-1.4570	-.1473
	4.00	-.34845	.17426	.722	-1.0033	.3064
	5.00	.52565	.17426	.196	-.1292	1.1805
	6.00	-.24037	.17426	.965	-.8952	.4145
	7.00	-.11626	.15586	1.000	-.7020	.4694
	9.00	.27456	.15586	.846	-.3111	.8603
	10.00	.34276	.15586	.603	-.2429	.9285
	11.00	-.17196	.15586	.994	-.7577	.4137
	12.00	-.60598	.17426	.086	-1.2608	.0489
	13.00	.18975	.17426	.994	-.4651	.8446
9.00	*1.00*	-.38077	.17426	.611	-1.0356	.2741
	2.00	-.58528	.15586	.050	-1.1710	.0004

	3.00	-1.07671*	.17426	.000	-1.7315	-.4219
	4.00	-.62301	.17426	.071	-1.2778	.0318
	5.00	.25109	.17426	.953	-.4038	.9059
	6.00	-.51493	.17426	.217	-1.1698	.1399
	7.00	-.39083	.15586	.421	-.9765	.1949
	8.00	-.27456	.15586	.846	-.8603	.3111
	10.00	.06819	.15586	1.000	-.5175	.6539
	11.00	-.44652	.15586	.251	-1.0322	.1392
	12.00	-.88054*	.17426	.003	-1.5354	-.2257
	13.00	-.08481	.17426	1.000	-.7396	.5700
10.00	*1.00*	-.44897	.17426	.384	-1.1038	.2059
	2.00	-.65347*	.15586	.021	-1.2392	-.0678
	3.00	-1.14491*	.17426	.000	-1.7997	-.4901
	4.00	-.69121*	.17426	.033	-1.3460	-.0364
	5.00	.18289	.17426	.996	-.4719	.8377
	6.00	-.58312	.17426	.110	-1.2380	.0717
	7.00	-.45902	.15586	.220	-1.0447	.1267
	8.00	-.34276	.15586	.603	-.9285	.2429
	9.00	-.06819	.15586	1.000	-.6539	.5175
	11.00	-.51472	.15586	.119	-1.1004	.0710
	12.00	-.94873*	.17426	.002	-1.6036	-.2939
	13.00	-.15301	.17426	.999	-.8078	.5018
11.00	*1.00*	.06575	.17426	1.000	-.5891	.7206
	2.00	-.13876	.15586	.999	-.7245	.4469
	3.00	-.63019	.17426	.066	-1.2850	.0246
	4.00	-.17649	.17426	.997	-.8313	.4783
	5.00	.69761*	.17426	.031	.0428	1.3524
	6.00	-.06841	.17426	1.000	-.7232	.5864
	7.00	.05570	.15586	1.000	-.5300	.6414
	8.00	.17196	.15586	.994	-.4137	.7577
	9.00	.44652	.15586	.251	-.1392	1.0322
	10.00	.51472	.15586	.119	-.0710	1.1004
	12.00	-.43401	.17426	.430	-1.0889	.2208
	13.00	.36171	.17426	.677	-.2931	1.0165
12.00	*1.00*	.49977	.19089	.362	-.2176	1.2171
	2.00	.29526	.17426	.874	-.3596	.9501
	3.00	-.19617	.19089	.997	-.9135	.5212
	4.00	.25753	.19089	.970	-.4598	.9749
	5.00	1.13162*	.19089	.001	.4143	1.8490
	6.00	.36561	.19089	.769	-.3517	1.0829
	7.00	.48971	.17426	.273	-.1651	1.1445
	8.00	.60598	.17426	.086	-.0489	1.2608
	9.00	.88054*	.17426	.003	.2257	1.5354
	10.00	.94873*	.17426	.002	.2939	1.6036

	11.00	.43401	.17426	.430	-.2208	1.0889
	13.00	.79573*	.19089	.022	.0784	1.5131
13.00	*1.00*	-.29596	.19089	.925	-1.0133	.4214
	2.00	-.50047	.17426	.248	-1.1553	.1544
	3.00	-.99190*	.19089	.003	-1.7092	-.2746
	4.00	-.53820	.19089	.269	-1.2555	.1791
	5.00	.33590	.19089	.847	-.3814	1.0532
	6.00	-.43012	.19089	.570	-1.1475	.2872
	7.00	-.30601	.17426	.848	-.9608	.3488
	8.00	-.18975	.17426	.994	-.8446	.4651
	9.00	.08481	.17426	1.000	-.5700	.7396
	10.00	.15301	.17426	.999	-.5018	.8078
	11.00	-.36171	.17426	.677	-1.0165	.2931
	12.00	-.79573*	.19089	.022	-1.5131	-.0784

For *figure 44A*:

One-way ANOVA:

	Sum of Squares	df	Mean Square	F	Sig.
Between Groups	5274.881	12	439.573	51.129	0.000
Within Groups	214.932	25	8.597		
Total	5489.813	37			

Multiple comparison: Tukey HSD *post hoc* test

(I) Treatment		*Mean Difference (I-J)*	*Std. Error*	*Sig.*	*95% Confidence Interval*	
					Lower Bound	Upper Bound
1.00	*2.00*	-.56907	2.39406	1.000	-9.3010	8.1628
	3.00	-29.05084*	2.39406	.000	-37.7828	-20.3189
	4.00	-3.18435	2.39406	.976	-11.9163	5.5476
	5.00	-3.91556	2.39406	.902	-12.6475	4.8164
	6.00	-15.60824*	2.39406	.000	-24.3402	-6.8763
	7.00	-33.95632*	2.39406	.000	-42.6882	-25.2244
	8.00	-20.89835*	2.67664	.000	-30.6609	-11.1358
	9.00	-.26340	2.39406	1.000	-8.9953	8.4685
	10.00	-.00657	2.39406	1.000	-8.7385	8.7254
	11.00	.01358	2.39406	1.000	-8.7183	8.7455
	12.00	-.14760	2.39406	1.000	-8.8795	8.5843

	13.00	-.00320	2.39406	1.000	-8.7351	8.7287
2.00	*1.00*	.56907	2.39406	1.000	-8.1628	9.3010
	3.00	-28.48176*	2.39406	.000	-37.2137	-19.7498
	4.00	-2.61528	2.39406	.995	-11.3472	6.1166
	5.00	-3.34649	2.39406	.965	-12.0784	5.3854
	6.00	-15.03917*	2.39406	.000	-23.7711	-6.3072
	7.00	-33.38725*	2.39406	.000	-42.1192	-24.6553
	8.00	-20.32928*	2.67664	.000	-30.0919	-10.5667
	9.00	.30567	2.39406	1.000	-8.4263	9.0376
	10.00	.56250	2.39406	1.000	-8.1694	9.2944
	11.00	.58266	2.39406	1.000	-8.1493	9.3146
	12.00	.42147	2.39406	1.000	-8.3105	9.1534
	13.00	.56587	2.39406	1.000	-8.1660	9.2978
3.00	*1.00*	29.05084*	2.39406	.000	20.3189	37.7828
	2.00	28.48176*	2.39406	.000	19.7498	37.2137
	4.00	25.86649*	2.39406	.000	17.1346	34.5984
	5.00	25.13527*	2.39406	.000	16.4034	33.8672
	6.00	13.44260*	2.39406	.000	4.7107	22.1745
	7.00	-4.90548	2.39406	.694	-13.6374	3.8264
	8.00	8.15249	2.67664	.170	-1.6101	17.9151
	9.00	28.78743*	2.39406	.000	20.0555	37.5194
	10.00	29.04427*	2.39406	.000	20.3123	37.7762
	11.00	29.06442*	2.39406	.000	20.3325	37.7963
	12.00	28.90323*	2.39406	.000	20.1713	37.6352
	13.00	29.04764*	2.39406	.000	20.3157	37.7796
4.00	*1.00*	3.18435	2.39406	.976	-5.5476	11.9163
	2.00	2.61528	2.39406	.995	-6.1166	11.3472
	3.00	-25.86649*	2.39406	.000	-34.5984	-17.1346
	5.00	-.73122	2.39406	1.000	-9.4631	8.0007
	6.00	-12.42389*	2.39406	.001	-21.1558	-3.6920
	7.00	-30.77197*	2.39406	.000	-39.5039	-22.0401
	8.00	-17.71400*	2.67664	.000	-27.4766	-7.9514
	9.00	2.92094	2.39406	.987	-5.8110	11.6529
	10.00	3.17778	2.39406	.976	-5.5541	11.9097
	11.00	3.19793	2.39406	.975	-5.5340	11.9299
	12.00	3.03674	2.39406	.983	-5.6952	11.7687
	13.00	3.18115	2.39406	.976	-5.5508	11.9131
5.00	*1.00*	3.91556	2.39406	.902	-4.8164	12.6475
	2.00	3.34649	2.39406	.965	-5.3854	12.0784
	3.00	-25.13527*	2.39406	.000	-33.8672	-16.4034
	4.00	.73122	2.39406	1.000	-8.0007	9.4631
	6.00	-11.69267*	2.39406	.003	-20.4246	-2.9608
	7.00	-30.04076*	2.39406	.000	-38.7727	-21.3088

	8.00	-16.98279*	2.67664	.000	-26.7454	-7.2202
	9.00	3.65216	2.39406	.936	-5.0798	12.3841
	10.00	3.90900	2.39406	.903	-4.8229	12.6409
	11.00	3.92915	2.39406	.900	-4.8028	12.6611
	12.00	3.76796	2.39406	.922	-4.9640	12.4999
	13.00	3.91237	2.39406	.902	-4.8196	12.6443
6.00	*1.00*	15.60824*	2.39406	.000	6.8763	24.3402
	2.00	15.03917*	2.39406	.000	6.3072	23.7711
	3.00	-13.44260*	2.39406	.000	-22.1745	-4.7107
	4.00	12.42389*	2.39406	.001	3.6920	21.1558
	5.00	11.69267*	2.39406	.003	2.9608	20.4246
	7.00	-18.34808*	2.39406	.000	-27.0800	-9.6162
	8.00	-5.29011	2.67664	.738	-15.0527	4.4725
	9.00	15.34483*	2.39406	.000	6.6129	24.0768
	10.00	15.60167*	2.39406	.000	6.8697	24.3336
	11.00	15.62182*	2.39406	.000	6.8899	24.3537
	12.00	15.46063*	2.39406	.000	6.7287	24.1926
	13.00	15.60504*	2.39406	.000	6.8731	24.3370
7.00	*1.00*	33.95632*	2.39406	.000	25.2244	42.6882
	2.00	33.38725*	2.39406	.000	24.6553	42.1192
	3.00	4.90548	2.39406	.694	-3.8264	13.6374
	4.00	30.77197*	2.39406	.000	22.0401	39.5039
	5.00	30.04076*	2.39406	.000	21.3088	38.7727
	6.00	18.34808*	2.39406	.000	9.6162	27.0800
	8.00	13.05797*	2.67664	.003	3.2954	22.8206
	9.00	33.69292*	2.39406	.000	24.9610	42.4248
	10.00	33.94975*	2.39406	.000	25.2178	42.6817
	11.00	33.96990*	2.39406	.000	25.2380	42.7018
	12.00	33.80872*	2.39406	.000	25.0768	42.5406
	13.00	33.95312*	2.39406	.000	25.2212	42.6850
8.00	*1.00*	20.89835*	2.67664	.000	11.1358	30.6609
	2.00	20.32928*	2.67664	.000	10.5667	30.0919
	3.00	-8.15249	2.67664	.170	-17.9151	1.6101
	4.00	17.71400*	2.67664	.000	7.9514	27.4766
	5.00	16.98279*	2.67664	.000	7.2202	26.7454
	6.00	5.29011	2.67664	.738	-4.4725	15.0527
	7.00	-13.05797*	2.67664	.003	-22.8206	-3.2954
	9.00	20.63495*	2.67664	.000	10.8724	30.3975
	10.00	20.89178*	2.67664	.000	11.1292	30.6544
	11.00	20.91193*	2.67664	.000	11.1494	30.6745
	12.00	20.75075*	2.67664	.000	10.9882	30.5133
	13.00	20.89515*	2.67664	.000	11.1326	30.6577
9.00	*1.00*	.26340	2.39406	1.000	-8.4685	8.9953
	2.00	-.30567	2.39406	1.000	-9.0376	8.4263

	3.00	-28.78743*	2.39406	.000	-37.5194	-20.0555
	4.00	-2.92094	2.39406	.987	-11.6529	5.8110
	5.00	-3.65216	2.39406	.936	-12.3841	5.0798
	6.00	-15.34483*	2.39406	.000	-24.0768	-6.6129
	7.00	-33.69292*	2.39406	.000	-42.4248	-24.9610
	8.00	-20.63495*	2.67664	.000	-30.3975	-10.8724
	10.00	.25683	2.39406	1.000	-8.4751	8.9888
	11.00	.27699	2.39406	1.000	-8.4549	9.0089
	12.00	.11580	2.39406	1.000	-8.6161	8.8477
	13.00	.26021	2.39406	1.000	-8.4717	8.9921
10.00	*1.00*	.00657	2.39406	1.000	-8.7254	8.7385
	2.00	-.56250	2.39406	1.000	-9.2944	8.1694
	3.00	-29.04427*	2.39406	.000	-37.7762	-20.3123
	4.00	-3.17778	2.39406	.976	-11.9097	5.5541
	5.00	-3.90900	2.39406	.903	-12.6409	4.8229
	6.00	-15.60167*	2.39406	.000	-24.3336	-6.8697
	7.00	-33.94975*	2.39406	.000	-42.6817	-25.2178
	8.00	-20.89178*	2.67664	.000	-30.6544	-11.1292
	9.00	-.25683	2.39406	1.000	-8.9888	8.4751
	11.00	.02015	2.39406	1.000	-8.7118	8.7521
	12.00	-.14103	2.39406	1.000	-8.8730	8.5909
	13.00	.00337	2.39406	1.000	-8.7285	8.7353
11.00	*1.00*	-.01358	2.39406	1.000	-8.7455	8.7183
	2.00	-.58266	2.39406	1.000	-9.3146	8.1493
	3.00	-29.06442*	2.39406	.000	-37.7963	-20.3325
	4.00	-3.19793	2.39406	.975	-11.9299	5.5340
	5.00	-3.92915	2.39406	.900	-12.6611	4.8028
	6.00	-15.62182*	2.39406	.000	-24.3537	-6.8899
	7.00	-33.96990*	2.39406	.000	-42.7018	-25.2380
	8.00	-20.91193*	2.67664	.000	-30.6745	-11.1494
	9.00	-.27699	2.39406	1.000	-9.0089	8.4549
	10.00	-.02015	2.39406	1.000	-8.7521	8.7118
	12.00	-.16119	2.39406	1.000	-8.8931	8.5707
	13.00	-.01678	2.39406	1.000	-8.7487	8.7151
12.00	*1.00*	.14760	2.39406	1.000	-8.5843	8.8795
	2.00	-.42147	2.39406	1.000	-9.1534	8.3105
	3.00	-28.90323*	2.39406	.000	-37.6352	-20.1713
	4.00	-3.03674	2.39406	.983	-11.7687	5.6952
	5.00	-3.76796	2.39406	.922	-12.4999	4.9640
	6.00	-15.46063*	2.39406	.000	-24.1926	-6.7287
	7.00	-33.80872*	2.39406	.000	-42.5406	-25.0768
	8.00	-20.75075*	2.67664	.000	-30.5133	-10.9882
	9.00	-.11580	2.39406	1.000	-8.8477	8.6161
	10.00	.14103	2.39406	1.000	-8.5909	8.8730

	11.00	.16119	2.39406	1.000	-8.5707	8.8931
	13.00	.14441	2.39406	1.000	-8.5875	8.8763
13.00	*1.00*	.00320	2.39406	1.000	-8.7287	8.7351
	2.00	-.56587	2.39406	1.000	-9.2978	8.1660
	3.00	-29.04764*	2.39406	.000	-37.7796	-20.3157
	4.00	-3.18115	2.39406	.976	-11.9131	5.5508
	5.00	-3.91237	2.39406	.902	-12.6443	4.8196
	6.00	-15.60504*	2.39406	.000	-24.3370	-6.8731
	7.00	-33.95312*	2.39406	.000	-42.6850	-25.2212
	8.00	-20.89515*	2.67664	.000	-30.6577	-11.1326
	9.00	-.26021	2.39406	1.000	-8.9921	8.4717
	10.00	-.00337	2.39406	1.000	-8.7353	8.7285
	11.00	.01678	2.39406	1.000	-8.7151	8.7487
	12.00	-.14441	2.39406	1.000	-8.8763	8.5875

For *figure 44B*:

One-way ANOVA:

	Sum of Squares	df	Mean Square	F	Sig.
Between Groups	42.460	12	3.538	14.663	0.000
Within Groups	6.274	26	.241		
Total	48.734	38			

Multiple comparison: Tukey HSD *post hoc* test

(I) Treatment		*Mean Difference (I-J)*	*Std. Error*	*Sig.*	*95% Confidence Interval*	
					Lower Bound	Upper Bound
1.00	*2.00*	-.17884	.40109	1.000	-1.6364	1.2787
	3.00	-.25472	.40109	1.000	-1.7123	1.2029
	4.00	-3.16896*	.40109	.000	-4.6266	-1.7114
	5.00	-.31549	.40109	1.000	-1.7731	1.1421
	6.00	-.52497	.40109	.979	-1.9826	.9326
	7.00	-2.38119*	.40109	.000	-3.8388	-.9236
	8.00	-1.97388*	.40109	.002	-3.4315	-.5163
	9.00	-.28693	.40109	1.000	-1.7445	1.1707
	10.00	-.20049	.40109	1.000	-1.6581	1.2571
	11.00	.21710	.40109	1.000	-1.2405	1.6747
	12.00	.17535	.40109	1.000	-1.2822	1.6329

	13.00	-.03305	.40109	1.000	-1.4906	1.4245
2.00	*1.00*	.17884	.40109	1.000	-1.2787	1.6364
	3.00	-.07589	.40109	1.000	-1.5335	1.3817
	4.00	-2.99013*	.40109	.000	-4.4477	-1.5325
	5.00	-.13665	.40109	1.000	-1.5942	1.3209
	6.00	-.34613	.40109	.999	-1.8037	1.1115
	7.00	-2.20235*	.40109	.001	-3.6599	-.7448
	8.00	-1.79504*	.40109	.007	-3.2526	-.3375
	9.00	-.10809	.40109	1.000	-1.5657	1.3495
	10.00	-.02166	.40109	1.000	-1.4792	1.4359
	11.00	.39594	.40109	.998	-1.0617	1.8535
	12.00	.35418	.40109	.999	-1.1034	1.8118
	13.00	.14579	.40109	1.000	-1.3118	1.6034
3.00	*1.00*	.25472	.40109	1.000	-1.2029	1.7123
	2.00	.07589	.40109	1.000	-1.3817	1.5335
	4.00	-2.91424*	.40109	.000	-4.3718	-1.4567
	5.00	-.06077	.40109	1.000	-1.5184	1.3968
	6.00	-.27024	.40109	1.000	-1.7278	1.1873
	7.00	-2.12646*	.40109	.001	-3.5840	-.6689
	8.00	-1.71915*	.40109	.011	-3.1767	-.2616
	9.00	-.03220	.40109	1.000	-1.4898	1.4254
	10.00	.05423	.40109	1.000	-1.4034	1.5118
	11.00	.47182	.40109	.991	-.9858	1.9294
	12.00	.43007	.40109	.996	-1.0275	1.8877
	13.00	.22168	.40109	1.000	-1.2359	1.6793
4.00	*1.00*	3.16896*	.40109	.000	1.7114	4.6266
	2.00	2.99013*	.40109	.000	1.5325	4.4477
	3.00	2.91424*	.40109	.000	1.4567	4.3718
	5.00	2.85347*	.40109	.000	1.3959	4.3111
	6.00	2.64399*	.40109	.000	1.1864	4.1016
	7.00	.78778	.40109	.745	-.6698	2.2454
	8.00	1.19509	.40109	.190	-.2625	2.6527
	9.00	2.88203*	.40109	.000	1.4244	4.3396
	10.00	2.96847*	.40109	.000	1.5109	4.4261
	11.00	3.38606*	.40109	.000	1.9285	4.8436
	12.00	3.34431*	.40109	.000	1.8867	4.8019
	13.00	3.13592*	.40109	.000	1.6783	4.5935
5.00	*1.00*	.31549	.40109	1.000	-1.1421	1.7731
	2.00	.13665	.40109	1.000	-1.3209	1.5942
	3.00	.06077	.40109	1.000	-1.3968	1.5184
	4.00	-2.85347*	.40109	.000	-4.3111	-1.3959
	6.00	-.20948	.40109	1.000	-1.6671	1.2481
	7.00	-2.06570*	.40109	.001	-3.5233	-.6081

	8.00	-1.65839*	.40109	.016	-3.1160	-.2008
	9.00	.02856	.40109	1.000	-1.4290	1.4861
	10.00	.11500	.40109	1.000	-1.3426	1.5726
	11.00	.53259	.40109	.976	-.9250	1.9902
	12.00	.49084	.40109	.987	-.9668	1.9484
	13.00	.28244	.40109	1.000	-1.1751	1.7400
6.00	*1.00*	.52497	.40109	.979	-.9326	1.9826
	2.00	.34613	.40109	.999	-1.1115	1.8037
	3.00	.27024	.40109	1.000	-1.1873	1.7278
	4.00	-2.64399*	.40109	.000	-4.1016	-1.1864
	5.00	.20948	.40109	1.000	-1.2481	1.6671
	7.00	-1.85622*	.40109	.005	-3.3138	-.3986
	8.00	-1.44891	.40109	.052	-2.9065	.0087
	9.00	.23804	.40109	1.000	-1.2195	1.6956
	10.00	.32447	.40109	1.000	-1.1331	1.7821
	11.00	.74207	.40109	.808	-.7155	2.1997
	12.00	.70031	.40109	.858	-.7573	2.1579
	13.00	.49192	.40109	.987	-.9657	1.9495
7.00	*1.00*	2.38119*	.40109	.000	.9236	3.8388
	2.00	2.20235*	.40109	.001	.7448	3.6599
	3.00	2.12646*	.40109	.001	.6689	3.5840
	4.00	-.78778	.40109	.745	-2.2454	.6698
	5.00	2.06570*	.40109	.001	.6081	3.5233
	6.00	1.85622*	.40109	.005	.3986	3.3138
	8.00	.40731	.40109	.997	-1.0503	1.8649
	9.00	2.09426*	.40109	.001	.6367	3.5518
	10.00	2.18069*	.40109	.001	.7231	3.6383
	11.00	2.59828*	.40109	.000	1.1407	4.0559
	12.00	2.55653*	.40109	.000	1.0989	4.0141
	13.00	2.34814*	.40109	.000	.8906	3.8057
8.00	*1.00*	1.97388*	.40109	.002	.5163	3.4315
	2.00	1.79504*	.40109	.007	.3375	3.2526
	3.00	1.71915*	.40109	.011	.2616	3.1767
	4.00	-1.19509	.40109	.190	-2.6527	.2625
	5.00	1.65839*	.40109	.016	.2008	3.1160
	6.00	1.44891	.40109	.052	-.0087	2.9065
	7.00	-.40731	.40109	.997	-1.8649	1.0503
	9.00	1.68695*	.40109	.013	.2294	3.1445
	10.00	1.77338*	.40109	.008	.3158	3.2310
	11.00	2.19097*	.40109	.001	.7334	3.6486
	12.00	2.14922*	.40109	.001	.6916	3.6068
	13.00	1.94083*	.40109	.003	.4832	3.3984
9.00	*1.00*	.28693	.40109	1.000	-1.1707	1.7445
	2.00	.10809	.40109	1.000	-1.3495	1.5657

	3.00	.03220	.40109	1.000	-1.4254	1.4898
	4.00	-2.88203*	.40109	.000	-4.3396	-1.4244
	5.00	-.02856	.40109	1.000	-1.4861	1.4290
	6.00	-.23804	.40109	1.000	-1.6956	1.2195
	7.00	-2.09426*	.40109	.001	-3.5518	-.6367
	8.00	-1.68695*	.40109	.013	-3.1445	-.2294
	10.00	.08643	.40109	1.000	-1.3712	1.5440
	11.00	.50403	.40109	.984	-.9536	1.9616
	12.00	.46227	.40109	.992	-.9953	1.9199
	13.00	.25388	.40109	1.000	-1.2037	1.7115
10.00	*1.00*	.20049	.40109	1.000	-1.2571	1.6581
	2.00	.02166	.40109	1.000	-1.4359	1.4792
	3.00	-.05423	.40109	1.000	-1.5118	1.4034
	4.00	-2.96847*	.40109	.000	-4.4261	-1.5109
	5.00	-.11500	.40109	1.000	-1.5726	1.3426
	6.00	-.32447	.40109	1.000	-1.7821	1.1331
	7.00	-2.18069*	.40109	.001	-3.6383	-.7231
	8.00	-1.77338*	.40109	.008	-3.2310	-.3158
	9.00	-.08643	.40109	1.000	-1.5440	1.3712
	11.00	.41759	.40109	.997	-1.0400	1.8752
	12.00	.37584	.40109	.999	-1.0817	1.8334
	13.00	.16745	.40109	1.000	-1.2901	1.6250
11.00	*1.00*	-.21710	.40109	1.000	-1.6747	1.2405
	2.00	-.39594	.40109	.998	-1.8535	1.0617
	3.00	-.47182	.40109	.991	-1.9294	.9858
	4.00	-3.38606*	.40109	.000	-4.8436	-1.9285
	5.00	-.53259	.40109	.976	-1.9902	.9250
	6.00	-.74207	.40109	.808	-2.1997	.7155
	7.00	-2.59828*	.40109	.000	-4.0559	-1.1407
	8.00	-2.19097*	.40109	.001	-3.6486	-.7334
	9.00	-.50403	.40109	.984	-1.9616	.9536
	10.00	-.41759	.40109	.997	-1.8752	1.0400
	12.00	-.04175	.40109	1.000	-1.4993	1.4158
	13.00	-.25014	.40109	1.000	-1.7077	1.2074
12.00	*1.00*	-.17535	.40109	1.000	-1.6329	1.2822
	2.00	-.35418	.40109	.999	-1.8118	1.1034
	3.00	-.43007	.40109	.996	-1.8877	1.0275
	4.00	-3.34431*	.40109	.000	-4.8019	-1.8867
	5.00	-.49084	.40109	.987	-1.9484	.9668
	6.00	-.70031	.40109	.858	-2.1579	.7573
	7.00	-2.55653*	.40109	.000	-4.0141	-1.0989
	8.00	-2.14922*	.40109	.001	-3.6068	-.6916
	9.00	-.46227	.40109	.992	-1.9199	.9953
	10.00	-.37584	.40109	.999	-1.8334	1.0817

	11.00	.04175	.40109	1.000	-1.4158	1.4993
	13.00	-.20839	.40109	1.000	-1.6660	1.2492
13.00	*1.00*	.03305	.40109	1.000	-1.4245	1.4906
	2.00	-.14579	.40109	1.000	-1.6034	1.3118
	3.00	-.22168	.40109	1.000	-1.6793	1.2359
	4.00	-3.13592*	.40109	.000	-4.5935	-1.6783
	5.00	-.28244	.40109	1.000	-1.7400	1.1751
	6.00	-.49192	.40109	.987	-1.9495	.9657
	7.00	-2.34814*	.40109	.000	-3.8057	-.8906
	8.00	-1.94083*	.40109	.003	-3.3984	-.4832
	9.00	-.25388	.40109	1.000	-1.7115	1.2037
	10.00	-.16745	.40109	1.000	-1.6250	1.2901
	11.00	.25014	.40109	1.000	-1.2074	1.7077
	12.00	.20839	.40109	1.000	-1.2492	1.6660

For *figure 57A*:

One-way ANOVA:

	Sum of Squares	df	Mean Square	F	Sig.
Between Groups	260.518	8	32.565	79.181	.000
Within Groups	7.403	18	.411		
Total	267.921	26			

Multiple comparison: Tukey HSD *post hoc* test

(I) Treatment		***Mean Difference (I-J)***	***Std. Error***	***Sig.***	***95% Confidence Interval***	
					Lower Bound	Upper Bound
1.00	*2.00*	.04985	.52362	1.000	-1.7849	1.8845
	3.00	-4.34094*	.52362	.000	-6.1756	-2.5062
	4.00	.01578	.52362	1.000	-1.8189	1.8505
	5.00	-5.54768*	.52362	.000	-7.3824	-3.7130
	6.00	-7.80320*	.52362	.000	-9.6379	-5.9685
	7.00	-.31785	.52362	.999	-2.1526	1.5168
	8.00	-3.92443*	.52362	.000	-5.7591	-2.0897
	9.00	-7.54794*	.52362	.000	-9.3826	-5.7132
2.00	*1.00*	-.04985	.52362	1.000	-1.8845	1.7849
	3.00	-4.39079*	.52362	.000	-6.2255	-2.5561
	4.00	-.03407	.52362	1.000	-1.8688	1.8006

	5.00	-5.59753*	.52362	.000	-7.4322	-3.7628
	6.00	-7.85305*	.52362	.000	-9.6878	-6.0183
	7.00	-.36770	.52362	.998	-2.2024	1.4670
	8.00	-3.97428*	.52362	.000	-5.8090	-2.1396
	9.00	-7.59779*	.52362	.000	-9.4325	-5.7631
3.00	*1.00*	4.34094*	.52362	.000	2.5062	6.1756
	2.00	4.39079*	.52362	.000	2.5561	6.2255
	4.00	4.35672*	.52362	.000	2.5220	6.1914
	5.00	-1.20674	.52362	.388	-3.0414	.6280
	6.00	-3.46226*	.52362	.000	-5.2970	-1.6276
	7.00	4.02309*	.52362	.000	2.1884	5.8578
	8.00	.41651	.52362	.996	-1.4182	2.2512
	9.00	-3.20700*	.52362	.000	-5.0417	-1.3723
4.00	*1.00*	-.01578	.52362	1.000	-1.8505	1.8189
	2.00	.03407	.52362	1.000	-1.8006	1.8688
	3.00	-4.35672*	.52362	.000	-6.1914	-2.5220
	5.00	-5.56346*	.52362	.000	-7.3982	-3.7288
	6.00	-7.81898*	.52362	.000	-9.6537	-5.9843
	7.00	-.33363	.52362	.999	-2.1683	1.5011
	8.00	-3.94021*	.52362	.000	-5.7749	-2.1055
	9.00	-7.56372*	.52362	.000	-9.3984	-5.7290
5.00	*1.00*	5.54768*	.52362	.000	3.7130	7.3824
	2.00	5.59753*	.52362	.000	3.7628	7.4322
	3.00	1.20674	.52362	.388	-.6280	3.0414
	4.00	5.56346*	.52362	.000	3.7288	7.3982
	6.00	-2.25552*	.52362	.010	-4.0902	-.4208
	7.00	5.22983*	.52362	.000	3.3951	7.0645
	8.00	1.62325	.52362	.107	-.2114	3.4580
	9.00	-2.00026*	.52362	.027	-3.8350	-.1656
6.00	*1.00*	7.80320*	.52362	.000	5.9685	9.6379
	2.00	7.85305*	.52362	.000	6.0183	9.6878
	3.00	3.46226*	.52362	.000	1.6276	5.2970
	4.00	7.81898*	.52362	.000	5.9843	9.6537
	5.00	2.25552*	.52362	.010	.4208	4.0902
	7.00	7.48535*	.52362	.000	5.6506	9.3201
	8.00	3.87877*	.52362	.000	2.0441	5.7135
	9.00	.25526	.52362	1.000	-1.5794	2.0900
7.00	*1.00*	.31785	.52362	.999	-1.5168	2.1526
	2.00	.36770	.52362	.998	-1.4670	2.2024
	3.00	-4.02309*	.52362	.000	-5.8578	-2.1884
	4.00	.33363	.52362	.999	-1.5011	2.1683
	5.00	-5.22983*	.52362	.000	-7.0645	-3.3951
	6.00	-7.48535*	.52362	.000	-9.3201	-5.6506
	8.00	-3.60658*	.52362	.000	-5.4413	-1.7719
	9.00	-7.23009*	.52362	.000	-9.0648	-5.3954

8.00	*1.00*	3.92443*	.52362	.000	2.0897	5.7591
	2.00	3.97428*	.52362	.000	2.1396	5.8090
	3.00	-.41651	.52362	.996	-2.2512	1.4182
	4.00	3.94021*	.52362	.000	2.1055	5.7749
	5.00	-1.62325	.52362	.107	-3.4580	.2114
	6.00	-3.87877*	.52362	.000	-5.7135	-2.0441
	7.00	3.60658*	.52362	.000	1.7719	5.4413
	9.00	-3.62351*	.52362	.000	-5.4582	-1.7888
9.00	*1.00*	7.54794*	.52362	.000	5.7132	9.3826
	2.00	7.59779*	.52362	.000	5.7631	9.4325
	3.00	3.20700*	.52362	.000	1.3723	5.0417
	4.00	7.56372*	.52362	.000	5.7290	9.3984
	5.00	2.00026*	.52362	.027	.1656	3.8350
	6.00	-.25526	.52362	1.000	-2.0900	1.5794
	7.00	7.23009*	.52362	.000	5.3954	9.0648
	8.00	3.62351*	.52362	.000	1.7888	5.4582

For *figure 57B*:

One-way ANOVA:

	Sum of Squares	df	Mean Square	F	Sig.
Between Groups	3.092	8	.386	12.898	.000
Within Groups	.539	18	.030		
Total	3.631	26			

Multiple comparison: Tukey HSD *post hoc* test

(I) Treatment		***Mean Difference (I-J)***	***Std. Error***	***Sig.***	***95% Confidence Interval***	
					Lower Bound	Upper Bound
1.00	*2.00*	-.02187	.14133	1.000	-.5171	.4733
	3.00	.50345*	.14133	.045	.0082	.9987
	4.00	-.37725	.14133	.226	-.8725	.1180
	5.00	-.51649*	.14133	.037	-1.0117	-.0213
	6.00	.20339	.14133	.868	-.2918	.6986
	7.00	-.23770	.14133	.750	-.7329	.2575
	8.00	.43723	.14133	.109	-.0580	.9324
	9.00	.29603	.14133	.505	-.1992	.7912
2.00	*1.00*	.02187	.14133	1.000	-.4733	.5171
	3.00	.52532*	.14133	.033	.0301	1.0205

	4.00	-.35538	.14133	.288	-.8506	.1398
	5.00	-.49461	.14133	.050	-.9898	.0006
	6.00	.22526	.14133	.796	-.2700	.7205
	7.00	-.21583	.14133	.829	-.7110	.2794
	8.00	.45910	.14133	.082	-.0361	.9543
	9.00	.31790	.14133	.418	-.1773	.8131
3.00	*1.00*	-.50345*	.14133	.045	-.9987	-.0082
	2.00	-.52532*	.14133	.033	-1.0205	-.0301
	4.00	-.88069*	.14133	.000	-1.3759	-.3855
	5.00	-1.01993*	.14133	.000	-1.5151	-.5247
	6.00	-.30006	.14133	.489	-.7953	.1952
	7.00	-.74115*	.14133	.001	-1.2364	-.2459
	8.00	-.06622	.14133	1.000	-.5614	.4290
	9.00	-.20742	.14133	.856	-.7026	.2878
4.00	*1.00*	.37725	.14133	.226	-.1180	.8725
	2.00	.35538	.14133	.288	-.1398	.8506
	3.00	.88069*	.14133	.000	.3855	1.3759
	5.00	-.13924	.14133	.983	-.6345	.3560
	6.00	.58063*	.14133	.015	.0854	1.0758
	7.00	.13955	.14133	.982	-.3557	.6348
	8.00	.81447*	.14133	.000	.3193	1.3097
	9.00	.67327*	.14133	.004	.1781	1.1685
5.00	*1.00*	.51649*	.14133	.037	.0213	1.0117
	2.00	.49461	.14133	.050	-.0006	.9898
	3.00	1.01993*	.14133	.000	.5247	1.5151
	4.00	.13924	.14133	.983	-.3560	.6345
	6.00	.71987*	.14133	.002	.2247	1.2151
	7.00	.27879	.14133	.578	-.2164	.7740
	8.00	.95371*	.14133	.000	.4585	1.4489
	9.00	.81251*	.14133	.001	.3173	1.3077
6.00	*1.00*	-.20339	.14133	.868	-.6986	.2918
	2.00	-.22526	.14133	.796	-.7205	.2700
	3.00	.30006	.14133	.489	-.1952	.7953
	4.00	-.58063*	.14133	.015	-1.0758	-.0854
	5.00	-.71987*	.14133	.002	-1.2151	-.2247
	7.00	-.44108	.14133	.103	-.9363	.0541
	8.00	.23384	.14133	.764	-.2614	.7291
	9.00	.09264	.14133	.999	-.4026	.5879
7.00	*1.00*	.23770	.14133	.750	-.2575	.7329
	2.00	.21583	.14133	.829	-.2794	.7110
	3.00	.74115*	.14133	.001	.2459	1.2364
	4.00	-.13955	.14133	.982	-.6348	.3557
	5.00	-.27879	.14133	.578	-.7740	.2164
	6.00	.44108	.14133	.103	-.0541	.9363
	8.00	.67493*	.14133	.004	.1797	1.1701

	9.00	.53373*	.14133	.029	.0385	1.0289
8.00	*1.00*	-.43723	.14133	.109	-.9324	.0580
	2.00	-.45910	.14133	.082	-.9543	.0361
	3.00	.06622	.14133	1.000	-.4290	.5614
	4.00	-.81447*	.14133	.000	-1.3097	-.3193
	5.00	-.95371*	.14133	.000	-1.4489	-.4585
	6.00	-.23384	.14133	.764	-.7291	.2614
	7.00	-.67493*	.14133	.004	-1.1701	-.1797
	9.00	-.14120	.14133	.981	-.6364	.3540
9.00	*1.00*	-.29603	.14133	.505	-.7912	.1992
	2.00	-.31790	.14133	.418	-.8131	.1773
	3.00	.20742	.14133	.856	-.2878	.7026
	4.00	-.67327*	.14133	.004	-1.1685	-.1781
	5.00	-.81251*	.14133	.001	-1.3077	-.3173
	6.00	-.09264	.14133	.999	-.5879	.4026
	7.00	-.53373*	.14133	.029	-1.0289	-.0385
	8.00	.14120	.14133	.981	-.3540	.6364

For *figure 58*:

One-way ANOVA:

	Sum of Squares	df	Mean Square	F	Sig.
Between Groups	24.740	11	2.249	10.795	.000
Within Groups	4.375	21	.208		
Total	29.115	32			

Multiple comparison: Tukey HSD *post hoc* test

(I) Treatment		***Mean Difference (I-J)***	***Std. Error***	***Sig.***	***95% Confidence Interval***	
					Lower Bound	Upper Bound
1.00	*2.00*	.10994	.37269	1.000	-1.2526	1.4725
	3.00	-2.12355*	.37269	.001	-3.4861	-.7610
	4.00	-.03592	.37269	1.000	-1.3985	1.3266
	5.00	-.20743	.37269	1.000	-1.5700	1.1551
	6.00	-1.21472	.41669	.205	-2.7381	.3087
	7.00	.22884	.37269	1.000	-1.1337	1.5914
	8.00	-2.07124*	.41669	.003	-3.5946	-.5479
	9.00	.11698	.37269	1.000	-1.2456	1.4795
	10.00	-1.40005*	.37269	.041	-2.7626	-.0375

	11.00	.02819	.37269	1.000	-1.3344	1.3907
	12.00	-1.59404*	.41669	.035	-3.1174	-.0707
	1.00	-.10994	.37269	1.000	-1.4725	1.2526
	3.00	-2.23348*	.37269	.000	-3.5960	-.8709
	4.00	-.14586	.37269	1.000	-1.5084	1.2167
	5.00	-.31737	.37269	.999	-1.6799	1.0452
	6.00	-1.32466	.41669	.128	-2.8480	.1987
2.00	*7.00*	.11890	.37269	1.000	-1.2437	1.4815
	8.00	-2.18118*	.41669	.002	-3.7046	-.6578
	9.00	.00704	.37269	1.000	-1.3555	1.3696
	10.00	-1.50999*	.37269	.022	-2.8725	-.1474
	11.00	-.08175	.37269	1.000	-1.4443	1.2808
	12.00	-1.70398*	.41669	.020	-3.2274	-.1806
	1.00	2.12355*	.37269	.001	.7610	3.4861
	2.00	2.23348*	.37269	.000	.8709	3.5960
	4.00	2.08762*	.37269	.001	.7251	3.4502
	5.00	1.91612*	.37269	.002	.5536	3.2787
	6.00	.90882	.41669	.578	-.6146	2.4322
3.00	*7.00*	2.35239*	.37269	.000	.9898	3.7149
	8.00	.05230	.41669	1.000	-1.4711	1.5757
	9.00	2.24052*	.37269	.000	.8780	3.6031
	10.00	.72350	.37269	.724	-.6391	2.0860
	11.00	2.15174*	.37269	.000	.7892	3.5143
	12.00	.52951	.41669	.974	-.9939	2.0529
	1.00	.03592	.37269	1.000	-1.3266	1.3985
	2.00	.14586	.37269	1.000	-1.2167	1.5084
	3.00	-2.08762*	.37269	.001	-3.4502	-.7251
	5.00	-.17150	.37269	1.000	-1.5341	1.1911
	6.00	-1.17880	.41669	.236	-2.7022	.3446
4.00	*7.00*	.26476	.37269	1.000	-1.0978	1.6273
	8.00	-2.03532*	.41669	.003	-3.5587	-.5119
	9.00	.15290	.37269	1.000	-1.2096	1.5155
	10.00	-1.36412*	.37269	.050	-2.7267	-.0016
	11.00	.06412	.37269	1.000	-1.2984	1.4267
	12.00	-1.55811*	.41669	.042	-3.0815	-.0347
	1.00	.20743	.37269	1.000	-1.1551	1.5700
	2.00	.31737	.37269	.999	-1.0452	1.6799
	3.00	-1.91612*	.37269	.002	-3.2787	-.5536
	4.00	.17150	.37269	1.000	-1.1911	1.5341
5.00	*6.00*	-1.00730	.41669	.436	-2.5307	.5161
	7.00	.43627	.37269	.986	-.9263	1.7988
	8.00	-1.86381*	.41669	.009	-3.3872	-.3404
	9.00	.32441	.37269	.999	-1.0381	1.6870
	10.00	-1.19262	.37269	.123	-2.5552	.1699

	11.00	.23562	.37269	1.000	-1.1269	1.5982
	12.00	-1.38661	.41669	.096	-2.9100	.1368
	1.00	1.21472	.41669	.205	-.3087	2.7381
	2.00	1.32466	.41669	.128	-.1987	2.8480
	3.00	-.90882	.41669	.578	-2.4322	.6146
	4.00	1.17880	.41669	.236	-.3446	2.7022
	5.00	1.00730	.41669	.436	-.5161	2.5307
6.00	*7.00*	1.44356	.41669	.074	-.0798	2.9669
	8.00	-.85652	.45646	.760	-2.5253	.8123
	9.00	1.33170	.41669	.124	-.1917	2.8551
	10.00	-.18533	.41669	1.000	-1.7087	1.3381
	11.00	1.24291	.41669	.182	-.2805	2.7663
	12.00	-.37931	.45646	.999	-2.0481	1.2895
	1.00	-.22884	.37269	1.000	-1.5914	1.1337
	2.00	-.11890	.37269	1.000	-1.4815	1.2437
	3.00	-2.35239*	.37269	.000	-3.7149	-.9898
	4.00	-.26476	.37269	1.000	-1.6273	1.0978
	5.00	-.43627	.37269	.986	-1.7988	.9263
7.00	*6.00*	-1.44356	.41669	.074	-2.9669	.0798
	8.00	-2.30008*	.41669	.001	-3.8235	-.7767
	9.00	-.11186	.37269	1.000	-1.4744	1.2507
	10.00	-1.62889*	.37269	.011	-2.9914	-.2663
	11.00	-.20065	.37269	1.000	-1.5632	1.1619
	12.00	-1.82288*	.41669	.011	-3.3463	-.2995
	1.00	2.07124*	.41669	.003	.5479	3.5946
	2.00	2.18118*	.41669	.002	.6578	3.7046
	3.00	-.05230	.41669	1.000	-1.5757	1.4711
	4.00	2.03532*	.41669	.003	.5119	3.5587
	5.00	1.86381*	.41669	.009	.3404	3.3872
8.00	*6.00*	.85652	.45646	.760	-.8123	2.5253
	7.00	2.30008*	.41669	.001	.7767	3.8235
	9.00	2.18822*	.41669	.002	.6648	3.7116
	10.00	.67119	.41669	.887	-.8522	2.1946
	11.00	2.09943*	.41669	.002	.5760	3.6228
	13.00	.47720	.45646	.994	-1.1916	2.1460
	1.00	-.11698	.37269	1.000	-1.4795	1.2456
	2.00	-.00704	.37269	1.000	-1.3696	1.3555
	3.00	-2.24052*	.37269	.000	-3.6031	-.8780
	4.00	-.15290	.37269	1.000	-1.5155	1.2096
	5.00	-.32441	.37269	.999	-1.6870	1.0381
9.00	*6.00*	-1.33170	.41669	.124	-2.8551	.1917
	7.00	.11186	.37269	1.000	-1.2507	1.4744
	8.00	-2.18822*	.41669	.002	-3.7116	-.6648
	10.00	-1.51703*	.37269	.021	-2.8796	-.1545
	11.00	-.08879	.37269	1.000	-1.4513	1.2738

	12.00	-1.71102*	.41669	.019	-3.2344	-.1876
	1.00	1.40005*	.37269	.041	.0375	2.7626
	2.00	1.50999*	.37269	.022	.1474	2.8725
	3.00	-.72350	.37269	.724	-2.0860	.6391
	4.00	1.36412*	.37269	.050	.0016	2.7267
	5.00	1.19262	.37269	.123	-.1699	2.5552
10.00	*6.00*	.18533	.41669	1.000	-1.3381	1.7087
	7.00	1.62889*	.37269	.011	.2663	2.9914
	8.00	-.67119	.41669	.887	-2.1946	.8522
	9.00	1.51703*	.37269	.021	.1545	2.8796
	12.00	1.42824*	.37269	.035	.0657	2.7908
	13.00	-.19399	.41669	1.000	-1.7174	1.3294
	1.00	-.02819	.37269	1.000	-1.3907	1.3344
	2.00	.08175	.37269	1.000	-1.2808	1.4443
	3.00	-2.15174*	.37269	.000	-3.5143	-.7892
	4.00	-.06412	.37269	1.000	-1.4267	1.2984
	5.00	-.23562	.37269	1.000	-1.5982	1.1269
11.00	*7.00*	-1.24291	.41669	.182	-2.7663	.2805
	8.00	.20065	.37269	1.000	-1.1619	1.5632
	9.00	-2.09943*	.41669	.002	-3.6228	-.5760
	10.00	.08879	.37269	1.000	-1.2738	1.4513
	12.00	-1.42824*	.37269	.035	-2.7908	-.0657
	13.00	-1.62223*	.41669	.030	-3.1456	-.0988
	1.00	1.59404*	.41669	.035	.0707	3.1174
	2.00	1.70398*	.41669	.020	.1806	3.2274
	4.00	-.52951	.41669	.974	-2.0529	.9939
	5.00	1.55811*	.41669	.042	.0347	3.0815
	6.00	1.38661	.41669	.096	-.1368	2.9100
12.00	*7.00*	.37931	.45646	.999	-1.2895	2.0481
	8.00	1.82288*	.41669	.011	.2995	3.3463
	9.00	-.47720	.45646	.994	-2.1460	1.1916
	10.00	1.71102*	.41669	.019	.1876	3.2344
	11.00	.19399	.41669	1.000	-1.3294	1.7174
	13.00	1.62223*	.41669	.030	.0988	3.1456

VII. 11. Gene clusters identified with DAVID analysis

Clusters of genes down-regulated by IFN-α:

Gene Group 1 Enrichment Score: 22.194215092754717

UNIPROT ID Gene Name

270106 ribosomal protein L13 (Rpl13)
75617 ribosomal protein S25 (Rps25)
20055 ribosomal protein S16 (Rps16)
66489 ribosomal protein L35 (Rpl35)
16898 ribosomal protein S2 (Rps2)
67891 ribosomal protein L4 (Rpl4)
66481 ribosomal protein S21 (Rps21)
66480 ribosomal protein L15 (Rpl15)
20091 ribosomal protein S3A1 (Rps3a1)
319195 ribosomal protein L17 (Rpl17)
19944 ribosomal protein L29 (Rpl29)
20085 ribosomal protein S19 (Rps19)
19896 ribosomal protein L10A (Rpl10a)
20084 ribosomal protein S18 (Rps18)
19989 ribosomal protein L7 (Rpl7)
19988 ribosomal protein L6 (Rpl6)
27367 ribosomal protein L3 (Rpl3)
20116 ribosomal protein S8 (Rps8)

Gene Group 2 Enrichment Score: 19.707222786005513

17709 cytochrome c oxidase subunit II (COX2)
18674 solute carrier family 25 (mitochondrial carrier, phosphate carrier), member 3 (Slc25a3)
28080 ATP synthase, H+ transporting, mitochondrial F1 complex, O subunit (Atp5o)
66694 ubiquinol-cytochrome c reductase, Rieske iron-sulfur polypeptide 1 (Uqcrfs1)
66945 succinate dehydrogenase complex, subunit A, flavoprotein (Fp) (Sdha)
67680 succinate dehydrogenase complex, subunit B, iron sulfur (Ip) (Sdhb)
11950 ATP synthase, H+ transporting, mitochondrial F0 complex, subunit B1 (Atp5f1)
11949 ATP synthase, H+ transporting, mitochondrial F1 complex, γ polypeptide 1 (Atp5c1)
66043 ATP synthase, H+ transporting, mitochondrial F1 complex, δ subunit (Atp5d)
11947 ATP synthase, H+ transporting mitochondrial F1 complex, β subunit (Atp5b)
67003 ubiquinol cytochrome c reductase core protein 2 (Uqcrc2)

Gene Group 3 Enrichment Score: 15.981115871725025

17709 cytochrome c oxidase subunit II (COX2)
18674 solute carrier family 25 (mitochondrial carrier, phosphate carrier), member 3 (Slc25a3)
71803 solute carrier family 25 (mitochondrial carrier), member 18 (Slc25a18)
67863 solute carrier family 25 (mitochondrial carrier oxoglutarate carrier), member 11 (Slc25a11)
11950 ATP synthase, H+ transporting, mitochondrial F0 complex, subunit B1 (Atp5f1)
66525 translocase of inner mitochondrial membrane 50 (Timm50)
66477 upregulated during skeletal muscle growth 5 (Usmg5)
27376 solute carrier family 25 (mitochondrial carrier, dicarboxylate transporter), member 10 (Slc25a10)
68316 apolipoprotein O (Apoo)
67003 ubiquinol cytochrome c reductase core protein 2 (Uqcrc2)
76614 inner membrane protein, mitochondrial (Immt)
72542 phosphoglycerate mutase family member 5 (Pgam5)

Gene Group 4 Enrichment Score: 15.234748256234331

73710 tubulin, β 2B class IIB (Tubb2b)
22152 tubulin, β 3 class III (Tubb3)
545486 tubulin, β 1 class VI (Tubb1)
67951 tubulin, β 6 class V (Tubb6)
22146 tubulin, α 1C (Tuba1c)
22145 tubulin, α 4A (Tuba4a)
53857 tubulin, α 8 (Tuba8)
22154 tubulin, β 5 class I (Tubb5)

Gene Group 5 Enrichment Score: 14.434590025344846

12462 chaperonin containing Tcp1, subunit 3 (γ) (Cct3)
12469 chaperonin containing Tcp1, subunit 8 (theta) (Cct8)
21454 t-complex protein 1 (Tcp1)
12466 chaperonin containing Tcp1, subunit 6a (zeta) (Cct6a)
12464 chaperonin containing Tcp1, subunit 4 (δ) (Cct4)

Gene Group 6 Enrichment Score: 13.89506787916256

22608 Y box protein 1 (Ybx1)
15384 heterogeneous nuclear ribonucleoprotein A/B (Hnrnpab)
319765 insulin-like growth factor 2 mRNA binding protein 2 (Igf2bp2)
15382 heterogeneous nuclear ribonucleoprotein A1 (Hnrnpa1)
51810 heterogeneous nuclear ribonucleoprotein U (Hnrnpu)
19655 RNA binding motif protein, X chromosome (Rbmx)
59093 poly(rC) binding protein 3 (Pcbp3)
50926 heterogeneous nuclear ribonucleoprotein D-like (Hnrnpdl)
20382 serine/arginine-rich splicing factor 2 (Srsf2)
56258 heterogeneous nuclear ribonucleoprotein H2 (Hnrnph2)

Gene Group 7 Enrichment Score: 13.6047232828136

232440 H2A histone family, member J (H2afj)
50708 histone cluster 1, H1c (Hist1h1c)
15078 H3 histone, family 3A (H3f3a)
15441 heterochromatin protein 1, binding protein 3 (Hp1bp3)
100041230 histone cluster 1, H4m (Hist1h4m)
319189 histone cluster 2, H2bb (Hist2h2bb)
319177 histone cluster 1, H2ba (Hist1h2ba)

Gene Group 8 Enrichment Score: 12.77028867995201

16828 lactate dehydrogenase A (Ldha)
17449 malate dehydrogenase 1, NAD (soluble) (Mdh1)
16832 lactate dehydrogenase B (Ldhb)
14555 glycerol-3-phosphate dehydrogenase 1 (soluble) (Gpd1)
333433 glycerol-3-phosphate dehydrogenase 1-like (Gpd1l)

Gene Group 9 Enrichment Score: 12.431775536731928

50797 coatomer protein complex, subunit β 2 (β prime) (Copb2)
319670 echinoderm microtubule associated protein like 5 (Eml5)
18786 phospholipase A2, activating protein (Plaa)
13427 dynein cytoplasmic 1 intermediate chain 2 (Dync1i2)
17101 lysosomal trafficking regulator (Lyst)
22388 WD repeat domain 1 (Wdr1)

Gene Group 10 Enrichment Score: 11.401680937202153

16675 keratin 27 (Krt27)
74127 keratin 80 (Krt80)
16691 keratin 8 (Krt8)
16907 lamin B2 (Lmnb2)

Gene Group 11 Enrichment Score: 10.255814479261028

93747 enoyl Coenzyme A hydratase, short chain, 1, mitochondrial (Echs1)
97212 hydroxyacyl-Coenzyme A dehydrogenase/3-ketoacyl-Coenzyme A thiolase/enoyl-Coenzyme A hydratase (trifunctional protein), α subunit (Hadha)
66885 acyl-Coenzyme A dehydrogenase, short/branched chain (Acadsb)
52538 acetyl-Coenzyme A acyltransferase 2 (mitochondrial 3-oxoacyl-Coenzyme A thiolase) (Acaa2)

Gene Group 12 Enrichment Score: 10.044014527244453

15482 heat shock protein 1-like (Hspa1l)
15525 heat shock protein 4 (Hspa4)
15512 heat shock protein 2 (Hspa2)
15511 heat shock protein 1B (Hspa1b)

Gene Group 13 Enrichment Score: 7.382807945264915

11844 ADP-ribosylation factor 5 (Arf5)
11843 ADP-ribosylation factor 4 (Arf4)
19349 RAB7, member RAS oncogene family (Rab7)
68365 RAB14, member RAS oncogene family (Rab14)

Gene Group 14 Enrichment Score: 3.664447304141587

68316 apolipoprotein O (Apoo)
72736 thioredoxin-related transmembrane protein 1 (Tmx1)
54563 nucleoporin 210 (Nup210)
103963 ribophorin I (Rpn1)

Clusters of genes down-regulated by palmitate:

Gene Group 1 Enrichment Score: 27.340953338322766

UNIPROT ID Gene Name
110308 keratin 5 (Krt5)
13346 desmin (Des)
16682 keratin 4 (Krt4)
53622 keratin 85 (Krt85)

68239 keratin 42 (Krt42)
16680 keratin 84 (Krt84)
16678 keratin 1 (Krt1)
94179 keratin 23 (Krt23)
16675 keratin 27 (Krt27)
16907 lamin B2 (Lmnb2)
16905 lamin A (Lmna)
16669 keratin 19 (Krt19)
16668 keratin 18 (Krt18)
16667 keratin 17 (Krt17)
16666 keratin 16 (Krt16)
16664 keratin 14 (Krt14)
16663 keratin 13 (Krt13)
16661 keratin 10 (Krt10)
66809 keratin 20 (Krt20)
105866 keratin 72 (Krt72)
268481 keratin 222 (Krt222)
109052 keratin 75 (Krt75)
223917 keratin 79 (Krt79)
16691 keratin 8 (Krt8)
19132 peripherin (Prph)
16687 keratin 6A (Krt6a)
406222 keratin 74 (Krt74)

Gene Group 2 Enrichment Score: 22.546153995797393

68263 pyruvate dehydrogenase (lipoamide) β (Pdhb)
11429 aconitase 2, mitochondrial (Aco2)
13382 dihydrolipoamide dehydrogenase (Dld)
17448 malate dehydrogenase 2, NAD (mitochondrial) (Mdh2)
18597 pyruvate dehydrogenase E1 α 1 (Pdha1)
27402 pyruvate dehydrogenase complex, component X (Pdhx)
78920 dihydrolipoamide S-succinyltransferase (E2 component of 2-oxo-glutarate complex) (Dlst)
67834 isocitrate dehydrogenase 3 (NAD+) α (Idh3a)
12974 citrate synthase (Cs)

Gene Group 3 Enrichment Score: 21.491599483468587

68193 ribosomal protein L24 (Rpl24)
68052 ribosomal protein S13 (Rps13)
270106 ribosomal protein L13 (Rpl13)
19935 mitochondrial ribosomal protein L23 (Mrpl23)
16898 ribosomal protein S2 (Rps2)
67427 ribosomal protein S20 (Rps20)
20091 ribosomal protein S3A1 (Rps3a1)
66481 ribosomal protein S21 (Rps21)
20085 ribosomal protein S19 (Rps19)
26961 ribosomal protein L8 (Rpl8)

20084 ribosomal protein S18 (Rps18)
19989 ribosomal protein L7 (Rpl7)
26451 ribosomal protein L27A (Rpl27a)
319195 ribosomal protein L17 (Rpl17)
19896 ribosomal protein L10A (Rpl10a)
20102 ribosomal protein S4, X-linked (Rps4x)

Gene Group 4 Enrichment Score: 18.046271492856555

17709 cytochrome c oxidase subunit II (COX2)
18674 solute carrier family 25 (mitochondrial carrier, phosphate carrier), member 3 (Slc25a3)
28080 ATP synthase, H+ transporting, mitochondrial F1 complex, O subunit (Atp5o)
66694 ubiquinol-cytochrome c reductase, Rieske iron-sulfur polypeptide 1 (Uqcrfs1)
67680 succinate dehydrogenase complex, subunit B, iron sulfur (Ip) (Sdhb)
11950 ATP synthase, H+ transporting, mitochondrial F0 complex, subunit B1 (Atp5f1)
11949 ATP synthase, H+ transporting, mitochondrial F1 complex, γ polypeptide 1 (Atp5c1)
11947 ATP synthase, H+ transporting mitochondrial F1 complex, β subunit (Atp5b)
66043 ATP synthase, H+ transporting, mitochondrial F1 complex, δ subunit (Atp5d)
12866 cytochrome c oxidase subunit VIIa 2 (Cox7a2)
66525 translocase of inner mitochondrial membrane 50 (Timm50)
57279 solute carrier family 25 (mitochondrial carnitine/acylcarnitine translocase), member 20 (Slc25a20)
22273 ubiquinol-cytochrome c reductase core protein 1 (Uqcrc1)
66477 upregulated during skeletal muscle growth 5 (Usmg5)
27376 solute carrier family 25 (mitochondrial carrier, dicarboxylate transporter), member 10 (Slc25a10)
76614 inner membrane protein, mitochondrial (Immt)

Gene Group 5 Enrichment Score: 16.895639297974952

381314 isoleucine-tRNA synthetase 2, mitochondrial (Iars2)
70120 tyrosyl-tRNA synthetase 2 (mitochondrial) (Yars2)
353172 glycyl-tRNA synthetase (Gars)
226414 aspartyl-tRNA synthetase (Dars)

Gene Group 6 Enrichment Score: 15.19979199086473

16828 lactate dehydrogenase A (Ldha)
17449 malate dehydrogenase 1, NAD (soluble) (Mdh1)
16833 lactate dehydrogenase C (Ldhc)
17448 malate dehydrogenase 2, NAD (mitochondrial) (Mdh2)
14555 glycerol-3-phosphate dehydrogenase 1 (soluble) (Gpd1)
333433 glycerol-3-phosphate dehydrogenase 1-like (Gpd1l)

Gene Group 7 Enrichment Score: 13.544274556436427

12462 chaperonin containing Tcp1, subunit 3 (γ) (Cct3)
12469 chaperonin containing Tcp1, subunit 8 (theta) (Cct8)
21454 t-complex protein 1 (Tcp1)
12466 chaperonin containing Tcp1, subunit 6a (zeta) (Cct6a)

Gene Group 8 Enrichment Score: 12.954545575472325

545486 tubulin, β 1 class VI (Tubb1)
22146 tubulin, α 1C (Tuba1c)
22145 tubulin, α 4A (Tuba4a)
22144 tubulin, α 3A (Tuba3a)
22154 tubulin, β5 class I (Tubb5)

Gene Group 9 Enrichment Score: 11.987323744852933

18949 pinin (Pnn)
15382 heterogeneous nuclear ribonucleoprotein A1 (Hnrnpa1)
110809 serine/arginine-rich splicing factor 1 (Srsf1)
51810 heterogeneous nuclear ribonucleoprotein U (Hnrnpu)
18458 poly(A) binding protein, cytoplasmic 1 (Pabpc1)
23881 GTPase activating protein (SH3 domain) binding protein 2 (G3bp2)
56403 synaptotagmin binding, cytoplasmic RNA interacting protein (Syncrip)
50926 heterogeneous nuclear ribonucleoprotein D-like (Hnrnpdl)
140488 insulin-like growth factor 2 mRNA binding protein 3 (Igf2bp3)

Gene Group 10 Enrichment Score: 11.291158146169026

232440 H2A histone family, member J (H2afj)
50708 histone cluster 1, H1c (Hist1h1c)
14958 H1 histone family, member 0 (H1f0)
319189 histone cluster 2, H2bb (Hist2h2bb)

Gene Group 11 Enrichment Score: 10.89155859219692

15482 heat shock protein 1-like (Hspa1l)
15525 heat shock protein 4 (Hspa4)
15512 heat shock protein 2 (Hspa2)
15511 heat shock protein 1B (Hspa1b)

Gene Group 12 Enrichment Score: 10.583684643167981

11370 acyl-Coenzyme A dehydrogenase, very long chain (Acadvl)
110842 electron transferring flavoprotein, α polypeptide (Etfa)
93747 enoyl Coenzyme A hydratase, short chain, 1, mitochondrial (Echs1)
11363 acyl-Coenzyme A dehydrogenase, long-chain (Acadl)

Gene Group 13 Enrichment Score: 9.232047295064406

14827 protein disulfide isomerase associated 3 (Pdia3)
18453 prolyl 4-hydroxylase, β polypeptide (P4hb)
12304 protein disulfide isomerase associated 4 (Pdia4)
72736 thioredoxin-related transmembrane protein 1 (Tmx1)

Gene Group 14 Enrichment Score: 3.8351172602377406

98238 leucine rich repeat containing 59 (Lrrc59)
72736 thioredoxin-related transmembrane protein 1 (Tmx1)
54563 nucleoporin 210 (Nup210)
103963 ribophorin I (Rpn1)

109154 malectin (Mlec)

Clusters of genes up-regulated by palmitate:

Gene Group 1 Enrichment Score: 12.916387525035683

UNIPROT_ID Gene Name

56258 heterogeneous nuclear ribonucleoprotein H2 (Hnrnph2)

76936 heterogeneous nuclear ribonucleoprotein M (Hnrnpm)

225027 serine/arginine-rich splicing factor 7 (Srsf7)

233908 fused in sarcoma (Fus)

53379 heterogeneous nuclear ribonucleoprotein A2/B1 (Hnrnpa2b1)

20384 serine/arginine-rich splicing factor 5 (Srsf5)

20382 serine/arginine-rich splicing factor 2 (Srsf2)

56194 pre-mRNA processing factor 40A (Prpf40a)

71514 splicing factor proline/glutamine rich (polypyrimidine tract binding protein associated) (Sfpq)

319765 insulin-like growth factor 2 mRNA binding protein 2 (Igf2bp2)

17975 nucleolin (Ncl)

110611 high density lipoprotein (HDL) binding protein (Hdlbp)

15388 heterogeneous nuclear ribonucleoprotein L (Hnrnpl)

15384 heterogeneous nuclear ribonucleoprotein A/B (Hnrnpab)

59093 poly(rC) binding protein 3 (Pcbp3)

23983 poly(rC) binding protein 1 (Pcbp1)

19655 RNA binding motif protein, X chromosome (Rbmx)

11991 heterogeneous nuclear ribonucleoprotein D (Hnrnpd)

56215 apoptotic chromatin condensation inducer 1 (Acin1)

18521 poly(rC) binding protein 2 (Pcbp2)

22185 U2 small nuclear ribonucleoprotein auxiliary factor (U2AF) 2 (U2af2)

22608 Y box protein 1 (Ybx1)

Gene Group 2 Enrichment Score: 10.63922038334072

67891 ribosomal protein L4 (Rpl4)

66489 ribosomal protein L35 (Rpl35)

75617 ribosomal protein S25 (Rps25)

20044 ribosomal protein S14 (Rps14)

19899 ribosomal protein L18 (Rpl18)

19921 ribosomal protein L19 (Rpl19)

Gene Group 3 Enrichment Score: 7.899364663937192

50709 histone cluster 1, H1e (Hist1h1e)

15078 H3 histone, family 3A (H3f3a)

100041230 histone cluster 1, H4m (Hist1h4m)

319177 histone cluster 1, H2ba (Hist1h2ba)

51788 H2A histone family, member Z (H2afz)

319176 histone cluster 2, H2ac (Hist2h2ac)

Gene Group 4 Enrichment Score: 3.7185121222254582

104130 NADH dehydrogenase (ubiquinone) 1 β subcomplex, 11 (Ndufb11)
227197 NADH dehydrogenase (ubiquinone) Fe-S protein 1 (Ndufs1)
67003 ubiquinol cytochrome c reductase core protein 2 (Uqcrc2)
12859 cytochrome c oxidase subunit Vb (Cox5b)

Clusters of genes down-regulated by IFN-α and up-regulated by palmitate:

Gene Group 1 Enrichment Score: 4.443951870351887
UNIPROT_ID Gene Name
20382 serine/arginine-rich splicing factor 2 (Srsf2)
19655 RNA binding motif protein, X chromosome (Rbmx)
319765 insulin-like growth factor 2 mRNA binding protein 2 (Igf2bp2)
15384 heterogeneous nuclear ribonucleoprotein A/B (Hnrnpab)
56258 heterogeneous nuclear ribonucleoprotein H2 (Hnrnph2)
59093 poly(rC) binding protein 3 (Pcbp3)

Clusters of genes down-regulated by IFN-α and by palmitate:

Gene Group 1 Enrichment Score: 14.186454203920169

UNIPROT_ID Gene Name
270106 ribosomal protein L13 (Rpl13)
16898 ribosomal protein S2 (Rps2)
20091 ribosomal protein S3A1 (Rps3a1)
66481 ribosomal protein S21 (Rps21)
20085 ribosomal protein S19 (Rps19)
20084 ribosomal protein S18 (Rps18)
19989 ribosomal protein L7 (Rpl7)
19896 ribosomal protein L10A (Rpl10a)
319195 ribosomal protein L17 (Rpl17)

Gene Group 2 Enrichment Score: 13.760325061844586

17709 cytochrome c oxidase subunit II (COX2)
18674 solute carrier family 25 (mitochondrial carrier, phosphate carrier), member 3 (Slc25a3)
66694 ubiquinol-cytochrome c reductase, Rieske iron-sulfur polypeptide 1 (Uqcrfs1)
67680 succinate dehydrogenase complex, subunit B, iron sulfur (Ip) (Sdhb)
11950 ATP synthase, H+ transporting, mitochondrial F0 complex, subunit B1 (Atp5f1)
66525 translocase of inner mitochondrial membrane 50 (Timm50)
66477 upregulated during skeletal muscle growth 5 (Usmg5)
27376 solute carrier family 25 (mitochondrial carrier, dicarboxylate transporter), member 10 (Slc25a10)
76614 inner membrane protein, mitochondrial (Immt)

Gene Group 3 Enrichment Score: 10.608146960576038

12462 chaperonin containing Tcp1, subunit 3 (γ) (Cct3)
12469 chaperonin containing Tcp1, subunit 8 (theta) (Cct8)

21454 t-complex protein 1 (Tcp1)
12466 chaperonin containing Tcp1, subunit 6a (zeta) (Cct6a)

Gene Group 4 Enrichment Score: 10.054782828918649

66043 ATP synthase, H+ transporting, mitochondrial F1 complex, δ subunit (Atp5d)
28080 ATP synthase, H+ transporting, mitochondrial F1 complex, O subunit (Atp5o)
18674 solute carrier family 25 (mitochondrial carrier, phosphate carrier), member 3 (Slc25a3)
11950 ATP synthase, H+ transporting, mitochondrial F0 complex, subunit B1 (Atp5f1)
11949 ATP synthase, H+ transporting, mitochondrial F1 complex, γ polypeptide 1 (Atp5c1)
11947 ATP synthase, H+ transporting mitochondrial F1 complex, β subunit (Atp5b)

Gene Group 5 Enrichment Score: 9.365775548954282

68263 pyruvate dehydrogenase (lipoamide) β (Pdhb)
18597 pyruvate dehydrogenase E1 α 1 (Pdha1)
12974 citrate synthase (Cs)
27402 pyruvate dehydrogenase complex, component X (Pdhx)

Gene Group 6 Enrichment Score: 8.598916979719728

545486 tubulin, β 1 class VI (Tubb1)
22146 tubulin, α 1C (Tuba1c)
22145 tubulin, α 4A (Tuba4a)
22154 tubulin, β 5 class I (Tubb5)

Gene Group 7 Enrichment Score: 8.22309435226446

15482 heat shock protein 1-like (Hspa1l)
15525 heat shock protein 4 (Hspa4)
15512 heat shock protein 2 (Hspa2)
15511 heat shock protein 1B (Hspa1b)

Gene Group 8 Enrichment Score: 7.259714237111446

16828 lactate dehydrogenase A (Ldha)
17449 malate dehydrogenase 1, NAD (soluble) (Mdh1)
14555 glycerol-3-phosphate dehydrogenase 1 (soluble) (Gpd1)
333433 glycerol-3-phosphate dehydrogenase 1-like (Gpd1l)

Gene Group 9 Enrichment Score: 6.089571025094121

98238 leucine rich repeat containing 59 (Lrrc59)
72736 thioredoxin-related transmembrane protein 1 (Tmx1)
54563 nucleoporin 210 (Nup210)
103963 ribophorin I (Rpn1)